Constrained Urban Airspace Design

Exploring future rules, strategies, and risk

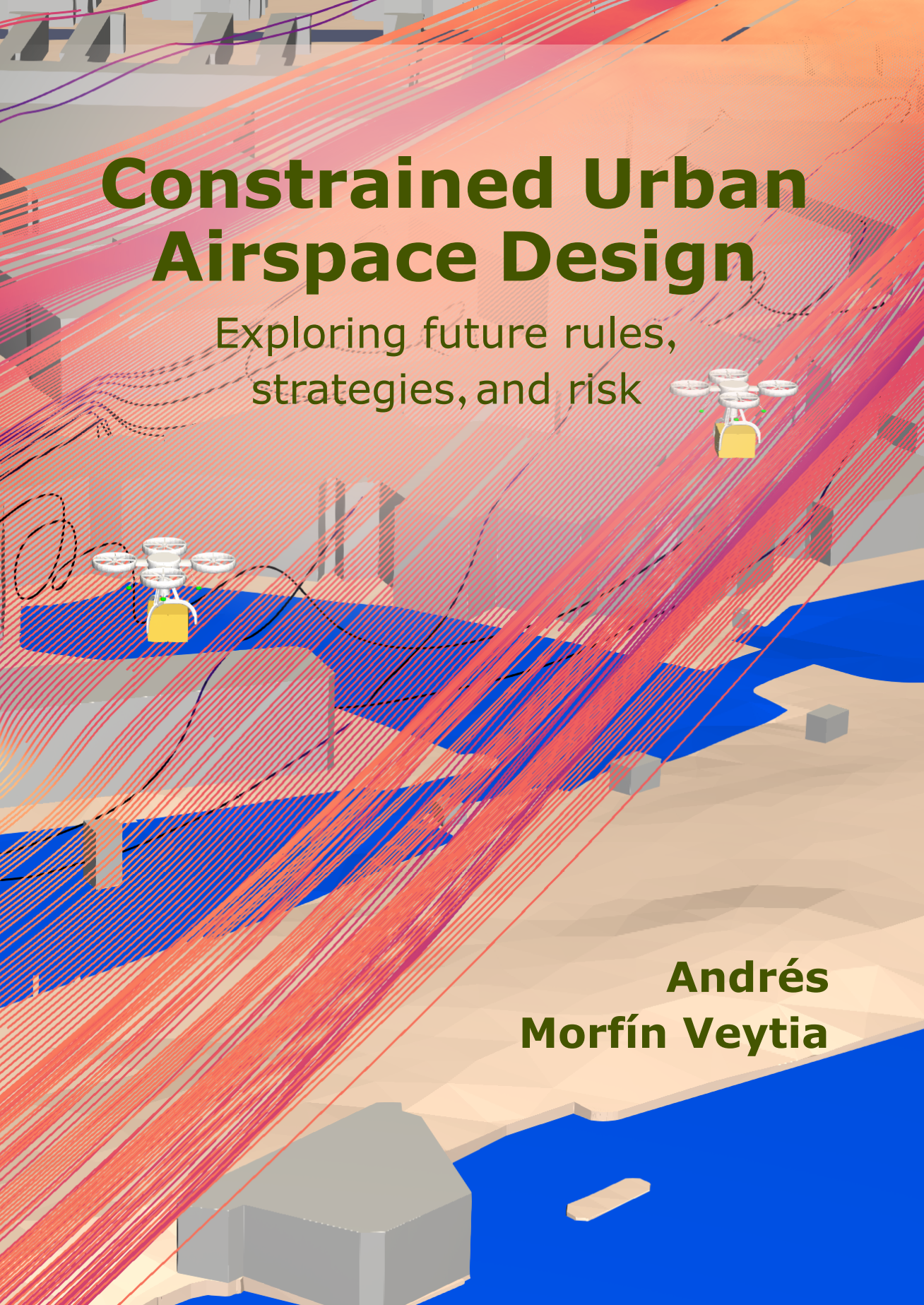

Andrés Morfín Veytia

Constrained Urban Airspace Design

Exploring future rules, strategies, and risk.

Constrained Urban Airspace Design

Exploring future rules, strategies, and risk.

Dissertation

for the purpose of obtaining the degree of doctor
at Delft University of Technology
by the authority of the Rector Magnificus, Prof. dr. ir. H. Bijl,
chair of the Board for Doctorates
to be defended publicly on
Monday, 16 March 2026 at 10:00 o'clock

by

Andres MORFIN VEYTIA

This dissertation has been approved by the promotors.

Composition of the doctoral committee:

Rector Magnificus,	chairperson
Dr.ir. J. Ellerbroek,	Delft University of Technology, *promotor*
Prof.dr.ir. J. M. Hoekstra,	Delft University of Technology, *promotor*
Independent members:	
Dr. C. Garcia Sanchez,	Delft University of Technology
Prof. dr. ir. S.P. Hoogendoorn,	Delft University of Technology
Prof. dr. D. Delahaye	Ecole Nationale de l'Aviation Civile, France
Prof. Dr.-Ing. D. Kügler,	Deutsches Zentrum für Luft- und Raumfahrt, Germany
Prof. Dr.-Ing. M. Schultz,	Universität der Bundeswehr München, Germany
Reserve member:	
Prof. dr. G.C.H.E. de Croon,	Delft University of Technology

Keywords: urban airspace, urban air mobility, conflict prevention, flow control, airspace structure, UTM, wind, air traffic management

Printed by: Ridderprint

Cover by: A. Morfin Veytia (drone model by Stinky Cheese Studios)

ISBN 978-94-6518-222-3

An electronic copy of this dissertation is available at
https://repository.tudelft.nl/.

To Barbora and Coco,

Barbora, thanks for the faith. Coco, thanks for the breaks.

Contents

SUMMARY

There is increasing interest in integrating autonomous air vehicles or drones into the current ground transportation system. In the European Union, the U-space framework has been established for the development of services that will enable drone missions in urban environments. These drone missions vary from typical package delivery to emergency medical transport, and have the potential to ease ground congestion and reduce greenhouse gas emissions in cities.

Operating in an urban environment poses challenges to air vehicles that are distinct from traditional air traffic management. Mainly, drones will constantly need to avoid both dynamic (other drones) and static (buildings and city infrastructure) obstacles during their flight. Additionally, the expected densities will be orders of magnitude larger than what is currently seen in conventional airspace.

This thesis focuses on addressing challenges and addressing risks of high-density air operations in constrained urban environments via two research goals. Thesis **goal 1** analyses how airspace designs and rules affect the safety and efficiency of the urban airspace at varying traffic density. Thesis **goal 2** develops and evaluates a method for analysing the operational feasibility of urban air missions considering local wind conditions.

Chapter 2 of this thesis details several urban airspace design considerations that are necessary for understanding the two thesis goals. Additionally, this chapter explains the reason for focusing on constrained airspace operations. In constrained airspace, drones operate in urban areas between tall buildings and/or other infrastructure. This means that drones are restricted to fly along a constrained network that is above the existing street network or any other pre-defined network with a fixed route topology. In constrained airspace, drones can no longer fly directly to their destination and have points of convergence at the intersections of the network.

Chapter 3 (**goal 1**) studies different airspace structures and rules to analyse how scarce vertical airspace can be effectively used in a simulated environment of Vienna. This chapter assumes air operations will happen in a layered constrained airspace and performs two sub-experiments that analyse the overall system safety, route duration, and route distance under increasing traffic demand. Note that in this part of the thesis, safety is measured with conflicts and intrusions that occur in the airspace. A conflict occurs when a drone is predicted to violate the safe separation distance of another drone within a look-ahead time if they continue along their current trajectory. An intrusion occurs if the safe separation distance is actually violated.

This first sub-experiment of this chapter shows the importance of establishing cruising layers versus other layer function assignments (such as turns). The second

sub-experiment shows how traffic demand can change the types of rules that are more desirable in the airspace. When there is high traffic demand, it is safer for traffic to be spread uniformly throughout the vertical space. However, at low traffic demands, there is less need to pre-allocate aircraft to specific heights. This allows aircraft to separate vertically only in areas where there is high local density.

Chapter 4 (**goal 1**) focuses on the effective use of horizontal airspace in the constrained network of Rotterdam. Some legs of a drone route through a network are preferred over others if all drones want the shortest route and demand is non-uniform. This creates hot-spots of high traffic density or high traffic complexity (converging aircraft). This thesis presents a decentralised dynamic traffic management method to ease these hot-spots. The method is decentralised because (1) not all airspace actors will want to freely share data, (2) the uncertainty of missions due to wind or other factors could make a previous plan inoperable, and (3) the ad hoc nature of urban missions makes them difficult to plan in advance.

This method uses current dynamic (current and constantly updated) aggregate flow data to identify and alter the cost of travelling through problematic clusters. Each drone individually uses the updated costs of the airspace to plan a new route with the goal of reducing local traffic density and complexity. Three different clustering strategies are presented that look at the current position of aircraft and recent safety events (conflicts and intrusions). Safety is improved significantly while limiting the distance increase compared to the shortest path route at high traffic demand levels. However, the method as developed in Chapter 4 does not significantly improve safety at low traffic demand levels.

Chapter 5 (**goal 1**) extends the method from Chapter 4 to improve the safety at low traffic demand levels. It uses historical conflicts to identify where high-complexity clusters tend to occur in the network of Rotterdam. Note that the method still uses current traffic data to dynamically alter the costs of travelling though the airspace. By using these pre-identified cluster zones, it was possible to increase the safety at low traffic demand levels. However, the safety improvement at high traffic demand levels is not as large when compared to using only current traffic data (Chapter 4).

Chapter 6 (**goal 2**) changes the focus of the thesis and studies the interaction of wind and the urban environment. This interaction can create safety risk and limit the operations of future urban air operations. This chapter compares a Computational Fluid Dynamics (CFD) simulation with the Reynolds-Averaged Navier Stokes (RANS) model to recorded wind measurements in the city centre of The Hague. The results show that while some measurement locations matched the simulation results, there are also large discrepancies. These discrepancies tend to occur in areas where the building models varies significantly from the reality. For example, one area had a large opening in the building that was not modelled.

Chapter 7 (**goal 2**) expands further on the simulations of Chapter 6. In this chapter, CFD simulations are performed to learn how wind affects airspace risk and yearly operational feasibility in Rotterdam. This chapter included an ensemble of simulations with varying wind conditions. The aim is to improve the results of a single RANS simulation with an uncertainty quantification framework to decide

several inflow conditions. The inflow conditions are selected considering the measured wind rose from 2022 at a weather station 10m over the ground in Rotterdam-Hague airport.

In this chapter, airspace zones are deemed unsafe if a certain wind speed and/or turbulence threshold is exceeded. The results show that a comprehensive city-wide risk analysis can be done with relatively few well-selected inflow conditions with a polynomial chaos expansion. Additionally, the results of the operational feasibility analysis show that 90 percent operational time in 2022 was possible if drones could withstand relatively medium turbulent kinetic energy and a 12 m/s average wind.

The thesis concludes with a comprehensive discussion and some recommendations for future work. Additionally, two appendices are included to supplement Chapters 4 and 7. The appendix for Chapter 4 includes a Wilcoxon signed-rank test that aim to test the hypothesis thoroughly across the different traffic demand levels. The appendix in Chapter 7 includes additional risk analysis and more operational feasibility analysis for the years of 2023 and 2024 in Rotterdam.

Finally, when applicable, the simulation environment and the results are provided via supplemental datasets (see **4TU Author datasets**). This is to (1) allow for replication and reproducibility of the work, and to (2) make the resulting data available for other research. For example, the wind fields generated by Chapter 7 may be valuable for other research not yet foreseen by the author.

SAMENVATTING

Er is toenemende belangstelling voor het integreren van autonome luchtvaartuigen of drones in het huidige verkeersnetwerk. In de Europese Unie is het U-space framework opgezet voor de ontwikkeling van diensten die dronemissies in stedelijke omgevingen mogelijk maken. Deze dronemissies kunnen variëren van typische pakketbezorging tot spoedeisend medisch transport en hebben het potentieel om om de druk op het verkeer te verminderen en broeikasgasemissies in steden te reduceren.

Het opereren in een stedelijke omgeving brengt uitdagingen met zich mee voor luchtvaartuigen die afwijken van de reguliere luchtvaart. Hoofdzakelijk moeten drones voortdurend zowel dynamische (andere drones) als statische (gebouwen en stadsinfrastructuur) obstakels vermijden tijdens hun vlucht. Bovendien zullen de verwachte dichtheden ordes van grootte groter zijn dan wat momenteel in de lucht is.

Dit proefschrift richtte zich op het aanpakken van uitdagingen en het adresseren van risico's van hoge verkeersdrukte in de lucht in beperkte stedelijke omgevingen via twee onderzoeksdoelen. Proefschrift **doel één** was het analyseren van hoe luchtruimontwerpen en regels de veiligheid en efficiëntie van het stedelijke luchtruim beïnvloeden bij toenemende verkeersdichtheid. Proefschrift **doel 2** was het ontwikkelen en evalueren van een methode voor het analyseren van de operationele haalbaarheid van stedelijke luchtmissies rekening houdend met lokale windomstandigheden.

Hoofdstuk 2 van dit proefschrift beschreef verschillende ontwerpoverwegingen voor stedelijk luchtruim die noodzakelijk zijn voor het begrijpen van de twee proefschriftdoelen. Daarnaast legde dit hoofdstuk de reden uit voor het focussen op beperkte luchtruimoperaties. In beperkt luchtruim opereren drones in stedelijke gebieden tussen hoge gebouwen en/of andere infrastructuur. Dit betekent dat drones beperkt zijn tot het vliegen langs een beperkt netwerk dat zich boven het bestaande stratennetwerk bevindt. In beperkt luchtruim kunnen drones niet langer direct naar hun bestemming vliegen en hebben convergentiepunten bij de kruispunten van het netwerk.

Hoofdstuk 3 (**doel 1**) bestudeerde verschillende luchtruimstructuren en regels om te analyseren hoe schaars verticaal luchtruim effectief kan worden gebruikt in een gesimuleerde omgeving van Wenen. Dit hoofdstuk nam aan dat luchtoperaties zullen plaatsvinden in een gelaagd beperkt luchtruim en voerde twee subexperimenten uit die de algehele systeemveiligheid, routeduur en routeafstand analyseerde onder toenemende verkeersvraag. In dit deel van het proefschrift werd veiligheid gemeten met conflicten en overschrijdingen van de minimaal veilige afstand die optreden in het luchtruim. Een conflict treedt op wanneer voorspeld wordt dat

een drone de veilige scheidingsafstand van een andere drone zal schenden binnen een vooruitkijktijd als ze hun huidige traject voortzetten. Een verlies van afstand treedt op als de veilige scheidingsafstand daadwerkelijk wordt geschonden.

Dit eerste sub-experiment van dit hoofdstuk toonde het belang aan van het vaststellen van cruise-lagen versus andere lagen met andere functies (zoals bochten). Het tweede sub-experiment toonde hoe verkeersdruk kan veranderen welke types regels wenselijker zijn in het luchtruim. Wanneer er hoge verkeersdruk is, is het veiliger voor verkeer om uniform verspreid te zijn door de verticale ruimte. Bij lage verkeersdruk is er echter minder behoefte om luchtvaartuigen vooraf toe te wijzen aan specifieke hoogtes. Dit maakt het mogelijk voor luchtvaartuigen om alleen verticaal te scheiden in gebieden waar er hoge lokale dichtheid is.

Hoofdstuk 4 (**doel 1**) richtte zich op het effectieve gebruik van horizontaal luchtruim in het beperkte netwerk van Rotterdam. Sommige segmenten van een droneroute door een netwerk zullen de voorkeur krijgen boven andere als alle drones de kortste route willen en de vraag niet-uniform is. Dit zal op zijn beurt hotspots van hoge verkeersdichtheid of hoge verkeerscomplexiteit (convergerende luchtvaartuigen) creëren. Dit proefschrift ontwikkelt een gedecentraliseerde dynamische verkeersmanagementmethode om deze hotspots te verlichten. De methode is gedecentraliseerd omdat (1) niet alle luchtruimactoren vrij gegevens willen delen, (2) de onzekerheid van missies vanwege wind of andere factoren een eerder plan onuitvoerbaar zou kunnen maken, en (3) de ad hoc-aard van stedelijke missies hen moeilijk vooraf te plannen maakt.

Deze methode gebruikte huidige dynamische (huidige en constant bijgewerkte) geaggregeerde stroomgegevens om clusters met hoge dichtheid te identificeren en de kosten van het reizen erdoorheen te verhogen. Elke drone gebruikt individueel de bijgewerkte kosten van het luchtruim om een nieuwe route te plannen die zou resulteren in het verminderen van lokale verkeersdichtheid en complexiteit. Drie verschillende clusteringstrategieën werden gepresenteerd die kijken naar de huidige positie van luchtvaartuigen en recente veiligheidsgebeurtenissen (conflicten en verliezen van afstand). Veiligheid werd significant verbeterd terwijl de afstandstoename beperkt werd vergeleken met de kortste route bij hoge verkeersvraagniveaus. De methode zoals ontwikkeld in Hoofdstuk 4 verbeterde echter niet significant de veiligheid bij lage verkeersvraagniveaus.

Hoofdstuk 5 (**doel 1**) breidde de methode uit Hoofdstuk 4 uit om de veiligheid bij lage verkeersdruk niveaus te verbeteren. Het gebruikte historische conflicten om te identificeren waar clusters met hoge complexiteit konden voorkomen in het netwerk van Rotterdam. MDe methode gebruikte echter nog steeds huidige verkeersgegevens om dynamisch de kosten van het reizen door het luchtruim te wijzigen. Door deze vooraf geïdentificeerde clusterzones te gebruiken, was het mogelijk om de veiligheid bij lage verkeersvraagniveaus te verhogen. De veiligheidsverbetering bij hoge verkeersvraagniveaus was echter niet zo groot vergeleken met het gebruik van alleen huidige verkeersgegevens (Hoofdstuk 4).

Hoofdstuk 6 (**doel 2**) veranderde de focus van het proefschrift en bestudeerde de interactie van wind en de stedelijke omgeving en hoe het risicos kan creëren en operaties van stedelijke luchtoperaties kan beperken. Dit hoofdstuk vergeleek een

Computational Fluid Dynamics (CFD) simulatie met het Reynolds-Averaged Navier Stokes (RANS) model met opgenomen windmetingen in het stadscentrum van Den Haag. De resultaten toonden dat hoewel sommige meetlocaties overeenkwamen met de simulatieresultaten, er ook grote discrepanties zijn. Deze discrepanties hebben de neiging om op te treden in gebieden waar het gebouwmodel aanzienlijk verschilt van de werkelijkheid. Zo had één gebied bijvoorbeeld een grote opening in het gebouw die niet was gemodelleerd.

Hoofdstuk 7 (**doel 2**) breidde verder uit op de simulaties van Hoofdstuk 6. In dit hoofdstuk werd een ensemble van CFD-simulaties uitgevoerd om te leren hoe wind luchtruimrisico en jaarlijkse operationele haalbaarheid in Rotterdam beïnvloedt. Dit hoofdstuk omvatte een ensemble van simulaties met variërende windomstandigheden. Het doel is de resultaten van een enkele RANS-simulatie te verbeteren door een onzekerheids analyse te gebruiken om verschillende instroomcondities te beslissen. De instroomcondities worden geselecteerd rekening houdend met de gemeten windroos van 2022 bij een weerstation 10m boven de grond op Rotterdam-Den Haag luchthaven.

In dit hoofdstuk werden luchtruimzones als onveilig beschouwd als een bepaalde windsnelheid en/of turbulentiedrempel werd overschreden. De resultaten toonden dat een uitgebreide stadsbrede risicoanalyse kan worden gedaan met relatief weinig goed geselecteerde instroomcondities met het gebruik van een polynomiale chaos-expansie. Daarnaast toonden de resultaten van de operationele haalbaarheidsanalyse dat 90 procent operationele tijd in 2022 mogelijk was als drones relatief gemiddelde turbulente kinetische energie en een gemiddelde wind van 12 m/s konden weerstaan.

Het proefschrift concludeert met een uitgebreide discussie en enkele aanbevelingen voor toekomstig werk. Daarnaast zijn twee appendices opgenomen om Hoofdstukken 4 en hoofdstuk 7 aan te vullen. De appendix voor Hoofdstuk 4 bevat een Wilcoxon signed-rank test van de hypothese. De appendix in Hoofdstuk 7 bevat aanvullende risicoanalyse en meer operationele haalbaarheidsanalyse voor de jaren 2023 en 2024 in Rotterdam.

Ten slotte, waar van toepassing, worden de simulatieomgeving en de resultaten verstrekt via aanvullende datasets (zie **4TU Author datasets**). Dit is om (1) replicatie en reproduceerbaarheid van het werk mogelijk te maken, en om (2) de resulterende gegevens beschikbaar te maken voor ander onderzoek. Bijvoorbeeld, de windvelden gegenereerd door Hoofdstuk 7 kunnen waardevol zijn voor ander onderzoek dat nog niet voorzien is door de auteur.

1

Introduction

The emergence of urban air operations presents unique challenges for air traffic management and safety. While we can draw valuable lessons from ground traffic, where vehicles must navigate within urban constraints while avoiding other vehicles, urban air traffic introduces a vertical dimension that changes the operational landscape. Additionally, aircraft operating in urban environments must also contend with turbulence generated by the atmospheric boundary layer, which is difficult to predict.

This thesis addresses these challenges with two main goals. The first is to analyse and develop urban airspace rules for constrained urban environments. The second is to establish a methodology for evaluating risk and operational feasibility considering urban wind conditions.

1

1.1. Background

People are increasingly moving to dense urban areas. According to United Nations projections, 68 percent of the world's population will reside in cities by 2050 [1]. This growing urban concentration will lead to ground traffic congestion, resulting in both wasted time in traffic and higher carbon emissions [2]. These challenges present an opportunity to restructure the systems for urban transportation of goods and people.

Recent years have seen growing interest in utilizing aircraft to replace part of the ground traffic. In some estimates, the volume of drone parcel deliveries is expected to surpass traditional air traffic levels [3, 4]. This potential transformation has led to extensive research initiatives that focus on developing urban air traffic management systems[5, 6].

Urban environments pose distinct challenges that do not typically affect traditional air traffic management. Aircraft must avoid both dynamic (other aircraft) and static (buildings and city infrastructure) obstacles during flight. Therefore, airspace rules and designs should consider these constraints. Additionally, the proximity to buildings and uneven terrain creates complex wind flows which lead to turbulent structures where each component in the three spatial dimensions has significant relative importance. This in contrast to the wind flows that commercial aircraft encounter at higher altitudes where they operate for the majority of their flight. This thesis addresses these challenges in urban airspace through two main goals. The first will be to analyse how airspace designs and rules affect the safety and efficiency of urban airspace, and the second is to develop and evaluate a method for analysing the operational feasibility of urban air missions considering local wind conditions.

Urban air missions at high densities will likely mirror the ad-hoc nature of ground traffic, making advance planning, like in traditional air traffic, difficult. Currently, Amazon is using delivery drones for packages needed within an hour of when the order was placed [7]. Additionally, air operators may be in competition with each other, so there may be a reluctance to share complete flight information with a central planner. For this reason, the airspace rules and designs presented in this work do not require a central entity to have complete knowledge of all airspace actors.

The Metropolis 2 project, a project which the author of this thesis was involved in, [8] demonstrated that both centralized pre-flight planning and decentralized in-flight decision-making can achieve comparable safety levels. Most notably, their research revealed that hybrid systems combining both approaches proved most effective, suggesting that individual flight autonomy is a viable avenue of research.

The second goal of this thesis addresses the operational feasibility of aircraft in urban wind conditions. Previous research has estimated that some aircraft may only be capable of flying 53% of the year in a city of Denmark due to weather factors [9]. To address this limitation, we develop an analytical framework that combines Computational Fluid Dynamics (CFD) with historical weather data, using Rotterdam as our test case.

Figure 1.1: Airbus© concept art showing urban air operations. At high traffic densities, aircraft would need to avoid both static and dynamic obstacles.

1.2. Conflict prevention with airspace Design and rules

A conflict arises when two aircraft are anticipated to approach each other within a distance that falls below an established separation minimum in the near future. If the separation minimum is violated, then an intrusion is said to occur (Fig 1.2). The goal in urban airspace safety is to prevent intrusions, as they may lead to collisions.

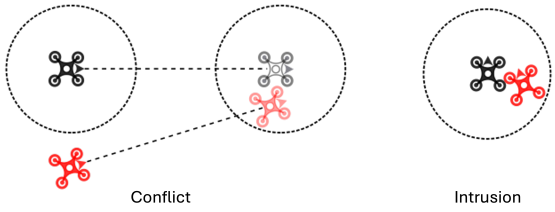

Figure 1.2: The difference between conflict and intrusions.

While conflict resolution aims to solve conflicts before they become intrusions, conflict prevention aims to prevent conflicts from ever occurring. Safe urban airspace design and rules work on the conflict prevention level. This means that they aim to reduce the probability that aircraft will encounter each other in an unsafe way. In this way, urban airspace designs and rules should lower the total number of conflicts and provide space to resolve conflicts that do end up

occurring.

Previous approaches to conflict prevention in open airspace rely on segmentation and alignment [10]. Aircraft with high relative velocities are segmented, while aircraft with low relative velocities are aligned to reduce conflict probability. The Metropolis project [11] developed a heading-based layered structure in open airspace that uses segmentation and alignment to improve safety. However, this thesis addresses constrained urban airspace, where aircraft are not able to fly straight-line routes to their destination.

Conflict prevention in constrained airspace has also been achieved by the use of layers in [3, 8, 12]. These layers can vary in function, among several others, they can be allocated for cruising, turning, resolving conflicts, or a combination of these. This thesis will present how allocating a specific function to different layers affects conflict prevention. Moreover, it will compare different methods to distribute aircraft vertically in this constrained environment.

As well as vertical separation, effective horizontal distribution of aircraft is also necessary to achieve airspace safety in constrained environments where some areas may be preferred by many aircraft. This work will also present a decentralised method in which aircraft can spread themselves over the available airspace by using current aggregate flow information. Moreover, it will extend the method by also including some historical data.

1.3. Wind effects on urban air operations

In traditional air traffic management, aircraft spend most of their flight high above the ground, where the air flow is relatively two-dimensional due to thermal stratification at cruise height [13]. Flights in urban environments occur inside the atmospheric boundary layer, where, the varying heat of the earth's surface causes forcings close to the ground, without considering buildings. With buildings in the mix, the situation can become even more difficult to forecast. There could be areas where the air speeds up, or slows down. And this can vary significantly across relatively small spaces and time.

To understand where and when drones will be able to fly, and to be able to do representative simulations of urban drone operations, will require tools that enable us to predict how a certain wind condition, will affect the urban airspace in a granular level relative to drone size and mission length. One option is to add several wind sensors in the city in tall buildings, another is to have wind sensors on the ground itself. However, these two options cannot predict. This, it is also useful to employ Computational Fluid Dynamics (CFD) simulations using historical data to establish time varying urban wind conditions.

The simplest CFD simulation that gives information about variation of the wind flow (turbulence) is the Reynolds Average Navier-Stokes (RANS) simulations [14, 15]. The advantage of the RANS approach is that it is computationally less expensive than other simulation methods. On the other hand, the drawback of RANS is that it only gives general information about the turbulent field and only an average velocity because it models turbulence with a linear eddy viscosity

approach. A more in depth simulation would be to simulate smaller scales in a Large Eddy Simulation (LES). However, this is quite computationally expensive, therefore this thesis performs a more advanced RANS approach which uses an ensemble of simulations to provide results that can be used to investigate the effects of wind on drone operations.

The thesis makes use Uncertainty Quantification and historical weather station data to decide on the relevant inflow conditions for the city of Rotterdam. Then based on the speed and turbulence thresholds of drones, the airspace risk can be quantified based on an overall inflow condition. Since the weather station provides data in 10-minute intervals, it is possible to identify unsafe airspace zones in that short interval and perform a yearly feasibility analysis for drone operations. Although, this is only applied to the city of Rotterdam, the goal is to develop the method so that it can be applied to other cities.

1.4. Research objectives

This thesis aims to address the two critical challenges for future high-density urban airspace: (1) effects of airspace design and rules on safety and efficiency and (2) evaluate and develop a method for assessing the feasibility of urban air operations considering local wind conditions. These two considerations will decide where and how drones fly safely in urban airspace. Safety is evaluated through different metrics for each challenge: for airspace design and rules, safety is quantified by the number of conflicts and intrusions (Fig. 1.2), while for wind effect analysis, safety is assessed by comparing local wind conditions against defined operational thresholds. Additionally, efficiency in this thesis refers to energy efficiency and is measured indirectly via route travel distance or time. For example, assume that concept (1) is more efficient than concept (2), this means that drones in concept (1) travel less distance or shorter time as compared to concept (2)

Overall research question (*RQ1*)

How do airspace design, operational rules, and local wind conditions affect the safety, efficiency and feasibility of high-density urban air operations?

The second chapter establishes some fundamental considerations for urban airspace design. Among several concepts, it explains separation management, flight planning, airspace layering, and wind. This chapter explains key principles that will be explored in the subsequent chapters.

Research question (*RQ2*): Chapter 2

What are the applicable considerations for constrained urban airspace design development?

The third chapter investigates the utilization of limited vertical airspace in the urban environment. As traffic density increases in urban airspace, the vertical allocation of space becomes critical for safety and efficiency. This chapter examines two key aspects: (1) the balance and trade-off between different airspace functions (particularly between cruising and turning layers) and (2) the effectiveness of dynamic versus pre-allocated height assignment strategies. Through simulations in Vienna's airspace, we evaluate how different vertical structuring and allocation approaches affect safety and efficiency at varying traffic demand levels.

Research question (*RQ3*): Chapter 3

How do vertical airspace layering strategies and height allocation methods impact urban air traffic safety and efficiency across varying traffic demand levels?

The fourth chapter develops a decentralised dynamic capacity balancing system that uses real-time aggregate flow data to reduce local traffic density and complexity in urban airspace. The system identifies high-complexity areas and incentivizes drones to take alternate routes. It does this by applying additional travel costs that do not overly increase the travel distance. The fifth chapter extends this approach and compares using historical data versus real-time data for identifying and managing these high-complexity areas.

Research question (*RQ4*): Chapter 4 & 5

How can decentralised dynamic capacity balancing with real-time and historical traffic data reduce local density and complexity in urban air operations?

The sixth and seventh chapters investigate the impact of urban wind conditions on air operation feasibility in city environments. The sixth chapter compares wind measurements to CFD simulations in a small area of The Hague. It then calls for more detailed analysis of wind effects on U-Space. The seventh chapter uses

an ensemble of CFD simulations and historical wind data of Rotterdam to make a risk and operational feasibility analysis. The analysis identifies regions where drone operations may be restricted or infeasible due to local wind conditions.

Research question (*RQ5*): Chapter 6 & 7

How do local wind conditions affect the risk and operational feasibility of urban air operations?

1

1.5. Structure of the thesis

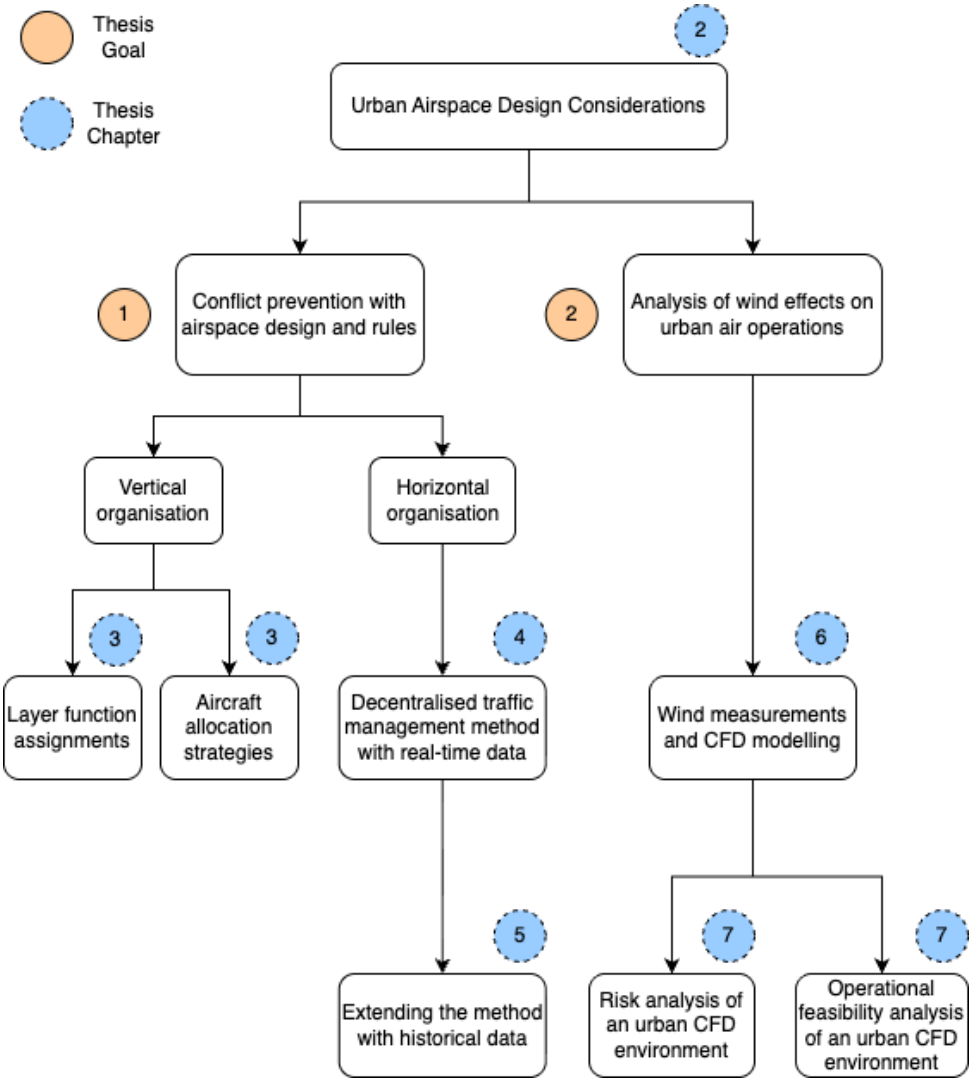

Figure 1.3: Thesis structure.

References

[1] U. Nations. *World Cities Report 2022: Envisaging the Future of Cities*. United Nations, 2022. URL: https://unhabitat.org/sites/default/files/2022/06/wcr_2022.pdf.

[2] R. Louf and M. Barthelemy. 'How congestion shapes cities: from mobility patterns to scaling'. In: *Scientific Reports* 4.1 (July 2014), p. 5561. ISSN: 2045-2322. DOI: 10.1038/srep05561. URL: https://doi.org/10.1038/srep05561.

[3] M. Doole, J. Ellerbroek, V. L. Knoop and J. Hoekstra. 'Constrained Urban Airspace Design for Large-Scale Drone-Based Delivery Traffic'. en. In: *Aerospace* 8.2 (2021). DOI: 10.3390/aerospace8020038.

[4] Single European Sky ATM Research 3 Joint Undertaking. *European drones outlook study: unlocking the value for Europe*. Publications Office, 2017. URL: https://data.europa.eu/doi/10.2829/085259.

[5] Single European Sky ATM Research 3 Joint Undertaking. *U-space : blueprint*. Publications Office, 2017. URL: https://data.europa.eu/doi/10.2829/335092.

[6] FAA. *Urban Air Mobility Concept of Operations*. Tech. rep. Version 2.0. Federal Aviation Administration, 2023. URL: https://www.faa.gov/sites/faa.gov/files/Urban%20Air%20Mobility%20%28UAM%29%20Concept%20of%20Operations%202.0_0.pdf.

[7] K. Roose. 'Are Amazon's Drones Finally Ready for Prime Time?' In: *The New York Times* (Dec. 2024). URL: https://www.nytimes.com/2024/12/20/technology/amazon-prime-air-drone-delivery.html (visited on 10/01/2025).

[8] A. Morfin Veytia, C. A. Badea, J. Ellerbroek, J. Hoekstra, N. Patrinopoulou, I. Daramouskas, V. Lappas, V. Kostopoulos, P. Menendez, P. Alonso, J. Rodrigo, V. Terrazas, D. Bereziat, A. Vidosavljevic and L. Sedov. 'Metropolis II: Benefits of Centralised Separation Management in High-Density Urban Airspace'. In: *12th SESAR Innovation Days*. 2022.

[9] T. Lundby, M. P. Christiansen and K. Jensen. 'Towards a Weather Analysis Software Framework to Improve UAS Operational Safety'. In: *2019 International Conference on Unmanned Aircraft Systems (ICUAS)*. 2019, pp. 1372–1380. DOI: 10.1109/ICUAS.2019.8798271.

[10] J. Hoekstra, J. Ellerbroek, E. Sunil and J. B. Maas. 'Geovectoring: Reducing Traffic Complexity to Increase the Capacity of UAV airspace'. en. In: *2018 International Conference on Research in Air Transportation* (2018). (Visited on 02/12/2020).

[11] E. Sunil, J. Hoekstra, J. Ellerbroek, F. Bussink, D. Nieuwenhuisen, A. Vidosavljevic and S. Kern. 'Metropolis: Relating Airspace Structure and Capacity for Extreme Traffic Densities'. en. In: *ATM seminar 2015, 11th USA/EUROPE Air Traffic Management R&D Seminar*. 2015.

[12] M. Ribeiro, J. Ellerbroek and J. Hoekstra. 'Velocity Obstacle Based Conflict Avoidance in Urban Environment with Variable Speed Limit'. In: *Aerospace* 8 (2021). DOI: 10.3390/aerospace8040093.

[13] U. Schumann. *Atmospheric physics : background, methods, trends*. English. Research topics in aerospace. Berlin: Springer, 2012. Chap. 14, p. 227. ISBN: 978-3-642-30183-4 3-642-30183-5. DOI: 10.1007/978-3-642-30183-4.

[14] R. B. Stull. *An Introduction to Boundary Layer Meteorology*. Vol. 13. Atmospheric and Oceanographic Sciences Library. Springer Dordrecht, 1988, p. 670. ISBN: 978-90-277-2768-8. DOI: 10.1007/978-94-009-3027-8.

[15] S. B. Pope. *Turbulent Flows*. Cambridge University Press, 2000.

2

Constrained Urban Airspace Design Considerations

Chapter 2 builds upon the concepts introduced in the Introduction. It also serves to explain and connect the key concepts that will be studied throughout the thesis. Specifically, it explains key considerations for urban airspace design, and it includes a section explaining the process of adapting existing street networks into constrained airspace networks.

This chapter is based on a section from the following publication:

- A. Morfin Veytia, C. A. Badea, N. Patrinopoulou, I. Daramouskas, J. Ellerbroek, V. Lappas, V. Kostopoulos and J. Hoekstra. 'U-Space Utilisation of Airspace under Various Layer Function Assignments and Allocations'. In: *Drones* 7.7 (2023). ISSN: 2504-446X. DOI: 10.3390/drones7070444. URL: https://www.mdpi.com/2504-446X/7/7/444

2.1. Introduction

The goal of this chapter is to outline and explain key concepts that will be studied throughout this thesis. Section 2.2 explains the choice for focusing on constrained airspace for thesis goal **(1)**. Section 2.3 outlines different airspace structures and explains a method for generating a fully connected network for drone flights in this airspace. Section 2.4 focuses on explaining the problem of limited vertical airspace, which is studied in Chapter 3. Section 2.5 explains how path planning and flow control are defined for Chapters 4 and 5. Section 2.6 focuses on thesis goal **(2)** and summarizes wind considerations for the urban airspace, which are studied in Chapters 6 and 7. Finally, Section 2.7 outlines some considerations that were not directly considered in this thesis.

2.2. Urban Environment

Flights operating in urban environments will need to regularly avoid static (i.e., buildings) and dynamic obstacles (i.e., other drones). The urban environment includes roads, geofences, and other infrastructure and these set the boundaries of where drones can operate. For example, drones may not be allowed to fly above parks or schools. The following section explains the different types of airspace environments (open and constrained) and how it relates to the urban environment. Furthermore, as the focus of this work is on constrained airspace, the effects of the city street network on constrained airspace design are described.

2.2.1. Types of Airspace

One study divided the urban airspace based on the height of the surrounding buildings [2]. In areas with low-rise buildings, the airspace spanned from 0 to 500 feet (152.4 m) above the ground level. In areas with high-rises, the airspace began at the highest obstacle and ended 1000 feet (304.8 m) above it. Other work [3–5] placed the airspace completely between buildings. In some cities (e.g., New York, Hong Kong) it may not be feasible for small drones to travel above the highest obstacle. Furthermore, for privacy considerations drones may avoid flying over buildings [6–8].

It can be more helpful to define two types of airspace based on the degree of constraints, as shown in [9]. In **open airspace**, drones can generally fly direct routes to their destination. Several researchers have developed concepts operating in mostly open airspace [10–12]. In **constrained airspace**, drones are restricted to a predefined constrained network. The network may be constrained by the existing buildings (i.e., above roads) or by some virtual constraints. Several works [3–5, 13–15] developed concepts in which drones follow the street network. It is important to note that the border between the two airspace types is not always clear. A mostly open airspace may have some geofenced areas and vice versa. However, this work separates them and specifically focuses on constrained airspace.

2.2.2. Effects of City-Layout on Constrained Airspace

Constrained airspace is highly dependent on the city layout [16] when drones fly between the existing buildings. Cities like New York have highly orthogonal intersections [17] which can simplify the urban airspace design parameters. For example, one airspace design may place drones on one of a set of four layers based on the cardinal directions of travel, north/east/south/west. This particular rule-set limits the chance of an encounter between drones travelling in different directions. Airspace designs in orthogonal networks were considered in [3, 4, 13].

Many older cities are non-orthogonal, like in Europe [17], which complicates the airspace design as there are now many different configurations of intersections. Applying the same design rule from the example in orthogonal networks is no longer trivial, as a street that is currently facing the north direction may turn and face east in a non-orthogonal network. Furthermore, in non-orthogonal cities there can be a common leg that the routes of many flights share. Drones sharing common legs create network hotspots if drones travel the shortest route to their destination. Airspace design in non-orthogonal networks were studied in [9, 18]. This work focuses on constrained airspace in a non-orthogonal network.

2.3. Airspace Structure

The Metropolis I project studied different urban airspace configurations above the buildings of Paris in open airspace [11]. The study concluded that a layered airspace can help mitigate detrimental emergent behaviour at high traffic densities. Therefore, this work focuses on layered airspace. This section first explains the safety benefits of a layered airspace, and then it shows how these are applied to constrained airspace.

2.3.1. Benefits of Layered Airspace Based on Track Angle

Figure 2.1 shows the layered open airspace from the Metropolis project [11]. Each layer only allows drones travelling in a specific heading range. This technique illustrates two interacting safety elements of a layered airspace, segmentation and alignment of the speed vector. The airspace structure reduces the conflict rate by segmentation, which separates groups of drones with high relative velocities. Using speed alignment lowers the relative velocity of drones in the same layer. An important takeaway is that adding constraints that segment aircraft with high relative velocity and align those with low relative velocity in an open airspace can have safety benefits [19].

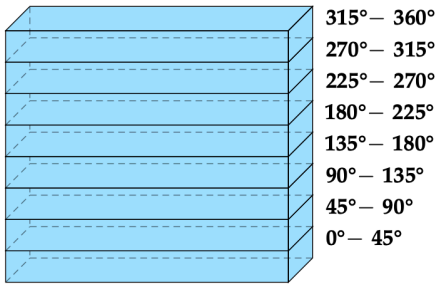

Figure 2.1: Example open airspace layering. Each layer has a 45° heading range.

2.3.2. Adding Other Layer Types for Constrained Airspace

Layering has also been used in constrained airspace to achieve segmentation and alignment of drones [3–5]. In [3, 4] layers are assigned depending on the orientation of the street. The goal is to ensure that cruising drones from different streets are vertically segmented at the shared intersections. However, as drones cannot travel directly to their destination, they need to make turns in the network. In order to not overshoot, turning drones slow down to make the turn. However, decelerating for turns can create bottlenecks if there is a cruising drone behind the turning drone. One solution is to create a separate turn layer to which drones vertically manoeuvre before slowing down.

The three types of layers used in this study are: (1) Cruise, (2) turn, (3) buffer (Figure 2.2). Cruise layers are where the drones spends the majority of the flight. Each cruise layer is assigned to a specific direction and it is assumed that drones cannot fly in parallel. Turn layers are used to transition from one cruise layer to another at an intersection. Finally, the buffer layers are an empty space created by the segmentation of the cruising layers, which also acts as a safety buffer against conflicts due to small vertical incursions.

There is a trade-off between the layer types because of the limited vertical space. Airspace designers cannot add an infinite number of layers. If there is more cruising space provided, it means that turning space is reduced and vice versa. In [3, 4], turn layers were alternated with cruise layers to create a ‘1-to-1’ structure. Other structures, like in [9], increased the number of cruise layers by only giving one turn layer for every two cruise layers.

Figure 2.2: Constrained airspace intersection example. Note how the blue and red cruise layers are vertically separated and contain a turn (yellow) layer in between. Note that this pattern is stacked until the top of airspace. The red circles and arrows signify the protected zone and current direction of travel of the drones, respectively.

2.3.3. Applying Layers in a Constrained Airspace

In orthogonal networks, the segmentation of layers can be achieved by considering the four possible directions of travel. Assuming that the network also aligns with the cardinal directions, the cruise directions are north, south, east and west. It is then possible to ensure that a north or south street never intersects at the same height as an east or west street.

It is more difficult to ensure segmentation in non-orthogonal networks than orthogonal ones because of the many different intersection configurations [18]. An initially north-facing street may end up facing east at the next intersection. This makes it difficult to ensure that each intersection has segmented streets if the layer assignments are based on the cardinal directions. Moreover, the airspace quickly runs out if each unique street is assigned to a specific height. So, using a cardinal assignment rule for segmentation means that there will be intersections where layers meet at the same height.

2.3.4. One-Way Networks and Layers

Studies have looked at comparing a one-way network versus a two-way network in orthogonal streets [3]. It is also assumed that aircraft are not allowed to fly next to each other on the same street. In a one-way network, a street that is on the north–south line will have all cruise layers in that street facing one direction. In a two-way network, the streets alternate in direction with increasing height. It was seen that a one-way network is safer as it reduces the chances of having head-on collisions because all drones in one street are aligned in their direction

of travel. In an orthogonal network, the directional of parallel streets alternates to ensure that all intersections can be reached.

In a non-orthogonal network, it is not always possible to ensure that all intersections are connected with one-way networks. It is dependent on the network layout. As a result, a one-way network must be specifically designed to ensure that all intersections can be reached. The following section will explain the process for designing an organic one-way fully connected network that can be used in constrained airspace.

2.3.5. Designing a one-way fully connected network

Fig. 2.3a shows how a street network can be represented as a graph, G, composed of a set of edges and nodes. The set of edges, E, refer to the streets and the set of nodes, N, correspond to intersections.

$$G = (N, E) \tag{2.1}$$

The goal of this section is to illustrate the method of designing a one-way fully- (or strongly-) connected graph. Aside from being strongly-connected and one-way, the resulting graph should reduce the number of nodes with potential head-on collisions and attempt to minimise the path lengths from all nodes to all other nodes. The method starts with an undirected graph that contains no dead-ends and no self-loops (edges that start and end at the same node). The overall steps of the method are:

- Apply the Continuity in streets algorithm (COINS) [20] to the street network. The COINS algorithm creates groups of edges (called strokes). A stroke is a connected group of edges which have a similar bearing. All edges in a stroke should align in the same direction in order to reduce head-on collisions at the nodes.

- Apply a genetic algorithm that decides the directionality of the graph. It acts by altering the directionality of the strokes rather than individual edges. The genetic algorithm minimises the total length of paths from all nodes to all other nodes. Additionally, it penalises any graph that is not strongly-connected.

Defining the problem

Fig. 2.3b shows an example graph, G, that will be used to illustrate the problem. The graph contains 5 nodes (labelled with letters A through E) and 6 edges which connect the nodes. The direction of the edge is defined as $u - v$ where, u is the starting node and v is the end node. To create the one-way graph, also called a **directed graph**, each edge must have a defined direction. Each edge can have two directions. For example, in Fig. 2.3b, the edge connecting nodes A and B can be defined as $A - B$ or $B - A$.

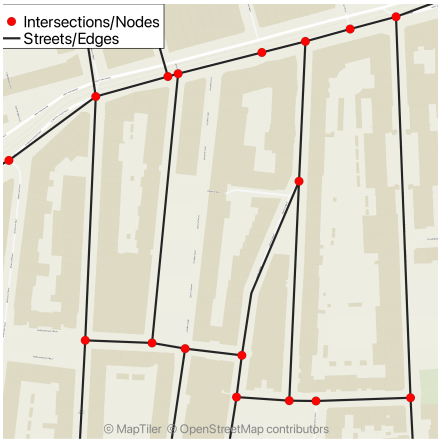

(a) A section of the Rotterdam street network represented by a graph. The intersections or nodes are shown with red dots and the edges or streets are shown with solid black lines.

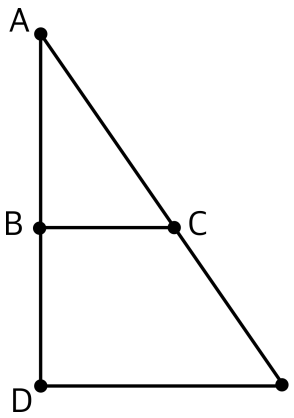

(b) An example graph G, that will be used to illustrate the method to design a strongly-connected one-way network. It contains 5 nodes (A, B, C, D, E) and 6 edges.

Figure 2.3: Rotterdam street network is shown in (a) and the example graph is shown in (b).

A directed graph is said to be strongly-connected when all nodes can be reached from all other nodes in the graph, so it ensures that all destinations are reachable. Therefore, the directionality of each edge needs to be individually defined. Creating a strongly-connected graph out of the example graph is trivial. However, Chapters 3, 4, and 5 contain street networks with around 5000 edges.

Since the direction of each edge can be set independently and each edge has two possible directions, it is possible to create $2^{N_{edges}}$ unique directed graphs, where N_{edges} is the total number of edges. In the example graph, there are $2^6 = 64$ unique directed graphs where only a subset is strongly-connected. For the street networks used in this thesis, there are 2^{5000} or around 10^{1505} unique directed graphs. This makes it very difficult to find a strongly-connected one-way graph by simply iterating. Therefore, the COINS algorithm is used to reduce the number of graphs that must be searched.

Continuity in streets algorithm (COINS)

The COINS algorithm [20] can be applied to street networks to group a set of edges into strokes. Strokes are made of connected edges with similar bearing angles. The algorithm works by iterating over each intersection in the network and calculating the interior angle between all intersecting edges. If the interior angle is between a certain range, say 60°-120°, then those two edges can be grouped in the same stroke. Also, if an edge intersects two other edges with interior angles falling within the range, then only the two edges with an interior angle closer to 180° will be part of the same stroke. This sets the continuity of the street network at each intersection.

The results of the COINS algorithm applied to the small street network of

Rotterdam and the example graph are shown in Figs. 2.4a and 2.4b, respectively. The edges that belong to the same stroke are shown in the same colour and are labelled with a number stating which stroke the edge belongs to.

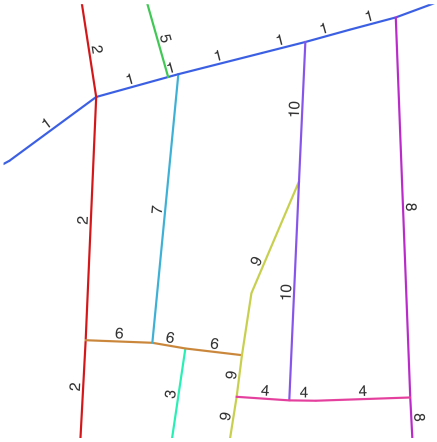

(a) The street network of Rotterdam after applying the COINS algorithm. Note that edges that are part of the same stroke share the same colour and number label. Ten strokes were identified.

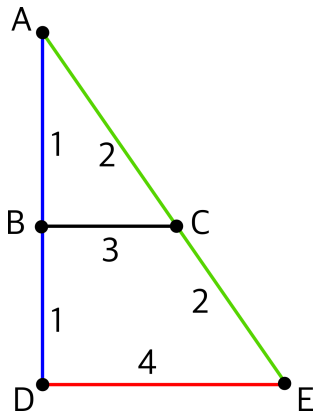

(b) The example graph labelled with the strokes from the COINS algorithm. Note that edges that are part of the same stroke share the same colour and number label. Four strokes were identified.

Figure 2.4: The COINS algorithm result for the Rotterdam street network is in (a) and the COINS algorithm result for the example graph is shown in (b).

For this thesis, it is required that each edge of the same stroke group faces the same direction. The edges of stroke 1 must be defined either in direction $[A-B, B-D]$ or direction $[D-B, B-A]$ in the example graph.

There are two advantages to applying the COINS algorithm. The first is that it reduces the potential for head-on collisions because two streets with a similar bearing will be in the same stroke. The second is that it reduces the unique graphs that must be searched to create a one-way strongly-connected graph.

In the example graph, G (Fig. 2.4b), there are four strokes, so there are now $2^4 = 16$ unique graphs. For the complete Rotterdam street network (Chapters 4 and 5) there are about 1000 strokes, so the set size of unique graphs is reduced to 2^{1000} or 10^{301}. This is orders of magnitude lower than the original size of 10^{1505}. Nevertheless, it is still quite a large set size. Therefore, this thesis employed a genetic algorithm to search for a one-way strongly-connected graph.

Genetic algorithm

A genetic algorithm is an evolutionary algorithm that uses a fitness function to operate a genome. In this thesis, the genome is a vector, $\mathbf{v}$, that contains the directionality of the street network. The index of each entry in the genome represents the direction of the stroke, so it can be either 0 or 1.

$$\mathbf{v} = \begin{bmatrix} v_1 & v_2 & v_3 & . & . & v_{N_{strokes}} \end{bmatrix} \tag{2.2}$$

The graphs in Figs. 2.4a and 2.4b have a genome with 10 and 4 strokes, respectively. The goal of the genetic algorithm is to create a one-way strongly-connected graph. However, it is useful if it also finds a graph that does not contain overly long routes. Therefore, the fitness or cost function is defined with these considerations.

The cost of travel from node u to node v is the summed length, $l_{u,v}$, of each edge that is taken in the path from u to v. For this thesis, the overall cost of travel, J_{length}, is defined as the length of all possible paths in the graph. However, to reduce computational time, this work uses a random subset of both origin nodes and destination nodes to create the paths. These nodes are about 5-10 percent of the total nodes. The second part of the fitness function considers if the graph is strongly-connected or not, J_{dir}. This cost is significantly higher than any J_{lengh}. This is so that unconnected graphs are quickly discouraged by the genetic algorithm. The complete fitness function, J, is:

$$J = J_{lengh} + J_{dir} \tag{2.3}$$

Once the genome and fitness function are defined, the genetic algorithm randomly searches, edits and evolves the solution until an appropriate solution is found [21]. The overall process of a genetic algorithm is as follows:

1. Initialisation of the genome.
2. Definition of the fitness function.
3. Generation of the population.
4. Crossover/mating of the population to create offspring.
5. Evolution/mutation of the offspring.

This is an iterative process that requires steps 3, 4, and 5 to continually evolve the solution. A pseudo-algorithm is shown in Algorithm 1.

Algorithm 1: The genetic algorithm pseudo-algorithm [22].

```
initialize population
repeat
    repeat
        crossover
        mutation
        map offspring to graph network
        fitness computation
    until population complete
    selection of new parental population
until termination condition
```

The initialisation of the population requires randomly generating several different individuals from the genome (Equation 2.2). This population is called the parent population. Then, several offspring are generated during the crossover step. The crossover step takes the genome of two parent solutions to generate an offspring genome. Each position of the genome has a 50 percent chance of belonging to one of the parents. After, this mating, the offspring are mutated with a certain probability (in this work, this is 20 percent).

The next steps are to map the offspring genomes into a graph and calculate the fitness function with Equation 2.3. Once the fitness function for each offspring has been calculated, it can become the new parent population for the next generation. This is then repeated until the termination condition is met. For this work, 1000 generations are made, as it is not given that a street network will ever reach the theoretical lowest value of the fitness function (the paths calculated using the shortest path algorithm in an undirected graph).

Fig. 2.5a shows the results of the genetic algorithm in an area of Rotterdam. Note that final directions chosen are shown with a red arrow. Fig. 2.5b shows a strongly-connected one-way network of the example graph. The resulting directions are shown with red arrows. The example graph is not to scale and is only for illustration purposes.

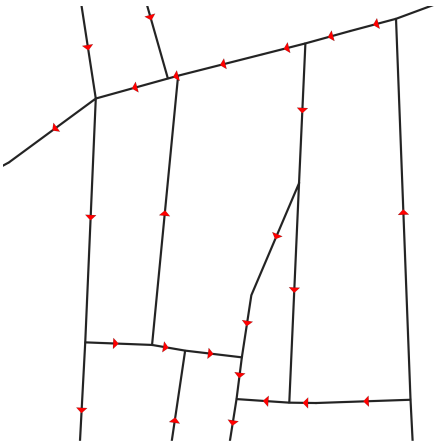

(a) A small area in Rotterdam showing the result of the genetic algorithm, with the edge directions shown in red arrows. The network is a one-way strongly-connected graph.

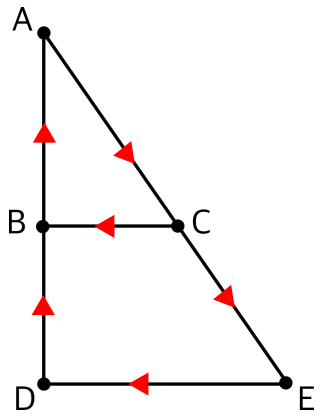

(b) The results of the genetic algorithm applied on the example graph, with the edge directions shown in red arrows. This network is a one-way strongly connected graph.

Figure 2.5: The genetic algorithm result for the Rotterdam street network is in (a) and the genetic algorithm result for the example graph is shown in (b).

2.4. Vertical Allocation Rules in a Layered Airspace

In a layered airspace, the allocation of traffic to the vertical airspace also impacts the safety of the airspace. Ideally, each cruise layer of open or constrained airspace should maintain uniform distributions so that one layer does not have denser traffic than another. Unfortunately, a uniform distribution is hard to achieve in urban air operations because some directions of travel may be preferred and can vary depending on the time of day. This section outlines a safety concern from vertical manoeuvres and then explains vertical rule-sets for constrained airspace.

2.4.1. Vertical Manoeuvres

It is possible to ensure that in open airspace (Figure 2.1) all layers are allocated a similar number of drones if there is a uniform distribution of origins and distributions. Moreover, there is no need to vertically transition between cruise layers except during take-off and landing. In [23] it was seen that the drones performing vertical manoeuvres highly impacted the safety of the airspace. In a layered open airspace, vertical manoeuvres should be limited because the manoeuvres create conflicts at high relative velocities with drones in other layers.

In the constrained airspace from Figure 2.2 vertical manoeuvres are necessary for turns. Merging from the turn layer back to the cruise layer has a large impact on safety [24]. However, it is not yet clear whether vertical manoeuvres between cruise layers in constrained airspace can also decrease the safety of the airspace.

2.4.2. Layer Allocation Rule-Sets in Constrained Airspace

In a one-way constrained layer airspace, such as in Figure 2.2 the direction of travel does not change with height, thus the vertical allocation is not part of the structure. Therefore, explicit rules should be set for how the airspace is utilised to ensure an efficient spread of traffic. Several explicit rules are defined and analysed in Ch. 3.

Two different rule-set strategies can be described. The first are those that allocate a set of layers depending on some rules. Drones are allocated to a specific height, and they must remain there until landing. An example rule allocation can use the distance of the mission. Short missions would be allocated to lower layers and long missions to higher layers. These strategies were used in [3, 4] but were not a focus of the study.

Another strategy is one that does not try to pre-allocate layer sets and allows the drones to separate themselves based on the local density. An analogy is the ‘keep-right‘ car highway rule where cars must remain on the right unless they perform an overtake [25]. In the Metropolis II project [9], drones started their missions at the lowest layer set. However, if a drone approached a slower drone then it could vertically manoeuvre to a higher cruise layer, overtake, and then

manoeuvre down again. This had the effect of ensuring that all drones remained in the available lower layers.

2.5. Horizontal distribution strategies in a constrained network

2.5.1. Flight Planning

Flight planning is a main component of a safe traffic management system. In general, it can encompass planning for the complete route in four dimensions (spatial and temporal). However, in this thesis, it is typically referred to as the path from node-to-node in the constrained network. It is therefore used as a means to spread the traffic horizontally.

It is possible to attempt to deconflict all flight plans prior to take-off, such as in [26]. This requires to modify which nodes that make up the path (spatial) and the time in which they are reached (temporal). This is typically done by a centralised planner that must have information about the complete path of all aircraft. Drone traffic is expected to be more ad-hoc than traditional air traffic management, and missions may not be known with sufficient time.

Other works in constrained airspace [3] had drones plan their own shortest-path route through constrained airspace. However, this will create local hotspots along some legs of the route if the airspace is non-orthogonal and the demand is not uniform.

2.5.2. Flow control

The creation of local hotspots can be attributed to increased traffic density or complexity in that area. In this thesis, traffic complexity refers to areas of the airspace where aircraft tend to converge [27]. It is possible that an area with low traffic density has high complexity, such as converging aircraft at an intersection. The opposite is also true, that an area with high traffic density has a low complexity, such as areas where air traffic is aligned and travelling in similar directions with a low relative velocity.

In this thesis, flow control occurs when either the centralised planner and/or individual airspace actors attempt to reduce local traffic density or complexity while en-route. Therefore, it is related but different from path planning. The result of flow control may be a new path for a drone due to increased density and complexity in the airspace. The goal of flow control is to perform local capacity balancing and attempt to route aircraft through unused zones of the airspace.

2.6. Wind considerations for urban airspace

2.6.1. Wind challenges in drone operations

As drones are expected to fly at low altitudes, they will interact within the turbulent atmospheric boundary layer. The buildings, trees and uneven terrain

of urban environments creates turbulence which makes wind more unpredictable. Therefore, some areas may experience speed-up/slow-down of the wind speed with respect to the global conditions.

Moreover, radiation emitted by streets and building can create additional turbulence due to the buoyant effects caused by temperature differentials [28]. In Rotterdam, it has been observed that there is a 2 $°C$ difference between the city and the surrounding air temperature [29].

Path planning in a windy environment can be complicated because the wind can vary from street to street and may lead to delayed arrivals. There have been previous worked that attempted to plan drones by considering the wind [30–32]. However, they considered meso-scale wind conditions that do not always capture the effects of the built environment through course parametrization.

Apart from causing disruptions in path planning, the wind can also make the airspace unsafe to operate. Several studies have considered this effect [33–35] but these also considered meso-scale wind conditions. More recent research [36] defined no-fly zones for drones using Computational Fluid Dynamics (CFD) but only considered the wind speed and not the unpredictability caused by turbulence.

2.6.2. Simulating wind in urban environments

There are different approaches for simulating wind in urban environments. This thesis mostly focuses on CFD approaches. A more comprehensive review of the different CFD methods in urban environments can be found in [37]. Urban wind flows can be described by the Navier-Stokes equations [38]. However, these equations are highly non-linear, and a general solution has not been found.

Two different approaches to reduce the complexity are described here. The first is the Reynolds-Averaged Navier-Stokes (RANS) equations. The RANS approach aims to solve for the mean flow and therefore provides an average view of the airspace. The fluctuating field (turbulence) effects on the mean flow must be modelled when using the RANS approach. The RANS method is known as being relatively less accurate but more computationally feasible than other CFD methods for urban flows. The RANS approach was used in [36] to find the areas with high average velocity.

For a more detailed view of turbulence, a Large Eddy Simulation (LES) is made. In an LES, the larger turbulent scales are solved numerically while the smaller scales are modelled. This approach was used by [28]. Compared to RANS, it provides a more accurate view of the turbulent flow, but it is significantly more computationally expensive. Therefore, this has led to methods that aim to improve the results of a singular RANS simulation by using reduced-order modelling. One important approach is through uncertainty quantification [39–41] techniques. The goal is to create an ensemble of RANS simulations where individual cases are simulated with varying conditions.

2.7. Other considerations

The urban airspace cannot be designed without other components of a complete traffic management system, these are separation management and flight planning [10]. These components are highly interdependent and should be designed in tandem. One reason is that the air traffic densities are expected to be orders of magnitude higher than what is seen in conventional air traffic [42, 43]. Another is that the expected missions (parcel and food delivery) are harder to plan in advance [44]. For example, food delivery drones may be requested several minutes before the expected delivery rather than hours.

2.7.1. Separation Management

Separation management is the component that attempts to maintain safe separation of UAVs during their flight. Separation can be reached by de-conflicting paths prior to take-off (strategic) and by providing manoeuvres en-route that maintain separation minima (tactical). These separation minima and the prediction horizon have an impact on the design of the airspace structure. For example, in a layered airspace the separation minima influences the height of an airspace layer. There have been several U-Space projects that specifically focus on separation management [45, 46].

2.7.2. Out of Scope Considerations

There are other important considerations for urban airspace design that are not considered for this work. These are take-off and landing procedures, vertiport locations, noise, communication latency, emergency management, weather phenomena not directly related to wind, and societal acceptance. These can be found in several concepts of operations from [47, 48].

References

[1] A. Morfin Veytia, C. A. Badea, N. Patrinopoulou, I. Daramouskas, J. Ellerbroek, V. Lappas, V. Kostopoulos and J. Hoekstra. 'U-Space Utilisation of Airspace under Various Layer Function Assignments and Allocations'. In: *Drones* 7.7 (2023). ISSN: 2504-446X. DOI: 10.3390/drones7070444. URL: https://www.mdpi.com/2504-446X/7/7/444.

[2] C. Barrado, M. Boyero, L. Brucculeri, G. Ferrara, A. Hately, P. Hullah, D. Martin-Marrero, E. Pastor, A. P. Rushton and A. Volkert. 'U-Space Concept of Operations: A Key Enabler for Opening Airspace to Emerging Low-Altitude Operations'. In: *Aerospace* 7.3 (2020). ISSN: 2226-4310. DOI: 10.3390/aerospace7030024. URL: https://www.mdpi.com/2226-4310/7/3/24.

[3] M. Doole, J. Ellerbroek, V. L. Knoop and J. Hoekstra. 'Constrained Urban Airspace Design for Large-Scale Drone-Based Delivery Traffic'. en. In: *Aerospace* 8.2 (2021). DOI: 10.3390/aerospace8020038.

[4] M. Ribeiro, J. Ellerbroek and J. Hoekstra. 'Velocity Obstacle Based Conflict Avoidance in Urban Environment with Variable Speed Limit'. In: *Aerospace* 8 (2021). DOI: 10.3390/aerospace8040093.

[5] D.-S. Jang, C. A. Ippolito, S. Sankararaman and V. Stepanyan. 'Concepts of Airspace Structures and System Analysis for UAS Traffic flows for Urban Areas'. en. In: *AIAA Information Systems-AIAA Infotech @ Aerospace*. 2017. ISBN: 978-1-62410-449-7. DOI: 10.2514/6.2017-0449. (Visited on 21/12/2020).

[6] A. Bauranov and J. Rakas. 'Designing airspace for urban air mobility: A review of concepts and approaches'. In: *Progress in Aerospace Sciences* 125 (2021), p. 100726. ISSN: 0376-0421. DOI: 10.1016/j.paerosci.2021.100726.

[7] D. Lee, D. J. Hess and M. A. Heldeweg. 'Safety and privacy regulations for unmanned aerial vehicles: A multiple comparative analysis'. In: *Technology in Society* 71 (2022), p. 102079. ISSN: 0160-791X. DOI: 10.1016/j.techsoc.2022.102079.

[8] EASA. *Study on the societal acceptance of Urban Air Mobility in Europe*. https://www.easa.europa.eu/en/full-report-study-societal-acceptance-urban-air-mobility-europe. 2021.

[9] A. Morfin Veytia, C. A. Badea, J. Ellerbroek, J. Hoekstra, N. Patrinopoulou, I. Daramouskas, V. Lappas, V. Kostopoulos, P. Menendez, P. Alonso, J. Rodrigo, V. Terrazas, D. Bereziat, A. Vidosavljevic and L. Sedov. 'Metropolis II: Benefits of Centralised Separation Management in High-Density Urban Airspace'. In: *12th SESAR Innovation Days*. 2022.

[10] T. McCarthy, L. Pforte and R. Burke. 'Fundamental Elements of an Urban UTM'. In: *Aerospace* 7.7 (2020). ISSN: 2226-4310. DOI: 10.3390/aerospace7070085.

[11] E. Sunil, J. Hoekstra, J. Ellerbroek, F. Bussink, D. Nieuwenhuisen, A. Vidosavljevic and S. Kern. 'Metropolis: Relating Airspace Structure and Capacity for Extreme Traffic Densities'. en. In: *ATM seminar 2015, 11th USA/EUROPE Air Traffic Management R&D Seminar*. 2015.

[12] L. Sedov and V. Polishchuk. 'Centralized and Distributed UTM in Layered Airspace'. en. In: *International conference on research in air transportation (ICRAT) 2020*. 2018.

[13] S. Bae, H.-S. Shin and A. Tsourdos. 'Structured Urban Airspace Capacity Analysis: Four Drone Delivery Cases'. en. In: *Applied Sciences* 13.6 (2023). Number: 6 Publisher: Multidisciplinary Digital Publishing Institute, p. 3833. ISSN: 2076-3417. DOI: 10.3390/app13063833.

[14] W. Qu, C. Xu, X. Tan, A. Tang, H. He and X. Liao. 'Preliminary Concept of Urban Air Mobility Traffic Rules'. en. In: *Drones* 7.1 (2023). Number: 1 Publisher: Multidisciplinary Digital Publishing Institute, p. 54. ISSN: 2504-446X. DOI: 10.3390/drones7010054.

[15] D. Sacharny, T. Henderson and V. Marston. 'Lane-Based Large-Scale UAS Traffic Management'. In: *IEEE Transactions on Intelligent Transportation Systems* 23.10 (2022), pp. 18835–18844. ISSN: 1524-9050. DOI: 10.1109/TITS.2022.3160378.

[16] J. Cho and Y. Yoon. 'Extraction and Interpretation of Geometrical and Topological Properties of Urban Airspace for UAS Operations'. In: *ATM Seminar*. 2019.

[17] G. Boeing. 'Urban spatial order: street network orientation, configuration, and entropy'. In: *Applied Network Science* 4.1 (2019), pp. 1–19. DOI: 10.1007/s41109-019-0189-1.

[18] C. Badea, A. Morfin Veytia, M. Ribeiro, M. Doole, J. Ellerbroek and J. Hoekstra. 'Limitations of Conflict Prevention and Resolution in Constrained Very Low-Level Urban Airspace'. In: *11th SESAR Innovation Days*. 2021.

[19] E. Sunil, J. Ellerbroek, J. Hoekstra, A. Vidosavljevic, M. Arntzen, F. Bussink and D. Nieuwenhuisen. 'Analysis of Airspace Structure and Capacity for Decentralized Separation Using Fast-Time Simulations'. In: *Journal of Guidance, Control, and Dynamics* 40.1 (2017), pp. 38–51. DOI: 10.2514/1.G000528.

[20] P. Tripathy, P. Rao, K. Balakrishnan and T. Malladi. 'An open-source tool to extract natural continuity and hierarchy of urban street networks'. In: *Environment and Planning B: Urban Analytics and City Science* (2020). DOI: 10.1177/2399808320967680.

[21] R. D. Goswami, S. Chakraborty and B. Misra. 'Variants of Genetic Algorithms and Their Applications'. en. In: *Applied Genetic Algorithm and Its Variants: Case Studies and New Developments*. Ed. by N. Dey. Singapore: Springer Nature, 2023, pp. 1–20. ISBN: 978-981-9934-28-7. DOI: 10.1007/978-981-99-3428-7_1. URL: https://doi.org/10.1007/978-981-99-3428-7_1 (visited on 28/05/2024).

[22] O. Kramer. *Genetic algorithm essentials*. English. Studies in computational intelligence; v. 679; volume 679. Cham, Switzerland: Springer, 2017. DOI: 10.1007/978-3-319-52156-5. URL: http://rave.ohiolink.edu/ebooks/ebc/9783319521565.

[23] E. Sunil, J. Ellerbroek, J. M. Hoekstra and J. Maas. 'Three-dimensional conflict count models for unstructured and layered airspace designs'. In: *Transportation Research Part C: Emerging Technologies* 95 (2018), pp. 295–319. ISSN: 0968-090X. DOI: 10.1016/j.trc.2018.05.031.

[24] M. Doole, J. Ellerbroek and J. M. Hoekstra. 'Investigation of Merge Assist Policies to Improve Safety of Drone Traffic in a Constrained Urban Airspace'. In: *Aerospace* 9.3 (2022). DOI: 10.3390/aerospace9030120.

[25] G. of the Netherlands. *Regulations Traffic Rules and Traffic Signs*. Government of the Netherlands, 1990.

[26] D. Bereziat, S. Cafieri and A. Vidosavljevic. 'Metropolis II: Centralised and strategical separation management of UAS in urban environment'. In: *12th SESAR Innovation Days*. 2022.

[27] D. Delahaye and S. Puechmorel. 'Air Traffic Complexity: Towards an Intrinsic Metric'. In: *Proceeding of the 3rd USA/Europe Air Traffic Management R and D Seminar*. Unknown, Unknown Region, 2000. URL: https://enac.hal.science/hal-01205255.

[28] S. Giersch, O. El Guernaoui, S. Raasch, M. Sauer and M. Palomar. 'Atmospheric flow simulation strategies to assess turbulent wind conditions for safe drone operations in urban environments'. In: *Journal of Wind Engineering and Industrial Aerodynamics* 229 (2022), p. 105136. ISSN: 0167-6105. DOI: https://doi.org/10.1016/j.jweia.2022.105136. URL: https://www.sciencedirect.com/science/article/pii/S016761052200232X.

[29] Atlas Natural Capital. *Climate control in cities*. Online resource. 2024. URL: https://www.atlasnatuurlijkkapitaal.nl/en/node/681 (visited on 15/05/2025).

[30] Ö. Gürel and S. Serdarasan. 'Drone-Assisted Last-Mile Delivery Under Windy Conditions: Zero Pollution Solutions'. In: *Smart Cities* 7.6 (2024), pp. 3437–3457. ISSN: 2624-6511. DOI: 10.3390/smartcities7060134. URL: https://www.mdpi.com/2624-6511/7/6/134.

[31] A. Thibbotuwawa, G. Bocewicz, G. Radzki, P. Nielsen and Z. Banaszak. 'UAV Mission Planning Resistant to Weather Uncertainty'. In: *Sensors* 20.2 (2020). ISSN: 1424-8220. DOI: 10.3390/s20020515. URL: https://www.mdpi.com/1424-8220/20/2/515.

[32] Y. Chan, K. K. Ng, C. Lee, L.-T. Hsu and K. Keung. 'Wind dynamic and energy-efficiency path planning for unmanned aerial vehicles in the lower-level airspace and urban air mobility context'. In: *Sustainable Energy Technologies and Assessments* 57 (2023), p. 103202. ISSN: 2213-1388. DOI: https://doi.org/10.1016/j.seta.2023.103202. URL: https://www.sciencedirect.com/science/article/pii/S2213138823001959.

[33] M. Gao, C. H. Hugenholtz, T. A. Fox, M. Kucharczyk, T. E. Barchyn and P. R. Nesbit. 'Weather constraints on global drone flyability'. In: *Scientific Reports* 11.1 (June 2021), p. 12092. ISSN: 2045-2322. DOI: 10.1038/s41598-021-91325-w. URL: https://doi.org/10.1038/s41598-021-91325-w.

[34] K. O. Ploetner, C. Al Haddad, C. Antoniou, F. Frank, M. Fu, S. Kabel, C. Llorca, R. Moeckel, A. T. Moreno, A. Pukhova, R. Rothfeld, M. Shamiyeh, A. Straubinger, H. Wagner and Q. Zhang. 'Long-term application potential of urban air mobility complementing public transport: an upper Bavaria example'. In: *CEAS Aeronautical Journal* 11.4 (Dec. 2020), pp. 991–1007. ISSN: 1869-5590. DOI: 10.1007/s13272-020-00468-5. URL: https://doi.org/10.1007/s13272-020-00468-5.

[35] T. Lundby, M. P. Christiansen and K. Jensen. 'Towards a Weather Analysis Software Framework to Improve UAS Operational Safety'. In: *2019 International Conference on Unmanned Aircraft Systems (ICUAS)*. 2019, pp. 1372–1380. DOI: 10.1109/ICUAS.2019.8798271.

[36] S. Jiang, J. Wang, C. Li, J. Ou, P. Duan and L. Li. 'Identification of no-fly zones for delivery drone path planning in various urban wind environments'. In: *Physics of Fluids* 36.8 (Aug. 2024), p. 085166. ISSN: 1070-6631. DOI: 10.1063/5.0221281. eprint: https://pubs.aip.org/aip/pof/article-pdf/doi/10.1063/5.0221281/20121043/085166_1_5.0221281.pdf. URL: https://doi.org/10.1063/5.0221281.

[37] B. Blocken. 'Computational Fluid Dynamics for urban physics: Importance, scales, possibilities, limitations and ten tips and tricks towards accurate and reliable simulations'. In: *Building and Environment*. Fifty Year Anniversary for Building and Environment 91 (2015), pp. 219–245. ISSN: 0360-1323. DOI: 10.1016/j.buildenv.2015.02.015.

[38] S. B. Pope. *Turbulent Flows*. Cambridge University Press, 2000.

[39] D. Xiu and G. E. Karniadakis. 'Modeling uncertainty in flow simulations via generalized polynomial chaos'. In: *Journal of Computational Physics* 187.1 (2003), pp. 137–167. ISSN: 0021-9991. DOI: https://doi.org/10.1016/S0021-9991(03)00092-5. URL: https://www.sciencedirect.com/science/article/pii/S0021999103000925.

[40] C. García-Sánchez, G. Van Tendeloo and C. Gorlé. 'Quantifying inflow uncertainties in RANS simulations of urban pollutant dispersion'. In: *Atmospheric Environment* 161 (2017), pp. 263–273. ISSN: 1352-2310. DOI: https://doi.org/10.1016/j.atmosenv.2017.04.019. URL: https://www.sciencedirect.com/science/article/pii/S1352231017302571.

[41] H. Bijl. *Uncertainty quantification in computational fluid dynamics*. Vol. 92. Lecture notes in computational science and engineering. 1 online resource (xi, 333 pages) : illustrations (some color). Cham: Springer, 2013. ISBN: 9783319008851. DOI: 10.1007/978-3-319-00885-1. URL: https://tudelft.on.worldcat.org/oclc/859778838.

[42] F. Borghetti, C. Caballini, A. Carboni, G. Grossato, R. Maja and B. Barabino. 'The Use of Drones for Last-Mile Delivery: A Numerical Case Study in Milan, Italy'. en. In: *Sustainability* 14.3 (2022). Number: 3 Publisher: Multidisciplinary Digital Publishing Institute, p. 1766. ISSN: 2071-1050. DOI: 10.3390/su14031766.

[43] Single European Sky ATM Research 3 Joint Undertaking. *European drones outlook study: unlocking the value for Europe*. Publications Office, 2017. URL: https://data.europa.eu/doi/10.2829/085259.

[44] C. Chin, K. Gopalakrishnan, H. Balakrishnan, M. Egorov and A. Evans. 'Tradeoffs between Efficiency and Fairness in Unmanned Aircraft Systems Traffic Management'. en. In: *"ICRAT 2020"*. 2020.

[45] *USEPE: U-space Separation in Europe*. https://cordis.europa.eu/project/id/890378/results. The Community Research and Development Information Service. 2022. (Visited on 01/05/2023).

[46] *BUBBLES: Defining the BUilding Basic BLocks for a U-Space SEparation Management Service*. https://cordis.europa.eu/project/id/893206/results. The Community Research and Development Information Service. 2022. (Visited on 01/05/2023).

[47] DLR. *DLR Blueprint Concept for Urban Airspace Integration*. DLR, 2017. URL: https://www.dlr.de/de/medien/publikationen/sonstige-publikationen/2017/blueprint-concept-for-urban-airspace-integration_2933.

[48] Single European Sky ATM Research 3 Joint Undertaking. *U-space : blueprint*. Publications Office, 2017. URL: https://data.europa.eu/doi/10.2829/335092.

3

Utilisation of Airspace under Various Layer Function Assignments and Allocations

Vertical airspace is a scarce resource in the urban environment. If aircraft fly at higher altitudes, missions may increase interaction with civil aviation and potentially become unfeasible. Therefore, this chapter aims to study the function of vertical airspace and how aircraft should be distributed among two related but distinct sub-experiments.

Sub-experiment 1 examines the impact of assigning different functions to airspace layers by comparing two airspace structures. Sub-experiment 2 explores the influence of varying rule-sets that distribute aircraft among available airspace layers.

This chapter is based on the following publications:

- A. Morfin Veytia, C. A. Badea, N. Patrinopoulou, I. Daramouskas, J. Ellerbroek, V. Lappas, V. Kostopoulos and J. Hoekstra. 'U-Space Utilisation of Airspace under Various Layer Function Assignments and Allocations'. In: *Drones* 7.7 (2023). ISSN: 2504-446X. DOI: 10.3390/drones7070444. URL: https://www.mdpi.com/2504-446X/7/7/444

Abstract

The interest in urban air mobility as a potential solution for urban congestion is steadily growing. Air operations in urban areas can present added complexity as compared with traditional air traffic management. As a result, it is necessary to test and develop novel airspace designs and rules. As airspace in urban areas is a scarce resource, creating structures and rules that effectively utilise the airspace is an important challenge. This work specifically focuses on layered airspace design in urban operations constrained to fly between the existing buildings. Two design parameters of airspace design are investigated with two sub-experiments. Sub-experiment 1 investigates layer function assignment by comparing concepts from previous research with different layer assignment distributions. Sub-experiment 2 investigates the flight rules of vertical distribution of traffic within the airspace, to determine whether this is best achieved in a static (pre-allocated) or dynamic manner. Both sub-experiments analyse the overall system safety, route duration, and route distance under increasing traffic demand. Results reveal that the importance of cruising airspace is apparent at high densities. Results also shows that the safest layer allocation flight rule depends on the traffic density. At lower densities dynamic rules help to spread traffic locally. However, when the airspace is saturated it is safer to pre-allocate flight heights if achieved uniformly.

3.1. Introduction

In recent years there has been increasing interest in the use of drones, also known as unmanned aerial vehicles (UAVs), in urban areas for human, parcel, and food transportation in response to increasing urbanisation and climate change. The UN estimates that 68% of the world population will live in urban areas by 2050[2]. Transitioning part of ground transportation to the air can free up space on the surface. Furthermore, drone delivery has the potential to be more environmentally viable than current day ground-delivery[3].

The European drone outlook study[4] expects that there will be 400,000 drones in the air by 2050. Other estimates also point at densities previously unseen by traditional air traffic management[5]. The U-space platform was established to support the creation of an infrastructure that provides a safe urban airspace in the European Union[6].

Several projects developed comprehensive traffic management systems[7, 8]. The main components of an air traffic management system are path planning, separation management, and airspace structure and rules. In highly-dense urban airspace these are interdependent and cannot be designed without considering the others. This work focuses specifically on the airspace structure and rules. An analogy from road traffic is useful to explain the difference between the structure and rules. Imagine a two-lane road (structure) in which each lane is reserved for a certain direction (rules). The rules provide guidance on how traffic is allowed to travel through the structure.

Urban airspace structures will be constrained by the existing urban environment

[9]. UAVs may have to operate above the road network in areas where buildings are tall. It may also be necessary to avoid flying over buildings for privacy reasons [10]. Furthermore, the airspace is limited in height to reduce interference with general and civil aviation aircraft and because of limited energy capacity of drones so it is important to create rules that use the airspace effectively.

This work is interested in how different airspace structures and rules affect interactions between vehicles at a tactical level. As the density of the airspace increases, drones are more likely to encounter other drones. This can cause emergent behaviour that is detrimental to system safety. For this reason, the work uses separation minima as the measure of safety. This means that other factors of safety, such as meteorological impact or navigational performance are out of scope of this work. Moreover, the work also measures the route duration and route distances to provide an estimation of how the energy usage varies in the different airspace structures and rules.

Metropolis I [11] investigated how different degrees of airspace structuring affect safety. The results showed that a layered concept was the safest. An important conclusion was that modifying the airspace structure and rules is an effective way to deal with detrimental emergent behaviour.

The work at hand aims to study emergent behaviour and evaluate the performance of a U-space system when applying strategic and tactical deconfliction methods. Various airspace structure and vertical altitude allocation rules, combined with established tactical deconfliction methods, are investigated under increasing level of traffic demand.

For this purpose, two sub-experiments are performed in order to isolate the effect of each on the performance of a U-space system. Sub-experiment 1 investigates different airspace structures in which layers are assigned a specific function (turning, cruising, deconflicting)[12, 13]. Assigning layers for cruising will reduce the available airspace for other functions. Moreover, it is important to effectively utilise the available airspace because of the constrained nature of the airspace. Sub-experiment 2 investigates if it is beneficial to allocate drones to specific layers in the airspace or if it is better to allow the drones to redistribute based on the local situation.

Section 3.2 presents the proposed airspace design configurations and the measures to analyse them. Section 3.3 presents the experimental set up. The results of the experiments are presented in Section 3.4. Finally, a discussion on the results and the conclusion are in Sections 3.5 and 3.6,respectively.

3.2. Proposed urban airspace concepts

Using the urban airspace design considerations in Section 2 for the airspace structure and vertical flight rules, this section first proposes different airspace structures and allocation rule-sets. These also serve as independent variables in the experiments described further in this work. Following this, the dependent measures to evaluate the structures and rule-sets are presented. The airspace and rules are in the context of a non-orthogonal network under increasing imposed

travel demand.

3.2.1. Layered Airspace Structures

This section illustrates two airspace structures that can be defined with the considerations from Ch. 2. The function assignment of the layers is the main difference between the structures. Note that all layers have the same vertical thickness.

Baseline Constrained Airspace Structure

In the Baseline structure, the pattern seen in Figure 2.2 where two orthogonal directions cross at different altitudes is repeated to reach the configuration seen in Figure 3.1. This is the structure that was used in the Metropolis II study [8]. The left and right stacks show the east/west and north/south layer configurations, respectively. Note that the grey layers in each structure correspond to altitudes where the other structure would have a cruising layer. For example, the lowest grey layer in the left image showing the east/west cruising layers corresponds to a blue cruising layer from the north/south assignment. The grey airspace is generally only used when making a vertical manoeuvre.

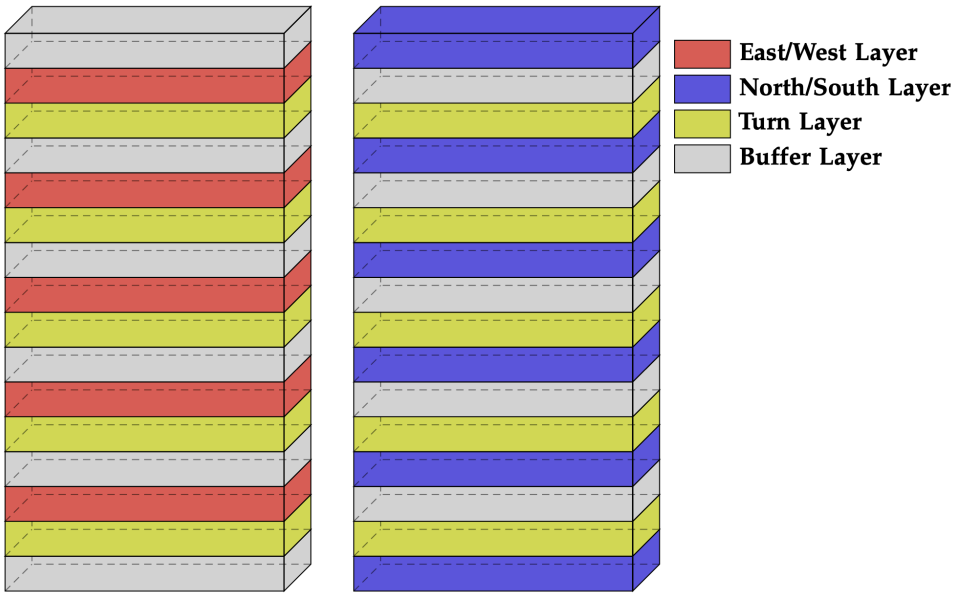

Figure 3.1: Constrained airspace layer assignments for the Baseline structure. The left image shows the cruising layer for streets categorised as east/west. The image on the right shows the cruising layers for streets categorised as north/south. Note that the turn layers are in the same height and the buffer layers correspond to the cruise layers in the other categorisation.

'1-to-1' Constrained Airspace Structure

The '1-to-1' structure alternates one cruise layer and one turn layer. It is a similar structure as that from [12, 13]. The '1-to-1' structure can be seen in Figure 3.2. The alternation of layers reduces the amount of cruising space as compared to the Baseline structure. The '1-to-1' structure has more layers for turning traffic. There are a total of 8 cruising layers in the '1-to-1' structure versus 11 in the Baseline structure.

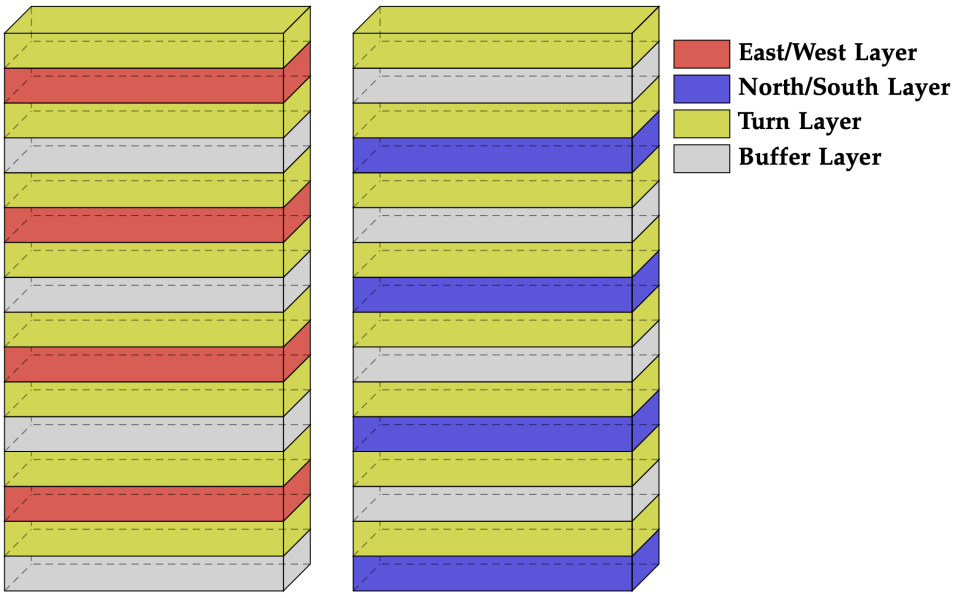

Figure 3.2: Constrained airspace layer assignments for the '1-to-1' structure. The left image shows the cruising layer for streets categorised as east/west. The image on the right shows the cruising layers for streets categorised as north/south. Note that the turn layers are in the same height and the buffer layers correspond to the cruise layers in the other categorisation.

3.2.2. Vertical Allocation Rule-Sets in Layered Airspace Structures

This section illustrates four different vertical allocation rules. The Baseline concept attempts to give more freedom to how drones travel in an already constrained network. The three pre-allocated layer sets make drones more predictable because the heights at which drones may travel are predetermined.

Baseline Airspace Allocation

The Baseline rule-set aims to give freedom in how drones vertically separate themselves. This strategy is called the dynamic density redistribution algorithm which can be seen in Algorithm 2 [8]. Essentially, the principle is the same as in the 'keep-right' case for highways, the drones remain on the lowest cruise

layer. However, if a faster drone approaches a slower drone in front, then it can perform a vertical manoeuvre to move up a layer, then overtake manoeuvre and then return to the lower layer. The conflict resolution (CR) algorithm can also call for vertical solutions if necessary. However, the extra freedom in vertical manoeuvres comes at the cost of increased airspace complexity.

Figure 3.3 illustrates the procedure for performing a vertical overtake. Drones A and B are both travelling in the lower cruise layer with a speed of 30 and 20 knots (15.4 m/s and 10.3 m/s), respectively. As drone A approaches drone B, it checks if the cruise layer above is empty. If there are no drones above then it can ascend.

Figure 3.4 illustrates the procedure of returning back to the lowest layer after an overtake. If there are no drones in the cruise layer below, then the drone can descend.

These proactive manoeuvres aim to reduce congestion at the local level. However, it is also important to note that not all transitions are proactive. Turn transitions are those that occur when a drone transitions to a turn layer from a cruise layer or vice versa. These are 'forced' transitions and occur at all turns of the flight. The CR algorithm may also perform some 'reactive' vertical transitions.

Algorithm 2: Dynamic density redistribution algorithm.

```
1:  for each drone in constrained airspace do
2:      if drone in conflict then:          ▷ conflict resolution algorithm takes over
3:          return CR manoeuvre
4:      else:
5:          if drone in lowest cruise layer then:
6:              if no drone in front then:                          ▷ drone remains
7:                  return Maintain altitude, continue cruising
8:              else:                                               ▷ drone ascends
9:                  return Drone received ascend command
10:         else:
11:             if no drone in cruise layer below then:             ▷ drone descends
12:                 return Drone receives descent command
13:             else if drone in front then:                        ▷ drone ascends
14:                 return Drone receives ascent command
15:             else:                          ▷ drone remains in current layer:
16:                 return Maintain altitude, continue cruising
```

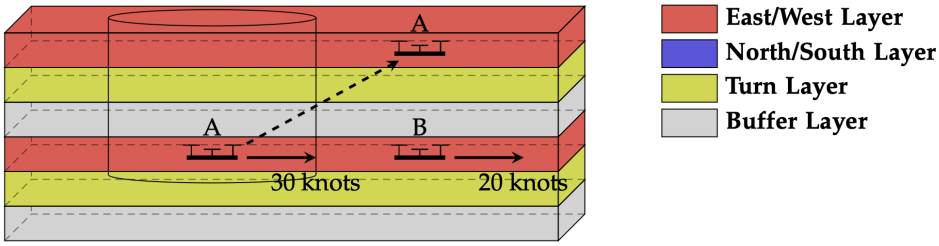

Figure 3.3: Dynamic density redistribution example. Drone A is stuck behind Drone B because it is travelling at a faster speed. Drone A then checks the cruise layer above for any drones within 2× protected zone radius. Drone A then climbs if the space above is empty. The solid and dotted arrows start from the current position of the drones prior to a vertical manoeuvre. The solid arrow shows the direction of travel. The dotted arrow points to the future position of the drone after the vertical manoeuvre has been performed.

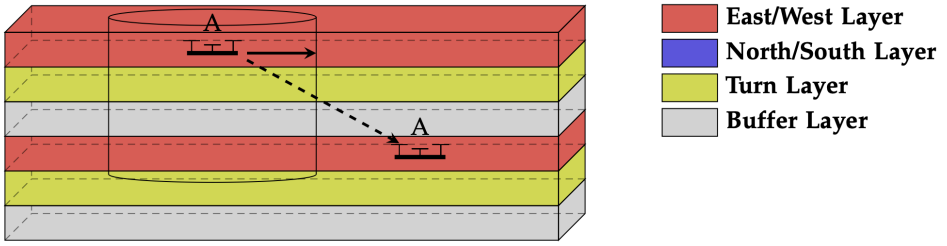

Figure 3.4: Dynamic density redistribution example. Drone A is not at the lowest cruise layer. Drone A continually checks the cruise layer below for any drone within 2× protected zone radius. If there is space, then Drone A descends. The solid and dotted arrows start from the current position of the drones prior to a vertical manoeuvre. The solid arrow shows the direction of travel. The dotted arrow points to the future position of the drone after the vertical manoeuvre has been performed.

Other Allocation Methods

The pre-allocated rule-sets aim to distribute drones uniformly over the layers to create a ‘keep-lane‘ strategy. Figure 3.5 shows five different layer set allocations stacked on top of each other. In the allocation concepts, drones transition to a pre-determined layer set and stay there throughout their route. Each layer set has one north/south cruise layer and one east/west cruise layer. Note that these sets do not use the highest layer as it does not have an accompanying red cruise layer. However, the effect is minimal when compared to the dynamic density redistribution algorithm because it ensures that the highest layer of the airspace is rarely used. The three different height allocations strategies are:

1. **Density allocation**: This allocation uses the current density in constrained airspace. When a drone enters the airspace it is allocated to the layer set

with the least number of drones in it. If there are two or more sets with the same number of drones then it gets allocated to the lowest layer set.

2. **Random allocation**: Whenever a drone enters the airspace it is randomly allocated to a layer set. This method attempts to give a uniform distribution without the need for any knowledge of the current occupation levels of the layer sets.

3. **Flight distance allocation**: Drones are allocated to a layer set depending on the flight distance. Shorter flights are in lower layers and longer ones are higher. The distances per layer set are seen in Table 3.1. They are based on one experimental scenario and attempt to set the same density at each layer set. So it is similar to using historical distance-distribution traffic data for the airspace rules.

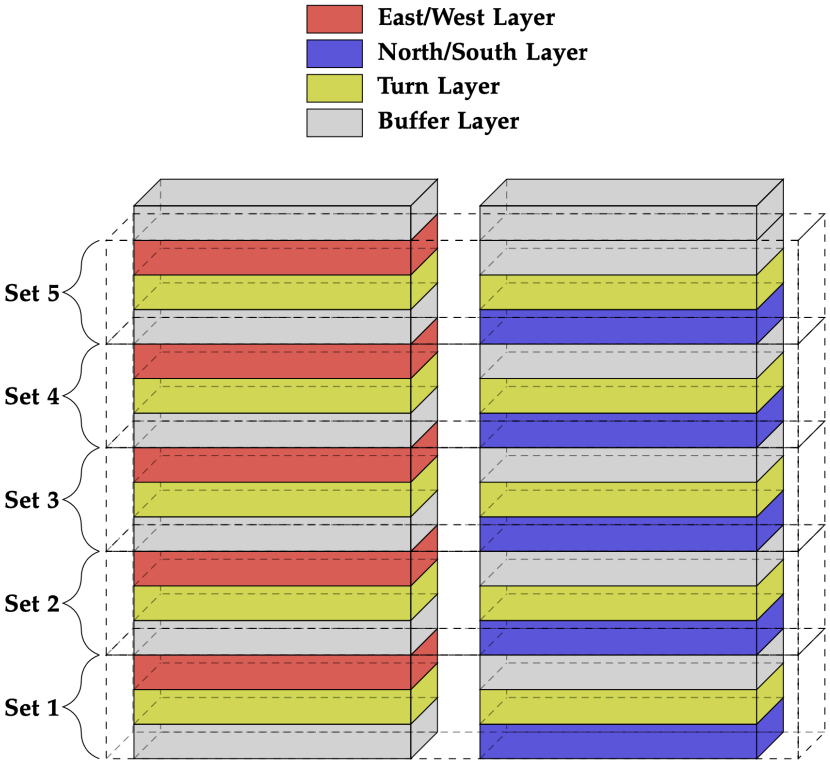

Figure 3.5: Constrained airspace layer configuration. The left image shows the cruising layer for streets categorised as east/west. The image on the right shows the cruising layers for streets categorised as north/south. Note that the turn layers are in the same height and the buffer layers correspond to the cruise layers in the other categorisation.

Table 3.1: Flight distance range per each allocated layer set.

Layer Set	Distance Range (m)
Set 1	distance < 2800
Set 2	$2800 \leq$ distance < 4500
Set 3	$4500 \leq$ distance < 6300
Set 4	$6300 \leq$ distance < 8200
Set 5	distance ≥ 8200

3.2.3. Evaluating the Concepts

This section explains the dependent measures that are used to evaluate the different proposed structures and vertical allocation rule-sets. Four different categories of dependent measures are used, (1) achieved density, (2) vertical transitions, (3) airspace safety, and (4) route duration and distance.

Achieved Density

The safety of a layered airspace is directly related to the density of drones in that layer [14]. The more drones there are the higher chance that they may encounter each other. With more interactions, drones may slow down as they must adjust their speed, like cars in busy highways.

In this study, the total airspace area is kept constant, therefore the concurrent number of drones in the air can be used as a way to measure resulting traffic density. Additionally, for the allocation rule-sets, it is also helpful to measure the concurrent number of drones in the airspace per layer set.

Vertical Transitions

The different allocation rule-sets affect how the drones vertically manoeuvre in the airspace. As it was seen in [14], vertical transitions can destabilise layered open airspace as they increase the vehicle to vehicle interactions. Therefore, this work measures the average number of vertical transitions per flight when comparing rule-sets to analyse if this is indeed the case for constrained airspace.

There are different types of vertical transitions. These are (1) dynamic density redistribution transitions, (2) turning and (3) conflict resolution. It is also possible that a transition is interrupted due to an unforeseen conflict.

Safety

In the current work, safety is evaluated by counting conflicts and intrusions. Conflicts and intrusions are tactical dependent measures as they give an idea on the vehicle-to-vehicle interactions. These are safety dependent measures that have been used in previous research [8, 11–13]. Those were inherited from traditional air traffic management (ATM) in which aircraft have a cylindrical

protected zone, i.e., a horizontal circle with a vertical height. These make up the horizontal and vertical separation minima that is used in this work.

An intrusion occurs when the distance between two drones is less than the predefined separation minima. A conflict is a predicted intrusion. State-based conflict detection can be used for conflict counting. At each time step the current state of the drones is linearly extrapolated into the future with a certain look-ahead time. If an intrusion is expected to occur, then a conflict is counted. A drone may alter its current state to avoid the intrusion by performing conflict resolution. Performing conflict resolution manoeuvres may lead to longer missions.

Figure 3.6 illustrates the difference between a conflict and an intrusion in two dimensions. The left side illustrates a conflict between the ownship (black) and intruder (red). The horizontal minima is illustrated with a dotted black circle around the ownship. If both drones maintain their current state it is predicted that the intruder will enter the protected zone of the ownship within the lookahead time. The right image shows an intrusion. An intrusion occurs when the conflict is not solved and the intruder enters the dotted circle. Each drone performs conflict resolution manoeuvres to ensure that conflicts do not become intrusions. This work measures the average number of conflicts and intrusions per flight.

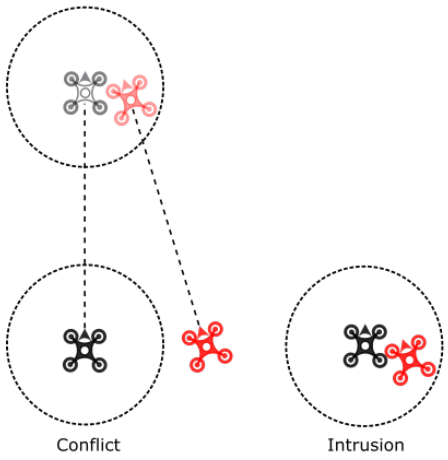

Figure 3.6: A diagram showing an example of a conflict (**left**) and an intrusion (**right**).

Since, the allocation rule-sets also study the vertical transition types it is useful to identify the average number of conflicts per flight attributed to a transition and the percentage of those in regards to the total conflicts per flight. Additionally, it is also possible to analyse the layer-types of two drones in an intrusion. If the drones are in the same layer, then it means that the intrusion was likely caused by a merging or in-trail conflict. Alternatively, if they are in different layers then the intrusion was caused by a vertical transition.

Defining the safety dependent measures in terms of conflicts and intrusions can provide some limitations. For example, the separation distances and look-ahead times will affect the observed number of conflicts and intrusions. As a result, the actual values of the separation distances and look-ahead times are not important for this work. The absolute number of conflicts and intrusions do not provide sufficient information to asses safety. A meaningful analysis can be made by making comparisons between the concepts and studying how that difference is affected by increasing traffic demand.

In the future, the separation standards of drones should consider several factors. These are communications, navigation and surveillance (CNS) factors which affect accuracy of position detection, and data transmission latencies [15]. Moreover, the separation distance may be affected by the local weather conditions, size of the aircraft, type of mission, and ground risk [16].

Route Duration and Distance

This work does not include an energy model to calculate the energy usage. Therefore, it is indirectly evaluated by looking at the average route duration and distance of flights. Due to the simplicity of the calculation, the absolute numbers are not important. Meaningful results are attained with relative comparisons. The route duration and distance dependent measures are shown as percentages of the Baseline concept. For example, the vertical distance percentage for a non-baseline concept is defined by the following equation:

$$p_{distance_{vertical}} = \frac{concept_{distance_{vertical}}}{baseline_{distance_{vertical}}} * 100\%, \tag{3.1}$$

Where $p_{distance_{vertical}}$ is the vertical distance percentage travelled by a specific concept as function of the Baseline, $concept_{distance_{vertical}}$ is the average vertical distance travelled in a specific concept, and $baseline_{distance_{vertical}}$ is the average vertical distance travelled in the Baseline concept. The same can be achieved for 3D distance and route duration. For these dependent measures, the value is larger than 100% when drones tended to travel more distance or time when compared to the Baseline structure or allocation method.

3.3. Comparative experiment

With the proposed concepts in Section 3.2 this section first outlines experimental hypotheses. Then, it introduces the independent variables, dependent measures, and the simulation set up.

There are two sub-experiments. Sub-experiment 1 studies how varying layer function assignment of the airspace structure affects the overall system safety, and route distance, and route duration. Sub-experiment 2 studies how modifying the vertical allocation rule-sets affects the overall system safety, and route distance, and route duration.

3.3.1. Hypotheses

These airspace structures and vertical allocation rule-sets can be compared against each other under increasing traffic demand. In Sub-Experiment 1 the baseline structure (Fig. 3.1) is compared to the '1-to-1' structure (Fig. 3.2). In Sub-Experiment 2, the dynamic density redistribution algorithm (Algorithm 2) is compared to the three pre-allocated methods (Sec. 3.2.2).

Sub-Experiment 1

Hypothesis: Structures 1 (S1): In the lower traffic demands, safety differences are not expected. However, as the demand increases, Baseline structure is hypothesised to be safer than the '1-to-1' structure because the '1-to-1' contains less cruising layers. Having more cruising space will help drones in the Baseline deal with detrimental emergent behaviour at high demands. The lower amount of cruise layers in the '1-to-1' structure will mean that there are more drones per cruise layer. Therefore, drones in the '1-to-1' concept are more likely to encounter each other and cause higher number of conflicts and intrusions per flight.

Hypothesis: Structures 2 (S2): In the all traffic demands, drones in the Baseline structures are hypothesised to have shorter route distances because there is less space between cruise layers as compared to the '1-to-1' structure. The less space between cruise layers would mean that drones travel less vertical distance when making a vertical manoeuvre. As traffic demand increases, and the number of conflicts and intrusions increase (Hypothesis S1), drones in the '1-to-1' concept will begin to have longer route durations as they must slow down due to interactions with other drones.

Sub-Experiment 2

Hypothesis: Allocation 1 (A1): At all traffic demands, the Baseline is expected to have the highest amount of drones in the lowest layer set. The three allocation rules are hypothesised to spread traffic evenly across each layer set despite the different allocation method at all traffic demands.

Hypothesis: Allocation 2 (A2): Differences in safety are not expected in the lower traffic demands. At higher demands, the Baseline concept is hypothesised to be safer than the three allocated concepts because drones are able to vertically redistribute themselves based on the local traffic conditions. These proactive vertical transitions may lead to fewer conflicts and intrusions per flight. Moreover, differences in safety between the three pre-allocated rule-sets should not be observed across traffic demands because they all attempt to spread traffic uniformly across the airspace.

Hypothesis: Allocation 3 (A3): At all traffic demands, drones in the the

Baseline concept are hypothesised to travel longer distances and route durations than the other allocation rule-sets. Even though drones stay lower in the airspace, the increased vertical manoeuvres are expected to create longer travel times and distances. Between the three pre-allocated concepts, the Flight Distance method is expected to have shorter distances and route durations because drones with the shortest paths will have shorter take-off distances.

3.3.2. Independent Variables

The two experiments presented in this work are structured around different sets of independent variables. Sub-experiment 1, which investigates the effects of airspace structure on the performance of the U-Space system, includes the following independent variables:

- Airspace structure configuration, consisting of two independent conditions:
  1. the Baseline airspace structure, presented in Section 3.2.1.
  2. the 1-to-1 layer configuration, presented in Section 3.2.1.
- Hourly traffic demand level, represented by five levels of take-off request frequency values, presented further in this work in Section 3.3.4.

The second sub-experiment, which investigates the effects of the vertical allocation rule-set on the overall performance of the U-space system, includes the following independent variables:

- Vertical allocation rule-set, consisting of four independent conditions:
  1. the Baseline allocation method, presented in Section 3.2.2.
  2. the Density allocation method presented in Section 3.2.2
  3. the Random allocation method presented in Section 3.2.2
  4. the Flight distance allocation method presented in Section 3.2.2.
- Hourly traffic demand level, same five levels as used for the first sub-experiment, presented in Section 3.3.4.

It should be noted that Sub-experiment 1 uses the baseline allocation method described in Section 3.2.2 throughout all the experiment conditions. Similarly, Sub-experiment 2 uses the baseline airspace structure throughout all the experiment conditions, described in Section 3.2.1.

3.3.3. Dependent Measures

The following section presents a summary of the dependent measures (first introduced in Section 3.2.3) used for each sub-experiment. Not all measures were deemed relevant for the first sub-experiment. Thus, the following set of dependent measures were used for Sub-experiment 1:

1. Number of drones concurrently in flight.

2. Conflicts per flight.
3. Intrusions per flight.
4. Vertical distance travelled as a percentage relative to the baseline condition of the sub-experiment.
5. Route duration as a percentage relative to the baseline condition of the sub-experiment.

All the dependent measures used for Sub-experiment 1 are also relevant for Sub-experiment 2, and are thus also recorded. However, additional measures applicable to Sub-experiment 2 only were also recorded:

1. Number of drones concurrently in flight per layer set.
2. Number of vertical transitions per flight (includes total, dynamic density redistribution, turn, and interrupted transitions).
3. Percentage of conflicts attributed to a vertical transition.
4. Number of intrusions within each layer type per flight.
5. The three-dimensional distance travelled as a percentage with respect to the baseline condition of the sub-experiment.

3.3.4. Simulation Set-Up

Imposed Traffic Demand

Each concept is tested under five imposed traffic demands with increasing number of flights, similar to [8]. Table 3.2 shows the imposed concurrent average number of drones and the average instantaneous traffic density. The flight plans are created prior to the simulation. Take-offs are then scheduled so that the concurrent number of drones in the area remains approximately constant if all drones depart on time and travel with their average speed. For each imposed demand there are nine scenarios (or repetitions) with varying flight plans. Each scenario accommodates 1 h of spawning traffic.

Table 3.2: The average number of hourly take-off requests, and per square kilometre, for each traffic demand level.

Traffic Demand Level	Hourly Take-Off Requests	Hourly Take-Off Requests per km^2
Very Low	1672	8.32
Low	3343	16.63
Medium	5041	25.07
High	6628	32.96
Very High	8262	41.09

Simulation Area

This work considers the airspace of Vienna as used in Metropolis II [8]. The airspace is an 8 km radius circle, see Figure 3.7. The area seen in the middle is constrained airspace, Drones must follow the existing road network in this area. The existing road network is sourced from OpenStreetMap [17] using the OSMnx python library [18]. Drones may travel directly to their destination in the part of the airspace that is open.

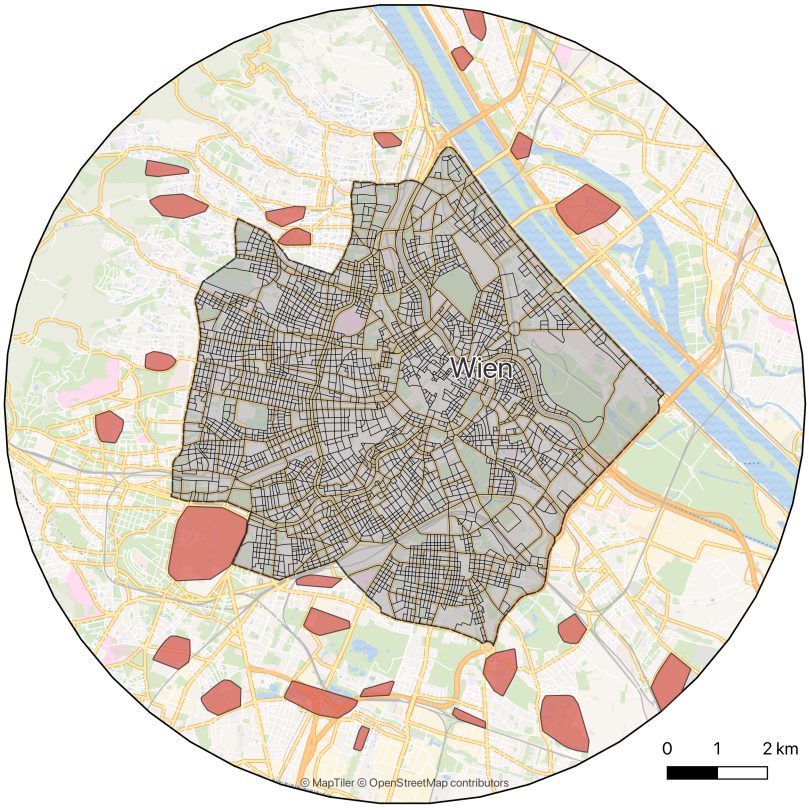

Figure 3.7: Vienna airspace. The area in the middle with the dark street network is constrained airspace. The red polygons on the outskirts are geofences in open airspace.

Although the simulation area also includes open airspace, the focus of the analysis is on constrained airspace. Figure 3.8 shows the layer assignments of each street in constrained airspace. Red layers are generally in the north or south directions. Blue layers are generally in the east or west direction. Note that the constrained network is one-way so each street only allows one direction of travel.

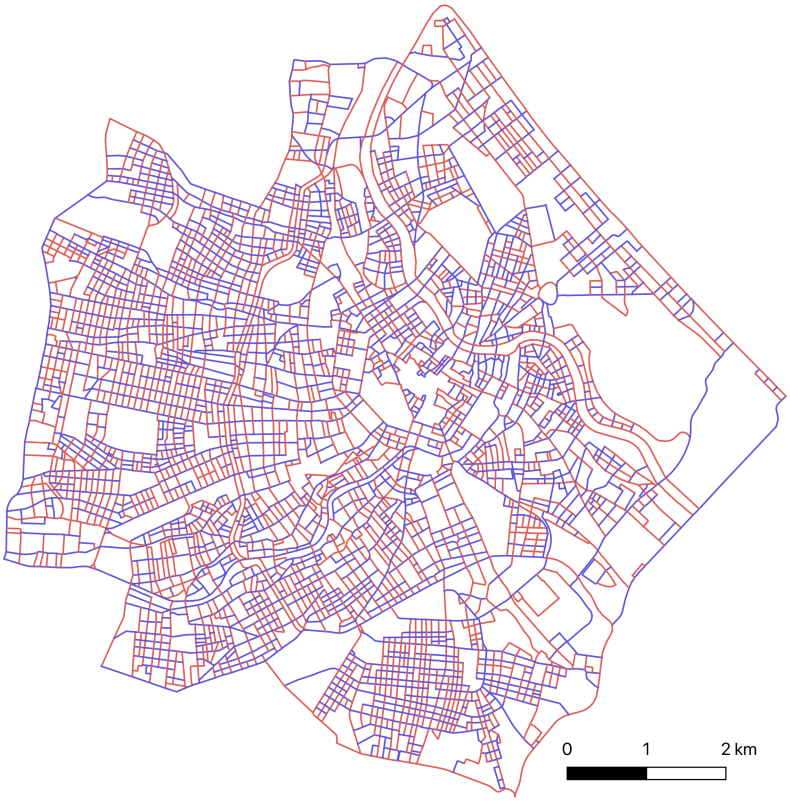

Figure 3.8: Constrained airspace allocation.

Vertical Airspace and Layer Heights

The vertical airspace ranges from 0 to 500 feet (152.4 m) with each vertical layer measuring 30 feet (9.14 m) for a total of 16 layers. The first layer is centred at 30 feet above the ground. Note that this work does not suggest that vertical layers in urban airspace are mandated to be 30 feet. The real value will depend on safe separation specifications (Section 3.2.3). The 30 feet is an arbitrary value to fit several layers inside the airspace. The absolute number of layers can be increased or decreased depending on the necessary specification.

Vertiports and Distribution Centres

Vertiports are spaced throughout the districts of Vienna. Each vertiport covers a maximum of 0.5 square km. The vertiports are uniformly distributed per district and the number of vertiports in a district depends on financial and population metrics [8]. Additionally, there are 16 distribution centres placed around Vienna (see Figure 1 of [8]).

For this work, it is assumed that 40 percent of traffic originates from the

distribution centres and goes to a vertiport. The other 60 percent of traffic starts and ends at a vertiport.

Missions

There are three different types of missions in the simulations: (A) Point-to-point, (B) distribution centre-to-point, (C) emergency. This was defined in order to differentiate between parcel deliveries, which typically originate in a distribution centre, and missions like food deliveries, which would be labelled as point-to-point. Emergency vehicles are a small percentage of the traffic and are allowed to violate the rules of the airspace to reach their destination.

Mission types (A) and (B) were also given a priority. Each of these drones were assigned to low, medium, or high priorities. Each priority accounted for about a third of the traffic. Drones with higher priority (e.g., medical deliveries) have more importance in the separation management decisions.

All missions start at ground level and then begin take-off. Drones take-off if there are no other drones near them. If the drone is not able to find space within 5 min of its scheduled departure then it takes-off. Note the the landing portion of the mission is removed and the drone disappears from the simulation once it is above the destination. The missions are designed to take an average of 15 min and is at least 1 km long.

Drone Models

For this experiment two drone types based on the DJI Matrice 600 Pro hexacopter drone model was used for the simulations. Their only difference is the average cruising speed (Table 3.3).

Table 3.3: Drone models used in this work.

	MP20	**MP30**
Max horizontal speed	25 knots (12.9 m/s)	35 knots (18.0 m/s)
Avg. horizontal speed	20 knots (10.3 m/s)	30 knots (15.4 m/s)
Min horizontal speed	0	0
Max vertical speed	5 m/s	5 m/s
Min vertical speed	0	0
Max take-off mass	15 kg	15 kg
Max (acc/dec)eleration	3.5 m/s^2	3.5 m/s^2

Path Planning and Capacity Monitoring

The output of the flight planning module was a list of sequential waypoints to guide drones to their selected destination. Each mission created a flight plan through the airspace that did not violate the rules.

Flight planning was achieved via the D* Lite algorithm [19]. The path planning graph was based on the street network, with the street sections acting as graph edges and the street intersections acting as graph nodes (Figure 3.8). The path planning algorithm computed the most efficient path on the described path graph, minimising the duration of the path.

Two optimisation parameters were used to indirectly minimise the duration of the flight: (1) The length of the path, and (2) the number of turns. Each turn required additional time for slowing down to turn to ensure that they do not overshoot, therefore it was assumed that the duration of the path depended on the number of turns. Both the cost and heuristic functions, used by the D* Lite algorithm implemented for this system, implemented the two optimisations. The path's length was divided by the nominal speed from Table 3.3 to compute the duration of the path. Then, an additional cost due to turning of 1.83 s per turn was added to the cost and heuristic functions.

There is a central capacity monitoring module active for Sub-experiment 1. Capacity monitoring gathered position data from all drones and estimated the current image of the traffic density. The cost of traversing a street was updated, depending on the current traffic density, and sent to the drones for replanning. Note that the capacity monitoring was turned off in Sub-experiment 2 as it was not applicable because it acted on two dimensions and sub-experiment distributes traffic in three dimensions.

Conflict Detection And Resolution

The current work used conflicts and intrusions as safety measures. An intrusion occured when the distance between two drones was less than a predefined separation minima. In the current work, the horizontal distance was 32 m and the vertical was 7.62 m [20] (Table 3.7.2.4-1). State-based conflict detection with a 10 s look-ahead time was used.

Drones may employ altitude and speed-based conflict resolution manoeuvres. Note that for the pre-allocation rule-sets, the vertical conflict resolution manoeuvres were not performed because of the rules of the airspace. The conflict resolution algorithm can be studied more in detail in [8].

Turning in Constrained Airspace

Drones in constrained airspace performed turns to avoid collisions with buildings. However, drones must slow down from the cruising speeds in order to avoid overshooting the turn. In this work drones vertically transitioned from cruise layers to turn layers prior to turning. The drones then decelerated to make the turn. After making the turn, the drones accelerated and then merged back into the cruise layer. Note that the conflict resolution algorithm may interrupt the vertical transitions associated with turning.

Simulation Software

This work used the BlueSky air traffic simulator for the experiments [21]. BlueSky can be extended via plugins and conditional commands in flight plans such that different airspace structure and rules can be compared against each other with similar conditions. This work also made use of the Metropolis II developments for BlueSky. These developments improved the capabilities of simulating traffic in urban environments.

3.4. Results

The following section shows the results of the two sub-experiments. Unless noted otherwise, the density plots show the number of drones in the vertical axis and the time in the horizontal. The vertical transition and safety plots have the corresponding measure on the vertical axis and the imposed traffic demand in the horizontal. The route duration and route distance plots are similar to the vertical transition and safety plots, with the difference being that the Baseline is seen as a horizontal line at 100%.

3.4.1. Sub-Experiment 1: structure comparison

Sub-experiment 1 compared the Baseline structure to the '1-to-1' structure. The results are presented in the following section. Note that there were no observed differences in achieved density between structures.

Safety

Figure 3.9a,b show the number of conflicts and the intrusions per flight in constrained airspace, respectively, for the two structures. The Baseline structure had more conflicts than the '1-to-1' structure at all imposed demands. In terms of intrusions, the two structures were similar at the lower imposed demands. However, the '1-to-1' structure had more intrusions at the high and very high demand.

Route Duration and Distance

Figure 3.10a shows the percent of vertical distance travelled of the '1-to-1' structure compared to the Baseline at all imposed demands. The drones in the '1-to-1' structure travelled more vertical distance.

Figure 3.10b shows the percent of route duration with respect to the Baseline. It is clear that at most imposed demands the difference between the structures is negligible. At the very high demand, drones in the '1-to-1' structure spend more time in the air than drones in the Baseline.

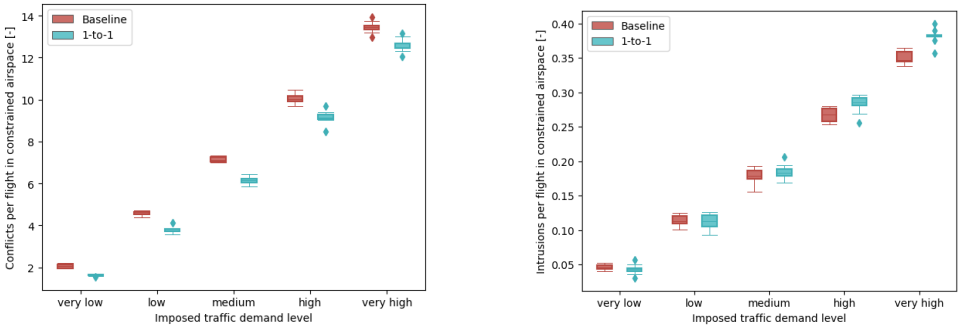

(a) (b)

Figure 3.9: Number of conflicts and intrusions per flight in constrained airspace. (**a**) Number of conflicts per flight in constrained airspace as a function of imposed traffic demand. (**b**) Number of intrusions per flight in constrained airspace as a function of imposed traffic demand.

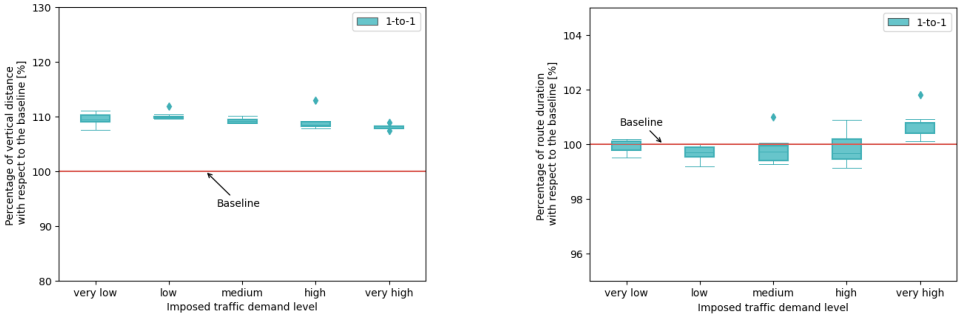

(a) (b)

Figure 3.10: Percentage of vertical distance and route duration with respect to the Baseline concept. A value larger than 100 percent indicates that the concept travelled a longer distance and/or time than the Baseline. (**a**) Percentage of vertical distance travelled with respect to Baseline concept. (**b**) Percentage of route duration with respect to the Baseline concept.

3.4.2. Sub-Experiment 2: vertical allocation comparison

Sub-experiment 2 compares the density redistribution algorithm to three other pre-allocation methods.

Density

The total achieved densities were comparable across the four rule-sets. However, there were clear differences in the achieved densities per layer set.

Figure 3.11 shows the actual traffic distribution in a high demand scenario for different layer sets. On the right, the heights of these layers are included, these correspond to the sets in Figure 3.8. In the lower layer set the number of drones

for the Baseline is about two times that of the Random and Density allocation concepts.

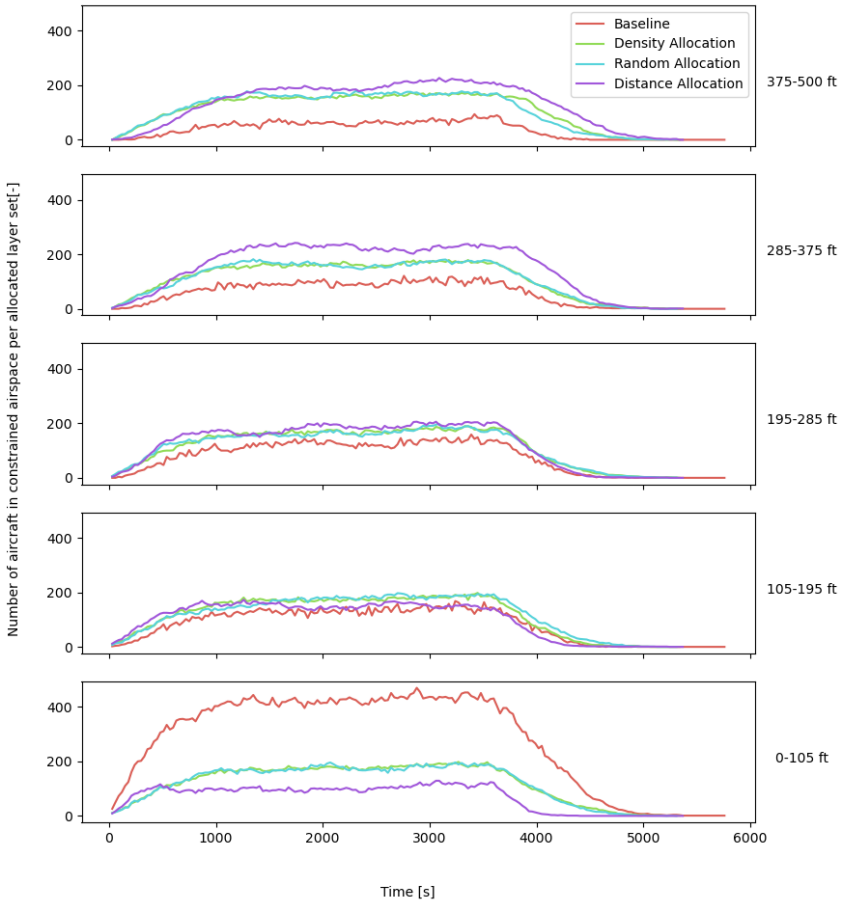

Figure 3.11: Sub-experiment 2:Number of instantaneous drones in constrained airspace for a high imposed traffic demand in the different layer sets. On the right of the image the heights at which the drone count is taken can be seen.

As the height increases, it is clear that the Baseline concept decreased in the number of drones. This was the intended effect, as drones are encouraged to remain as low as possible. The Density and Random allocation concepts remained relatively constant with a peak of 200 drones at one time.

It is also interesting to note that the Distance allocation concept had less drones in the lowest layer set than the other allocation methods but the highest number of drones in the higher layer sets.

Vertical Transitions

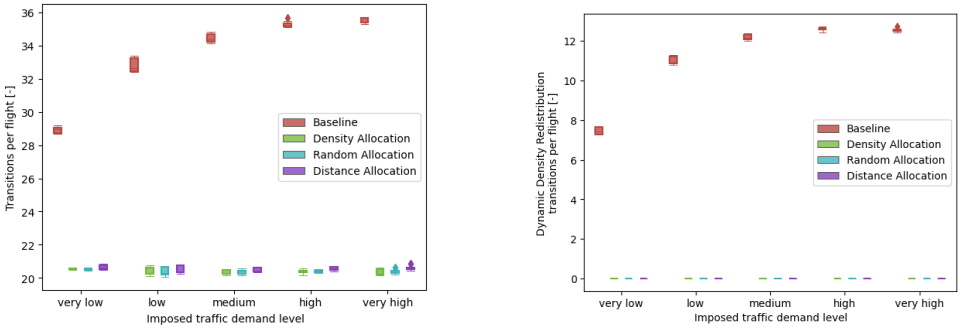

(a) (b)

Figure 3.12: Number of transitions per flight for the different transition types. (**a**) Number of vertical transitions per flight. (**b**) Number of dynamic density redistributing transitions.

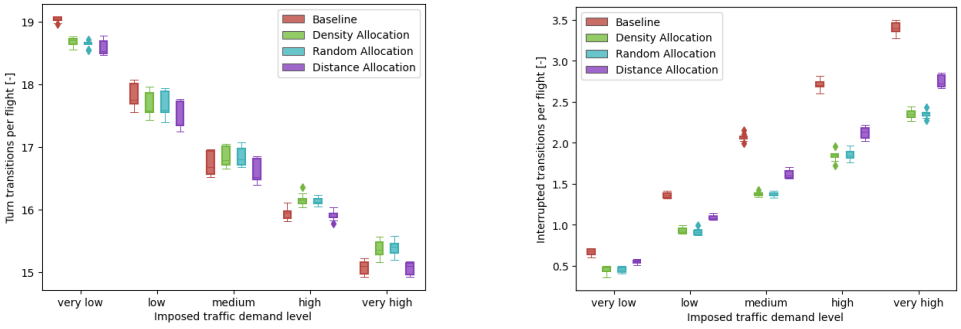

(a) (b)

Figure 3.13: Number of transitions per flight for the different transition types. (**a**) Number of turn vertical transitions per flight. (**b**) Number of interrupted vertical transitions per flight.

Figure 3.12a shows the total number of transitions per flight for all concepts. The Baseline concept had the highest number of vertical transitions for all imposed demands. This was expected because of the dynamic density redistribution algorithm. Although the number of transitions increased with demand, the increase was not linear as the airspace became denser. The three other allocation methods were relatively similar across the different demands.

Figure 3.13a,b show only the turn and interrupted transitions per flight, respectively. The turn transitions decreased with the demand because as the density of the airspace increased, there was a higher chance that the transition was interrupted. This is explained by Figure 3.13b, which shows the opposite trend, increasing conflict interrupted transitions with the imposed demand.

The Baseline concept had more interrupted transitions because it also

performed the dynamic density redistributing transitions. These transitions can be seen in Figure 3.12b. These transitions increased as the imposed demand increased but hit a ceiling at the higher demands.

Safety

Figure 3.14a,b show the number of conflicts and intrusions per flight. At the very low and low imposed demands the number of conflicts was similar for the Baseline, Density, and Random allocation concepts. However, as the demand increased, the number of conflicts in the Baseline concept was larger than in the Density and Random allocation concepts. Moreover, the Distance allocation concept had the largest number of conflicts for all densities.

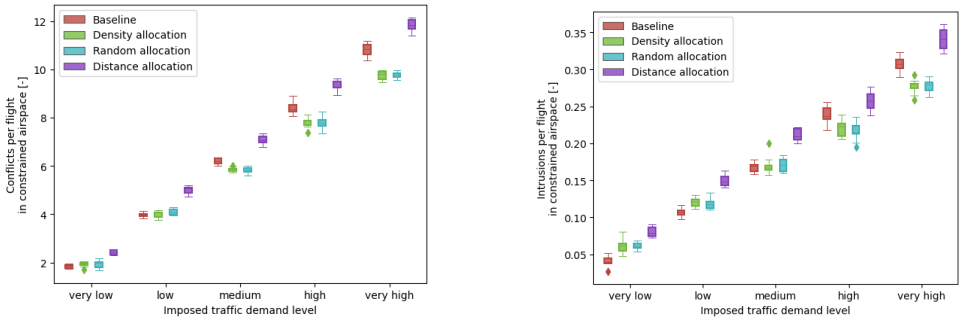

(a) (b)

Figure 3.14: Number of conflicts and intrusions in constrained airspace. (**a**) Number of conflicts per flight in constrained airspace as a function of imposed traffic demand. (**b**) Number of intrusions per flight in constrained airspace as a function of imposed traffic demand.

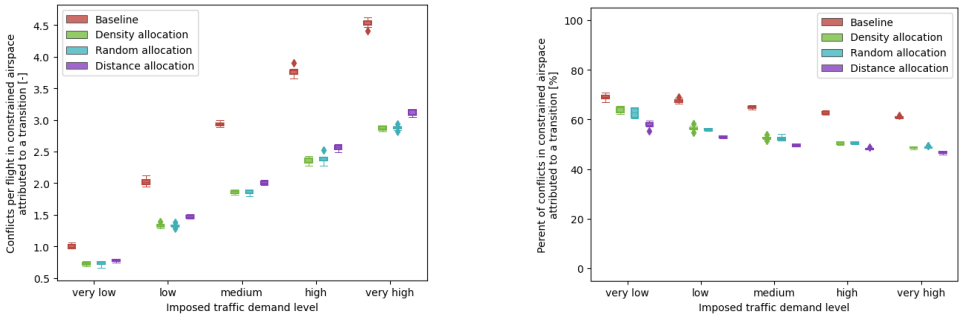

(a) (b)

Figure 3.15: Conflicts per flight and percent of conflicts attributed to vertical transitions. (**a**) Conflicts per flight attributed to a vertical transition. (**b**) Percent of conflicts attributed to a vertical transition.

The trend in the intrusions (Figure 3.14b) was similar but there were some

important differences. The Distance allocation concept maintained the highest number of intrusions at all imposed demands. At the lower densities, the Baseline concept had fewer intrusions than the Random and Density allocation concepts. At the medium demand the intrusions were similar and in the high and very high demand, both the Density and Random allocations had the least number of intrusions.

Figure 3.15a shows the total number of conflicts per flight that can be attributed to a vertical transition. The Baseline concept has the largest amount of transition conflicts because it performs more transitions (Figure 3.12a). Out of the other allocated methods, the Distance allocation concept has the largest number of conflicts attributed to transitions because it has more conflicts (Figure 3.14a).

Figure 3.15b shows the percentage of conflicts that can be attributed to a transition. Here, it is clear that the majority of conflicts in the Baseline (70%) were due to vertical manoeuvres. There was a slight decrease as the imposed demand increased which suggests that in-trail or merging conflicts were becoming more prevalent as the demand increased. The Random and Density allocation concepts were similar and decreased with imposed demand. Interestingly, the percentage of conflicts for the Distance allocation was lower than the others which suggested that there was more importance in horizontal conflicts when compared to the other concepts.

Figure 3.16 shows the number of intrusions per flight on the vertical axis and a given layer pair in the horizontal axis for the high demand scenarios. The layer pair were the layers where the drone-pair were flying when the intrusion occurred. It can either be a cruise (C), turn (T), or buffer (B). The Baseline case had the least amount of intrusions when both drones were in similar layers (C-C, T-T). These were largely in-trail or crossing intrusions. The Density and Random allocation concepts were slightly higher than the Baseline in these cases. Finally, the Distance allocation concept shows the highest number intrusions when drones were in the same layer.

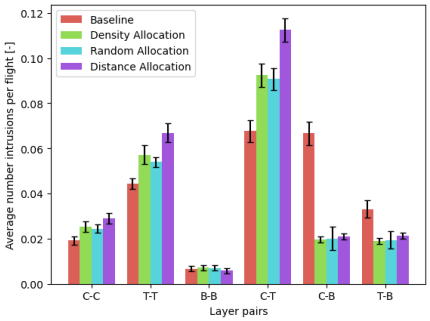

Figure 3.16: Average intrusions per flight per layer type for the high demand scenarios.

The C-T intrusions happened due to turning transitions. The Baseline concept had the lowest number of intrusions. In the other allocated methods, the Density

and Random allocations were fairly similar, while the Distance allocation had the highest intrusions. C-B and T-B intrusions were the largest in the Baseline concept because the Baseline concept made dynamic density redistribution transitions which forced drones to travel in the buffer layers.

Route Duration and Distance

Figure 3.17a shows the percentage of the vertical distance travelled with respect to the Baseline. Drones in the Density and Random allocation concepts travelled less vertical distance than drones in the Baseline. Additionally, drones in the Distance allocation travelled slightly less vertical distance than drones in the other allocation methods. In the very high densities, the other allocated concepts travelled 50% less distance vertically than the Baseline.

Figure 3.17b shows the percentage of route duration with respect to the Baseline. It can be seen that the other allocation concepts performed worse than the Baseline. The Distance allocation concept performed slightly worse than the other allocation concepts. However, the average difference was within 5% of the Baseline concept.

Figure 3.18 shows the percentage of the total distance travelled of each concept with respect to the Baseline. The non-baseline allocation methods are roughly similar to each other and better than the Baseline. Most of the distance travelled is horizontal and that is the same across all concepts so the difference is less than 2%.

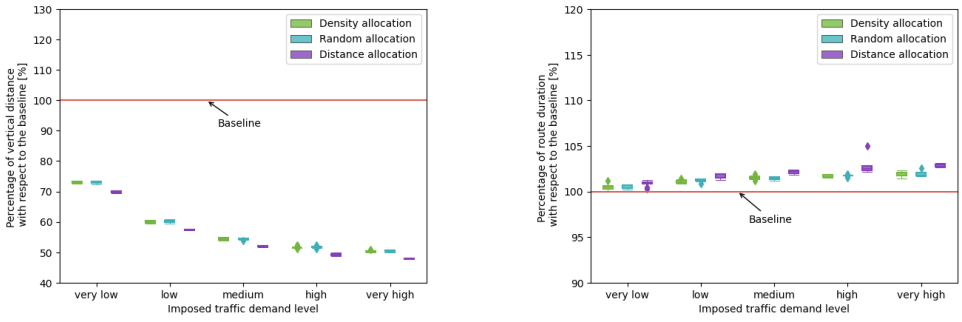

(a) (b)

Figure 3.17: Percentage of vertical distance and route duration with respect to the Baseline concept. A value larger than 100 percent indicates that the concept travelled a longer distance and/or time than the Baseline. (**a**) Percentage of vertical distance travelled with respect to Baseline concept. (**b**) Percentage of route duration with respect to the Baseline concept.

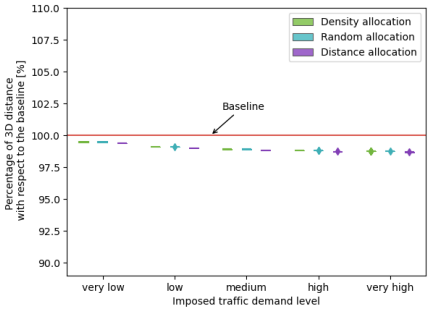

Figure 3.18: Percentage of total distance duration with respect to the Baseline concept.

3.5. Discussion

3.5.1. Sub-Experiment 1: structure comparison

The layer function assignment directly affected the amount of space provided for different parts of the flight phase. This in turn had an effect on the overall system safety and route distances and durations. In Sub-experiment 1 the Baseline structure had more cruise space than the '1-to-1' structure. Conversely, the '1-to-1' structure allowed for more turn space.

Safety

It was hypothesised (Hypothesis S1) that the difference between structures would not be visible for the lower traffic demands. As the demand increased, it was hypothesised that the Baseline concept would be safer than the '1-to-1' structure at higher traffic demands. This is not true when analysing the conflicts per flight because the Baseline concept had fewer conflicts at all demands. However, Hypothesis S1 can be confirmed by looking at the intrusions. When the airspace density was low enough there was no significant difference between structures. There is a critical traffic density in which there was detrimental emergent behaviour and the '1-to-1' structure had more intrusions than the Baseline.

In the Baseline concept, cruise layers were closer than in the '1-to-1' structure; therefore, drones were more likely to encounter drones from other layers when making a vertical transition. This explains why there were more conflicts in the Baseline. However, this also meant that there were more cruising layers available in the Baseline structure. As a result, there were less drones per layer and more space for vertical transitions.

Even though drones in the Baseline structure had more conflicts, they were able to solve the conflicts before they become intrusions. This suggests that at higher densities, cruising space became more important than turning space, thus the choice of having more cruising layers was beneficial at higher densities in terms of intrusions. Considering that intrusions were violations of the separation minima, their occurrences were more serious than conflicts.

Route Duration and Distance

It was hypothesised (Hypothesis S2) that drones in the Baseline concept would travel less distance than the '1-to-1' concept. This can be confirmed by looking at the vertical distance travelled. Drones in the '1-to-1' structure needed to travel more distance when performing dynamic density redistribution manoeuvres or conflict resolution manoeuvres because cruise layers were further apart.

However, this did not have a large impact in the route duration as both concepts were similar at most demands. At the very high demand, drones in the '1-to-1' structure had a slightly higher ($<2\%$) route duration. Therefore, the hypothesis can only be confirmed for the vertical distance travelled.

3.5.2. Sub-Experiment 2: vertical allocation comparison

The layer allocation rule-sets directly affect how the vertical airspace was utilised. This sub-experiment compared four concepts with a different layer allocation rule-set.

Density

It was hypothesised (Hypothesis A1) that the Baseline concept would have the highest number of drones in the lowest layer set. This was clearly seen in (Figure 3.11). The intention of the Baseline rule-set was to encourage drones to travel in the lowest layer set and the results showed that most drones travelled there.

However, it was also hypothesised that the three pre-allocation methods would maintain similar number of drones in all layer sets. This was only true for the Density and Random Allocation methods. Interestingly, the Flight Distance allocation method did not manage to keep the number of drones equal at all layer sets. This was because only one scenario was used to decide the distance distribution of all of the Flight Distance scenarios. Therefore, it was not able to keep a constant number of drones across layer sets.

The difference in the number of drones between the layers in the Flight Distance allocation method illustrate the potential pitfalls of using historical distance distribution information for planning traffic in urban operations. The dynamic nature of the missions makes planning them more difficult than traditional air traffic which is planned long before take-off. Airspace structures and rules should be able to cope with a dynamic traffic demand.

Vertical Transitions

In the Baseline concept, the dynamic density redistribution transitions per flight hit a ceiling at the higher imposed demands. As the airspace becomes more congested, it was more difficult to manoeuvre. The increased congestion made it increasingly difficult to create space dynamically.

It is also interesting to note that for all methods the turn transitions decreased while the CR interrupted transitions increased with the demand. As the density of the airspace increased, drones were more likely to encounter other drones.

The emergent behaviour at higher demands made vertical transitions more detrimental for safety.

Safety

It was hypothesised (Hypothesis A2) that there would be no safety differences between the concepts at the lower demands. However, at the higher demands the hypothesis stated that the Baseline concept would be safer than the pre-allocated methods because it is able to redistribute traffic based on the local situation. This hypothesis is not true as the results show a different trend.

In the lower demands, the Baseline concepts had less intrusions than the pre-allocated concepts. This means that at low demands, drones in the Baseline rule-set were able to dynamically create space and prevent intrusions. However, as the airspace became more congested (high and very high demands), the Baseline concept had more intrusions than the Density and Random allocation methods. This showed detrimental emergent behaviour of vertical transitions at increasing demands. In higher demands it was more beneficial for drones to be more predictable. Interestingly, the Baseline concept had less intrusions than the Flight Distance allocation method. The unequal distribution of drones across layer sets decreased the overall safety.

It is also interesting to note that more than half the conflicts in all methods can be attributed to vertical manoeuvres. Moreover, in the Baseline rule-set, the vertical manoeuvre conflict proportion was even higher (above 60%). The rest of the conflict can be attributed to horizontal conflicts which were either in-trail conflicts or crossing conflicts at an intersection. The safety issues with vertical manoeuvres were also visualised in the number of intrusions per layer pairs. The Baseline had more intrusions in cases where drones were vertically manoeuvring C-U, T-U cases. However, the pre-allocated methods had more conflicts in cases where drones were in similar layers C-C, T-T. Moreover, both cases show several intrusions due to drones in turn, C-T. This shows a need to create better turning strategies in a layered constrained airspace.

Route Duration and Distance

It was hypothesised (Hypothesis A3) that at all traffic demands drones in the Baseline concept would travel more distance and have longer route durations. The results show that this was only true in terms of route duration. Drones in the Baseline rule-set travelled the most distance because of the high number of vertical transitions. The initial vertical distance (to reach the assigned layer-set) travelled by the pre-allocated methods was lower than the total distance manoeuvred in the Baseline. However, because the horizontal distance travelled was significantly larger than the vertical distance, the differences were not very large in overall distance (2.5%).

It was also hypothesised that drones in the Flight Distance Allocation method would travel less distance and have shorter route durations than the Random and Density methods. There were no significant differences regarding the 3D distance.

However, the route durations were slightly longer because drones in the Flight Distance had more conflicts that force drones to slow down. Similarly, drones in the Flight Distance method travelled slightly less vertical distance because more of their vertical transitions were interrupted.

3.6. Conclusion

The airspace structure and vertical flight rules are an essential part of an urban traffic management system. This work specifically compared structures with different layer assignments and rule-sets with different allocation methods in a layered constrained airspace.

It was seen that providing more cruising layers is more beneficial for safety in highly dense airspace. As the airspace became congested, having more layers dedicated to cruising spaces became more important than other functions. The additional cruise layers allowed the structure to mitigate detrimental emergent behaviour at high densities more effectively since it reduced the vehicle to vehicle interactions.

Since high densities are expected in the future, research should focus on improving the use of the available airspace. Allowing for a more dynamic layer function assignment could improve the overall system safety. For example, the rarely used buffer layer could also be used as a deconfliction layer.

The airspace structure should also be developed with effective vertical allocation rule-sets. In this work it was seen that there was a trade-off between allowing drones freedom to redistribute between layers or on pre-allocating their flight layers.

At low densities, there is a beneficial effect in safety of allowing drones to redistribute themselves vertically depending on the local situation. However, at higher densities it became clear that staying in one layer was more beneficial. This was similar to what was seen in open airspace by [14]. At increasing densities there was a detrimental emergent behaviour due to vertical manoeuvres. It was also interesting to note that if the allocation method does not distribute equally amongst layer sets, then the dynamic density redistribution algorithm was safer.

Future research could consider combining both pre-allocation and redistribution into a unified concept. For example, it could be possible to allow for drones to change allocated layer sets mid flight. The local density in one area may not match another area. Ensuring safe transitions between allocated sets might be required when combining these.

This research did not see large differences between the route duration and distance measures. However, it was a limited analysis because the work did not consider real energy used. It would be helpful to consider the energy performance model of the drones and measure energy usage directly. Moreover, work should also focus on improving the other components of a traffic management system. Path planning that reduces local hotspots could improve the safety of the system. Moreover, including uncertainties introduced by meteorological conditions or

drone navigation performance would help mitigate limitations of this work.

Layer function assignment and vertical allocation rule-sets are important concepts in the future of U-space because airspace is not infinite. In general, future research should look to improve airspace structure and develop rules that effectively utilise it.

References

[1] A. Morfin Veytia, C. A. Badea, N. Patrinopoulou, I. Daramouskas, J. Ellerbroek, V. Lappas, V. Kostopoulos and J. Hoekstra. 'U-Space Utilisation of Airspace under Various Layer Function Assignments and Allocations'. In: *Drones* 7.7 (2023). ISSN: 2504-446X. DOI: 10.3390/drones7070444. URL: https://www.mdpi.com/2504-446X/7/7/444.

[2] United Nations, Department of Economic and Social Affairs, Population Division. *World Urbanization Prospects: The 2018 Revision (ST/ESA/SER.A/420)*. New York: United Nations, 2019.

[3] J. K. Stolaroff, C. Samaras, E. R. O'Neill, A. Lubers, A. S. Mitchell and D. Ceperley. 'Energy use and life cycle greenhouse gas emissions of drones for commercial package delivery'. en. In: *Nature Communications* 9.1 (2018), p. 409. DOI: 10.1038/s41467-017-02411-5.

[4] Single European Sky ATM Research 3 Joint Undertaking. *European drones outlook study: unlocking the value for Europe*. Publications Office, 2017. URL: https://data.europa.eu/doi/10.2829/085259.

[5] F. Borghetti, C. Caballini, A. Carboni, G. Grossato, R. Maja and B. Barabino. 'The Use of Drones for Last-Mile Delivery: A Numerical Case Study in Milan, Italy'. en. In: *Sustainability* 14.3 (2022). Number: 3 Publisher: Multidisciplinary Digital Publishing Institute, p. 1766. ISSN: 2071-1050. DOI: 10.3390/su14031766.

[6] Single European Sky ATM Research 3 Joint Undertaking. *U-space : blueprint*. Publications Office, 2017. URL: https://data.europa.eu/doi/10.2829/335092.

[7] T. McCarthy, L. Pforte and R. Burke. 'Fundamental Elements of an Urban UTM'. In: *Aerospace* 7.7 (2020). ISSN: 2226-4310. DOI: 10.3390/aerospace7070085.

[8] A. Morfin Veytia, C. A. Badea, J. Ellerbroek, J. Hoekstra, N. Patrinopoulou, I. Daramouskas, V. Lappas, V. Kostopoulos, P. Menendez, P. Alonso, J. Rodrigo, V. Terrazas, D. Bereziat, A. Vidosavljevic and L. Sedov. 'Metropolis II: Benefits of Centralised Separation Management in High-Density Urban Airspace'. In: *12th SESAR Innovation Days*. 2022.

[9] J. Cho and Y. Yoon. 'Extraction and Interpretation of Geometrical and Topological Properties of Urban Airspace for UAS Operations'. In: *ATM Seminar*. 2019.

[10] EASA. *Study on the societal acceptance of Urban Air Mobility in Europe*. https://www.easa.europa.eu/en/full-report-study-societal-acceptance-urban-air-mobility-europe. 2021.

[11] E. Sunil, J. Hoekstra, J. Ellerbroek, F. Bussink, D. Nieuwenhuisen, A. Vidosavljevic and S. Kern. 'Metropolis: Relating Airspace Structure and Capacity for Extreme Traffic Densities'. en. In: *ATM seminar 2015, 11th USA/EUROPE Air Traffic Management R&D Seminar*. 2015.

[12] M. Ribeiro, J. Ellerbroek and J. Hoekstra. 'Velocity Obstacle Based Conflict Avoidance in Urban Environment with Variable Speed Limit'. In: *Aerospace* 8 (2021). DOI: 10.3390/aerospace8040093.

[13] M. Doole, J. Ellerbroek, V. L. Knoop and J. Hoekstra. 'Constrained Urban Airspace Design for Large-Scale Drone-Based Delivery Traffic'. en. In: *Aerospace* 8.2 (2021). DOI: 10.3390/aerospace8020038.

[14] E. Sunil, J. Ellerbroek, J. M. Hoekstra and J. Maas. 'Three-dimensional conflict count models for unstructured and layered airspace designs'. In: *Transportation Research Part C: Emerging Technologies* 95 (2018), pp. 295–319. ISSN: 0968-090X. DOI: 10.1016/j.trc.2018.05.031.

[15] DLR. *DLR Blueprint Concept for Urban Airspace Integration*. DLR, 2017. URL: https://www.dlr.de/de/medien/publikationen/sonstige-publikationen/2017/blueprint-concept-for-urban-airspace-integration_2933.

[16] C. Barrado, M. Boyero, L. Brucculeri, G. Ferrara, A. Hately, P. Hullah, D. Martin-Marrero, E. Pastor, A. P. Rushton and A. Volkert. 'U-Space Concept of Operations: A Key Enabler for Opening Airspace to Emerging Low-Altitude Operations'. In: *Aerospace* 7.3 (2020). ISSN: 2226-4310. DOI: 10.3390/aerospace7030024. URL: https://www.mdpi.com/2226-4310/7/3/24.

[17] OpenStreetMap contributors. *Planet dump retrieved from https://planet.osm.org*. https://www.openstreetmap.org. 2017.

[18] G. Boeing. 'OSMNX: New Methods for Acquiring, Constructing, Analyzing, and Visualizing Complex Street Networks'. In: *Computers Environment and Urban Systems* 65 (2017), pp. 126–139. DOI: 10.1016/j.compenvurbsys.2017.05.004.

[19] L. Yang, J. Qi, J. Xiao and X. Yong. 'A literature review of UAV 3D path planning'. In: *Proceeding of the 11th World Congress on Intelligent Control and Automation*. 2014, pp. 2376–2381. DOI: 10.1109/WCICA.2014.7053093.

[20] International Civil Aviation Organisation. *Annex 10 - Aeronautical Telecommunications - Volume I - Radio Navigational Aids*. 7th ed. ICAO, 2018. ISBN: 978-92-9265-233-3.

[21] J. Hoekstra and J. Ellerbroek. 'BlueSky ATC Simulator Project: an Open Data and Open Source Approach'. In: *International Conference for Research on Air Transportation*. 2016.

4

Decentralised traffic management for constrained urban airspace: dynamically generating and acting upon aggregate flow data

The previous chapter (Ch. 3) analysed the importance of vertical airspace organization in urban environments. This chapter shifts the focus to effective utilization of the horizontal space in constrained environments. Due to the dynamic nature of urban traffic, strategic planning may not be feasible because missions may not be known with enough lead-time.

This chapter introduces a decentralised approach to airspace management, where aircraft leverage real-time flow data to navigate efficiently and avoid areas of high traffic complexity and density. This dynamic strategy aims to improve airspace safety while not overly increasing extra distance travelled.

This chapter is based on the following publications:

- A. Morfin Veytia, J. Ellerbroek and J. Hoekstra. 'Decentralised Traffic Management for Constrained Urban Airspace: Dynamically Generating and Acting Upon Aggregate Flow Data'. In: *Journal of Open Aviation Science* 2.1 (2024). DOI: 10.59490/joas.2024.7716. URL: https://journals.open.tudelft.nl/joas/article/view/7716

Abstract

There are several efforts to explore employing drones to replace ground transportation in cities. However, this would mean that the expected traffic densities would be significantly higher than existing air traffic management. A decentralised system for traffic management may be necessary in this future because (1) not all airspace actors will want to freely share data, (2) the uncertainty of missions due to wind or other factors could make a previous plan inoperable, and (3) the ad hoc nature of urban missions makes them difficult to plan in advance. This work focuses on the challenges of drone operations within constrained urban airspace. We define constrained airspace as a virtual network overlaid on the physical environment, where tall buildings and urban infrastructure dictate the allowed routes. Drones are restricted to flying within this virtual network, either above the existing street network or along other predetermined segments. A dynamic and decentralised traffic management method is presented. The method uses current aggregate flow data to identify and alter the cost of travelling through high-density clusters. The goal is to reduce local traffic density and complexity by encouraging alternate routes. Three different clustering strategies are presented that look at the current position of aircraft and recent safety events. The dynamic traffic management method is first illustrated with two simple example scenarios. Then an experiment is conducted with different traffic demand levels within the city of Rotterdam. It was observed that when using traffic complexity indicators, the method is able to reduce safety events by 30 percent while only increasing the distance travelled by 6 percent.

4.1. Introduction

Ground transportation within urban areas creates congestion, which worsens air quality due to the increased number of vehicles on the road and results in economic losses [2]. A solution may be to transfer a portion of ground transportation to the air, as it has the potential to be more beneficial for the environment [3, 4]. Several government-led research initiatives focusing on drone operations [5–8] illustrate that there is significant interest in exploring urban drone operations to mitigate issues arising from ground transportation.

An estimate by the European Union predicts 400,000 drones in operation by 2040 [9]. This would result in urban air traffic densities that are significantly higher than traditional air traffic management [10]. Moreover, a significant difference with conventional aviation is that air traffic in cities will need to regularly avoid both dynamic (other aircraft) and static (buildings and geofences) obstacles

In major urban areas, aircraft may need to operate within a constrained airspace, defined here as a virtual network overlaid on the physical environment. This virtual network primarily aligns with and exists above the existing road network, but may also include other predetermined segments. In cities with tall buildings (e.g., New York), flying above the tallest structures could be inefficient. Also, even in areas with shorter buildings, it may still be necessary to fly above

the road network, as these paths are typically on public property and may be required by urban regulators. Furthermore, in areas where there are no roads, such as over busy waterways, aircraft may also need to follow the virtual network to ensure predictability. This may help the adoption of drones in cities that do not currently allow flights over busy waterways, such as the Nieuwe Mass River in Rotterdam[11].

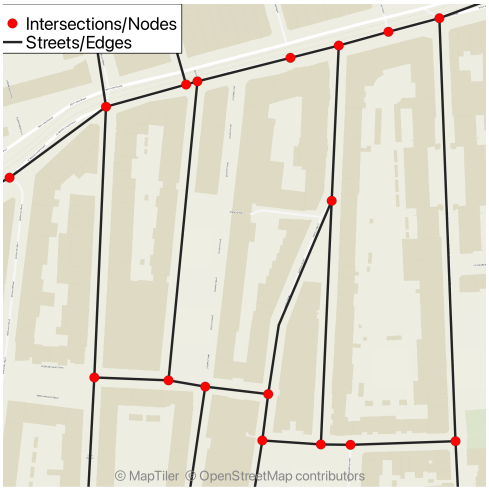

Figure 4.1: A small virtual network creates a constrained airspace in Rotterdam. The edges of the network are aligned with streets and the nodes are aligned with intersections when the network is above land.

A virtual network creates a constrained airspace that can be described as a graph with nodes and edges. The edges are generally aligned with the streets and the intersections of the edges are nodes (Fig. 4.1). In this constrained airspace, the manoeuvrability of aircraft is greatly limited. Aircraft are not able to perform heading changes to solve any potential conflicts with other aircraft. Therefore, it is important to have an even spread of traffic over the available airspace to minimize the local traffic complexity and density, as this will lead to a lower conflict probability[12].

The Metropolis II project [13] studied how separation management, flight planning, and airspace structure can be managed in a constrained urban airspace. The project concluded that a hybrid system that combines a central entity, which deconflicts aircraft prior to take-off, and allowing aircraft to perform decentralised conflict resolution was able to combine the benefits of both a centralised and decentralised system.

A question that remains, however, is to what extent central strategic planning is (economically and practically) feasible. It is for instance likely that not all airspace actors will want to freely share operational data, which would be required for central planning. Also, uncertainty of missions due to wind or other factors can make the current plan inoperable. Finally, the ad hoc nature of urban

missions makes them difficult to plan in advance in a centralised manner [14]. As such, the current work focuses on a decentralised system in which a set of dynamic rules are incorporated into the current traffic situation.

It has been observed that when following a virtual network [15, 16], drones typically share similar travel legs towards their destination, which creates hot-spots in the airspace and increases the local traffic density and complexity. Traffic complexity attempts to describe the disorder in the airspace based on aircraft interactions [17, 18]. Some measures of traffic complexity try to capture the disorder by observing the proximity and convergence of aircraft [19]. The more convergence present in the airspace, the more unsafe it can become. Additionally, following a virtual network may force aircraft trajectories to converge at the intersections. This makes it a difficult problem to mitigate, especially in a decentralised system.

Previous work in traditional air traffic management [20] created a method for defining dynamic sectors based on the local density. Other works, in urban airspace, used static and historical data to identify zones of high-density traffic [21] and perform capacity management in those zones to reduce local traffic density and complexity. The current work will present a novel dynamic traffic management method that attempts to decentrally reduce local density and complexity by dynamically identifying high-density zones. The method uses real-time aggregate flow information to subdivide the airspace into low and high density zones and applies an additional cost of travel on high density areas.

The dynamic traffic management method can be summarized as follows. (1) Observations of current positions or safety incidents are gathered. The safety incidents are indicators of traffic complexity, and position is an indicator of traffic density. (2) The observations are clustered to create dynamic zones that can receive an additional cost of travel depending on the relative density. (3) Aircraft can then check (decentrally / autonomously) whether their future route intersects these dynamic clusters and update their route taking into account the updated costs. Note that this process happens continuously, the clusters always reflect a recent snapshot of the airspace. This is similar to how highway operators apply speed limits or metering of lanes during rush hour.

The individual agents or drones are responsible for adjusting their own routes that account for the additional cost of travel and find a new optimal path. This will increase the flight distance as aircraft are incentivized to avoid the clustered areas. This creates a trade-off between safety and efficiency when a longer route is chosen.

The dynamic traffic management method will be tested in a simulated urban environment. First, the overall method will be presented along with two example scenarios. The example scenarios are meant to illustrate how the dynamic traffic management method behaves under simplified traffic patterns. Then, the method will be tested in an experiment using a city-wide demand estimation of the city of Rotterdam [22].

4.2. Method: Using aggregate flow data for dynamic traffic management

This section will outline the method used for performing dynamic traffic management in a constrained urban environment. The method uses aggregate flow statistics to identify and apply additional cost of travel to high-density zones in the airspace. The aggregate flow statistics can be the current position of aircraft or safety events.

Two different but related safety events (conflicts and intrusions) are considered. State-based conflict detection linearly extends the position of aircraft using their current state to check if an intrusion will occur in the near future. A conflict is detected when it is predicted that an aircraft will enter the protected zone of another within a certain look-ahead time. An intrusion occurs when an aircraft actually enters the protected zone of another aircraft.

The difference is illustrated in Figure 4.2. The protected zone is the dashed circle, in which the radius is the horizontal safe separation distance between aircraft (32 metres, refer to Section 4.3.2 for more information). It is up to the conflict resolution algorithm to ensure that conflicts are solved before they become intrusions. This can be done tactically by performing speed, heading, or altitude changes. In constrained airspace, this is limited to only speed or altitude changes.

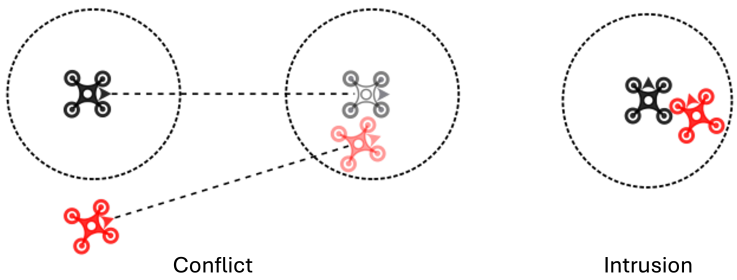

Figure 4.2: Conflict and intrusion diagram. Note that the protected zone is the dashed circle. The radius of this circle is the safe separation distance between aircraft.

The overall goal of this method is to incentivise aircraft to fly around areas with a high likelihood for conflicts, as this will lead to fewer intrusions and create additional space to tactically solve conflicts. The overall steps of this method are illustrated in Figure 4.3 and are as follows:

1. Aggregate flow data from urban airspace is gathered into clusters. Figure 4.3a.

2. The airspace is categorised into a high or low category based on the relative density observed in the clusters. An additional cost of travel is applied to high density zones, Figure 4.3b.

3. Individual aircraft check if their path will go through areas categorised as high density, Figure 4.3c.
4. Aircraft find a new optimal plan considering the additional cost of travel of the clusters, Figure 4.3d.

These steps are continuously repeated over time to provide an updated view of the airspace, occurring every 10 seconds. As a result, different clusters with varying categories are generated every 10 seconds. This 10-second interval comes from the methodology used in [13, 21] to update the densities of high-density zones.

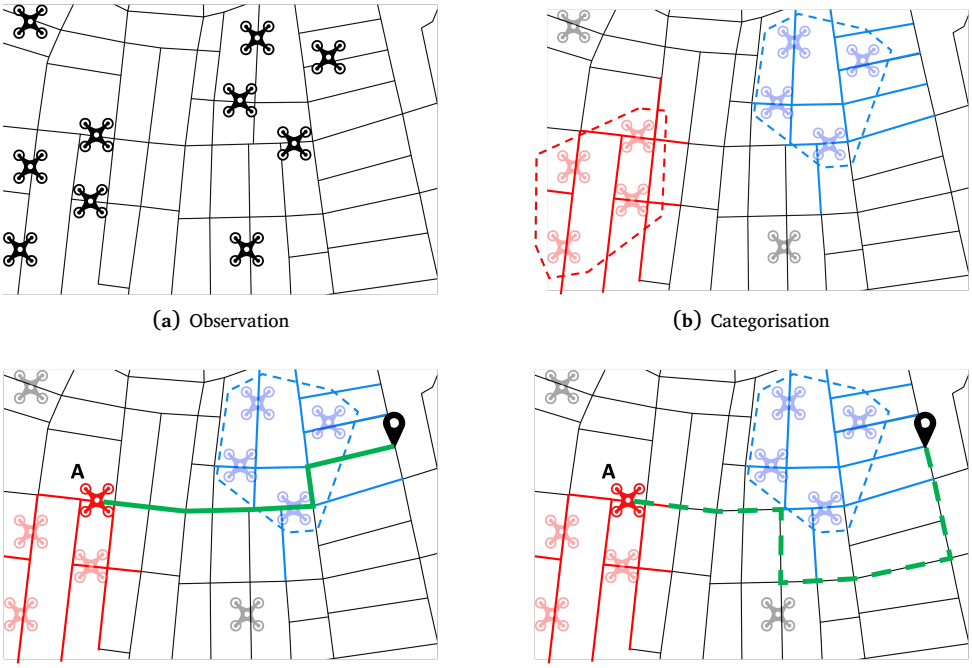

(a) Observation (b) Categorisation

(c) Original plan (d) New plan

Figure 4.3: The dynamic traffic management method. Note that in this example, the blue cluster is a high-density cluster. Drone A originally has a path that travels through the blue area. However, due to the additional cost of travel applied to the blue area, Drone A creates a new plan that avoids the blue cluster.

4.2.1. Gathering aggregate flow data

The first step in the method is to make the observation of the aggregate flow data. This work considers three different types of observation strategies to create clusters:

1. Position-based observations: This strategy gathers the current position of all aircraft.

2. Conflict-based observations: This strategy gathers the positions of all conflict events that have occurred in the past ten minutes.

3. Intrusion-based observations: This strategy gathers the position of all intrusion events that have occurred in the past ten minutes.

The observations are gathered into an observation vector, $v_{observation}$:

$$v_{observation} = \begin{bmatrix} (x_1, y_1) \\ (x_2, y_2) \\ .. \\ (x_N, y_N) \end{bmatrix} \tag{4.1}$$

Each row contains the Cartesian coordinates (x_j, y_j) of each observation and N is the total number of observations. For the position-based strategy N is the number of aircraft in the air. Alternatively, for the conflict-based and intrusion-based strategies, the observation vector containts the Cartesian coordinates of aircraft when they entered into a conflict or intrusion, respectively, within the past ten minutes.

The conflict-based and intrusion-based based observations are indicators of traffic complexity. They indicate locations where aircraft may converge (conflicts) or have converged (intrusions). On the other hand, the position-based observations are an indicator of the traffic density and does not include any past information.

4.2.2. Clustering the observations

In this study, hierarchical clustering, specifically Ward clustering [23], is employed for its distinct advantage over other methods like K-means, which require a predetermined cluster count. Ward clustering involves iteratively merging clusters to minimize the with-in cluster variance during merging. The Ward cluster distance is defined as the Euclidean distance variance when clusters are merged. A Ward distance threshold can be applied to prevent merging of clusters if the variance exceeds this threshold. This approach is similar to the variance-minimizing principle in K-means clustering. Specifically, the Ward cluster distance corresponds to half the squared Euclidean distance between the clusters [24].

$$d_{ward} = \frac{d^2_{euclidean}}{2} \tag{4.2}$$

This work sets a Ward cluster distance threshold of 4000 m^2, which is about 90 metres, for all three strategies. Note that a sensitivity analysis can be found in the supporting data set [25]. The sensitivity analysis shows how other cluster distances affect the effectiveness of the method. In general, a larger cluster distance corresponds to larger clusters. It was seen in [21] that relatively smaller clusters are preferred in dynamic traffic flow management because it allows for more flexibility to plan around them.

Applying this clustering algorithm to the 2D observation vector will return an array that contains a cluster label for each observation. These clusters are called position-based, conflict-based or intrusion-based clusters depending on the observation vector information.

4.2.3. Categorising the airspace

After each entry of the observation vector has been placed into a cluster, the airspace can be categorised into areas of relatively lower and higher density airspace. This is illustrated in Figure 4.3b. Each cluster is represented by a convex hull polygon that contains all observations inside it [26].

Density calculation

The aircraft are operating in a constrained environment in which a virtual network is followed (Fig. 4.1). Therefore, the density of a cluster is calculated by considering the summed length of the edges that intersect the cluster convex polygon as shown in Equation 4.3:

$$\text{Linear cluster density} = \frac{\text{Number of observations in cluster}}{\text{Summed length of edges intersecting polygon}} \tag{4.3}$$

Note that it is possible for clusters to intersect with the same edge or with each other. When this happens, the edge is given the categorisation of the cluster where the edge has its longest segment. Figure 4.3b illustrates how edges are linked to a convex polygon. The advantage of using 2D space for clustering and 1D space for the density calculation is that the 2D distance matrix is symmetric. This gives a clear indication of the distance between two nodes in the graph. A distance matrix in a one-way fully-connected graph may not be symmetric [27]. For example, the distance from a given node A to node B may not the same as from node B to node A. This makes the graph distance matrix non-trivial for clustering. The reason for choosing a one-way virtual network is that it has been shown to be safer than a two-way virtual network [28].

Apply an additional cost of travel

After the density of each cluster has been calculated, they can be categorised as low- or high-density based on their relative density calculated from Equation 4.3. For this work, the densities are categorised based on percentiles. The clusters in the lower 25th percentile are labelled as low-density and no cost multiplier is applied. Clusters that are above the 25th percentile are labelled as high-density (refer to the sensitivity analysis for other percentiles).

The unaltered cost of travel is simply equal to the length of the path. At the start of the mission, all aircraft plan their route with the Dijkstra algorithm [29]. The additional cost of travel applies a cost multiplier to the edges that are part

of a high-density cluster. The cost multiplier used in the city-wide scenarios is 2 (refer to the sensitivity analysis for effects of the other cost multipliers).

This method ensures that only a current view of the airspace affects the additional cost multipliers, and this is only related to the observation method. An ideal cost multiplier would increase the safety of the airspace while not forcing aircraft to fly needlessly long routes.

4.2.4. Checking and modifying the original plan

After the airspace has been categorised, each individual aircraft performs a check to see if their path goes through any high density edges. If the new plan intersects any of the high-density clusters, then a new plan is calculated. The new plan uses the Dijkstra algorithm to calculate an updated path, considering the length and additional cost multipliers.

Note that the method acts every ten seconds, therefore, there is a possibility that all aircraft replan at the same time and get into a formation where they all move to the same areas. This oscillation has been observed to happen in road traffic when people use route planning mobile apps like Google Maps [30].

4.2.5. Example scenarios

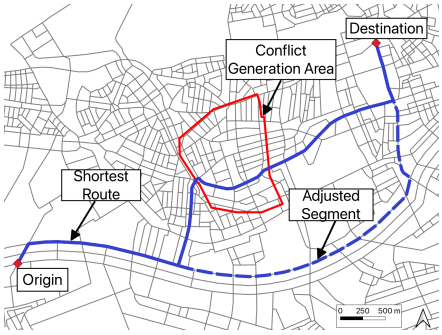

(a) Example scenario 1. In this scenario, the aircraft that follow the blue solid line pass through a conflict generation area. The next shortest route that does not pass through the conflict generation area is shown as a dashed line.

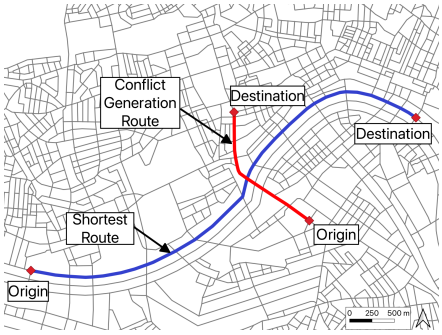

(b) Example scenario 2. In this scenario, the aircraft that follow the blue solid line pass through a conflict generation route. There is no other route that avoids the red line when applying the additional cost multiplier of 1.5.

Figure 4.4: This figure contains both example scenarios. Example scenario 1 illustrates how the three observations strategies work in the dynamic traffic management method. Example scenario 2 illustrates a scenario in which all additional paths of the blue route go through the red line. This shows that coupling the method with conflict resolution is helpful for cases where the dynamic traffic management method cannot avoid the clustered area.

This section will illustrate two example scenarios that showcase how the concept behaves in two simple cases. The example scenarios are illustrated in Figure 4.4. They are simulated in a small section of the Rotterdam virtual network using the BlueSky software (refer to Section 4.3 for more information about the airspace

and software). For a more detailed analysis of the example scenarios, refer to the supporting dataset [25].

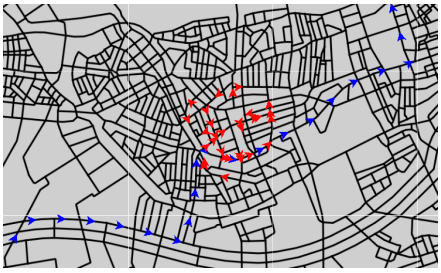

(a) Baseline (no clustering)

(b) Conflict-based clustering

(c) Intrusion-based clustering

(d) Position-based clustering

Figure 4.5: Simulation snapshot for Example scenario 1. It shows each different observation strategy and a baseline (no clustering) case that does not use the dynamic traffic management method. The red arrows represent individual aircraft flying in the conflict generation area. The blue arrows represent individual aircraft that were initially given the shortest route through the conflict generation area.

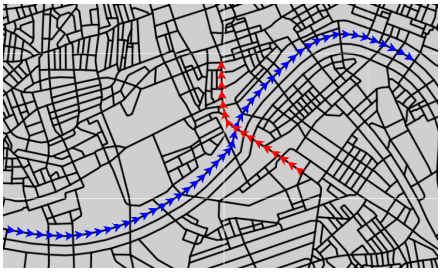

(a) Baseline (no clustering)

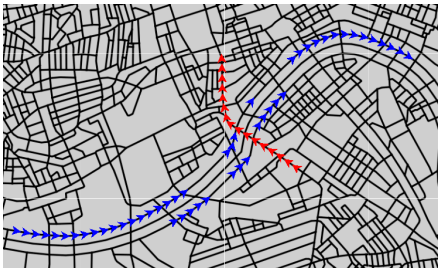

(b) Conflict-based clustering

Figure 4.6: Simulation snapshot for Example scenario 2. This shows the baseline (no clustering) case and the conflict-based clustering strategy. The red arrows represent individual aircraft flying the conflict generation route. The blue arrows represent individual aircraft that were initially given the shortest route through the conflict generation route.

Example scenario 1

Figure 4.4a shows the first example scenario. This scenario illustrates how the dynamic traffic management method behaves under the three different clustering strategies. The aircraft following the blue route originally pass through a conflict generation area (red polygon). In the conflict generation area, aircraft spawn and randomly choose a destination within the area. This will create complex traffic in the conflict generation areas as aircraft are converging. The dynamic traffic management method will act and apply an additional cost of travel to observed clusters. The next shortest route that does not pass through the conflict generation area is shown in the blue dashed line.

Figure 4.5 shows a snapshot of a simulation for the three clustering strategies and a baseline case that does not use the dynamic traffic management method. The red arrows represent individual aircraft flying in the conflict generation area. The blue arrows represent individual aircraft that were initially given the shortest route through the conflict generation area. Figure 4.5a shows the baseline case. Since the dynamic traffic management method is disabled, the blue aircraft pass through the conflict generation area. Figure 4.5b shows the conflict-based clustering strategy. Here it is clear that the aircraft in blue are avoiding the high complexity traffic in the conflict generation area. Figure 4.5c shows the intrusion-based strategy. There are usually fewer intrusions than conflicts, and conflicts between aircraft occur before an intrusion. This is why the blue aircraft in the intrusion-based strategy take both paths to their destination (the shortest route and the adjusted segment). Finally, Figure 4.5d shows the position-based strategy. The clusters are created using the positions of the aircraft. Therefore, the aircraft in blue are also part of a cluster. This is why some blue aircraft take a parallel route compared to the adjusted segment. These blue aircraft are also avoiding the high complexity area. However, by taking a parallel route, the method is also making the traffic more complex for the blue aircraft.

Example scenario 2

Figure 4.4b shows the set-up for Example scenario 2. This scenario illustrates how the dynamic traffic management method may not always be able to avoid clusters without taking an excessively long route. In this case, the blue aircraft cross a stream of red aircraft. The scenario is designed so that even with an additional cost multiplier, the blue aircraft cannot avoid the red aircraft. The aim of this example scenario is to only focus on benefits provided to the blue aircraft. The red aircraft in this scenario are not allowed to replan.

Figure 4.6 shows a snapshot of a simulation for the baseline case and the conflict-based strategy. The red arrows represent individual aircraft flying the conflict generation route. The blue arrows represent individual aircraft that were initially given the shortest route through the conflict generation route. Figure 4.6a shows that the blue aircraft in the baseline case do not change their route in response to the red aircraft. Figure 4.6b shows the conflict-based clustering strategy. It is clear that some aircraft in blue are taking a different route

compared to the shortest routes. These new routes are in response to the clusters created by the observed conflicts. However, this route does not avoid crossing the red aircraft. The traffic complexity of the scenario is not simplified by the dynamic management method. Nevertheless, the dynamic traffic management method is spreading out the blue traffic to parallel edges, thereby reducing the local density at the intersections. If there is a robust conflict resolution strategy, the additional space created by the dynamic traffic management method may improve the effect of the conflict resolution algorithm.

4.3. Experimental design

The previously presented method aimed to identify and mitigate traffic hotspots to reduce the number of safety incidents (conflicts and intrusions). By dynamically redistributing aircraft, the local traffic density and complexity may be reduced, and more space can be provided for conflict resolution.

An experiment was designed to test the dynamic traffic management method under several city-wide scenarios with varying traffic demand level. The three clustering strategies will be compared against each other and to the baseline case that does not use the method.

4.3.1. Hypotheses

H1: It is hypothesized that all three clustering strategies will have higher safety levels than the baseline (no clustering). The method is expected to be able to identify locations with conflict, intrusion, and positional hot-spots.

H2: It is hypothesized that traffic complexity clusters (conflicts and intrusions) will have higher safety levels than density clusters (position). This is because complexity clusters will identify sectors where aircraft are converging. On the other hand, density clusters may increase the cost of travel to areas with a relative high traffic density but low complexity.

H3: It is hypothesized that the intrusion-based clustering will have higher safety levels than the conflict-based clustering strategy. The usage of state-based conflict detection in constrained airspace has been known to create false conflicts. Therefore, using conflicts may increase the cost of travel in more low traffic complexity areas as compared to clustering with intrusions.

These three hypotheses will be evaluated with a Wilcoxon signed-rank test [31]. The null hypothesis is that the differences between strategies is not statistically significant, therefore the listed hypotheses will be accepted when $p_{value} < 0.01$. Refer to Appendix A for the detailed results of the hypothesis testing.

4.3.2. Common Elements

The common elements of the experiment will be shown in the following section. They include the urban airspace, the traffic demand patterns, origins

and destinations, the conflict resolution algorithm, aircraft models, and the simulation software.

Rotterdam Airspace

This work simulates air traffic in the centre of Rotterdam. The Rotterdam airspace is particularly interesting because the city is traversed by the Nieuwe Maas river, see Fig. 4.7. The airspace illustrates that when the virtual network is over land, it is aligned with the street network. Additionally, in Rotterdam there are a limited number of land bridges connecting north and south. Therefore, several new drone ”bridges” have been proposed to ease congestion and ensure that the graph is well-connected (all nodes can reach all other nodes). Currently, the government of the Netherlands does not allow any drone flights over the river due to maritime operations [11]. Therefore, enhancing the predictability of drones over waterways could lead to increased acceptance over these areas.

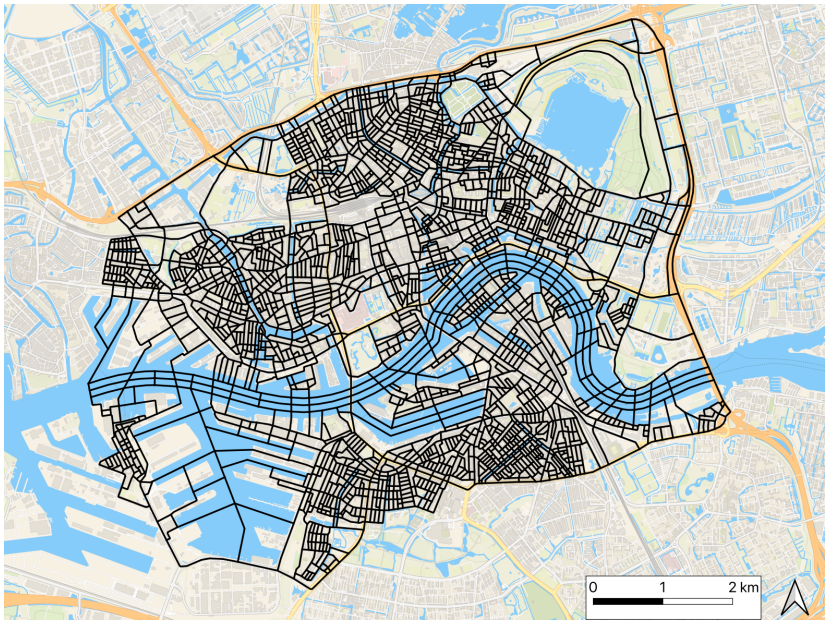

Figure 4.7: Rotterdam airspace

The process of adapting a street network to a virtual network is derived from [15]. The street network is download from OpenStreetMap [32] with osmnx [33]. After downloading, the street network is simplified by removing parallel streets, roundabouts, and dead-ends. Following the simplification, several edges are added to the virtual network that are in parallel to waterways. The distance between these parallel edges is three times the safe separation distance of aircraft. This is about the distance that an aircraft would travel with their average speed for the conflict look-ahead time of 10 seconds. Finally, the edges above land that

are dead-ends are extended to the ones parallel to the waterways.

This work assumes that all edges are one-way, since it is generally safer than two-way edges [28]. However, in a one-way non-orthogonal network, it is not apparent what the direction of each edge should be to ensure that all intersections are reachable from each other. The process of choosing the direction of the edges is described in detail in [15] and [13] and involves two important steps.

The first step is to group the edges so that edges in the same group are continuous at intersections. This is done with the Continuity in Street Networks algorithm [34] which uses the edge geometry to assign the groups based on continuity. The second step is to use a genetic algorithm to decide the direction of each group. The goal of the genetic algorithm is to (1) create a network that is strongly connected, and (2) find a suboptimal solution where the overall cost of travel between all intersections is minimized, and (3) ensure that head on situations are not created as those create high relative velocities which lead to decreased safety [35]. The result is a one-way and fully-connected virtual network with intersections that do not create head-on collisions. The final network used in this work is seen in Fig. 4.7.

Note that, the traffic management system proposed in Sec. 4.2 should be independent of the virtual network that it operates in. Therefore, the sensitivity analysis [25] shows how the method performs in the virtual network of Vienna, from [13], in which the virtual network is always above the existing street network.

Traffic demand pattern

This section will present the results of testing the method on city-wide traffic scenarios. The MASS-GT [22, 36] project made an estimate of the daily parcel demand for South Holland. With this data, each neighbourhood of Rotterdam can be given a demand percentage relative to other neighbourhoods. The relative demand of each neighbourhood can be seen in Fig. 4.8.

Origins and destinations

About two-hundred random intersections are selected as possible take-off locations (Fig. 4.8), they are at least 300 metres away from each other. Then for each possible origin, a path is created to all other intersections in the network with the following constraints. For each mission, the origin and destination are at least 1000 metres apart, and it cannot start or end in a node that is inside water. This creates around 500.000 possible routes. Each route is created with the Dijkstra algorithm [29] using the length as a cost to select the shortest route.

To create the scenarios, random origins are selected from the possible take-off locations, then a destination is selected considering the weighted probabilities of the destination nodes based on the parcel demand. All missions take place at 30 feet above the ground.

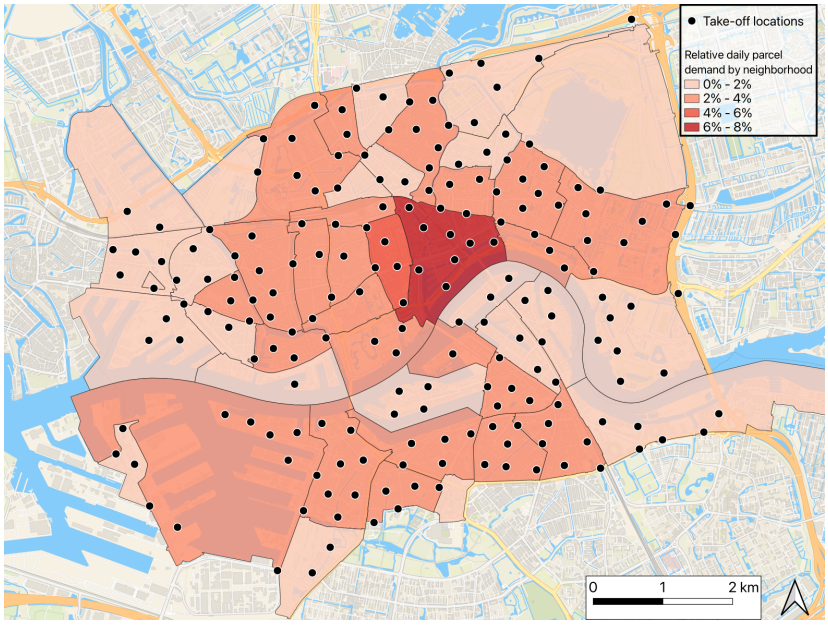

Figure 4.8: Rotterdam parcel demand with the possible take-off locations.

Conflict detection and resolution

This work uses state-based conflict detection. This method linearly extrapolates the current position of all aircraft with a given look-ahead time and checks if they will violate the protected zone (Fig. 4.2). A known effect of using state-based conflict detection in non-orthogonal constrained airspace is that it may detect false conflicts [15]. These are detected conflicts that do not actually become intrusions.

The drones in this work use a tactical speed-based conflict resolution algorithm from [37] to solve conflicts in constrained airspace. This method has a horizontal protected radius of 32 metres based on the horizontal accuracy signal-in-space requirements (Table 3.7.2.4-1) [38]. The work uses a 10 second lookahead time that was used in previous urban airspace research works [13, 15, 21, 37]. Note that the tactical conflict resolution is independent of the dynamic traffic management method, as it only forces aircraft to slow down or speed up.

Aircraft models

This work used a performance model based on the DJI Matrice 600 Pro hexacopter [39]. The model parameters are shown in Table 4.1.

Simulation software

This work used the BlueSky air traffic simulator for the experiments [40]. BlueSky is a fast-time simulator that can be extended via plugins so that a

Table 4.1: Performance model parameters.

Parameter	Value
Max. horizontal speed	12.9 m/s
Avg. horizontal speed	10.3 m/s
Min. horizontal speed	0 m/s
Max. take-off mass	15 kg
Acceleration/Deceleration	3.5 m/s^2

cluster observation strategy and flight planning module can be added. This work also made use of the Metropolis II developments for BlueSky to improve the capabilities of simulating traffic in urban environments [13].

4.3.3. Independent variables

- Dynamic traffic management method clustering strategy: baseline (no clustering), position-based, conflict-based, intrusion-based.
- Imposed traffic demand level: 100, 200, 300, 400, 500 instantaneous aircraft.

Moreover, each case is repeated 20 times with a different random seed that generate different origin-destination pairs. This creates 4 (clustering strategies + baseline) x 5 (traffic demand levels) x 20 (randomly selected random seeds) = 400 different scenarios. Each scenario has a simulation time of 2 hours. The work was simulated on an AMD Ryzen 9 5950X 16-Core Processor with 96 GB of RAM. It took about 25 hours of real time to simulate 800 hours (400 scenarios * 2 hours).

4.3.4. Dependent variables

This section will present the dependent variables used in the city-wide scenario experiment. There are three different overall categories of dependent variables (safety, efficiency and clustering). Note that the results of the first 10 minutes are ignored because that is the observation time required for the conflict-based and intrusion-based clustering strategies.

Safety: conflicts and intrusions

The safety metrics used to evaluate the results are conflicts and intrusions. However, these are not presented as absolute values. Note that because the number of intrusions and conflicts scales with the separation distance and look-ahead time, it is more useful to consider the relative difference between concepts when comparing them.

The metrics are presented in terms of conflicts and intrusions per flight. These are calculated by dividing the total amount of conflicts and intrusions by the

amount of flights. Additionally, the safety metrics are also presented per distance travelled as a percentage of the baseline (no clustering). For example, assume that the conflict-based strategy shows 105 conflicts per distance percentage. This indicates that aircraft in this clustering strategy have 5 percent more conflicts per distance travelled than aircraft travelling in the baseline.

Finally, a heat-map of the intrusions is also presented to show how the clustering strategy visually change the traffic patterns. It uses the kernel density estimation [41] with a radius of 300 metres.

Efficiency: distance travelled and number of replans

The distance travelled percentage is presented as a percentage of the total distance travelled by aircraft in the baseline.

The number of replans per flight is also presented. A replan generally indicates that the aircraft took a longer route. Note that by definition, aircraft in the baseline case do not make any replans. Note that an aircraft may receive a flight plan that it does not execute because a newer plan is issued before the previous update is implemented. Consequently, the number of replans per flight reflects only the executed updates, not the attempts.

Clustering: cluster percentage and stability

Since there is a new observation vector made every 10 seconds (Section 4.2), the clusters at one time may differ from the clusters at the next time step. If the clusters change significantly, this may affect the stability of the airspace, because there will be less coherence in replanning.

Therefore, two metrics are presented. The first is the percent of clustered airspace. This shows on average how much of the airspace is part of a cluster during each observation. The second is the cluster temporal stability. This represents the average percentage overlap of the clusters from one observation to the next. A value of 100 percent would indicate that the cluster polygons are completely identical from one observation time step to the other.

Finally, an example map of the clusters with a high density categorisation at 400 aircraft for each of the three strategies is presented to help visualise the method.

4.4. Results

This section presents the results of the city-wide scenarios. Unless noted otherwise, the box plots show the metric on the vertical axis and the imposed traffic demand level on the horizontal axis.

4.4.1. Safety: conflicts and intrusions

Fig. 4.9a shows the conflict occurrence per flight. It shows that the number of conflicts per flight increase with traffic demand level for all cases. Also,

the conflict-based strategy resulted in the lowest number of conflicts per flight, starting from 200 aircraft. The position-based and intrusion-based strategies both have a number of conflicts per flight that is similar to the baseline (no clustering) at most demand levels, except at 500 aircraft, where they are slightly lower.

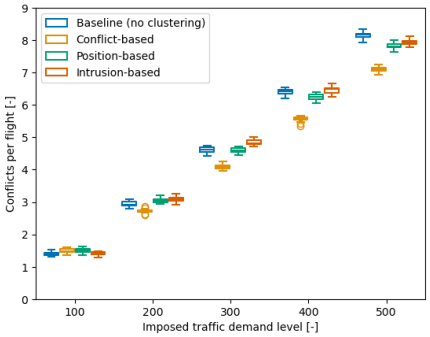

(a) Conflicts per flight.

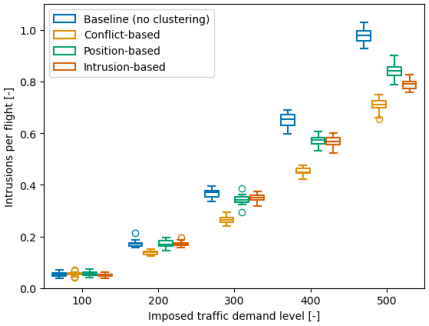

(b) Intrusions per flight.

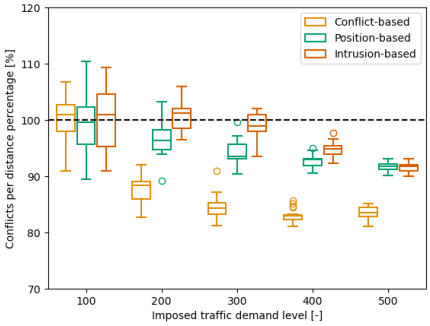

(c) Conflicts per distance percentage.

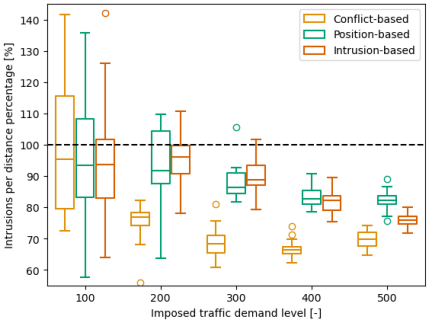

(d) Intrusions per distance percentage.

Figure 4.9: Safety: These plot show the conflicts and intrusions per flight in Fig. 4.9a and Fig. 4.9b, respectively. It also shows the conflicts and intrusions per distance percentage in Fig. 4.9c and Fig. 4.9d, respectively.

Fig. 4.9b shows the number of intrusions per flight. This plot shows that the number of intrusions per flight increase with traffic demand level. Moreover, the conflict-based strategy resulted in the lowest number of intrusions per flight at most traffic demands. The intrusion-based and position-based clustering strategies are only better than the baseline, starting at 400 aircraft. At these higher demands, the intrusion-based clustering strategy is slightly better than the position-based strategy.

Fig. 4.9c shows the occurrence of conflicts per distance as a percentage of the baseline. The baseline is illustrated by a dashed line at 100 percent. Similar to the previous plots, the conflict-based strategy has the lowest conflicts per distance percentage. Reaching the maximum improvement of 85 percent at 300

aircraft. The position-based and intrusion-based strategies are slightly below 100 percent at 300 aircraft, but are not able to reach the level of the conflict-based strategy.

Fig. 4.9d shows the occurrence of intrusions per distance as a percentage of the baseline. This plot shows that the conflict-based strategy has a 70 percent improvement from the baseline at most traffic demand levels. The position-based and intrusion-based strategies have similar values and show improvement over the baseline case at 300 aircraft. Again, they are not able to reduce the number of intrusions per distance travelled as much as the conflict-based strategy.

Fig. 4.10 shows a cumulative intrusion map for one scenario of 400 aircraft in the air. Figs. 4.10a, 4.10b, show the baseline and conflict-based, strategies, respectively. It can be seen that the baseline case has noticeably brighter hot-spots relating to a higher number of intrusions. Note that the position-based and intrusion-based clustering strategies had a similar map as the conflict-based, so they are not shown here. (refer to the supporting dataset [25]).

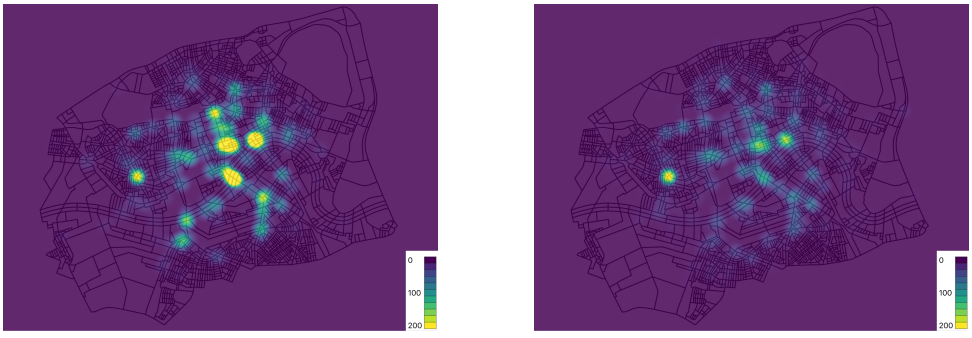

(a) Baseline (no clustering) (b) Conflict-based clustering

Figure 4.10: Safety: This figure shows the cumulative intrusion maps for one of the 400 aircraft scenarios for the baseline (no clustering) case and the conflict-based clustering strategy. The colours of the heat map represent the number of intrusions at that location.

4.4.2. Efficiency: distance travelled and number of replans

Fig. 4.11a shows the distance travelled as a percentage of the baseline case. The plot shows that all clustering strategies force aircraft to travel longer than the baseline. However, this increase never exceeds 10 percent of the baseline value. The intrusion-based clustering strategy forces aircraft to travel the least amount of distance at 100 and 200 aircraft as compared to the other strategies. Interestingly, it has the highest distance travelled at 400 and 500 aircraft. The conflict-based strategy has slightly lower distances than the position-based at most traffic demand levels. The conflict-based strategy is also the lowest at 400 and 500 aircraft.

Fig. 4.11b shows the number of replans per flight. The position-based clustering strategy has the highest number of replans per flight at low demand

levels. Conversely, at the low demand levels, the intrusion-based strategy has the lowest number of replans per flight. However, starting at 300 aircraft in the air, the conflict-based strategy has the lowest number of replans per flight, while the intrusion-based has the highest. It is also interesting to note that the conflict-based and position-based strategies show a similar decreasing trend of replans per flight. On the other hand, the replans per flight in the intrusion-based strategy increases from 100 to 300 aircraft and then tapers at 400 and 500 aircraft.

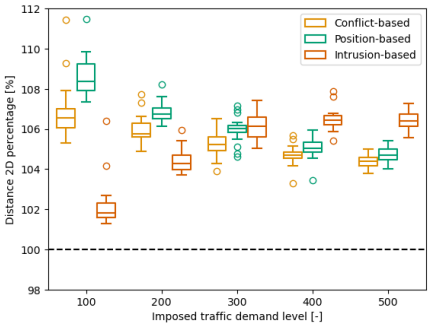

(a) Distance as percentage of the Baseline case.

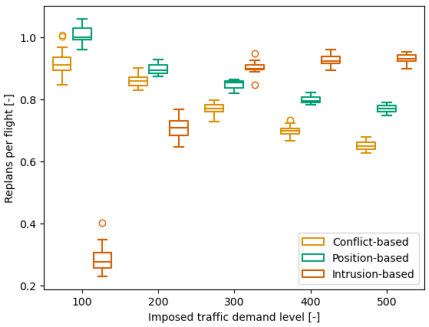

(b) Replans per flight.

Figure 4.11: Efficiency: These plot show the distance percentage and amount of replans per flight in Fig. 4.11a and Fig. 4.11b, respectively.

4.4.3. Clustering: cluster percentage and stability

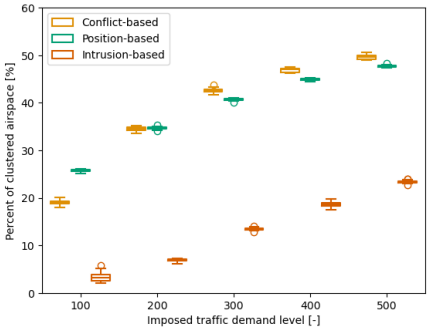

(a) Percent of clustered airspace.

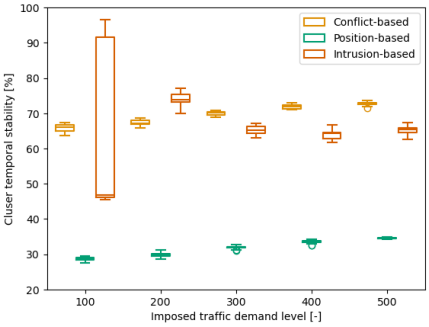

(b) Temporal cluster stability.

Figure 4.12: Clustering: These plots show the percent of clustered airspace and temporal cluster stability in Fig. 4.12a and Fig. 4.12b, respectively.

Fig. 4.12a shows the percent of the airspace that is part of a cluster. Note that at all traffic demand levels, the intrusion-based strategy has the least amount of airspace in a cluster. Varying from 5 percent to a maximum value of around 20

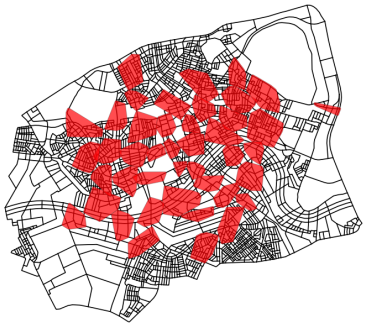

(a) Conflict-based clusters with a high density categorisation at 50 minutes of a simulation with 400 aircraft.

(b) Intrusion-based clusters with a high density categorisation at 50 minutes of a simulation with 400 aircraft.

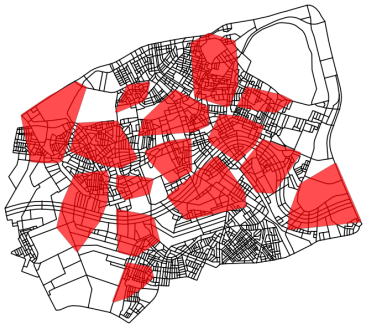

(c) Position-based clusters with a high density categorisation at 50 minutes of a simulation with 400 aircraft.

Figure 4.13: Clustering: These maps show the cluster with a high density at 50 minutes of a simulation with 400 aircraft for the three strategies.

percent. At 100 aircraft, the position-based strategy has the highest amount of clustered airspace. However, at higher demand levels the conflict-based strategy tends to have more clustered airspace, up until almost 50 percent at 500 aircraft.

Fig. 4.12b shows the cluster temporal stability. The results show that the intrusion-based strategy has a large amount of variation at 100 aircraft, this is because there are few intrusions at this density. It then stabilizes at around 65 percent for higher demand levels. The temporal stability of the conflict-based strategy slightly increases, with traffic demand reaching around 70 percent. The temporal cluster stability of the position-based strategy is the lowest for all traffic demand levels, with a maximum of 35 percent.

Fig. 4.13 shows clusters categorised as high density, at 50 minutes of a simulation with 400 aircraft in the air. Note that these plots only show a single moment in time so they should be analysed in conjuction with Figs. 4.12a and 4.12b. Fig. 4.13a shows that the conflict-based clusters are concentrated in the

middle of the airspace. Fig. 4.13b shows that there significantly less clusters identified with the intrusion-based strategy. Finally, Fig. 4.13c shows that the position-based clusters tend to spread over more of the airspace.

4.5. DISCUSSION

The dynamic traffic management method aimed to improve the overall safety of the airspace by applying an additional cost of travel to high-density clustered zones. These clustered zones are created and continually updated by using current observations of positions, conflicts, and intrusions. Each individual aircraft checks if it will intersect clustered areas and makes a new plan to avoid them. The goal is for aircraft to avoid areas with high local traffic density and complexity.

Hypothesis **H1** can only be partially accepted because the clustering strategies did not show improvements over the baseline at all traffic demand levels. When comparing the baseline to the conflict-based clustering strategy, the safety improvements over the baseline case are only significant starting at 200 aircraft in the air ($p_{value} < 0.01$). The intrusion-based and position-based strategies are only better than the baseline, starting at 300 aircraft in the air. These results indicate that the method's effectiveness depends on the presence of sufficient safety event data to form meaningful clusters.

Interestingly, the method is able to limit the extra distance travelled to less than 110 percent of the baseline case. At higher demand levels, when the method is effective for all cluster strategies, the extra distance travelled is around 106 percent of the baseline, while the intrusions per distance percentage is on average lower than 90 percent of the baseline. This shows the trade-off made in the dynamic management method between efficiency and safety.

The intrusion maps show that the clustering strategies are able to dissipate the intrusion hot-spots seen by the baseline case. At higher demand levels, all the strategies are better than the baseline case. The method has achieved the goal of dissipating the intrusion hot-spots without creating new ones due to the replanning at high demand levels. The supplemental documents [25] show the other heat-maps and some animations of the traffic.

Additionally, the results highlight the reactive nature of the dynamic traffic management method. The airspace must have clusters of positions or safety events to be able to solve them. Clusters mean that aircraft are close to each other, which then leads to conflicts and intrusions. A strategic approach might be able to solve these issues before they happen. However, for a strategic planner to work, the flight plans will need to be provided to a central entity to deconflict them prior to take-off. This could make it more difficult to deal with uncertainties such as wind. Moreover, if urban air traffic is meant to replace a portion of ground operations, the dynamic and ad-hoc nature of ground operations will also add some complexity to the strategic planner.

Hypothesis **H2** can be partially accepted. The conflict-based clustering strategy has higher safety levels than the position-based strategy, starting at 200 aircraft

in the air, ($p_{value} < 0.01$). However, the intrusion-based strategy only performs better than the position-based at 500 aircraft in the air. The clusters that take into account traffic complexity tend to have higher safety levels than those that consider traffic density for clusters. This can be seen in Example scenario 1 which shows that the position-based clustering forces aircraft to replan even when they are in a relatively low traffic complexity situation. However, it can also be seen that as the traffic demand level increases, the position-based clustering moves closer to the safety level of the conflict-based clustering.

It was observed that the aircraft replans in the position-based clusters has a similar trend than that of the conflict-based concepts. However, these replans are not as effective as reducing the number of intrusions as in the conflict-based strategy. This can be explained by two reasons: (1) the percent of clustered airspace is relatively high (maximum at 50 percent) and the cluster temporal stability is relatively low (maximum 30 percent). Therefore, the location of the clusters is not generally overlapping, causing some oscillatory effects that change the locations of the high-cost airspace. Also, because the traffic demand pattern is not uniform, the location of the high traffic density areas will vary, making traffic density a less effective clustering strategy than traffic complexity. Note that for the intrusion-based strategy, there is only a statistically significant difference with the position-based strategy at 500 aircraft in the air. Therefore, complexity metrics that indicate locations where aircraft may converge (conflicts) are generally more effective than traffic density clustering strategies. The conflict-based complexity indicator is less likely to cluster areas where there is a high traffic density but aligned aircraft (Example scenario 1).

Hypothesis **H3** is rejected. The results show that the conflict-based clustering strategy achieved a higher level of safety than the intrusion-based strategy, starting at 200 aircraft in the air. While the null hypothesis is rejected, meaning there is statistically significance when comparing these two strategies ($p_{value} < 0.01$), the trend is the opposite to what was hypothesized. It has been shown that using state-based conflict detection in constrained urban airspace tends to create false conflicts (conflicts that never become intrusions) [15]. However, the conflict-based strategy is more effective at avoiding areas with higher traffic complexity and density than the intrusion-based strategy at most traffic demands.

At lower demand levels, the number of intrusions per flight is an order of magnitude less than the conflicts per flight. Therefore, for the intrusion-based strategy, the method does not have enough information to avoid complex traffic areas. This is also why the distance travelled and replans per flight is initially low for the intrusion-based strategy, there are not many intrusion events that create clusters and force aircraft to replan at the low demand levels. At higher demand levels, there is enough information about complex traffic areas, since there are many more intrusions. This is why the intrusion-based strategy is reaching the safety levels of the conflict-based strategy.

The conflict-based strategy has both a high percent of clustered airspace and a high temporal stability. This means that the conflict-based strategy limits the

oscillatory effects seen in the position-based strategy and has enough clustered airspace to redistribute aircraft through lower cost routes. Note that the highest percentage of clustered airspace is never more than 50 percent of the total airspace. In contrast, the intrusion-based strategy has a very low amount of clustered airspace at low demand levels. This is also why aircraft travel the least amount of distance and replan the least amount of times at these low densities. There is simply not enough data to identify the high traffic complexity areas. However, as the traffic demand level increases, and there are more intrusions events, the replans per flight are the highest for the intrusion-based strategy. At these high demand levels, the intrusion-based strategy has higher safety levels than the position-based strategy and is approaching the level of the conflict-based strategy.

It is interesting to note that the intrusion-based strategy has a downward trend for the conflicts and intrusions per distance percentage. In contrast, the conflict-based strategy achieves its lowest relative gain of intrusions per distance at 200-300 aircraft. With increasing demand levels, the conflict-based strategy is not able to decrease more than 70 percent. While it shows that the conflict-based strategy is robust with the increasing demand level, it is possible that the false conflicts detected are making it difficult to keep improving.

4.6. Conclusion

It was observed that the dynamic traffic management method improves the safety of the airspace. The maximum improvement reduced the intrusions per distance to 70 percent of the baseline (no clustering). It accomplishes this without suggesting excessively long alternate routes. The distance travelled was always less than 10 percent higher than the baseline, and around 6 percent for the best performing strategy (conflict-based).

The work shows that using different aggregate flow data strategies has varying success in avoiding intrusions between aircraft. The clustering strategies that take into account traffic complexity (conflict-based and intrusion-based) were more successful than considering only traffic density (position-based). Amongst the complexity cluster strategies, the conflict-based strategy was the most successful at reducing the number of observed intrusions while limiting extra distance travelled. It is better performing than the intrusion-based strategy because it provides more information about complex traffic areas. This also means that even false conflicts, which are generally seen as unfavourable, can have some beneficial effect. However, they may also limit the performance of the method when the traffic demand levels are high. It is also possible to create a traffic complexity metric by smoothing the traffic density over a certain time limit. This adjusted position-based strategy may mitigate the issues caused by false conflicts.

The proposed method is able to show that a decentralised traffic management system is able to improve upon a baseline (no clustering) case, especially when using traffic complexity metrics. However, this should be compared against other decentralised capacity management system such as those in [21] that use

static zones. Additionally, the reactive nature of the method means that there must be a certain number of safety events observed to work effectively. This is illustrated by the improved safety performance in the intrusion-based strategy with traffic demand level. Therefore, research that combines this strategy with a more strategic planner could further improve the safety.

Further research should focus on trying to improve the understanding of this method. Mainly, it can focus on studying how the parameters, such as additional cost and cluster distance threshold, affect the effectiveness of the method on different virtual networks. It is also possible to further refine how the zones are categorised. Currently, a convex polygon is used to categorise groups of edges. This means that some edges without any traffic may be categorised as high density. However, it might be better to only consider edges where aircraft are actually flying and creating conflicts or intrusions. Moreover, rather than having two airspace categories, making the additional cost multiplier proportional to the measured density of the edges may improve the method.

Moreover, data transmission latency was not considered in this work. It should be studied in concurrence with the cluster update rate to learn the feasibility of the level of communication required. As it was observed that not all aircraft actually make new plans, further research can also focus on limiting the ratio of aircraft that are allowed to replan. It might be that only a certain number of aircraft need to alter their plans in order to see a beneficial effect on safety.

References

[1] A. Morfin Veytia, J. Ellerbroek and J. Hoekstra. 'Decentralised Traffic Management for Constrained Urban Airspace: Dynamically Generating and Acting Upon Aggregate Flow Data'. In: *Journal of Open Aviation Science* 2.1 (2024). DOI: 10.59490/joas.2024.7716. URL: https://journals.open.tudelft.nl/joas/article/view/7716.

[2] F. Creutzig, A. Javaid, N. Koch, B. Knopf, G. Mattioli and O. Edenhofer. 'Adjust urban and rural road pricing for fair mobility'. In: *Nature Climate Change* 10.7 (July 2020), pp. 591–594. ISSN: 1758-6798. DOI: 10.1038/s41558-020-0793-1. URL: https://doi.org/10.1038/s41558-020-0793-1.

[3] J. K. Stolaroff, C. Samaras, E. R. O'Neill, A. Lubers, A. S. Mitchell and D. Ceperley. 'Energy use and life cycle greenhouse gas emissions of drones for commercial package delivery'. en. In: *Nature Communications* 9.1 (2018), p. 409. DOI: 10.1038/s41467-017-02411-5.

[4] A. Raghunatha, E. Lindkvist, P. Thollander, E. Hansson and G. Jonsson. 'Critical assessment of emissions, costs, and time for last-mile goods delivery by drones versus trucks'. In: *Scientific Reports* 13.1 (July 2023), p. 11814. ISSN: 2045-2322. DOI: 10.1038/s41598-023-38922-z. URL: https://doi.org/10.1038/s41598-023-38922-z.

[5] DLR. *DLR Blueprint Concept for Urban Airspace Integration*. DLR, 2017. URL: https://www.dlr.de/de/medien/publikationen/sonstige-publikationen/2017/blueprint-concept-for-urban-airspace-integration_2933.

[6] Single European Sky ATM Research 3 Joint Undertaking. *U-space : blueprint*. Publications Office, 2017. URL: https://data.europa.eu/doi/10.2829/335092.

[7] P. Kopardekar, J. Rios, T. Prevot, M. Johnson, J. Jung and J. E. Robinson III. 'UAS Traffic Management (UTM) Concept of Operations to Safely Enable Low Altitude Flight Operations'. In: *16th AIAA Aviation Technology, Integration, and Operations Conference*. 2016. DOI: 10.2514/6.2016-3292.

[8] FAA. *Urban Air Mobility Concept of Operations*. Tech. rep. Version 2.0. Federal Aviation Administration, 2023. URL: https://www.faa.gov/sites/faa.gov/files/Urban%20Air%20Mobility%20%28UAM%29%20Concept%20of%20Operations%202.0_0.pdf.

[9] Single European Sky ATM Research 3 Joint Undertaking. *European drones outlook study: unlocking the value for Europe*. Publications Office, 2017. URL: https://data.europa.eu/doi/10.2829/085259.

[10] M. Doole, J. Ellerbroek and J. Hoekstra. 'Estimation of traffic density from drone-based delivery in very low level urban airspace'. en. In: *Journal of Air Transport Management* 88 (2020), p. 101862. DOI: 10.1016/j.jairtraman.2020.101862.

[11] Government of the Netherlands. *GoDrone Interactive Map*. https://map.godrone.nl/. Accessed: 2024-08-20.

[12] E. Sunil, J. Ellerbroek, J. M. Hoekstra and J. Maas. 'Three-dimensional conflict count models for unstructured and layered airspace designs'. In: *Transportation Research Part C: Emerging Technologies* 95 (2018), pp. 295–319. ISSN: 0968-090X. DOI: 10.1016/j.trc.2018.05.031.

[13] A. Morfin Veytia, C. A. Badea, J. Ellerbroek, J. Hoekstra, N. Patrinopoulou, I. Daramouskas, V. Lappas, V. Kostopoulos, P. Menendez, P. Alonso, J. Rodrigo, V. Terrazas, D. Bereziat, A. Vidosavljevic and L. Sedov. 'Metropolis II: Benefits of Centralised Separation Management in High-Density Urban Airspace'. In: *12th SESAR Innovation Days*. 2022.

[14] S. Bharadwaj, S. Carr, N. Neogi and U. Topcu. 'Decentralized Control Synthesis for Air Traffic Management in Urban Air Mobility'. In: *IEEE Transactions on Control of Network Systems* 8.2 (2021), pp. 598–608. DOI: 10.1109/TCNS.2021.3059847.

[15] C. Badea, A. Morfin Veytia, M. Ribeiro, M. Doole, J. Ellerbroek and J. Hoekstra. 'Limitations of Conflict Prevention and Resolution in Constrained Very Low-Level Urban Airspace'. In: *11th SESAR Innovation Days*. 2021.

[16] M. Doole, J. Ellerbroek and J. M. Hoekstra. 'Investigation of Merge Assist Policies to Improve Safety of Drone Traffic in a Constrained Urban Airspace'. In: *Aerospace* 9.3 (2022). DOI: 10.3390/aerospace9030120.

[17] D. Delahaye and S. Puechmorel. 'Air Traffic Complexity: Towards an Intrinsic Metric'. In: *Proceeding of the 3rd USA/Europe Air Traffic Management R and D Seminar*. Unknown, Unknown Region, 2000. URL: https://enac.hal.science/hal-01205255.

[18] Z. Wang, D. Delahaye, J.-L. Farges and S. Alam. 'Complexity optimal air traffic assignment in multi-layer transport network for Urban Air Mobility operations'. In: *Transportation Research Part C: Emerging Technologies* 142 (2022), p. 103776. ISSN: 0968-090X. DOI: https://doi.org/10.1016/j.trc.2022.103776. URL: https://www.sciencedirect.com/science/article/pii/S0968090X22002054.

[19] A. Vidosavljevic, D. Delahaye, E. Sunil, F. Bussink and J. Hoekstra. 'Complexity Analysis of the Concepts of Urban Airspace Design for METROPOLIS Project'. In: *EIWAC 2015, 4th ENRI International Workshop on ATM/CNS*. ENRI. Tokyo, Japan, Nov. 2015. URL: https://enac.hal.science/hal-01234078.

[20] K. Bilimoria and H. Lee. 'Analysis of Aircraft Clusters to Measure Sector-Independent Airspace Congestion'. In: *AIAA 5th ATIO and16th Lighter-Than-Air Sys Tech. and Balloon Systems Conferences*. Arlington, Virginia, 2005.

[21] N. Patrinopoulou, I. Daramouskas, C. A. Badea, A. M. Veytia, V. Lappas, J. Ellerbroek, J. Hoekstra and V. Kostopoulos. 'Dynamic Capacity Management for Air Traffic Operations in High Density Constrained Urban Airspace'. In: *Drones* 7.6 (2023). DOI: 10.3390/drones7060395.

[22] M. de Bok and L. Tavasszy. 'An empirical agent-based simulation system for urban goods transport (MASS-GT)'. In: *Procedia Computer Science* 130 (2018). The 9th International Conference on Ambient Systems, Networks and Technologies (ANT 2018) / The 8th International Conference on Sustainable Energy Information Technology (SEIT-2018) / Affiliated Workshops, pp. 126–133. ISSN: 1877-0509. DOI: https://doi.org/10.1016/j.procs.2018.04.021. URL: https://www.sciencedirect.com/science/article/pii/S1877050918303715.

[23] J. H. Ward. 'Hierarchical Grouping to Optimize an Objective Function'. In: *Journal of the American Statistical Association* 58.301 (1963), pp. 236–244. ISSN: 01621459. URL: http://www.jstor.org/stable/2282967 (visited on 28/11/2023).

[24] B. Mirkin. *Hierarchical Clustering*. en. Ed. by B. Mirkin. Undergraduate Topics in Computer Science. London: Springer, 2011, pp. 283–313. ISBN: 978-0-85729-287-2. DOI: 10.1007/978-0-85729-287-2_7. URL: https://doi.org/10.1007/978-0-85729-287-2_7 (visited on 28/11/2023).

[25] A. Morfin Veytia, J. Ellerbroek and J. Hoekstra. *Supporting data and code for Decentralised Traffic Management for Constrained Urban Airspace: Dynamically Generating and Acting Upon Aggregate Flow Data*. en. 2024. DOI: 10.4121/54825F14-8743-447D-8346-3AFA46D319D6. URL: https://data.4tu.nl/datasets/54825f14-8743-447d-8346-3afa46d319d6.

[26] S. R. Lay 1944-. 'Convex sets and their applications'. English. In: Pure and applied mathematics (John Wiley & Sons). New York: Wiley, 1982, p. 48. ISBN: 9780471095842.

[27] C. Reinhart. 'The distance matrix and its variants for graphs and digraphs'. Available at https://dr.lib.iastate.edu/handle/20.500.12876/RwyqEbkw. PhD thesis. Ames, Iowa: Iowa State University, 2021.

[28] M. Doole, J. Ellerbroek, V. L. Knoop and J. Hoekstra. 'Constrained Urban Airspace Design for Large-Scale Drone-Based Delivery Traffic'. en. In: *Aerospace* 8.2 (2021). DOI: 10.3390/aerospace8020038.

[29] E. W. Dijkstra. 'A note on two problems in connexion with graphs'. In: *Numerische mathematik* 1.1 (1959), pp. 269–271.

[30] G. Bianchin and F. Pasqualetti. 'Routing Apps May Cause Oscillatory Congestions in Traffic Networks'. In: *2020 IEEE Conference on Decision and Control*. Dec. 2020, pp. 253–260. DOI: 10.1109/CDC42340.2020.9303866.

[31] F. Wilcoxon. 'Individual Comparisons by Ranking Methods'. In: *Biometrics Bulletin* 1.6 (1945). Publisher: [International Biometric Society, Wiley], pp. 80–83. ISSN: 00994987. DOI: 10.2307/3001968. URL: http://www.jstor.org/stable/3001968 (visited on 14/08/2024).

[32] OpenStreetMap contributors. *Planet dump retrieved from https://planet.osm.org*. https://www.openstreetmap.org. 2017.

[33] G. Boeing. 'OSMNX: New Methods for Acquiring, Constructing, Analyzing, and Visualizing Complex Street Networks'. In: *Computers Environment and Urban Systems* 65 (2017), pp. 126–139. DOI: 10.1016/j.compenvurbsys.2017.05.004.

[34] P. Tripathy, P. Rao, K. Balakrishnan and T. Malladi. 'An open-source tool to extract natural continuity and hierarchy of urban street networks'. In: *Environment and Planning B: Urban Analytics and City Science* (2020). DOI: 10.1177/2399808320967680.

[35] J. Hoekstra, J. Ellerbroek, E. Sunil and J. B. Maas. 'Geovectoring: Reducing Traffic Complexity to Increase the Capacity of UAV airspace'. en. In: *2018 International Conference on Research in Air Transportation* (2018). (Visited on 02/12/2020).

[36] M. de Bok, L. Tavasszy, I. Kourounioti, S. Thoen, L. Eggers, V. M. Nielsen and J. Streng. 'Simulation of the Impacts of a Zero-Emission Zone on Freight Delivery Patterns in Rotterdam'. In: *Transportation Research Record* 2675.10 (2021), pp. 776–785. DOI: 10.1177/03611981211012694. eprint: https://doi.org/10.1177/03611981211012694. URL: https://doi.org/10.1177/03611981211012694.

[37] C. Badea, A. Morfin Veytia, J. Ellerbroek, J. Hoekstra, N. Patrinopoulou, I. Daramouskas, V. Lappas and V. Kostopoulos. 'Tactical conflict detection and resolution for a decentralised U-space traffic management system'. Unpublished. 2023.

[38] International Civil Aviation Organisation. *Annex 10 - Aeronautical Telecommunications - Volume I - Radio Navigational Aids*. 7th ed. ICAO, 2018. ISBN: 978-92-9265-233-3.

[39] DJI. *DJI Matrice 600 Pro Support Page*. Acessed in 2024. 2024. URL: https://www.dji.com/nl/support/product/matrice600-pro (visited on 14/05/2024).

[40] J. Hoekstra and J. Ellerbroek. 'BlueSky ATC Simulator Project: an Open Data and Open Source Approach'. In: *International Conference for Research on Air Transportation*. 2016.

[41] A. Gramacki. *Nonparametric kernel density estimation and its computational aspects*. English. Studies in big data; v. 37; volume 37. Cham, Switzerland: Springer, 2018. ISBN: 9783319716886. DOI: 10.1007/978-3-319-71688-6. URL: https://search.ebscohost.com/login.aspx?direct=true&scope=site&db=nlebk&db=nlabk&AN=1668756.

5

DYNAMIC CAPACITY BALANCING IN URBAN AIRSPACE: COMPARING HISTORICAL AND REAL-TIME AGGREGATE FLOW DATA

Although the previous chapter (Ch. 4) demonstrated the potential of real-time data to enhance airspace safety, it also revealed limitations in scenarios with low aircraft demand. To address this, this chapter expands on the previous approach by incorporating historical data into the decision-making process. This chapter compares the original method with a strategy that uses historical traffic patterns to identify and predict areas of high complexity, thus improving airspace safety across a wider range of demand levels.

This chapter is based on the following publication:

- A. Veytia, J. Ellerbroek and J. Hoekstra. 'Dynamic capacity balancing in urban airspace: comparing historical and real-time aggregate flow data'. In: *14th SESAR Innovation Days*. 2024

Abstract

As urban ground transportation congestion increases, there is growing interest in urban air transportation, such as delivery drones and air taxis. However, managing air traffic in densely populated urban areas poses significant challenges, which require effective flight planning, separation management, and airspace design. This paper investigates dynamic capacity balancing methods to manage air traffic in constrained urban airspace, where drones must fly above the existing road network. Specifically, it compares the effectiveness of labelling high-complexity zones using historical data versus real-time aggregate flow data. The results indicate that while both approaches reduce airspace intrusions and improve safety, the best approach depends on traffic demand levels. At lower demand levels, using historical data yields better safety outcomes, whereas using real-time data is more effective at higher demand levels due to its flexibility. At their best, both methods increase the travel distance by less than 6% while reducing airspace intrusions by 30% compared to a case without dynamic capacity balancing.

5.1. Introduction

Ground transportation is becoming increasingly dense, particularly in cities like London, where people spend an average of 148 additional hours per year in traffic congestion [2]. This growing challenge has led to interest in employing delivery drones and air taxis to alleviate ground congestion [3–6]. In addition to reducing the time spent in traffic, urban air transportation could mitigate economic losses [7] and reduce emissions [8, 9].

However, anticipated densities in urban airspace far exceed those of traditional air traffic management [10]. At such high densities, flight planning, separation management, capacity management, and urban airspace design become interdependent. Therefore, an integrated approach is essential to enable safe urban operations [11]. Moreover, in some cities, tall buildings and critical infrastructure may constrain aircraft above the existing road network, further complicating flight operations [12]. This constrained airspace limits aircraft manoeuvrability and poses unique challenges for navigation.

In constrained airspace, aircraft cannot fly directly to their destinations and must follow a network. Coupled with non-uniform traffic demand, certain legs of the network may be more preferred than others, which can create hot-spots (zones of traffic convergence). Traffic convergence leads to increased traffic complexity [13, 14], which can decrease airspace safety. To address this, capacity balancing can be used to reduce local traffic and complexity in urban airspace.

Capacity balancing can be achieved centrally, with a single entity managing take-off delays [15] or dynamic airspace modifications [16]. However, such systems rely on operators to freely share operational data. Moreover, uncertainties such as wind and operational delay can complicate central planning. The ad hoc nature of urban missions further challenges advance planning

[17]. As a result, we have previously developed decentralized dynamic capacity balancing concepts, allowing individual drones to adjust routes based on current airspace congestion [18, 19].

Our previous work on dynamic capacity balancing has utilized both real-time [18] and historical data [19] to aid in the creation of dynamic high-complexity zones so that aircraft may re-plan around them. The advantage of real-time data is that it provides current insight into airspace conditions. Conversely, historical traffic data offers a broader perspective on traffic patterns, which helps identify persistent congestion areas. This work aims to compare the performance of a dynamic capacity balancing method when relying solely on real-time data versus incorporating historical data to identify high-complexity zones. The work simulates air traffic above the city of Rotterdam under varying traffic demand levels.

Section 5.2 will explain the general capacity balancing system and explain the differences in using historical or real-time data for labelling high-complexity zones. Section 5.3 presents an experiment to compare the two methods for labelling high-complexity zones. Section 5.4 will show the results of the experiment. Finally, Sections 5.5 and 5.6 contain the Discussion and Conclusion, respectively.

5.2. Dynamic capacity balancing

Capacity balancing can be used to improve safety by reducing local traffic complexity and density in urban airspace. In this work, we perform capacity balancing by spreading traffic over the available airspace while attempting to limit the extra distance travelled (safety and efficiency trade-off). In this way, the local traffic density and complexity can be lowered dynamically. The overall process in which dynamic capacity balancing employed is as follows:

1. **Observation**: The safety events that have occurred in the past ten minutes in the airspace are gathered in the observation step. The safety events considered for the observations are unique conflict events (see Sec. Fig 5.1).

2. **High-complexity zone labelling**: Using conflict observations, the airspace is labelled into areas with high and low complexity. The areas of high-complexity airspace have an additional cost of travel.

3. **Replanning**: Aircraft use the updated cost of travel to decentrally create a new optimal route that considers the additional costs.

In this work, we consider two different methods for labelling high-complexity airspace. The first method additionally uses **historical data** to help label the airspace, while the second only uses the **real-time data** from the observation step. The historical method will use static and stable zones, while the real-time data will create dynamic zones that adapt to traffic fluctuations. Note that both

methods will use real-time data to decide which airspace zones can be considered high-complexity.

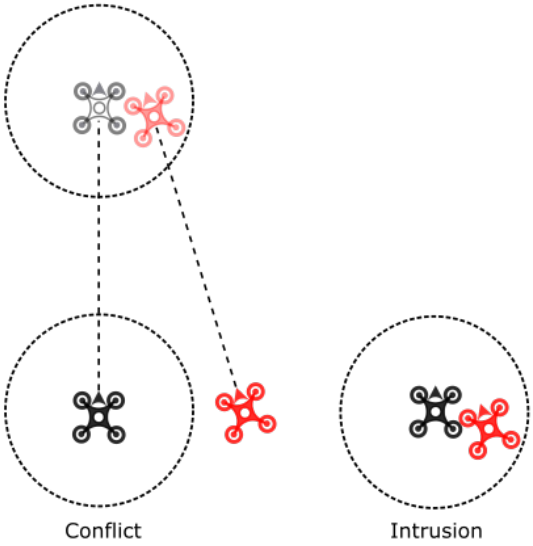

Figure 5.1: Conflict and intrusion diagram. An intrusion occurs when an aircraft enters the protected area of another aircraft (dashed circle). A conflict is counted when an aircraft is expected to become an intrusion within a lookahead time. It is up to the conflict resolution algorithm to solve conflicts before they become intrusions.

5.2.1. High-complexity labelling with historical data

Using historical traffic patterns for capacity balancing can identify general trends and locations prone to high complexity. By incorporating this historical perspective, we can remove fluctuations arising solely from real-time data, leading to more consistent labelling of high-complexity zones. Previous research has demonstrated that using historical data for capacity balancing can improve airspace safety [19]. We define historical data as the conflict locations derived from a scenario without any capacity balancing applied (see Sec. 5.3.2). It is important to note that the historical data source in this work was developed from the same traffic demand distribution as the other scenarios within the experiment. However, in practical applications, capacity balancing methods would likely need to account for variable traffic demand patterns.

Once all conflict events from the historical scenario are collected, they are clustered using Ward's method [20]. Ward clustering is a variance-minimizing approach, similar to K-means, which takes a distance threshold for merging nearby clusters (90 meters). After clustering, we use the centroid of the clusters to create a Voronoi diagram. A Voronoi diagram creates polygons in which all points in a particular polygon are always closer to its centroid than any other

centroid [21].

The resulting Voronoi diagram is illustrated in Fig. 5.2. Note that the shape and location of these zones remain constant throughout each scenario. During flight, every 10 seconds, the conflict-density of each Voronoi polygon is calculated by dividing the number of conflicts (within 10 minutes) by the total length of streets within that polygon. Subsequently, polygons with a conflict-density greater than zero are ranked based on their relative conflict-density. The top 75 percent of these polygons are then assigned an additional cost multiplier and are considered high-complexity zones. Any drone whose planned path traverses these high-complexity zones must recalculate a new path that takes this additional cost into account. The cost of travelling through a high-complexity zone is twice that of travelling through a low-complexity zone. The reason to choose 75 percent of clusters to receive the additional cost multiplier of two comes from the sensitivity analysis performed in [18].

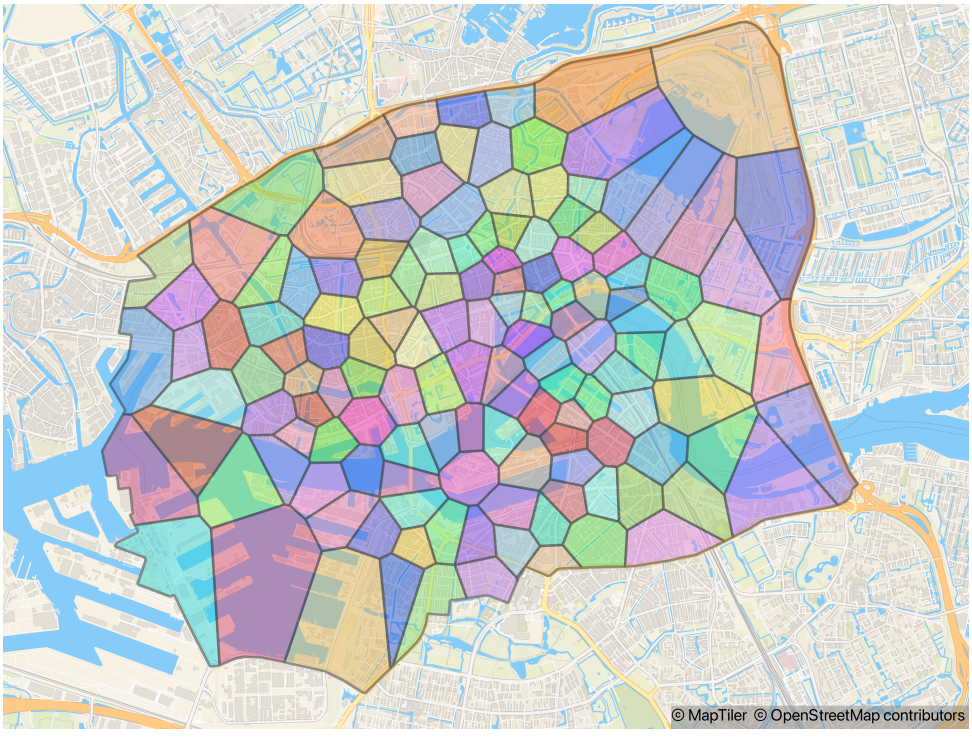

Figure 5.2: Static zones identified in Rotterdam airspace using historical conflict data. The location of these zones do not change. However, the zones labelled as high-complexity can change every 10 seconds.

5.2.2. High-complexity labelling with real-time data

Unlike labelling with historical data, using real-time conflict data for capacity balancing allows the aircraft to respond to the current condition of the airspace. This approach would be useful in mitigating situations that are not visible in the historical data timescale.

The method for high-complexity labelling with real-time data is derived from [18]. In this method, potential zones are not defined a priori: they are dynamic. Labelling the high-complexity zones only depends on the current observations. First, only the conflict events that have occurred within the last ten minutes (observations) are clustered with the Ward method. Then a convex hull polygon [22] is created which contains all members of the clusters.

Similarly to the historical data method, the conflict-density of the polygons is calculated and the top 75 percent of clusters receive the additional cost multiplier of two. An example of these dynamic high-complexity zones is seen in Fig. 5.3. Note that the size, location, shape, and label of the zones is changing every 10 seconds. All aircraft with a path that intersects these high-complexity zones must create a new optimal plan.

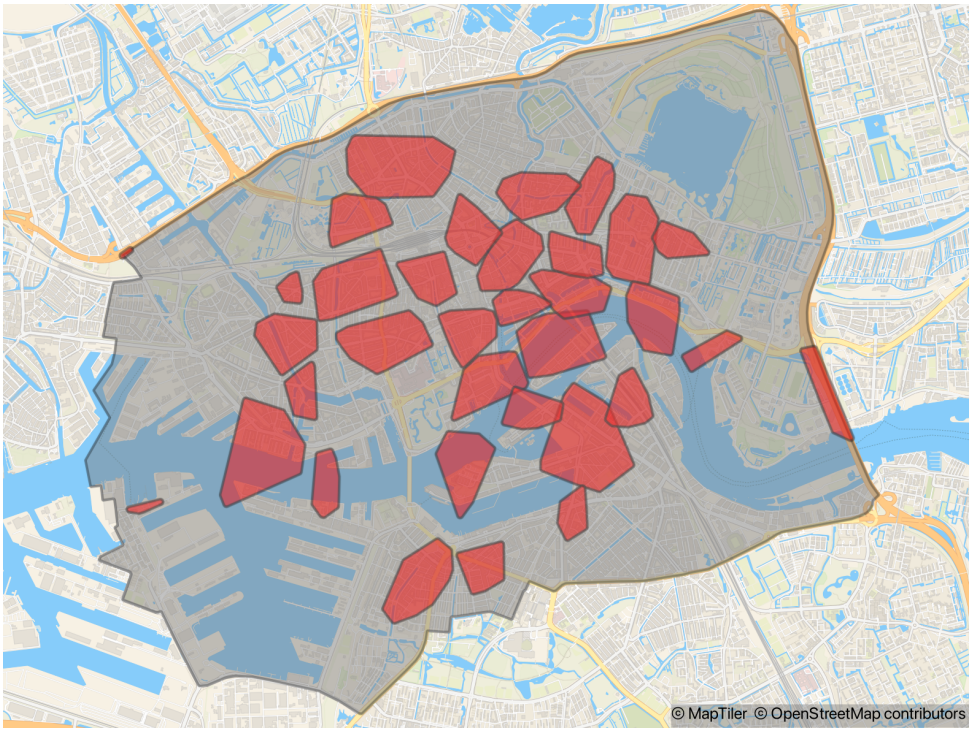

Figure 5.3: Dynamic zones identified in Rotterdam airspace using real-time conflict data. Note that the image shows the high-complexity zones at one specific moment in time. The amount, size, shape, and locations of these zones can change every 10 seconds.

5.3. Experiment

The experiment will compare using historical versus real-time data to label the high-complexity zones of a dynamic capacity balancing system. It will also present a baseline case that does not perform any dynamic capacity balancing.

5.3.1. Common Elements

Urban Airspace

The urban airspace used in this work is the city of Rotterdam (Fig. 5.4). The street network was downloaded from OpenStreetMap using the OSMNX python package [23, 24]. After downloading, the street network is processed so that roundabouts and parallel streets are simplified. Moreover, virtual 'bridges' were added to provide additional crossing points over the waterways of Rotterdam.

Previous research has shown that a one-way network for urban airspace is safer than a two-way network [25]. Therefore, a one-way network is designed to ensure that all intersections are reachable. The first step is to group continuous streets into groups using the COINS algorithm [26]. In the second step, a genetic algorithm is used to determine the directionality of the groups. More information about the urban airspace set-up can be found in [12] and [18].

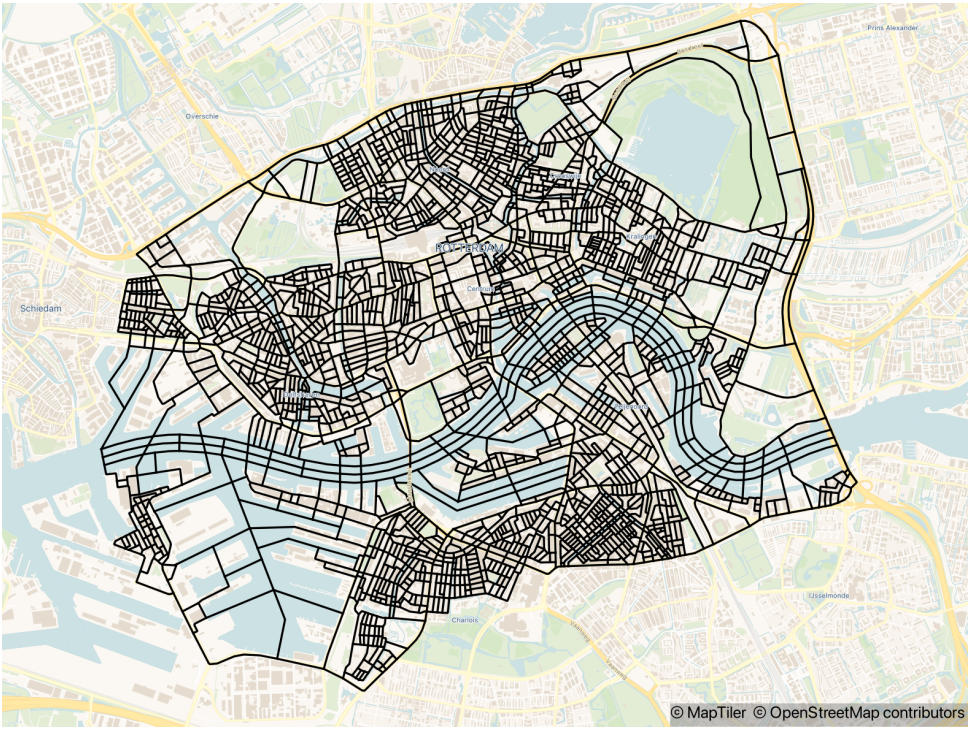

Figure 5.4: The constrained airspace in Rotterdam (Area= 50 km^2).

Aircraft missions

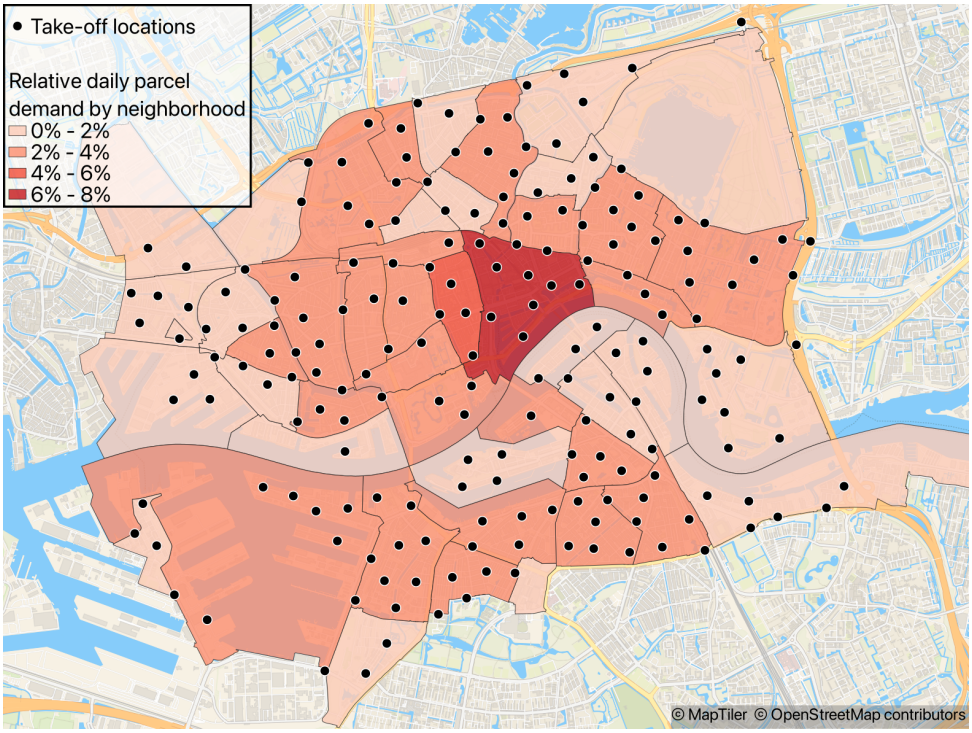

Figure 5.5: Take off locations and relative parcel demands by neighbourhood. The relative parcel demand is from the MASS-GT project [27, 28].

The MASS-GT [27, 28] project made an estimate of the neighbourhood parcel demand in the city of Rotterdam. Fig. 5.5 shows the relative demand of the neighbourhoods in the Rotterdam airspace seen from Fig. 5.4. This demand is used to create the traffic distribution considering the take-off locations and destinations.

The take-off locations for all potential missions are also shown in Fig. 5.5. They are placed at least 300 metres from each other and are ensured to be outside of water bodies. The destinations are all other nodes in the street network that are outside of water bodies. Each mission starts by randomly selecting one of the take-off locations. The destination is chosen by considering the weighted probabilities and by ensuring that the mission is at least 1000 metres long. The plan is created by finding the shortest path between the two nodes considering the length with the Dijkstra algorithm[29]. All missions take place at 30 feet above ground.

Replanning module

Aircraft that intersect any high-complexity zone in their future path must search for a new optimal plan. Since a new observation is made every ten seconds, aircraft continuously check for lower cost plans. The new plans are created by finding the shortest path between the current position and the destination with the Dijkstra algorithm. The streets in high-complexity zones receive a cost multiplier of 2.

Conflict detection and resolution

This work uses state-based conflict detection. This method linearly extrapolates the current position of all aircraft with a given look-ahead time and checks whether they will violate the protected zone (Fig. 5.1). The drones use a tactical speed-based conflict resolution algorithm from [30] to solve conflicts before they become intrusions. The method relies on a horizontal protected radius of 32 metres (Table 3.7.2.4-1)[31] and a 10 second look-ahead time. Note that a limitation of state-based conflict detection in constrained airspace is that it detects a large amount of false conflicts [12]. However, these false conflicts provide information where aircraft are near each other, so they are also taken into account for this work.

Aircraft model

All aircraft in this work are modelled after a Matrice 600 pro drone with performance parameters described in Table 5.1.

Table 5.1: DJI Matrice 600 pro drone performance parameters [32].

Parameter	Value
Max. horizontal speed	12.9 m/s
Avg. horizontal speed	10.3 m/s
Min. horizontal speed	0 m/s
Max. take-off mass	15 kg
Acceleration/Deceleration	3.5 m/s^2

Simulation software

This work used the BlueSky air traffic simulator for the experiments [33]. BlueSky is a fast-time simulator that can be extended via plugins so that different methods of labelling high-complexity zones can be compared.

5.3.2. Independent variables

The independent variables of the experiment are as follows

- Aggregate flow data labelling: Baseline (no capacity balancing), Historical data, Real-time data.
- Imposed traffic demand level: 100, 200, 300, 400, 500 simultaneous aircraft in the air. These correspond to densities of 2, 4, 6, 8, 10 $drones/km^2$, respectively. The low value is similar to what was estimated in [10], while the high value is about 2 times the highest density in [10].

Each case is repeated 5 times with a different random seed that generate different origin-destination pairs. This creates 3 (data methods + baseline) x 5 (traffic demand levels) x 5 (randomly selected random seeds) = 75 different scenarios. Each scenario simulates aircraft missions for 2 simulation hours.

The historical data scenario was created with 300 aircraft with the demand distribution in Fig. 5.5. Capacity balancing is not employed (baseline) in the historical scenario and a different random seed is used to select the origins and destinations. The conflict events of the historical scenario created the zones shown in Fig. 5.2.

5.3.3. Dependent measures

This work will use three different dependent measure categories. These are **Safety**, **Efficiency**, and **Airspace**.

Safety: conflicts and intrusions

We consider conflicts and intrusions as the relevant safety metrics. However, these are not presented in absolute terms. First, the conflicts and intrusions are scaled by the total number of flights. This gives the number of conflicts and intrusions per flight.

We also present the safety metrics scaled with the distance travelled as a percentage of the baseline case. The metrics are conflicts and intrusions per distance percentage. For example, assume the results show that using real-time or historical data yields 105 intrusions per distance percentage. This means that on average, aircraft encountered 5 percent more intrusions per distance when compared to the baseline. Conflict/intrusions per distance are useful metrics for this experiment because an aircraft with an initial identical route may fly a different route depending on the data labelling method.

Efficiency: distance travelled and number of replans

Efficiency metrics are related to how much distance aircraft fly. As the flight distance increases, the efficiency of the flight decreases. For this category, two metrics are observed.

First, the horizontal distance travelled as a percentage of the baseline case is shown. Assuming that one concept shows a distance percentage of 105 percent, it would mean that, on average, aircraft flew 5 percent more distance as compared to the baseline case without dynamic traffic management.

Second, the number of replans per flight is shown. The number of replans per flight will indicate how many times aircraft are changing their original plan. A value equal to one would show that all aircraft make on average one new plan during flight. Note that this metric is not shown for the baseline case because they do not perform any replans.

Airspace: high-complexity percentage and stability

There is an observation of the airspace made every 10 seconds to find the high-complexity zones. This means that the amount and location of airspace labelled as high-complexity can vary throughout the simulation. Therefore, two metrics related to the airspace are presented.

The first metric measures on average the percentage of airspace that is labelled as high-complexity. The second metric measures the temporal stability of high-complexity airspace. This represents the average percentage overlap of the clusters from one observation to the next. A value of 100 percent would indicate that the high-complexity airspace is completely identical from one observation time step to the other.

5.4. Results

The following section presents the results of the simulations. Unless otherwise noted, all figures show the imposed traffic demand level on the horizontal axis and the dependent variable in the vertical axis.

5.4.1. Safety: conflicts and intrusions

Figs. 5.6a and 5.6b shows the number of conflicts and intrusions per flight, respectively. Both plots show similar trends. All three concepts, baseline, historical data, and real-time data, show an upward trend in conflicts and intrusions per flight as the traffic demand increases. However, it is clear that the dynamic capacity management concepts perform better than the baseline concept. Moreover, it is seen that using real-time data for dynamic capacity management is better than historical data, especially at the higher demand levels.

Figs.5.6c and 5.6d show the conflicts and intrusions per distance as a percentage of the baseline, respectively. The dashed horizontal line represents the baseline concept. Regarding the conflicts, both the historical and real-time data concepts show little improvement over the baseline at a traffic density of 100 simultaneous aircraft. However, they both decrease to about 85 percent of the baseline at the higher demand levels, with the real-time data concept showing a slightly lower number of conflicts per distance travelled. The intrusions per distance percentage is similar but exhibits some important differences. First, at 100 aircraft in the air, it is clear that using historical data reduces the intrusions per distance to an average of 71 percent of the baseline. Meanwhile, at the same demand level, using real-time data does not show an improvement. As the demand level increases, using historical data keeps the intrusions per distance

percentage constant. However, at 300 and 400 aircraft in the air, using real-time data for dynamic capacity management show a 10 percent improvement over using historical data. At 500 aircraft in the air, using real-time data for dynamic capacity management is not as efficient as lowering the intrusions per distance percentage, as with 300 and 400 aircraft.

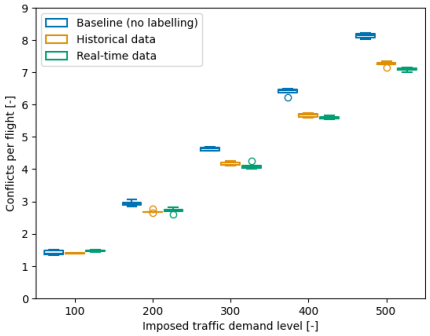

(a) Conflicts per flight.

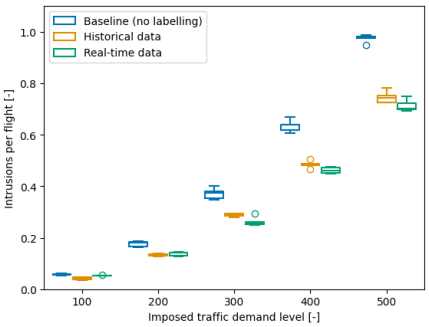

(b) Intrusions per flight.

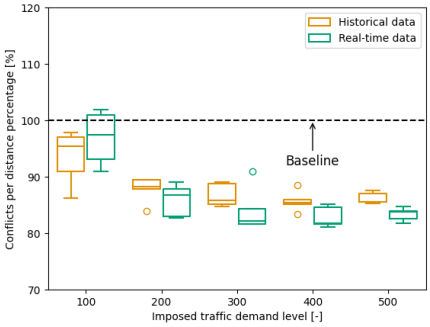

(c) Conflicts per distance percentage, where the baseline represents 100 percent.

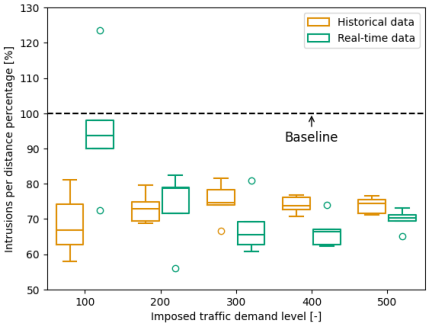

(d) Intrusions per distance percentage, where the baseline represents 100 percent.

Figure 5.6: Safety: These plot show the conflicts and intrusions per flight in Fig. 5.6a and Fig. 5.6b, respectively. It also shows the conflicts and intrusions per distance percentage in Fig. 5.6c and Fig. 5.6d, respectively.

5.4.2. Efficiency: distance travelled and number of replans

Fig. 5.7a shows the distance travelled as a percentage of the baseline concept without any dynamic capacity management. As expected, using historical and real-time data for dynamic capacity management increases the overall distance travelled. The figure also shows that as the demand level increases, the additional distance travelled also decreases when using historical and real-time data. However, it is clear that considering historical data does not increase the extra distance travelled as much as when using real-time data.

Fig. 5.7b shows the number of re-plans per flight. This shows a similar trend to Fig. 5.7a, which is that re-plans per flight tend to decrease with increasing demand level. Moreover, considering historical data for dynamic traffic management tends to reduce the number of re-plans per flight as when using real-time data.

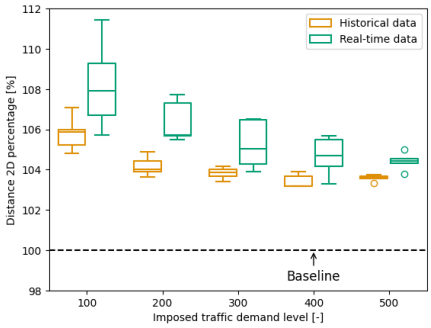

(a) Distance as percentage of the baseline case.

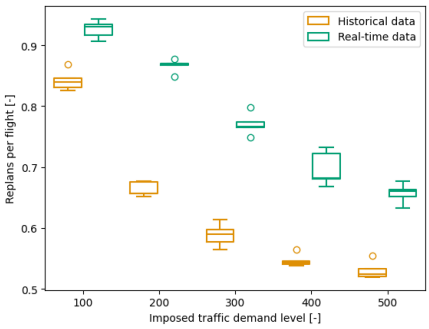

(b) Replans per flight.

Figure 5.7: Efficiency: These plots show the distance percentage and amount of replans per flight in Fig. 5.7a and Fig. 5.7b, respectively.

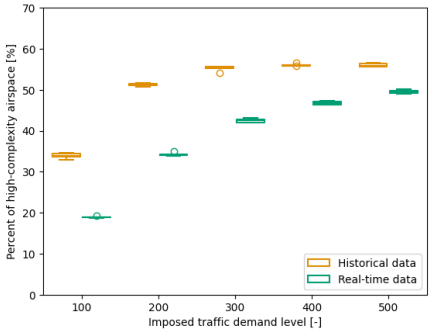

(a) Percent of high-complexity airspace.

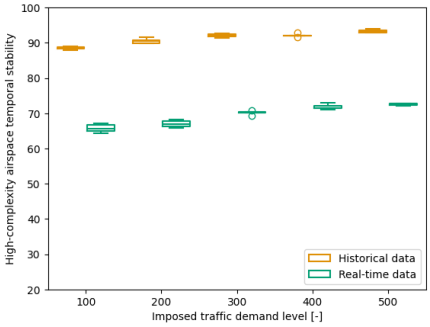

(b) High-complexity temporal stability.

Figure 5.8: Airspace: These plots show the percent of high-complexity airspace and high-complexity temporal stability in Fig. 5.8a and Fig. 5.8b, respectively.

5.4.3. Airspace: high-complexity percentage and stability

Fig. 5.8a shows the percentage of airspace that is considered high density. Using historical data for dynamic capacity management tended to label more high density compared to using real-time data. Both concepts increase the percent of high-complexity airspace with increasing demand level. However, the increase is faster at the lower demand levels and then tapers at higher demand levels.

With historical data, a maximum of 60 percent of the airspace is labelled as high-complexity, while with real-time it is less than 50 percent.

Fig. 5.8b shows the high-complexity temporal stability. Note that it measures how stable the locations of high-complexity are, an average between observations steps. A value of 100 percent indicates that high-complexity airspace does not change between observation steps. The figure exhibits that using historical data creates very stable high-complexity zones that are on average 90 percent the same from one density observation to the next step. Using real-time data for dynamic traffic management tends to have lower high-complexity stability than when using historical data. It increases from around 65 percent at lower demand levels to around 70 percent.

5.5. Discussion

5.5.1. Safety: conflicts and intrusions

Interestingly, the results showed that the strategy used to label high-complexity zones changes the effectiveness of the dynamic capacity balancing method at different demand levels. When the demand level is low (100 aircraft), using historical data was able to reduce the conflicts per distance to about 70 percent of the baseline. Meanwhile, real-time data is not as effective. This is because the historical data method is able to identify the shape of the zones that are high-complexity. This means that the stability provided by historical data is beneficial when there is not enough real-time data to create useful high-complexity zones.

However, as the airspace becomes increasingly dense, using real-time data begins to yield better results. This means that there is enough information so that the dynamic capacity balancing system can effectively reduce the number of intrusion events. Using real-time data also starts to outperform using historical data. This again shows that using historical data can help increase safety when there is not enough information in the airspace. However, with increasing density, the flexibility allowed with real-time information becomes more important in finding and avoiding high-complexity airspace.

Moreover, using real-time information tends to show constant relative improvement over the baseline in terms of intrusions. Using real-time information reaches its maximum improvement over the baseline at around 400 aircraft, and then starts to decrease in effectiveness at the highest demand level. At very high densities, there is more of a chance of encountering false conflicts. False conflicts are typically encountered in constrained airspace, when using state-based conflict detection. Due to the orientation of the street, a detected conflict may never actually become an intrusion.

5.5.2. Efficiency: distance travelled and replans

Both high-complexity labelling concepts increase the extra distance travelled as compared to the baseline by less than 10 percent, and the difference between

both is quite small. However, it is clear that as the traffic demand level increases, the aircraft travel less additional distance. Due to the increased conflicts observed in the airspace, the amount of high-complexity zone airspace increases. This makes it difficult to plan around, so there are fewer re-plans per flight. Interestingly, it also means that not all aircraft need to replan to see a beneficial effect in safety.

It can be seen that using historical data for dynamic capacity balancing makes aircraft more predictable, since they tend to perform fewer re-plans and travel less distance. However, this predictability is more useful at low demand levels when the airspace does not provide enough information to make real-time data useful. At higher demand levels, more replans per flight allow the real-time data zones to better distribute traffic.

5.5.3. Airspace: high-complexity percentage and stability

It is also seen that about 30 percent of the airspace should be high-complexity in order to see the beneficial effects in terms of intrusions. At the lowest demand level, using historical data makes 30 percent of the airspace classified as high-complexity. This is around 20 percent for when using real-time data. However, when the real-time data is at 30 percent at 200 aircraft, a relative improvement in the number of intrusions matches that of historical data. Moreover, at the higher demand levels, too much of the airspace is high-complexity as compared to real-time data, which allows the real-time data more flexibility in isolating the high-complexity zones and therefore spreading traffic better.

The airspace results also illustrate the reason why the distance travelled and number of replans per flight decrease with increasing traffic demand level for both concepts. As more of the airspace is labelled as high-complexity, more aircraft are not able to find an alternative route that decreases the overall cost of travel. Therefore, they perform less replans which means the extra distance travelled tends to decrease with density.

The predictability of using historical data is again seen in the high-complexity temporal stability. On average, about 90 percent of the airspace labelled as high density is the same from one observation time step to the next when using historical data. The predictability of the real-time data high-complexity zones only reaches a maximum of around 70 percent.

5.6. Conclusion

The aim of the study was to study the differences between using historical and real-time conflict data to create areas high-complexity with dynamic capacity balancing. The results show that a decentralised dynamic capacity balancing method always shows improvement in terms of intrusion events at low and high demand levels. However, at lower demand levels, the dynamic capacity balancing method performs better in terms of safety if it uses historical data

to label high-complexity zones because it used past information to generate the likely problematic zones.

As the traffic demand level increases, it is better for safety to use real-time data to identify high-complexity zones. The increased flexibility with real-time data means the high-complexity areas can be identified and aircraft can plan around them. Nevertheless, both data labelling methods increase the extra distance travelled by less than 6 percent while reducing the observed intrusions to around 70 percent of a case without dynamic capacity balancing. In practice, a dynamic capacity balancing should make use of both real-time and historical data. Therefore, future research should study how best to combine the benefits of both data sources.

Moreover, the historical data in this work was derived from a similar demand distribution than what was experienced in the experimental scenarios. In reality, the demand distribution can vary. Therefore, more research should be made that considers the demand distribution variation between the historical data and the actual missions, especially at low demand levels, since depending on real-time data is least effective there.

Also, both data labelling methods have a reactive nature. There need to be conflicts in the airspace so that zones can be labelled as high-complexity. This is the decentralised nature of the dynamic capacity balancing method. Therefore, research into combining this system with a more strategic approach could be beneficial.

Additionally, there are a number of limitations in the general dynamic capacity balancing method itself that require further study. Although [18] studied the effect of modifying the percentage of clusters with an additional cost-multiplier, it was still one dimensional. A more granular approach that adapts this percentage based on local density or complexity could yield better results. Similarly, other factors of the method (the 10-second update rate and the 10-minute data gathering) should be studied further. Future research should focus on how this balancing method fits within the broader U-Space framework.

References

[1] A. Veytia, J. Ellerbroek and J. Hoekstra. 'Dynamic capacity balancing in urban airspace: comparing historical and real-time aggregate flow data'. In: *14th SESAR Innovation Days*. 2024.

[2] TomTom. *Annual TomTom Traffic Index Major Traffic Trends Shaping Cities Globally in 2023*. Tech. rep. TomTom, 2023. URL: https://a.storyblok.com/f/178460/x/863802b48e/major-traffic-trends-shaping-cities-globally-in-2023-eu.pdf.

[3] Single European Sky ATM Research 3 Joint Undertaking. *U-space : blueprint*. Publications Office, 2017. URL: https://data.europa.eu/doi/10.2829/335092.

[4] SESAR. *U-space concept of operations (ConOPs) – Fourth edition*. Publications Office of the EU, 2023. DOI: doi/10.2829/207917. URL: https://data.europa.eu/doi/10.2829/207917.

[5] P. Kopardekar, J. Rios, T. Prevot, M. Johnson, J. Jung and J. E. Robinson III. 'UAS Traffic Management (UTM) Concept of Operations to Safely Enable Low Altitude Flight Operations'. In: *16th AIAA Aviation Technology, Integration, and Operations Conference*. 2016. DOI: 10.2514/6.2016-3292.

[6] FAA. *Urban Air Mobility Concept of Operations*. Tech. rep. Version 2.0. Federal Aviation Administration, 2023. URL: https://www.faa.gov/sites/faa.gov/files/Urban%20Air%20Mobility%20%28UAM%29%20Concept%20of%20Operations%202.0_0.pdf.

[7] F. Creutzig, A. Javaid, N. Koch, B. Knopf, G. Mattioli and O. Edenhofer. 'Adjust urban and rural road pricing for fair mobility'. In: *Nature Climate Change* 10.7 (July 2020), pp. 591–594. ISSN: 1758-6798. DOI: 10.1038/s41558-020-0793-1. URL: https://doi.org/10.1038/s41558-020-0793-1.

[8] J. K. Stolaroff, C. Samaras, E. R. O'Neill, A. Lubers, A. S. Mitchell and D. Ceperley. 'Energy use and life cycle greenhouse gas emissions of drones for commercial package delivery'. en. In: *Nature Communications* 9.1 (2018), p. 409. DOI: 10.1038/s41467-017-02411-5.

[9] A. Raghunatha, E. Lindkvist, P. Thollander, E. Hansson and G. Jonsson. 'Critical assessment of emissions, costs, and time for last-mile goods delivery by drones versus trucks'. In: *Scientific Reports* 13.1 (July 2023), p. 11814. ISSN: 2045-2322. DOI: 10.1038/s41598-023-38922-z. URL: https://doi.org/10.1038/s41598-023-38922-z.

[10] M. Doole, J. Ellerbroek and J. Hoekstra. 'Estimation of traffic density from drone-based delivery in very low level urban airspace'. en. In: *Journal of Air Transport Management* 88 (2020), p. 101862. DOI: 10.1016/j.jairtraman.2020.101862.

[11] T. McCarthy, L. Pforte and R. Burke. 'Fundamental Elements of an Urban UTM'. In: *Aerospace* 7.7 (2020). ISSN: 2226-4310. DOI: 10.3390/aerospace7070085.

[12] C. Badea, A. Morfin Veytia, M. Ribeiro, M. Doole, J. Ellerbroek and J. Hoekstra. 'Limitations of Conflict Prevention and Resolution in Constrained Very Low-Level Urban Airspace'. In: *11th SESAR Innovation Days*. 2021.

[13] D. Delahaye and S. Puechmorel. 'Air Traffic Complexity: Towards an Intrinsic Metric'. In: *Proceeding of the 3rd USA/Europe Air Traffic Management R and D Seminar*. Unknown, Unknown Region, 2000. URL: https://enac.hal.science/hal-01205255.

[14] A. Vidosavljevic, D. Delahaye, E. Sunil, F. Bussink and J. Hoekstra. 'Complexity Analysis of the Concepts of Urban Airspace Design for METROPOLIS Project'. In: *EIWAC 2015, 4th ENRI International Workshop on ATM/CNS*. ENRI. Tokyo, Japan, Nov. 2015. URL: https://enac.hal.science/hal-01234078.

[15] S. Chen, A. D. Evans, M. Brittain and P. Wei. 'Integrated Conflict Management for UAM With Strategic Demand Capacity Balancing and Learning-Based Tactical Deconfliction'. In: *IEEE Transactions on Intelligent Transportation Systems* 25.8 (2024), pp. 10049–10061. DOI: 10.1109/TITS.2024.3351049.

[16] Y. Tang, Y. Xu and G. Inalhan. 'An Integrated Approach for On-Demand Dynamic Capacity Management Service in U-Space'. In: *IEEE Transactions on Aerospace and Electronic Systems* 58.5 (2022), pp. 4180–4195. DOI: 10.1109/TAES.2022.3159317.

[17] S. Bharadwaj, S. Carr, N. Neogi and U. Topcu. 'Decentralized Control Synthesis for Air Traffic Management in Urban Air Mobility'. In: *IEEE Transactions on Control of Network Systems* 8.2 (2021), pp. 598–608. DOI: 10.1109/TCNS.2021.3059847.

[18] A. Morfin Veytia, J. Ellerbroek and J. Hoekstra. 'Decentralised Traffic Management for Constrained Urban Airspace: Dynamically Generating and Acting Upon Aggregate Flow Data'. In: *Journal of Open Aviation Science* 2.1 (2024). DOI: 10.59490/joas.2024.7716. URL: https://journals.open.tudelft.nl/joas/article/view/7716.

[19] N. Patrinopoulou, I. Daramouskas, C. A. Badea, A. M. Veytia, V. Lappas, J. Ellerbroek, J. Hoekstra and V. Kostopoulos. 'Dynamic Capacity Management for Air Traffic Operations in High Density Constrained Urban Airspace'. In: *Drones* 7.6 (2023). DOI: 10.3390/drones7060395.

[20] J. H. Ward. 'Hierarchical Grouping to Optimize an Objective Function'. In: *Journal of the American Statistical Association* 58.301 (1963), pp. 236–244. ISSN: 01621459. URL: http://www.jstor.org/stable/2282967 (visited on 28/11/2023).

[21] H. Edelsbrunner and R. Seidel. 'Voronoi diagrams and arrangements'. In: *Discrete & Computational Geometry* 1.1 (Mar. 1986), pp. 25–44. ISSN: 1432-0444. DOI: 10.1007/BF02187681. URL: https://doi.org/10.1007/BF02187681.

[22] S. R. Lay 1944-. 'Convex sets and their applications'. English. In: Pure and applied mathematics (John Wiley & Sons). New York: Wiley, 1982, p. 48. ISBN: 9780471095842.

[23] OpenStreetMap contributors. *Planet dump retrieved from https://planet.osm.org*. https://www.openstreetmap.org. 2017.

[24] G. Boeing. 'OSMNX: New Methods for Acquiring, Constructing, Analyzing, and Visualizing Complex Street Networks'. In: *Computers Environment and Urban Systems* 65 (2017), pp. 126–139. DOI: 10.1016/j.compenvurbsys.2017.05.004.

[25] M. Doole, J. Ellerbroek, V. L. Knoop and J. Hoekstra. 'Constrained Urban Airspace Design for Large-Scale Drone-Based Delivery Traffic'. en. In: *Aerospace* 8.2 (2021). DOI: 10.3390/aerospace8020038.

[26] P. Tripathy, P. Rao, K. Balakrishnan and T. Malladi. 'An open-source tool to extract natural continuity and hierarchy of urban street networks'. In: *Environment and Planning B: Urban Analytics and City Science* (2020). DOI: 10.1177/2399808320967680.

[27] M. de Bok and L. Tavasszy. 'An empirical agent-based simulation system for urban goods transport (MASS-GT)'. In: *Procedia Computer Science* 130 (2018). The 9th International Conference on Ambient Systems, Networks and Technologies (ANT 2018) / The 8th International Conference on Sustainable Energy Information Technology (SEIT-2018) / Affiliated Workshops, pp. 126–133. ISSN: 1877-0509. DOI: https://doi.org/10.1016/j.procs.2018.04.021. URL: https://www.sciencedirect.com/science/article/pii/S1877050918303715.

[28] M. de Bok, L. Tavasszy, I. Kourounioti, S. Thoen, L. Eggers, V. M. Nielsen and J. Streng. 'Simulation of the Impacts of a Zero-Emission Zone on Freight Delivery Patterns in Rotterdam'. In: *Transportation Research Record* 2675.10 (2021), pp. 776–785. DOI: 10.1177/03611981211012694. eprint: https://doi.org/10.1177/03611981211012694. URL: https://doi.org/10.1177/03611981211012694.

[29] E. W. Dijkstra. 'A note on two problems in connexion with graphs'. In: *Numerische mathematik* 1.1 (1959), pp. 269–271.

[30] C. Badea, A. Morfin Veytia, J. Ellerbroek, J. Hoekstra, N. Patrinopoulou, I. Daramouskas, V. Lappas and V. Kostopoulos. 'Tactical conflict detection and resolution for a decentralised U-space traffic management system'. Unpublished. 2023.

[31] International Civil Aviation Organisation. *Annex 10 - Aeronautical Telecommunications - Volume I - Radio Navigational Aids*. 7th ed. ICAO, 2018. ISBN: 978-92-9265-233-3.

[32] DJI. *DJI Matrice 600 Pro Support Page*. Acessed in 2024. 2024. URL: https://www.dji.com/nl/support/product/matrice600-pro (visited on 14/05/2024).

[33] J. Hoekstra and J. Ellerbroek. 'BlueSky ATC Simulator Project: an Open Data and Open Source Approach'. In: *International Conference for Research on Air Transportation*. 2016.

6

Urban Wind Measurement and Modelling for U-space Operations

The previous chapters focused on developing rule-sets and methods of how aircraft should navigate the horizontal and vertical airspace to improve conflict prevention.

This chapter moves to the second goal of this thesis, which is to focus on how the urban wind affects air operations. The chapter will emphasize the need for more accurate computational fluid dynamics models and wind measurements to ensure the safety of future urban air operations.

This chapter is based on the following publications:

- C. Badea, A. Morfin Veytia, J. Ellerbroek and J. Hoekstra. 'Urban Wind Measurement and Modelling for U-space Operations'. English. In: *Proceedings International Conference on Research in Air Transportation*. Ed. by E. Neiderman, M. Bourgois, D. Lovell and H. Fricke. International Conference on Research in Air Transportation, ICRAT 2024 ; Conference date: 01-07-2024 Through 04-07-2024. 2024

Abstract

Urban air mobility can be a potential solution for urban congestion, and high-level concepts of operations (e.g., UTM, U-space) have been developed with the help of large-scale simulations of multi-agent systems. However, one aspect that should be researched more is the effect of wind on the safety and efficiency of missions in an urban environment. While studies that analyse the potential effect of wind on U-space operations exist, they mostly use constant wind fields, or highly simplified wind models.

The study at hand investigates whether medium-fidelity CFD models can be used to predict and match recorded wind data in the city centre of The Hague. Six locations with distinct urban features were chosen, and wind measurements were recorded on two separate days. Using the rooftop wind properties obtained during the measurement sessions, computational fluid dynamics (CFD) simulations were performed within a large urban model of the city. Results indicate that there are large discrepancies between the simulated and measured values. Some wind phenomena observed within the measured wind data were also replicated by the CFD model. Thus, based on the results presented in this work, future research should focus on improving computer city models and wind measurement methods to ensure the development of concepts of operations that maximise the safety and efficiency of future U-space operations.

6.1. Introduction

With the increase in density of major population centres around the world, solutions for congestion are being investigated across a wide spectrum of domains. Urban air mobility holds the potential to add another mode of transportation for goods and people within high density population centres [2]. To facilitate and create an operational framework for the implementation of urban air mobility, the concept of U-space was developed [3]. This research domain focuses on the study and creation of rules to ensure the safe and efficient operations of aircraft within urban environments.

The main medium through which potential large-scale deployments of aircraft are studied is through multi-agent simulations [4–6]. These provide a feasible and fast way of determining the effects of operational decisions on the safety and efficiency of large-scale U-space systems. However, one important element that is typically understudied within such simulations is the effect of wind.

Much of the currently available research on urban wind modelling focuses on other applications and on simplified urban patters or isolated buildings [7], and are thus lacking the global picture of wind patterns at a citywide level. High-fidelity computational fluid dynamics (CFD) simulations have been run on wider areas [8] at the relatively low altitudes at which U-space operations will be conducted. However, the building and terrain models that are used in these are also simplified, and the results themselves are not validated using live-recorded data.

Methods to collect live wind data within cities have been proposed, such as the

METSIS project [9], which tested a method through which live hyperlocal wind data can be collected by aircraft in flight. This real-time method is promising for future large-scale operations, and also for the contribution it could make to help develop and verify computer-generated wind models.

However, to study and understand the effect of wind on the safety and efficiency of U-space operations through computer simulations, new wind models may need to be developed specifically for this purpose, with a degree of fidelity high enough to account for most possible scenarios, but limited in complexity as to lower computational requirements and maintain the ability to perform fast-time simulations. Realistic wind models are especially important for testing the capabilities and robustness of both tactical [10] and strategic [11–13] conflict detection and resolution algorithms and procedures.

The aim of the research at hand is to investigate whether a medium complexity CFD simulation of an urban area can produce results that are similar to live-recorded data, and determine the requirements for future work in this domain to improve large-scale multi-agent U-space simulations.

6.2. Methods

The following sections present the methods through which both simulated and live-recorded data were obtained.

6.2.1. Urban environment

The city centre of The Hague, Netherlands was chosen as the location for wind measurements. This area has a high degree of variability in terms of urban features, with diverse street widths and building heights. Six locations were chosen for this study, described below as well as presented in Fig. 6.1:

1. **Zwartebrug** (52.0798 N, 4.3222 E)
   Open area close to the central station on East-West direction.
2. **Turfmarkt 552** (52.0793 N, 4.3213 E)
   Wide street surrounded by tall buildings on East-West direction.
3. **Kalvermarkt 32** (52.0781 N, 4.3168 E)
   Wide street surrounded by medium-sized buildings on East-West direction.
4. **Voldersgracht 40** (52.0768 N, 4.3138 E)
   More narrow street surrounded by medium-sized buildings on North-South direction.
5. **Venestraat 48** (52.0772 N, 4.3101 E)
   Narrow street surrounded by low buildings on North-South direction.
6. **Papestraat 11** (52.0791 N, 4.3082 E)
   Narrow street surrounded by low buildings on East-West direction.

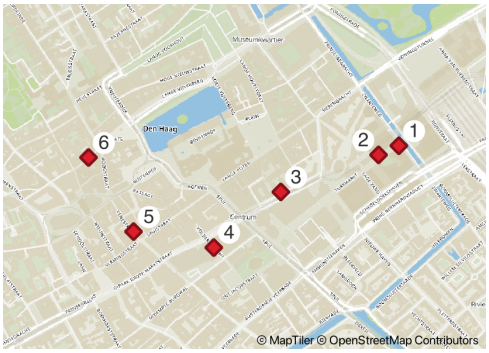

Figure 6.1: Locations chosen for data collection in The Hague.

6.2.2. Measurement instrumentation and procedure

The live wind measurements were taken on two different days of the year 2023: 11th of June and 13th of September. The instrument used to measure the wind magnitude and direction is a Bresser 5-in-1 PC Weather Station, as shown in Fig. 6.2. The sensor was attached to a pole, raising the direction sensor to a height of 217 cm above ground, and the magnitude sensor at 233 cm, to lessen the ground effects on the measurements. The station was connected to a radio data receiver, which is then connected to a computer.

The weather station was set in an open space and calibrated such that it would point in the geographical North direction. Data measurements would then be started and logged on the laptop for approximately 15 minutes with a frequency of six measurement points per minute. This data was post processed to obtain the average and the standard deviation. The data of interest within the logs consists of wind direction, wind magnitude, and wind gust level. The global wind characteristics would be recorded at the beginning of the measurement using the Meteostat[1] Python package, and is assumed constant throughout the duration of a single measurement. The Meteostat package provides open weather and climate data.

6.2.3. Computational fluid dynamics wind simulation

An Urban Computational Fluid Dynamics (CFD) simulation was used to attempt to re-create the measured wind values given the same global wind properties. Buildings inside a 1-kilometre radius circle centred in The Hague were included in the simulation. The building models were obtained from [14]. Fig. 6.3a shows the buildings included in the simulation. The goal was to include enough buildings around the measurement location such that the simulation can capture the effects of the surrounding urban landscape. The buildings were simplified to level of detail LOD1.1 [15] in order reduce the complexity of the mesh, and buildings that share a wall were merged.

[1] https://github.com/meteostat/meteostat-python (Accessed: 28-09-2023)

Figure 6.2: Instruments used to measure wind direction and magnitude: weather station, support pole, USB radio receiver, and a laptop.

The height of the buildings were taken from a publicly available government dataset [16]. Additionally, City4CFD [17] was used to generate a 3D model from the building polygons and government dataset.

The CFD domain dimensions were selected using the guidelines from [18] to create a rectangular mesh. The ground is assumed to be flat, as the variance in terrain elevation is minimal. An Open-Source CFD software (OpenFOAM [19]) was used to generate a mesh and simulate the global wind conditions of the two measurement days. Two CFD simulations were performed, one per measurement day. The mesh contains about 9 million cells. The resolution of the mesh is not constant and increase near the buildings and the ground. Near the buildings and the ground, the horizontal resolution is around 2.5 metres per cell and around 1.3 metres vertical.

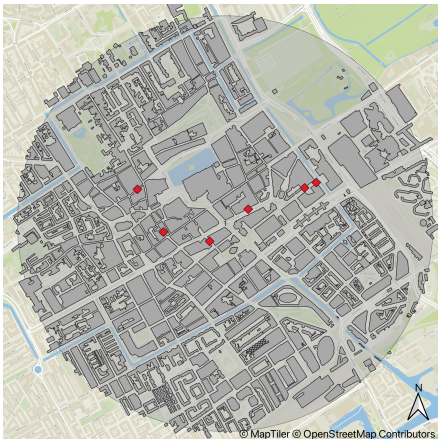

(a) Buildings included for CFD simulations.

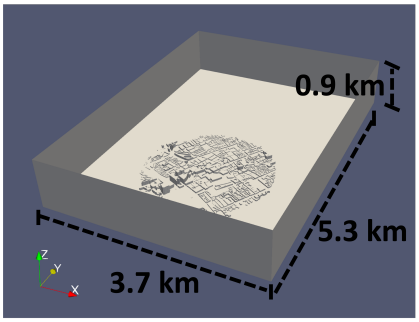

(b) CFD domain, wind is acting in the y-direction.

Figure 6.3: The buildings included in the CFD simulation and the domain.

Incompressibility can be assumed, as the wind speeds in urban areas are significantly below the speed of sound and below the transonic regime. This work uses the incompressible Reynolds-Averaged Navier Stokes (RANS) Equations, meaning the Navier Stokes equations are separated into mean and fluctuating parts using the Reynolds decomposition. The decomposed equations are then averaged over time. This creates the well-known turbulence closure problem, which requires the use of models.

This is a commonly used approach for solving urban flow problems [18]. The RANS approach solves for the average velocity field and requires the use of a turbulence model. The advantage of the RANS approach over a more accurate model, such as a Large Eddy Simulation (LES), is that it does not use nearly as much computational power and still produces robust results[20, 21]. The main drawback is that RANS cannot resolve the fluctuating components of the velocity field and therefore can only provide a modeled view of turbulence.

This work uses the standard k - ϵ (k-epsilon) model for turbulence [22], where k is the turbulent kinetic energy and ϵ is the dissipation rate. This is the typical model used for RANS simulations in urban environments, as it can provide an accurate view of the flow field [18]. The turbulent kinetic energy is defined as follows:

$$k = \frac{1}{2}(\langle uu \rangle + \langle vv \rangle + \langle ww \rangle), \tag{6.1}$$

u, v, and w are instantaneous fluctuations from the average velocities in the 3 Cartesian directions, and $\langle\rangle$ is the average operator. A low value of turbulent kinetic energy at a certain location means that the instantaneous velocity has a higher probability of matching the average velocity. Conversely, a high value of turbulence indicates that the instantaneous velocity has a lower probability of

matching the average velocity. This may mean that instantaneous velocities can be significantly higher or lower than the average value.

An inlet boundary condition of a neutral atmospheric boundary layer was used with a wall function from [23]. The reference velocity was set to 8 m/s and 6 m/s for the first and second day, respectively. In both cases, the reference height was set to 10 metres. The area around The Hague is accurately described as "very rough" due to the scattered buildings. However, in accordance to the recommendations in [18], the aerodynamic roughness parameter in the simulations ($z_0 = 0.2$) is set as "rough" [24]. Thus, the boundary layer is faster at the inlet and thus more conservative.

In accordance to the method described in [18], the simulations were performed with second-order numerical discretisation schemes. The *simpleFOAM* (Semi-Implicit Method for Pressure Linked Equations) solver [25] is used, as it is a steady-state solver for turbulent, incompressible flow that has been used previously in literature [26, 27].

One of the aims of this work is to perform a medium-fidelity simulation with relatively low computational intensity. The solution of a high-fidelity RANS simulation typically requires the flow field variables to reach numerical convergence less than 10^{-4} [18]. In these simulations, the large domain size and computational power limit the resolution of the mesh that would provide a high-fidelity solution. Therefore, the convergence criterium is relaxed to less than 10^{-2}. The velocity, dissipation, and turbulent kinetic energy converged below 10^{-3} and the pressure was less than 10^{-2}. More information about the mesh, boundary conditions, numerical schemes, as well as the source code can be found at [28].

6.3. Results

6.3.1. Global wind data

At the beginning of each measurement session, the global wind field and direction were obtained using the Meteostat Python package. As this package provides data with a frequency of one hour, both days only have two data points for this. However, on both days, the global wind did not experience significant variations in magnitude and direction during the measurement sessions, and thus the measured values were averaged, presented in Table 6.1.

Table 6.1: Average global wind values over the course of the measurement sessions, and Beaufort scale equivalent values.

Day	Speed [m/s]	Gust intensity [m/s]	Direction [deg]	BFT
1	7.9	11.4	217	4-5
2	5.6	9.1	28	3-4

6.3.2. Measured live wind results

The measured live wind data for each location is presented as wind-rose graphs in Fig. 6.4. The wind-rose graphs are placed at the approximate locations of the measurements on the map of the centre of The Hague. The radial component of the wind-rose represents the frequency that the wind blows in said direction. The colours in each individual diagram show the measured speeds in the respective direction. Data points with wind speeds below 1 m/s were excluded from the dataset. This exclusion was necessary due to the decreased measurement reliability at low wind velocities, influenced by factors like the wind direction sensor's moment of inertia and its tendency to remain in its previous position when there is no wind.

The local wind is relatively consistent in direction in most locations on both days. However, some locations experienced low wind and high direction variance: Location 3 on Day 1, and Location 1 on Day 2. Other locations, such as Location 6 on both days, and Location 2 and 4 on Day 2, experienced low wind speeds with a relatively consistent direction.

Overall, in most locations, the local wind direction is consistent with the direction of the global wind mapped onto the street bearing. However, some interesting cases occurred on both days. On the first day, there was little to no wind at Location 3, despite the street being relatively wide and parallel to the streets of Locations 1 and 2. Furthermore, Location 4 experienced local wind that was perpendicular to the street direction, even if the street is relatively narrow and the surrounding buildings relatively tall. On the second day, the local wind directions were mostly matching expectations and were consistent with the street bearings. The only anomaly on that day is seen within the low wind speed magnitude for Location 1, and consequently, the high variance in wind direction.

6.3.3. Simulated wind results

Fig. 6.5 shows the results of the CFD simulations that were performed on the city section of The Hague using the global wind properties presented in Table 6.1. In some areas, the wind direction and magnitude are relatively close to the observations, such as Locations 2, 4, and 6 on Day 1, and Locations 2 and 6 on Day 2. However, the other locations show a discrepancy in either magnitude and wind direction between the measured and the simulated values, with the first location showing the largest differences.

6.3.4. Results overview

Tables 6.2, 6.3, 6.4, and 6.5 contains a summary of the measured and simulated wind data properties. The measured wind data is described using the mean (μ) and standard deviation (σ) of the data sets, adjusted to account for the circular properties of the direction. The simulated wind data was obtained by surveying the proximity of the measurement points within the simulated data, and determining the range in which the values for speed, direction and turbulent kinetic energy are found.

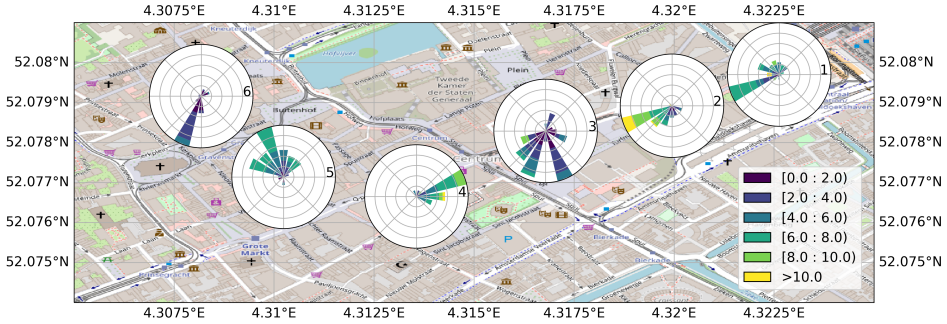

(a) Measured wind properties for the first day.

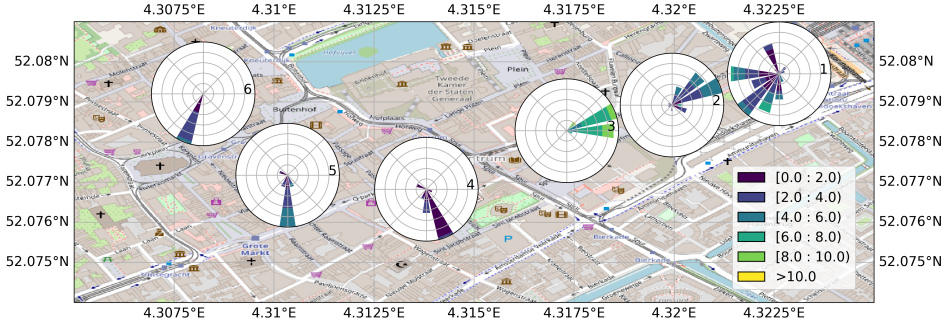

(b) Measured wind properties for the second day.

Figure 6.4: Measured data represented as wind-rose plots, speed represented in metres per second. Map courtesy of OpenStreetMap [14].

Table 6.2: Recorded wind properties for the first measurement day, with global wind magnitude of 7.9 m/s, gusts magnitude of 11.4 m/s, and direction 217 deg.

Location	Speed [m/s]		Direction [deg]		Max gust [m/s]
	μ	σ	μ	σ	
1	5.70	2.02	288	64	13.85
2	6.27	3.26	215	44	16.52
3	3.02	1.71	181	69	9.82
4	5.85	2.25	75	32	12.92
5	4.78	1.87	338	51	9.38
6	2.26	0.98	173	68	5.59

The simulated wind turbulence values are also presented in Tables 6.4 and 6.5. This metric cannot be reliably computed from the measured live data, as the latter was recorded at a single location for each measurement point, and the wind is recorded in 2 dimensions only. However, it can be related to the

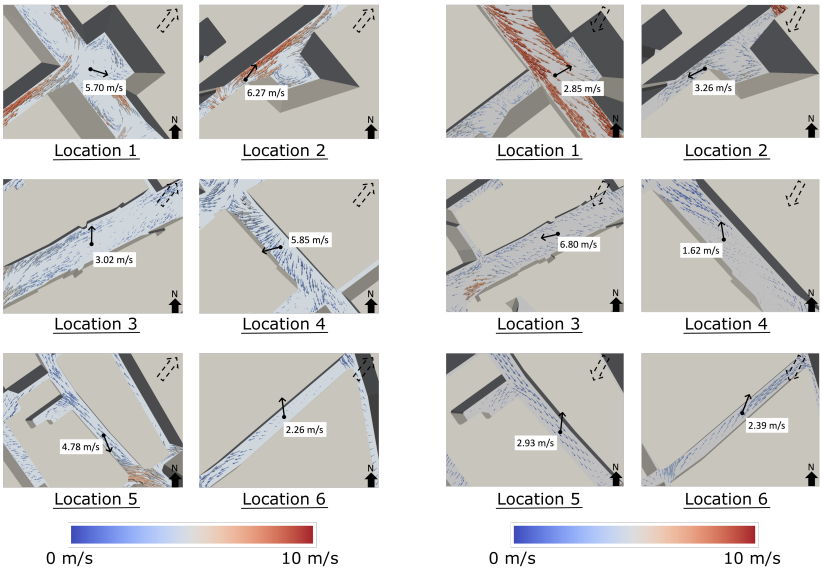

(a) Simulated wind data for the first day. **(b)** Simulated wind data for the second day.

Figure 6.5: Simulated wind velocity and direction at the measurement locations for each measurement day. The average measured magnitude and direction are shown as black arrows and labelled. The dotted arrow in each figure represents the direction of the global wind.

Table 6.3: Recorded wind properties for the second measurement day, with global wind magnitude of 5.6 m/s, gusts magnitude of 9.1 m/s, and direction 28 deg.

Location	Speed [m/s]		Direction [deg]		Max gust [m/s]
	μ	σ	μ	σ	
1	2.85	1.53	240	62	7.58
2	3.26	1.36	63	45	7.58
3	6.80	1.65	77	16	12.05
4	1.62	0.62	171	42	4.91
5	2.93	1.41	186	34	5.59
6	2.39	1.05	201	33	5.59

variation in the wind properties (variance of speed and direction, gust level).

For the first day, the most turbulent Locations were 2 and 4. If compared to the measured data in Table 6.2, these two locations had high gust values as well as the highest variance in wind speed. On the second day, the most turbulent locations were 1 and 2. This is reflected in the values presented Table 6.3, as these locations have the highest variation in wind direction, and relatively high gust levels.

For the first day, only Location 2 has matching measured and simulated results

Table 6.4: Summary of simulation results at the measurement locations for Day 1.

Location	Speed [m/s]		Direction [deg]		Turbulent kinetic energy [m^2/s^2]	
	lower bound	upper bound	lower bound	upper bound	lower bound	upper bound
1	2.0	4.0	110	170	0.1	0.4
2	5.0	6.9	235	235	1.5	2.0
3	1.0	2.5	230	250	0.2	0.3
4	1.4	3.0	30	50	0.7	1.0
5	2.0	3.5	140	140	0.2	0.4
6	0.4	1.0	80	105	0.2	0.2

Table 6.5: Summary of simulation results at the measurement locations for Day 2.

Location	Speed [m/s]		Direction [deg]		Turbulent kinetic energy [m^2/s^2]	
	lower bound	upper bound	lower bound	upper bound	lower bound	upper bound
1	6.6	6.6	300	300	1.3	1.3
2	2.9	4.5	65	75	0.3	0.4
3	1.9	2.4	90	90	0.2	0.3
4	0.2	0.8	330	8	0	0
5	1.4	1.6	320	320	0	0
6	1.9	2.7	220	220	0.2	0.2

in terms of wind speed, with the other locations being outside the value interval by a relatively large margin. In terms of wind direction, Location 2 is yet again the only point where the simulation is in agreement with the measured values, with the discrepancies being greatest for Locations 5 and 6.

The simulation data for the second day matches the measured data to a higher proportion than for the first day. For wind speed, the measured value for two locations (2 and 6) are contained within the simulated wind speed intervals. Locations 1 and 3 have relatively high discrepancies between simulated and measured values, while the simulated data of the remaining two locations (4 and 5) correctly predicts low wind speeds. In terms of wind direction, 4 locations (1, 2, 3, and 6) have simulated data values that resemble the live measurement values, with the other two locations (4 and 5) having large discrepancies.

6.4. Discussion

The results shown in the study at hand show that urban citywide wind models need to be improved to develop a complete set of rules and procedures to ensure the safe and efficient deployment of urban air mobility operations.

In most of the locations where live data was recorded, the simulations did not produce matching values. One of the locations with the greatest discrepancies was Location 1 (Zwartebrug). On the first day, a relatively strong wind with gusts up to 14 m/s was recorded in this location. However, the simulations predict a relatively calm area, with wind speeds of approximately 3 m/s.

This discrepancy may be produced by the mismatch between the real shape of the buildings and the city model. In reality, the building North-East of the measurement point is not fully solid, with a relatively large passageway on the ground level. The lack of this feature could have determined a high-pressure point to form within the simulation of Day 1, which produced lower than expected wind speeds and turbulence, and a large discrepancy in wind direction.

To mitigate this, one option could be the use of city models obtained from the creation of 3D cadastre models for buildings that have complex features should be made and used. These complex features, such as the large passageway at Location 1, affect the local wind flow, and need to be better studied. The development of such models has been underway for several years, with a steadily increasing interest [29]. However, the presence of legal, technological, and organisational impediments means that accessible citywide high-fidelity models are unavailable publicly.

In some cases, the simulations correctly predicted the magnitude and direction of the wind, most notably for Location 4 of the first day. The measurements for this day were surprising, as the wind direction was both inconsistent with the street bearing and the global wind direction. However, the simulation correctly predicted that wind in this area would not be directed along the street, like observed in other areas. This result shows that complex wind phenomena might indeed be captured within medium-fidelity simulations, and can provide valuable information about expected wind behaviour in urban environments, which should be accounted for when developing U-space concepts of operations. However, more measurements at this location are needed to confirm this.

Another notable finding of this study is that, for many measurement points, the direction of local wind was consistent with expectations based on mapping the global wind onto the bearing of the street. This can be seen for Locations 1 and 2 on Day 1 and Locations 2 and 3 on Day 2 (Fig. 6.4). Wind on streets that were less aligned to the global wind direction had a higher chance of having local wind that goes against expectations (e.g., Location 5 on both days). Thus, with more live measurements and data analysis, a set of general considerations could be developed that would help estimate expected urban wind level on streets without the need to run computationally intensive simulations.

Despite the discrepancies between measured and simulated wind values for each location, an overview of the results shows that simulations produced data within the range of measured values. Thus, realistic models can indeed be

created by only using medium-fidelity CFD methods, which would serve the purpose of better understanding the effects that wind has on aircraft within urban environments. However, a wider range of conditions need to be simulated to account for a larger variety of possible wind intensities and directions.

6.5. Conclusion

The study presented in this work aimed to investigate whether current computational fluid dynamics (CFD) methods applied on a large citywide scale can reliably predict and match wind data recorded at street level in an urban environment. Live wind data was recorded at six locations within The Hague on two different days, and compared to models generated using OpenFOAM.

Results indicate that there are large discrepancies between recorded and simulated values in terms of wind speed and direction at most of the locations. However, some unexpected observed phenomena (i.e., wind blowing perpendicular to the street bearing and opposite of rooftop wind direction at location 4 on Day 1) were correctly predicted, and the simulations provided values within the order of magnitude of the recorded values. Thus, despite some discrepancies, CFD simulations prove to be a good tool for studying wind patterns in urban environments, and for creating realistic wind models that can then be used to simulate and develop large-scale U-space operations.

More research and development is needed in several aspects of the problem at hand to produce better wind data for urban environments. Firstly, the methodology can be improved in several ways, one of which would be the use of better 3D city models to more accurately capture wind patterns in areas with complex building shapes. Most large-scale building model data sets are created by using aircraft, and are thus limited to capturing the 2D footprint of buildings. Terrain features should also be included in the analysis, such as changes in elevation and natural features (e.g., trees and water). The data quality for rooftop wind should also be improved, preferably with live measurements taken from tall buildings and vantage points, thus improving the potential accuracy of CFD simulations. Also, uncertainty in the boundary conditions, namely the reference height, velocity, and roughness parameter can affect the accuracy of the CFD results. Therefore, the methodology of the comparison can also be improved by using more accurate instruments at higher elevations than in this study to set improved boundary conditions.

Future research should pursue the development of better urban wind models and methods to capture live wind data. As wind is expected to affect U-space operations greatly, this information could be important in the development of operational concepts, with major implications in safety-critical systems (e.g., strategic and tactical conflict resolution) as well as flight planning and flow management.

ACKNOWLEDGMENTS

The authors would like to thank Dr. Clara Garcia-Sanchez from the 3Dgeoinformation group of Delft University of Technology for providing the code to create a computational mesh of The Hague.

References

[1] C. Badea, A. Morfin Veytia, J. Ellerbroek and J. Hoekstra. 'Urban Wind Measurement and Modelling for U-space Operations'. English. In: *Proceedings International Conference on Research in Air Transportation*. Ed. by E. Neiderman, M. Bourgois, D. Lovell and H. Fricke. International Conference on Research in Air Transportation, ICRAT 2024 ; Conference date: 01-07-2024 Through 04-07-2024. 2024.

[2] M. Doole, J. Ellerbroek and J. Hoekstra. 'Estimation of traffic density from drone-based delivery in very low level urban airspace'. en. In: *Journal of Air Transport Management* 88 (2020), p. 101862. DOI: 10.1016/j.jairtraman.2020.101862.

[3] CORUS consortium. *U-space Concept of Operations*. Edition 03.00.02. Vol 2.: SESAR Joint Undertaking, 2019.

[4] V. Lappas, G. Zoumponos, V. Kostopoulos, H. Shin, A. Tsourdos, M. Tantarini, D. Shmoko, J. Munoz, N. Amoratis, A. Maragkakis, T. Machairas and A. Trifas. 'EuroDRONE, A European UTM Testbed for U-Space'. In: *2020 International Conference on Unmanned Aircraft Systems (ICUAS)*. 2020, pp. 1766–1774. DOI: 10.1109/ICUAS48674.2020.9214020.

[5] T. Dubot and A. Joulia. 'Towards U-space conflict management services based on 4D protection bubbles'. In: *AIAA AVIATION 2021 FORUM*. American Institute of Aeronautics and Astronautics, 2021. DOI: 10.2514/6.2021-2347.

[6] N. Patrinopoulou, I. Daramouskas, V. Lappas, V. Kostopoulos, A. Morfin Veytia, C. A. Badea, J. Ellerbroek, J. Hoekstra, V. de Vries, J. van Ham, E. Sunil, P. M. Ponte Alonso, J. Pedrero Gonzalez, D. Bereziat, A. Vidosavljevic and L. Sedov. 'Metropolis II: Investigating the Future Shape of Air Traffic Control in Highly Dense Urban Airspace'. In: *2022 30th Mediterranean Conference on Control and Automation (MED)*. 2022. DOI: 10.1109/MED54222.2022.9837201.

[7] F. Silva, T. Kono, C. Peralta, O. Garcia and J. Chen. 'A review of computational fluid dynamics (CFD) simulations of the wind flow around buildings for urban wind energy exploitation'. In: *Journal of Wind Engineering and Industrial Aerodynamics* 180 (2018), pp. 66–87. ISSN: 0167-6105. DOI: 10.1016/j.jweia.2018.07.010.

[8] S. Giersch, O. El Guernaoui, S. Raasch, M. Sauer and M. Palomar. 'Atmospheric flow simulation strategies to assess turbulent wind conditions for safe drone operations in urban environments'. In: *Journal of Wind Engineering and Industrial Aerodynamics* 229 (2022), p. 105136. ISSN: 0167-6105. DOI: 10.1016/j.jweia.2022.105136.

[9] E. Sunil, R. Koerse, S. van Selling, J.-W. van Doorn, T. Brinkman and J. Sun. 'METSIS: Hyperlocal Wind Nowcasting for U-space'. In: *11th SESAR Innovation Days*. 2021.

[10] A. Joulia and T. Dubot. 'Analysis and assessment of U-space tactical conflict management services'. In: *AIAA AVIATION 2022 Forum*. American Institute of Aeronautics and Astronautics, 2022. DOI: 10.2514/6.2022-3543.

[11] C. Huang, I. Petrunin and A. Tsourdos. 'Strategic Conflict Management using Recurrent Multi-agent Reinforcement Learning for Urban Air Mobility Operations Considering Uncertainties'. en. In: *Journal of Intelligent & Robotic Systems* 107.2 (2023), p. 20. ISSN: 1573-0409. DOI: 10.1007/s10846-022-01784-0.

[12] Y. Xie, A. Gardi and R. Sabatini. 'Reinforcement Learning-Based Flow Management Techniques for Urban Air Mobility and Dense Low-Altitude Air Traffic Operations'. In: *2021 IEEE/AIAA 40th Digital Avionics Systems Conference (DASC)*. 2021, pp. 1–10. DOI: 10.1109/DASC52595.2021.9594384.

[13] F. Causa, A. Franzone and G. Fasano. 'Strategic and Tactical Path Planning for Urban Air Mobility: Overview and Application to Real-World Use Cases'. In: *Drones* 7.1 (2023), p. 11. ISSN: 2504-446X. DOI: 10.3390/drones7010011.

[14] OpenStreetMap contributors. *Planet dump retrieved from https://planet.osm.org*. https://www.openstreetmap.org. 2017.

[15] F. Biljecki, H. Ledoux and J. Stoter. 'An improved LOD specification for 3D building models'. In: *Computers, Environment and Urban Systems* 59 (2016), pp. 25–37. ISSN: 0198-9715. DOI: https://doi.org/10.1016/j.compenvurbsys.2016.04.005. URL: https://www.sciencedirect.com/science/article/pii/S0198971516300436.

[16] AHN. *Home*. Landingspagina. Publisher: AHN. 2023. URL: https://www.ahn.nl/ (visited on 21/09/2023).

[17] I. Paden, C. Garcia-Sanchez and H. Ledoux. 'Towards Automatic Reconstruction of 3D City Models Tailored for Urban Flow Simulations'. In: *Frontiers in Built Environment* 8 (2022). ISSN: 2297-3362. DOI: 10.3389/fbuil.2022.899332.

[18] B. Blocken. 'Computational Fluid Dynamics for urban physics: Importance, scales, possibilities, limitations and ten tips and tricks towards accurate and reliable simulations'. In: *Building and Environment*. Fifty Year Anniversary for Building and Environment 91 (2015), pp. 219–245. ISSN: 0360-1323. DOI: 10.1016/j.buildenv.2015.02.015.

[19] T. O. Foundation. *OpenFOAM | Free CFD Software | The OpenFOAM Foundation*. en-GB. URL: https://openfoam.org/ (visited on 21/09/2023).

[20] Y. Tominaga, L. Wang, Z. Zhai and T. Stathopoulos. 'Accuracy of CFD simulations in urban aerodynamics and microclimate: Progress and challenges'. In: *Building and Environment* 243 (2023), p. 110723. ISSN: 0360-1323. DOI: https://doi.org/10.1016/j.buildenv.2023.110723.

[21] C. García-Sánchez, J. van Beeck and C. Gorlé. 'Predictive large eddy simulations for urban flows: Challenges and opportunities'. In: *Building and Environment* 139 (2018), pp. 146–156. ISSN: 0360-1323. DOI: https://doi.org/10.1016/j.buildenv.2018.05.007.

[22] B. E. Launder and D. Spalding. 'The numerical computation of turbulent flows'. In: *Computer Methods in Applied Mechanics and Engineering* 3.2 (1974), pp. 269–289. ISSN: 0045-7825. DOI: https://doi.org/10.1016/0045-7825(74)90029-2.

[23] D. M. Hargreaves and N. G. Wright. 'On the use of the k–epsilon model in commercial CFD software to model the neutral atmospheric boundary layer'. In: *Journal of Wind Engineering and Industrial Aerodynamics* 95.5 (2007), pp. 355–369. ISSN: 0167-6105. DOI: https://doi.org/10.1016/j.jweia.2006.08.002.

[24] J. Wieringa. 'Updating the Davenport roughness classification'. In: *Journal of Wind Engineering and Industrial Aerodynamics* 41.1 (1992), pp. 357–368. ISSN: 0167-6105. DOI: https://doi.org/10.1016/0167-6105(92)90434-C.

[25] L. S. Caretto, A. D. Gosman, S. V. Patankar and D. B. Spalding. 'Two calculation procedures for steady, three-dimensional flows with recirculation'. In: *Proceedings of the Third International Conference on Numerical Methods in Fluid Mechanics*. Ed. by H. Cabannes and R. Temam. Berlin, Heidelberg: Springer Berlin Heidelberg, 1973, pp. 60–68. ISBN: 978-3-540-38392-5.

[26] C. García-Sánchez and C. Gorlé. 'Uncertainty quantification for microscale CFD simulations based on input from mesoscale codes'. In: *Journal of Wind Engineering and Industrial Aerodynamics* 176 (2018), pp. 87–97. ISSN: 0167-6105. DOI: https://doi.org/10.1016/j.jweia.2018.03.011.

[27] A. Ricci, I. Kalkman, B. Blocken, M. Burlando and M. Repetto. 'Impact of turbulence models and roughness height in 3D steady RANS simulations of wind flow in an urban environment'. In: *Building and Environment* 171 (2020), p. 106617. ISSN: 0360-1323. DOI: https://doi.org/10.1016/j.buildenv.2019.106617.

[28] C. A. Badea and A. M. Veytia. *The Hague Wind Measurements and CFD Simulations Dataset*. DOI: 10.4121/3ae69abd-6b84-49cf-9761-64680883de78. 2023.

[29] J. M. Paasch and J. Paulsson. 'Trends in 3D cadastre – A literature survey'. In: *Land Use Policy* 131 (2023), p. 106716. ISSN: 0264-8377. DOI: 10.1016/j.landusepol.2023.106716.

7

Investigating the Operational Feasibility for Drones Using Wind Simulations in Rotterdam

The previous chapter (Ch. 6) established the importance of computational fluid dynamics (CFD) simulations for U-space operations. This chapter dives deeper and performs a city-wide risk and yearly operational analysis for drone flights in Rotterdam. These in-depth simulation aim to assess how different wind conditions can affect the risk and feasibility of U-space operations. The chapter also establishes a replicable methodology for other urban environments where/when air operations may take place.

This chapter is based on an upcoming publication:

- A. Morfin Veytia, A. Patil, I. Pađen, J. Hoekstra, C. García-Sánchez and J. Ellerbroek. *Investigating the Operational Feasibility for Drones Using Wind Simulations in Rotterdam*. Available at SSRN. 2025. DOI: 10.2139/ssrn.5366294. URL: https://ssrn.com/abstract=5366294

7.1. Abstract

There is increasing interest in employing aerial vehicles or drones to replace ground traffic, especially in last-mile urban transportation systems. This last-mile transportation often occurs in the urban environment, where accurately quantifying the risk for future drone trajectories is of paramount importance. However, the varying wind conditions and urban morphologies in cities can create challenging unsafe airspace zones. These, in turn, affect the yearly operational feasibility of the drone missions, as they traverse through high wind speeds and turbulence. In this work, Computational Fluid Dynamics (CFD) is used to simulate how varying inflow conditions affect airspace risk and yearly operational feasibility. A weather station 10m over the ground in the Rotterdam-Hague airport with 10-minute averages of wind speed and direction for all of 2022 is employed to choose the relevant wind profiles/inflow conditions that enter the city. Airspace zones are deemed unsafe if a certain wind speed and/or turbulence threshold is exceeded there. This work uses an ensemble of simulations through an uncertainty quantification framework to determine the city-wide risk, and performs a yearly operational feasibility analysis. The results show that a comprehensive city-wide risk analysis can be done with relatively few well-selected inflow conditions with the use of a polynomial chaos expansion on the yearly wind rose. Additionally, the results of the operational feasibility analysis show that if drones can withstand a wind speed of 12 m/s and a medium relative turbulent kinetic energy, they could be operational at most 90% of the time in 2022.

7.2. Introduction

Urban areas accounted for about 70% of greenhouse gas emissions in 2020, with urban transport specifically contributing 8% of global carbon dioxide emissions [2, 3]. As the rate of urbanisation increases and traffic congestion becomes more problematic, these emissions are projected to increase unless stringent policies are put in place and adhered [4]. With increasing emissions, traffic congestion has been linked to adverse health effects, wasted time, and economic losses [5–7]. This has led to interest in alleviating ground traffic with air operations, as it also has the potential to reduce greenhouse gas emissions [8]. Potential applications for urban air operations include the transportation of humans, packages, and medical supplies, and other missions like surveillance and building inspections [9–12].

There are several research initiatives focusing on urban air traffic operations by the use of drones to alleviate ground traffic. Among them, there is the U-Space framework in Europe [13] and the Unmanned Aircraft System Traffic Management ecosystem in the United States [14]. Additionally, some cities such as Rotterdam have also shown interest in exploring drone traffic for their transportation infrastructure [15].

The European Union estimates that there will be 400,000 drones in operation by 2040 [16], which will create traffic densities orders of magnitude higher

than traditional air traffic management. In addition to avoiding other aircraft, drones will need to safely navigate around buildings, other urban infrastructure, and above populated regions. The study of the risk posed by drone flights in cities is a major challenge for the implementation of safe urban air operations [17]. These flights will be further complicated by complex wind flows in urban environments, which will create additional risk and limit the operational uptime of missions.

Wind in urban areas can be highly uncertain due to the turbulence created by the flow interaction with the urban environment. This complex flow makes it difficult to quantify the risk and operational feasibility. Previous works have attempted to perform risk [18, 19] and yearly operational feasibility analysis [20–24] by considering mesoscale wind conditions. They do not account for the effect of the city's buildings, terrain, water bodies, and vegetation on the wind field.

The simplified wind view is largely because obtaining comprehensive wind information requires Computational Fluid Dynamics (CFD) with the capability to reconstruct the urban environment accurately. There are two general techniques for research on CFD and drone operations in cities [25]. The first is with a lower-fidelity and lower-cost model, such as the Reynolds Averaged Navier Stokes (RANS) model that provides time-averaged wind flow fields [26–28]. The second is with higher-fidelity and higher-cost models, such as Large Eddy Simulations that can provide both time-resolved and time-averaged wind flow fields [29–31].

Since the RANS approach models all of the small-scale turbulence, the uncertainty associated with the time-averaged wind prediction is relatively larger when compared to that of the LES approach that resolves a portion of the requisite scales of motion [32]. However, due to the high computational cost of LES, it can be computationally prohibitive to perform a city-wide risk and yearly operational feasibility analysis that considers the yearly wind variability. This has led to research that attempts to improve RANS simulations with reduced-order modelling through data-assimilation [33, 34] and Uncertainty Quantification (UQ) [35–37] techniques.

To that end, in this work, we perform a city-wide risk and flight operational feasibility analysis using a RANS approach in Rotterdam. The city of Rotterdam is chosen due to its interesting urban morphology (tall buildings near the Nieuwe Maas river) and the city's proximity to the high wind speeds from the North Sea [38]. The relevant wind conditions for simulations are selected with a polynomial chaos expansion (PCE) based on an uncertainty quantification framework. The PCE is performed on the variable wind directions measured in a weather station in Rotterdam. In this way, the results of a RANS simulation can be augmented while still maintaining a lower computational cost than LES for an identical region of interest. The RANS approach does not resolve the small pressure fluctuations that relate to wind loads and gustiness that would be given by an LES. However, when looking at the city scale, it is possible to determine which areas are affected by high levels of turbulence, which likely correlates to areas

with dangerous wind loads and gustiness.

The goal of city-wide risk analysis is to identify unsafe airspace zones where there is a large probability that the local speed and turbulence exceed certain safety thresholds. The effects of different speed and turbulence safety thresholds are presented because there are currently no established criteria [39]. While there have been previous works that have attempted to identify high-wind speed regions based on weather conditions and CFD [27, 28], these are in smaller regions and do not include the variation of wind due to turbulence. Additionally, the differences between performing the city-wide risk analysis with an order 16 PCE and an order 40 PCE are shown to learn if it is possible to reduce the number of simulations in future cities.

After performing the city-wide risk analysis, a flight operational feasibility analysis for 2022 is performed for Rotterdam. The goal is to get an estimate of the operational time in a calendar year when the airspace is considered safe to use. Similar to the city-wide risk analysis, this considers different speed and turbulence safety thresholds. It is also possible to show 10-minute variations of the unsafe airspace areas by linking the simulation results to the 10-minute wind measurement. This is done by matching the measured wind direction and speed to the closest simulated condition from the order 40 PCE.

7.3. Methodology

7.3.1. Simulation set-up: modelling the urban environment

Selecting the urban environment and geometry

The city of Rotterdam is chosen as an Urban Environment test case, due to the city's interest in drone operations [40] and complex built environment that is split by the Nieuwe Maas river. Fig. 7.1 shows the location (Fig. 7.1a) and map of the area of interest (Fig. 7.1b), which is approximately a 9.2 km by 10.2 km rectangle. The area of interest was split into 4 equal regions with a 500-metre overlap to simplify meshing. A 200-metre overlap is considered to average the resulting fields from different regions. This splitting approach is relatively new and was first attempted in [41].

The city geometry was obtained using a variety of different data sources. Fig. 7.2 shows the water, vegetation, and building polygons in the area of interest. The building polygons were downloaded using 3DBAG [42] with a 1.2 level of detail. This level of detail extrudes the roofs of individual buildings to the same height while maintaining the actual shape of its perimeter [43]. This level was chosen to limit the size of the computational mesh. However, this level of detail means that the accuracy of the resulting speed and turbulence is lowered near the buildings. The water and vegetation polygons were downloaded from Publieke Dienstverlening Op de Kaart (PDOK) of The Netherlands [44]. Note that trees and other vegetation objects were not directly simulated, but represented with an aerodynamic roughness. The building perimeters were post-processed to simplify the mesh by smoothing abrupt changes in the geometry. Additionally, polygons

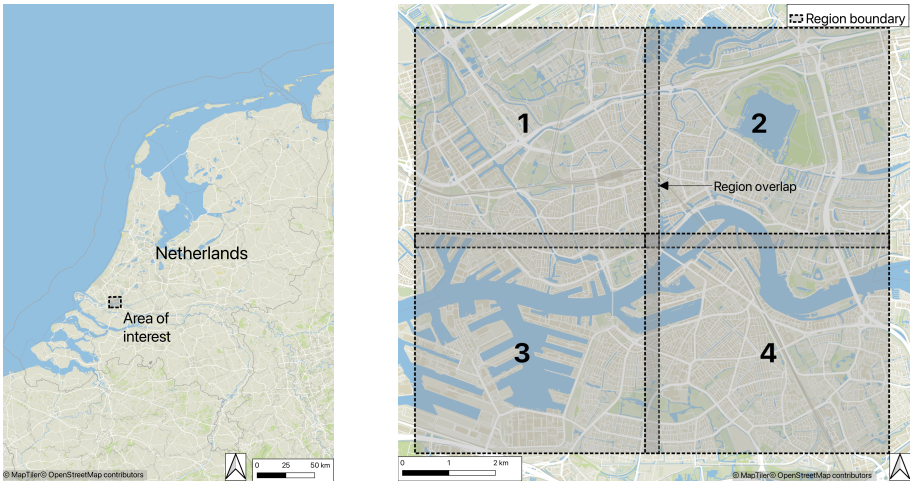

(a) Area of interest in Rotterdam. (b) Four regions that make up the area of interest.

Figure 7.1: Area of interest located in Rotterdam, The Netherlands. The total size of the area of interest is 9.2km by 10.2km. The right side shows the four regions along with the overlap of 500 metres. Note that only the inner 200 metres is considered for averaging the results.

with an area less than or equal to 10 metres squared were removed. The terrain and building elevations were downloaded from the Actueel Hoogtebestand Nederland (AHN4) [45].

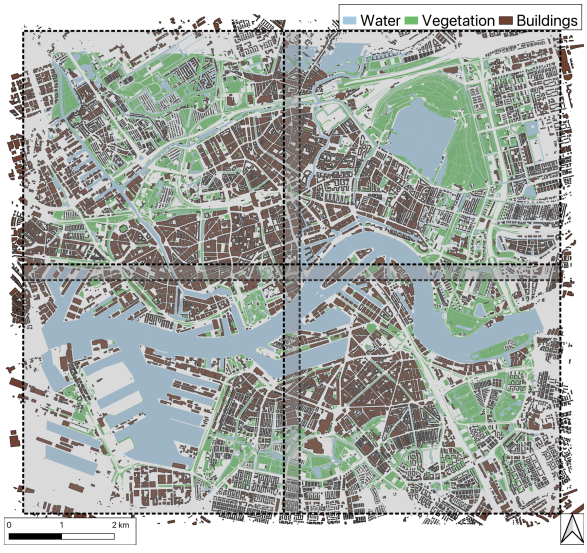

Figure 7.2: Map of Rotterdam showing the polygons included in the computational mesh. Building polygons were downloaded from [42]. Water and vegetation polygons were downloaded from [44].

Building the computational urban environment

Four three-dimensional regions of interest (ROI) were obtained through the reconstruction process using City4CFD [46]. City4CFD generated the input geometry corresponding to the buildings, water bodies, vegetation, and terrain within the specified ROI, which is subsequently used to obtain the computational mesh. Through the use of City4CFD, the input data processing is significantly reduced through the automated reconstruction of the ROI. Table 7.1 presents an overall summary of the mesh characteristics for each region. Note that the diameter and height of each domain were decided based on the best practice guidelines for urban microscale simulations [47]. The best practice guidelines set the minimum distances from the area of interest to the boundary of the computational mesh (see Fig. 10 in [47]). Fig. 7.3 shows the three-dimensional reconstructed output for region 1 using City4CFD.

Table 7.1: Summary of the meshes for the four regions of interest.

Mesh summary for four regions of interest

Region	Number of cells (millions)	Near-wall cell resolution (metres)	Cylinder diameter (kilometres)	Cylinder height (kilometres)	Average iteration time (seconds)
1	127	~1.5	15.7	1.1	9.3
2	137	~1.5	17.1	1.1	10.0
3	97	~1.5	16.4	1.2	7.2
4	119	~1.5	17.2	1.7	8.8

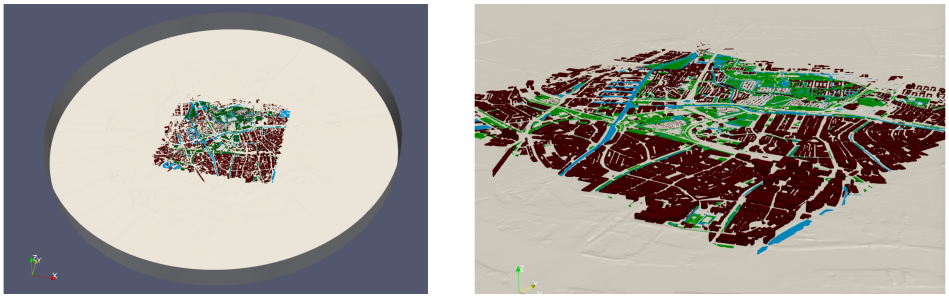

(a) Cylindrical domain for region 1. (b) Area of interest for region 1.

Figure 7.3: Three-dimensional reconstruction for region 1 showing buildings, terrain, water, and vegetation. Note that each region had its own unique domain with the dimensions mentioned in Table 7.1.

Governing equations and computational method

This work solves the steady-state incompressible Reynolds-averaged Navier-Stokes (RANS) equations [32, 48]. The RANS equations are derived by splitting the

velocity field given by the Navier-Stokes equation into a mean and fluctuating component. The equations are then averaged over time to remove most of the fluctuating components. The RANS equations are given by:

$$\underbrace{\partial_j \overline{u_j}\,\overline{u_i}}_{(1)} = \underbrace{-\frac{1}{\rho_o}\partial_i \overline{p}}_{(2)} + \underbrace{\nu \partial_j \partial_j \overline{u_i}}_{(3)} + \underbrace{\partial_j \overline{u_j' u_i'}}_{(4)} \tag{7.1}$$

and

$$\partial_i \overline{u_i} = 0, \tag{7.2}$$

where ρ_o is the density of the fluid, $\overline{u}_i$ represents the Reynolds-averaged velocity, ν is the kinematic viscosity of the fluid ($\nu_{\text{air}} = 1.5 \times 10^{-5} m^2/s$), $\overline{p}$ is the pressure, and $\partial_j \overline{u_j' u_i'}$ are the Reynolds-stresses, and u_i' represents the fluctuating component of the velocity. The governing equations described above make use of tensorial notation, where repeated indices imply summation. The coordinate axes x_1, x_2, and x_3 are aligned along the streamwise, spanwise, and vertical directions, respectively. The momentum equation (Eq. 7.1) contains the following terms: (1) convection by the mean flow, (2) mean pressure gradient, (3) mean viscous stress, and (4) Reynolds-stresses. The continuity equation (Eq. 7.2) represents the conservation of mass.

Since the Reynolds stresses (term 4 in Eq. 7.1) are unknown, the system of equations is mathematically unclosed, which is resolved through the widely used two-equation standard $k-\epsilon$ model [49]:

$$\overline{u_j' u_i'} = \frac{2}{3} k \delta_{ij} - 2\mu_t S_{ij} \tag{7.3}$$

and

$$\mu_t = C_\mu \frac{k^2}{\epsilon} \tag{7.4}$$

where k is the turbulent kinetic energy, ϵ is the turbulent kinetic energy dissipation rate, S_{ij} the time-averaged shear stress tensor, μ_t is the turbulence viscosity, and C_μ is a model constant equal to 0.09.

The integral form of the equations is discretised using the finite-volume method (FVM) using a collocated grid arrangement for the variables under consideration (i.e., $\overline{u}_i$ and $\overline{p}$) [50]. The numerical solution is obtained using the OpenFOAM computational framework (version 7) [51], which is parallelised through the Message-Passing-Interface (MPI) over an unstructured grid consisting primarily of hexahedral cells. To obtain a converged solution to the wind flow subject to suitable initial and boundary conditions (discussed later), the semi-implicit method for pressure-linked equations (SIMPLE) algorithm is used [52], which corresponds to the *simpleFoam* application within the OpenFOAM toolbox [53].

The numerical solutions are integrated for 4500 pseudo time steps (iterations) until the normalised residuals for the time-averaged pressure stabilise below 10^{-2} and the normalised residuals for other flow parameters of interest stabilise below 10^{-3}. All the simulations are run using the Snellius Dutch National Supercomputer, using AMD Genoa 9654 CPUs with 192 cores. This is a well-established method for solving urban flows [47]. Thanks to the efficiency of the RANS approach, where the resources required to run simulations are small, we can model the flow in large heterogeneous cities.

This work assumes a Neutral Atmospheric Boundary Layer for inflow conditions with a logarithmic velocity profile $U(x_3)$ given by [54]:

$$U(x_3) = \frac{u^*}{\kappa} \ln\left(\frac{x_3 + z_0}{z_0}\right) \tag{7.5}$$

where u^* is the friction velocity, κ is the von Kármán constant (0.41), x_3 is the height from the ground, and z_0 is the aerodynamic roughness. Different aerodynamic roughnesses are assumed for terrain, vegetation and water surfaces of 0.5, 0.03, 0.002, respectively [55]. An inflow speed of 10 m/s at a reference height of 10 metres is set to solve for u^* at the inlet. The inlet conditions for k and ϵ are:

$$k = \frac{u^{*2}}{\sqrt{C_\mu}} \tag{7.6}$$

and

$$\epsilon = \frac{u^{*3}}{\kappa(x_3 + z_0)} \tag{7.7}$$

Note that simulations will give the results for an inlet speed of 10 m/s. However, it is assumed that the results can be scaled linearly for other inlet speeds. This is due to the asymptotic behaviour of the bulk Reynolds number ($Re_b = U_{\text{in}}H/\nu \gg 10^6$), where H is the representative height of the tallest building in the domain [56].

7.3.2. Simulation set-up: inflow cases and safety thresholds

Yearly wind data

This work uses 10-minute weather data from 2022, that was recorded at a measuring station located 10m above the ground at Rotterdam-The Hague airport, maintained by the Royal Netherlands Meteorological Institute (KNMI) [57]. Fig. 7.4 shows the distribution of the yearly 10-minute data in terms of speed and direction. Figs. 7.4a and 7.4b show the probability density function of the average wind speed and wind rose, respectively.

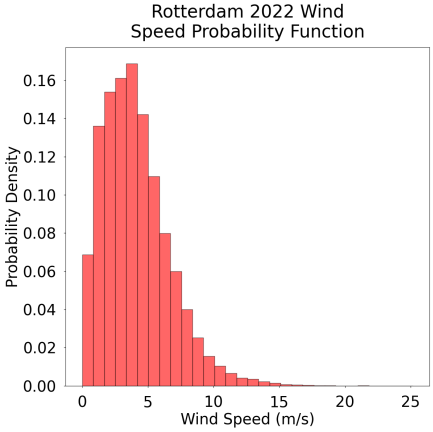

(a) Wind speed probability density function of Rotterdam in 2022.

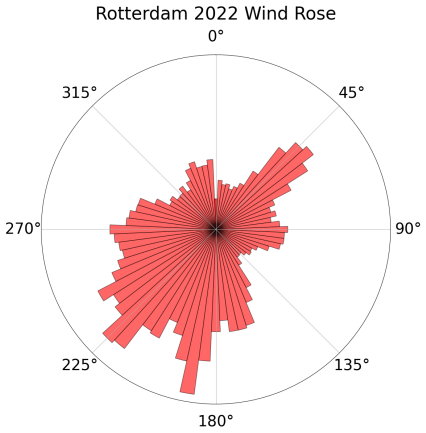

(b) Wind rose of Rotterdam in 2022.

Figure 7.4: Measured speed probability density function and wind rose for a weather station located at the Rotterdam-The Hague Airport in 2022. Note that the wind rose refers to the direction from which the wind is coming; 0 degrees corresponds to North and 90 degrees to East.

Simulated inflow speed

As seen in Fig. 7.4a, the average measured wind speed varied between 0 m/s to 17 m/s. This work sets an inflow speed of 10 m/s at a reference height of 10m. This means that the results of the simulation gave an average speed U_{sim} and the turbulent kinetic energy k_{sim} in the whole domain for an inflow speed of 10 m/s.

Recall that the inflow velocity shape is of the form of Eq. 7.5. Therefore, to scale the results for other inflow speeds, the scaling function $\phi(\gamma, x_3)$ is used where γ is the inflow speed at the reference height of 10m and x_3 is the height at which the scaling is performed.

$$U_\gamma = U_{sim}\phi(\gamma, x_3) \tag{7.8}$$

$$k_\gamma = k_{sim}\phi(\gamma, x_3)^2 \tag{7.9}$$

U_γ and k_γ refer to the scaled average velocity and turbulent kinetic energy, respectively, for a given reference inflow speed, γ. Refer to the Appendix for more details on the scaling process (Appendix B.1).

Simulated inflow angles

Choosing the relevant inflow angles to capture enough information to make a city-wide risk analysis and flight operational feasibility analysis is more difficult because of the complex shape of the urban environment. This work uses Uncertainty Quantification to select the relevant inflow wind directions to

represent the complete wind rose (Fig. 7.4b). Specifically, a polynomial chaos expansion (PCE) method is employed. The PCE was developed in [58] and later adapted to CFD applications in [35–37].

A PCE describes a response function, R, with coefficients η_i and an orthogonal basis, that is a function of a random variable $\psi_i(\theta)$. For this work, the wind direction is θ.

$$R(\theta) = \sum_{i=0}^{P} \eta_i \psi_i(\theta), \tag{7.10}$$

P is the order of the expansion. The polynomials chosen typically depends on the shape of the probability density function. The coefficients correspond to a set of inflow wind directions from the wind rose. These coefficients were derived using the least squares method with the Dakota [59] software. Two expansion orders (16 and 40) are used to select the relevant inflow angles. This was done to compare the results of the city-wide risk analysis made with 16 or 40 angles because CFD simulations are computationally expensive. The selected inflow angles are shown with dashed lines in Fig. 7.5.

A full PCE can be performed by selecting the relevant polynomials. Then, with Eq. 7.10, it is possible to rebuild the flow fields for inflow angles that were not directly simulated. However, the wind rose from Fig. 7.4b does not have an identifiable probability density function. This work attempted to rebuild the polynomials numerically, but the results were not as expected. Therefore, the PCE analysis was only used to select the relevant inflow directions (16 and 40) and in the future we will attempt to make use of the full PCE.

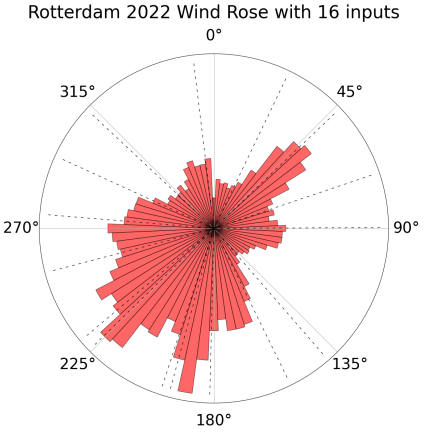

(a) Wind rose with 16 inflow angles shown as dashed lines.

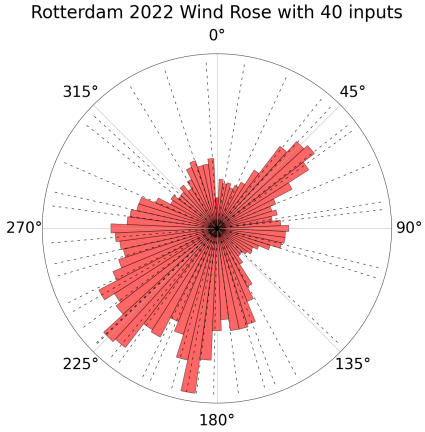

(b) Wind rose with 40 inflow angles shown as dashed lines.

Figure 7.5: The selected wind directions for both orders of 16 and 40 angles.

Drone wind speed and turbulence safety thresholds

Delivery drone manufacturers share varying details about maximum wind speed and turbulence limits for their drones. Some manufacturers share the wind speed and maximum allowable gusts, others share just the wind speed. For example, the flagship delivery drone of DJI has a maximum wind resistance of 12 m/s [60]. Matternet provides slightly more detail for the M2 Drone and states ”8 m/s gusting 12 m/s” [61]. Others are not as detailed and say that drones can fly in ”different types of weather” [62] and operate on ”windy days” [63].

The European Union Aviation Safety Agency has not yet established rules for aircraft operating in the Certified High-Risk category (risk category for drone operations in urban environments) [64]. Moreover, there is no consensus on allowable wind limits, and there will likely not be a single limit, as this may depend on several factors such as aircraft type, mission type and environment. Table 1 of [39] has a comprehensive list of different potential wind thresholds for drone limits. These vary from 11 to 40 knots (6 to 20 m/s) depending on the direction of wind and yearly operational time.

This work sets a variety of different limits depending on the analysis that is performed. For the city-wide risk analysis, a wind speed limit of 10 m/s is used, which is the same as that used in [18, 28] and is near the limit of several drones on the market. For the flight operational analysis, results for speed limits of 8, 10, and 12 m/s are shown. Note that the results and post-processing scripts are shared in the supporting dataset so that this work may be replicated for different limits [65].

Therefore, for a given reference inflow speed and direction, if the U_γ in any part of the city exceeds the safe speed limit, U_{limit}, then that part of the city is considered unsafe. In other words, it is unsafe airspace if the ratio exceeds the speed safety threshold $\alpha = 1$.

$$\frac{U_\gamma}{U_{limit}} \geq \alpha \tag{7.11}$$

Turbulence limits are rarely defined directly by manufacturers. When they do provide details, it is in the form of maximum allowable gusts [61]. This work attempts to include the turbulence because it gives an indication of the intensity of the gusts at a certain location. For a given inflow angle and reference speed, the simulation results give the turbulent kinetic energy, k_γ, throughout the domain. k_γ is scaled by U^2_{limit} and compared against the turbulence safety threshold β.

$$\frac{k_\gamma}{U^2_{limit}} \geq \beta \tag{7.12}$$

As with speed ratio, if this ratio exceeds the threshold, then that part of the city can be considered unsafe. The turbulence ratio can be defined as a ratio of the turbulent kinetic energy and the energy carried by the mean flow at the wind speed limit, similar to the turbulent intensity definition [32, 48].

This work presents results for three turbulent safety thresholds (β) of 0.02, 0.05, and 0.1, which we call low, medium and high thresholds, respectively, to streamline the discussion in the text.

7.4. Results and Discussion

7.4.1. Simulation results

Resulting velocity and turbulent kinetic energy fields were sampled (sliced) at above-ground levels (AGLs) of 2m, 5m, and from 10m to 150m at every 10m. The slices were then scaled as explained in Section 7.3.2. Fig. 7.6 shows two slices at 20 metres above terrain with a 10-degree inflow direction and γ =10m/s. Figs. 7.6a and 7.6b show the non-dimensionalised average velocity magnitude and turbulent kinetic energy, respectively.

In the velocity plot, a value over 1.0 indicates that the speed has exceeded the safe speed limit, U_{limit}. There is an observable slowdown in the centre of the city and a speed up above the water (See Fig. 7.2). Additionally, the overlapping area between regions is slightly visible in the direction perpendicular to the flow. This is somewhat expected since this overlapping methodology is still under development and further improvements need to be considered to eliminate such effect. For the turbulence plot, values higher than 0.02, 0.05, or 0.1 indicate low, medium, and high relative turbulence levels, respectively. Areas in red are high turbulence and can be seen in the wake of some buildings. As expected, most of the high turbulence regions are in the vicinity of the built infrastructure, as the flow separates behind the buildings, rendering a relatively complex flow response. While the distribution of the wind speed and the turbulence levels provides an insightful perspective on the risk associated, operational forecasting requires relatively quantified metrics, as will be discussed in the following sub-sections.

7.4.2. City-wide risk analysis of Rotterdam

This section shows the city-wide risk of Rotterdam for a given reference inflow speed (γ), safe speed limit ($U_{limit} = 10$ m/s), and speed (α) and turbulence (β) safety thresholds. The probability formulation of this risk is presented first. Then, risk maps are created with the riskMap tool [66] to show the probability that the safety thresholds are exceeded at a certain height. Finally, several aggregated contour plots of the unsafe airspace (probability equal to 1) are shown that show the relationship at different heights, inflow speeds, and safety thresholds.

Note that the presented results are shown with some inflow speeds, safety thresholds, and speed limits. It is possible to generate figures with different parameters in the supporting dataset [65].

Risk probability formulation

The formulation of the risk is made for two conditions. The first quantifies the probability that both safety thresholds, α **AND** β, are exceeded (Eq. 7.13) The second quantifies the probability that α **OR** β are exceeded (Eq. 7.14).

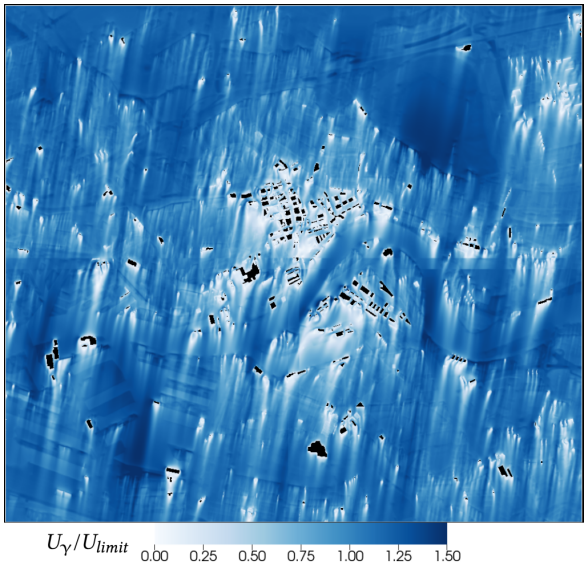

(a) Example simulation results of non-dimensionalised average velocity magnitude.

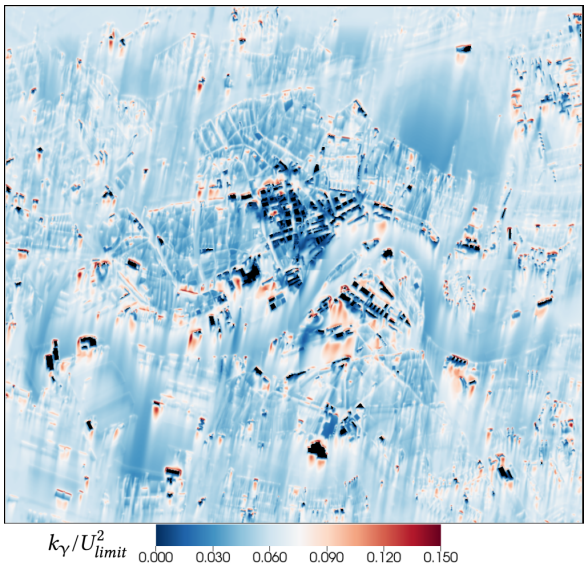

(b) Example simulation results of non-dimensionalised turbulent kinetic energy.

Figure 7.6: Example results for non-dimensionalised velocity magnitude and turbulence for a wind direction of 10 degrees and 20 metres above terrain with a reference inflow speed of 10 m/s. Buildings that reach at least 20m above ground are shown in black. U_γ and k_γ are the velocity magnitude and turbulence, respectively, given a certain reference inflow speed, γ. U_{limit} is the safe speed limit of the drone. In this plot, both γ and U_{limit} are set to 10 m/s.

$$P^{\cap}_{\alpha,\beta,\gamma} \equiv P\left(\frac{U_\gamma}{U_{lim}} \geq \alpha \cap \frac{k_\gamma}{U^2_{lim}} \geq \beta\right) \tag{7.13}$$

$$P^{\cup}_{\alpha,\beta,\gamma} \equiv P\left(\frac{U_\gamma}{U_{lim}} \geq \alpha \cup \frac{k_\gamma}{U^2_{lim}} \geq \beta\right) \tag{7.14}$$

$$\alpha = 1, \beta = 0.02, 0.05, \, or \, 0.1 \tag{7.15}$$

$$\gamma = [2, 4, 6, 8, 10] m/s, U_{lim} = 10 m/s \tag{7.16}$$

The probabilities are calculated by assigning weights to each individual wind direction using the area under the curve (Fig. 7.5), and then summing it for each angle. This is done for both 16 and 40 orders to study their differences and learn if running additional inflow angles creates significantly better results.

Risk maps at individual heights

Fig. 7.7 shows the weighted risk maps built with 16 angles at 20 metres above the ground with reference inflow speed $\gamma = 10 m/s$, speed safety threshold $\alpha = 1$, and turbulence safety threshold $\beta = 0.05$. Fig. 7.7a shows the probability that α **AND** β safety thresholds are exceeded (Eq. 7.13). Fig. 7.7b shows the probability that α **OR** β thresholds are exceeded (Eq. 7.14). The dark red regions correspond to areas that have a probability of 1, and the dark blue regions correspond to areas with a low probability of exceeding the thresholds.

It is evident that the **OR** condition is significantly more conservative because most of the airspace surrounding the centre of the city is completely red. This means that there is a high probability that the speed **OR** turbulent safety thresholds are exceeded. Conversely, the **AND** condition shows that the probability of the speed and turbulence thresholds is very low in the centre of the city.

Fig. 7.8 shows the weighted risk maps built with 40 angles at 20 metres above the ground with reference inflow speed $\gamma = 10 m/s$, speed safety threshold $\alpha = 1$, and turbulence safety threshold $\beta = 0.05$. Fig. 7.8a shows the probability that α **AND** β thresholds are exceeded (Eq. 7.13). Fig. 7.8b shows the probability that α **OR** β safety thresholds are exceeded (Eq. 7.14). The dark red regions correspond to areas that have a probability of 1, and the dark blue regions correspond to areas with a low probability of exceeding the thresholds.

Similarly, to the plots with 16 angles, the **OR** condition is significantly more conservative. However, it is clear that the increased resolution in angles creates a smoother risk map when compared to order 16. This can be seen in the lake at the top right of the **AND** maps (at the centre of region 2 from Fig. 7.1). Nevertheless, the shape and magnitudes of the risk areas are relatively similar for both 16 and 40 angles. Therefore, for a city-wide risk analysis, it is possible to use a lower number of angles to build the risk map.

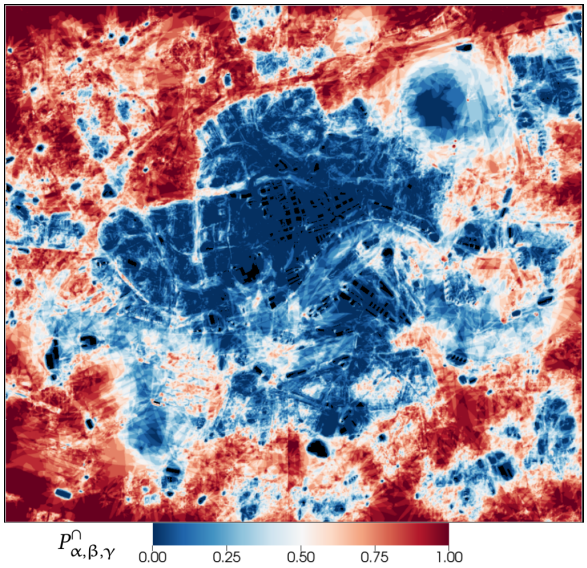

(a) Example risk map of the **AND** condition at 20 metres above terrain built with 16 inflow angles.

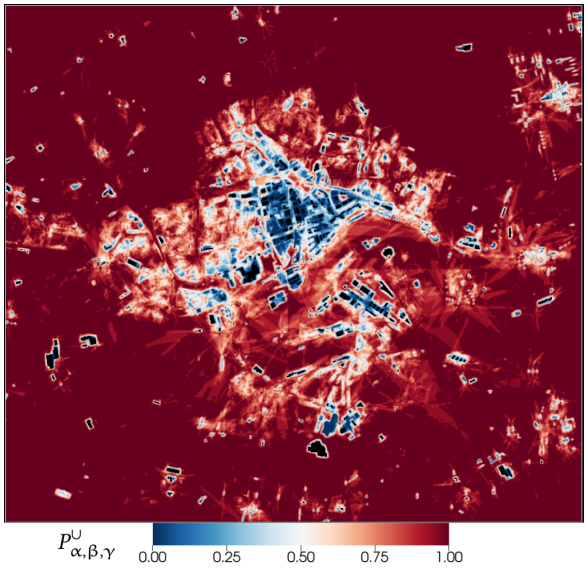

(b) Example risk map of the **OR** condition at 20 metres above terrain built with 16 inflow angles.

Figure 7.7: Example risk maps at 20 metres above terrain built with 16 inflow angles. The speed and turbulence safety thresholds are set to $\alpha = 1$ and $\beta = 0.05$, respectively, the reference inflow speed is set to $\gamma = 10$ m/s and the safe speed limit is $U_{limit} = 10$ m/s. Buildings that reach at least 20m above ground are shown in black.

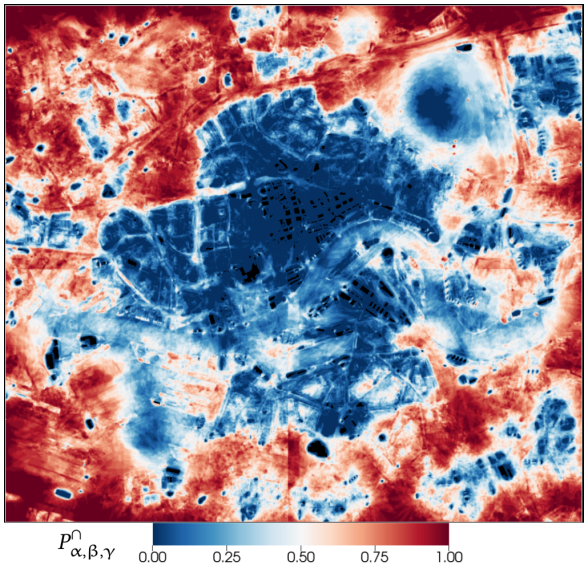

(a) Example risk map of the **AND** condition at 20 metres above terrain built with 40 inflow angles.

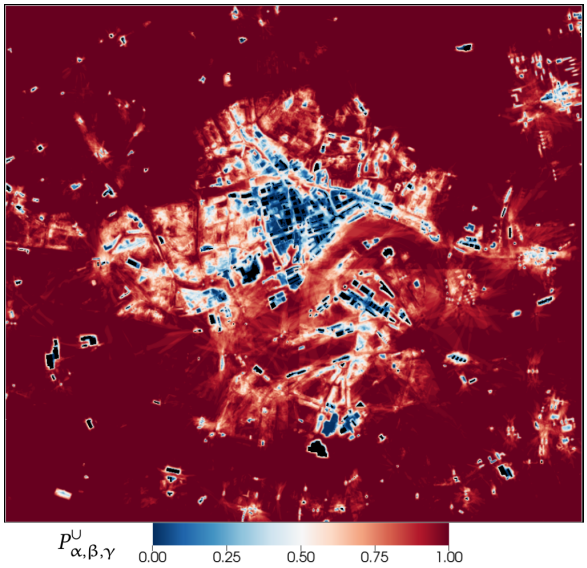

(b) Example risk map of the **OR** condition at 20 metres above terrain built with 40 inflow angles.

Figure 7.8: Example risk map at 20 metres above terrain built with 40 inflow angles. The speed and turbulence safety thresholds are set to $\alpha = 1$ and $\beta = 0.05$, respectively, the reference inflow speed is set to $\gamma = 10$ m/s, and the safe speed limit is $U_{limit} = 10$ m/s. Buildings that reach at least 20m above ground are shown in black.

Height and inflow speed aggregated risk

The risk maps can be created for several different heights, inflow speeds, and safety thresholds. This makes it possible to derive the relationship between unsafe airspace (probability equal to 1) to height and inflow speed.

Fig. 7.9 shows two contour plots for the **AND** (Fig. 7.9a) and **OR** (7.9b) conditions aggregated with 40 inflow angles and safe speed limit $U_{limit} = 10m/s$. Each different subplot refers to specific speed (α) and turbulence (β) safety thresholds. The purple regions are areas where 0% of the airspace exceeds probability greater than 1, while the yellow means 100% of the airspace exceeds 1 (Eqs. 7.13 and 7.14). See the appendix for the contours created with 16 inflow angles (Appendix B.2).

Again, it is evident that the **OR** case is significantly more conservative than the **AND** case. In the **OR** contour, the airspace is almost completely unsafe when the inflow speeds exceed 8 m/s if drones can only handle a low amount of turbulence ($\beta = 0.02$). However, if drones are able to withstand a medium ($\beta = 0.05$) or high turbulence ($\beta = 0.1$), then there is still a significant portion of airspace available up to 60 metres above the ground.

For the **OR** case, at medium and high turbulence thresholds, unsafe zones are created around 20 metres. This suggests that flying at this height will yield the highest operational time. The analysis assumes that unsafe airspace exists when the probability of exceeding the thresholds is greater than or equal to 1. In reality, the acceptable risk should be lower. This will further limit the amount of safe airspace. Refer to the appendix for plots where the probability thresholds are set to 0.9 and 0.8 (Appendix B.2).

7.4.3. Flight operational feasibility analysis

The flight operational analysis quantifies the amount of time in the calendar year that the airspace would have been safe enough for drone operations in 2022. In the future, the amount of drone missions during the day may be lower than at night. However, for this work, the complete 24-period is analysed.

This section first explains how the unsafe airspace is calculated. Using this calculation, it is possible to estimate the operational time for drone missions in 2022. Then, the section presents two short-term variable scenarios that show how the airspace can change within a relatively small 40-minute window. This is relevant because drone mission times are expected to be in the order of minutes rather than hours. Lastly, the section shows how the unsafe airspace changed day-to-day throughout 2022.

The following parameters are used for this analysis: safe speed limits are set to U_{limit} = 8, 10, or 12 m/s. Speed and turbulence safety thresholds are set to α =1 and β = 0.02, 0.05, or 0.1, respectively. Similar to the city-wide risk analysis, it is possible to generate figures with different values in the supporting dataset [65].

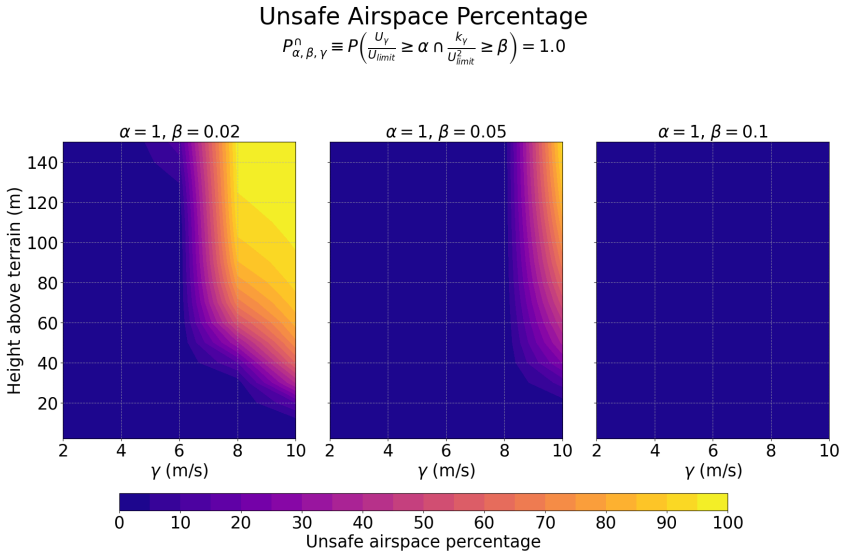

(a) Contour plot showing the **AND** condition for 40 inflow angles.

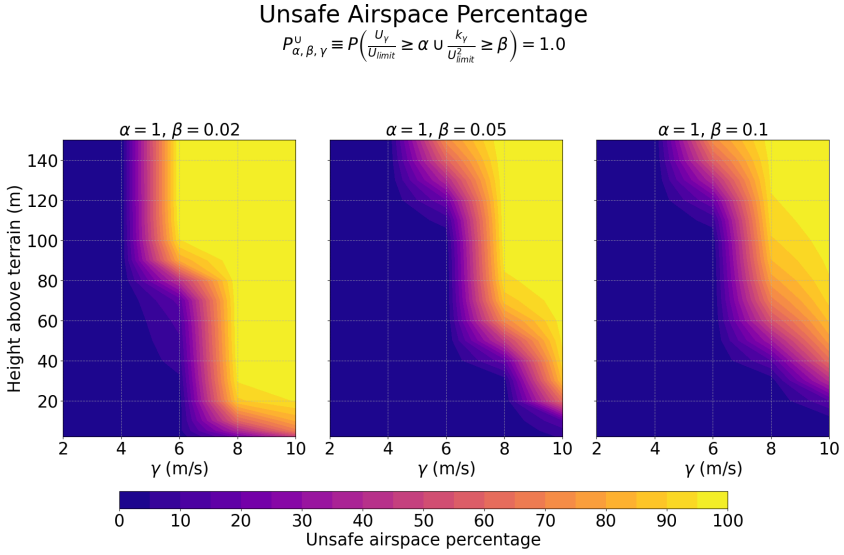

(b) Contour plot showing the **OR** condition for 40 inflow angles.

Figure 7.9: Contour plot of unsafe airspace with 40 inflow angles for safe speed limit $U_{limit} = 10m/s$ and different reference inflow speeds, γ. The different plots correspond to certain speed, α, and turbulence, β, safety thresholds. The plot shows the percent of unsafe airspace, where the probability that velocity magnitude and/or turbulence thresholds are exceeded is equal to 1.

Unsafe airspace calculation

The flight operational feasibility analysis makes use of the yearly ten-minute wind speeds and directions from Fig. 7.4. It is possible to go through the complete calendar year in ten-minute steps and obtain the unsafe airspace zones for that 10-minute time step with the CFD simulation results.

First, the speed (U_γ) and turbulent fields (k_γ) are obtained for that 10-minute time step. This is done by finding the closest simulated direction (from the order 40 inflow angles) and then scaling the raw simulation results using Eqs. 7.8 and 7.9. Second, the scaled results are non-dimensionalised with the safe speed limit (U_{limit}) and then compared to the speed (α) and turbulence (β) safety thresholds. For this analysis, only the **OR** condition is checked. Unsafe zones are areas in which the speed or turbulence thresholds are exceeded.

This is done for each 10-minute time step so it will be possible to calculate the yearly operational time that drones with certain U_{limit}, α, and β could have operated in 2022. It is important to note that this work consider the airspace as operational if more than 10 percent of the space is unsafe. The choice of 10 percent is made because a relatively small area can still have significant disruption. For example, the unsafe airspace zones have relatively high-aspect ratios that may force aircraft to increase their routes.

Yearly operational time

Table. 7.2 shows what percentage of the time during 2022 the airspace is safe for drones at two different heights (20m and 60m) for different speed limits and safety thresholds. Drones that can withstand at least a medium turbulence threshold, $\beta = 0.05$, are mostly limited by the speed threshold. Moreover, drones need to withstand a speed limit of 12 m/s and medium turbulence to achieve an operational time of 90% of the year up to 60m above ground. Refer to the appendix for an analysis for 2023 and 2024 (Appendix B.3)

Table 7.2: This table shows the amount of time as a percentage of 2022 that the airspace is operational for drones with different turbulence safety thresholds (β), and safe speed limits (U_{limit}) (The speed safety threshold is set to $\alpha = 1$ for all cases).

	Yearly operational time as percentage of 2022 in Rotterdam					
	Height = 20 m			**Height = 60 m**		
U_{limit}	β **=0.02**	β **=0.05**	β **=0.1**	β **=0.02**	β **=0.05**	β **=0.1**
8 m/s	58%	81%	82%	56%	69%	69%
10 m/s	73%	91%	91%	71%	82%	82%
12 m/s	83%	96%	96%	81%	90%	90%

Short-term variable scenarios

As the wind data is provided in 10-minute time steps, it is also interesting to study how the airspace can change in this time window. This is interesting

because the drone mission times are expected to be in the order of minutes rather than hours. Figs. 7.10 and 7.11 show scenarios from two different days of 2022 that portray how unsafe airspace areas (red polygons) can change within a 40-minute window at 60 metres above the terrain.

Fig. 7.10 shows a window where the wind direction changed by 116 degrees within 40 minutes, with speed safety thresholds of $\alpha = 1$ and turbulence safety thresholds $\beta = 0.02$ with the safe speed limit $U_{limit} = 10$m/s. The scenario shows that within 10 minutes, the airspace went from 11% unsafe to less than 1% unsafe. The plot shows that an 11 % coverage already can be quite disruptive for future drone missions. The unsafe airspace zones can have a high aspect ratio. This would cause drone paths to converge while avoiding these areas.

Fig. 7.11 shows a more extreme case where the airspace goes from completely safe to almost completely unsafe within 10 minutes (safety thresholds of $\alpha = 1$, $\beta = 0.05$, and $U_{limit} = 10$m/s). Therefore, without proper forecasting, the safety of the airspace can be compromised within a very short time limit. This also shows that the operational times in Table 7.2 will likely be even lower. This is because the airspace may need to be closed for some time before and after the airspace shutdown.

Seasonal variability analysis

The 40-minute scenarios show that airspace conditions can vary significantly, and days with large inflow speeds may disrupt airspace operations longer than their 10-minute window. Fig. 7.12 shows the percentage of daytime that had unsafe conditions for different drone speed limits (U_{limit}) and speed and turbulence safety threshold of $\alpha = 1$ and $\beta = 0.05$, respectively. The figure shows that as the drone speed limit increases, there are fewer unsafe zones. This is shown by the calendar showing more blue squares. The figure also shows that the high wind speeds of February 2022 would have caused significant disruption in the airspace. This would have been almost the whole month for drones with a $U_{limit} = 8m/s$ and 11 days for drones with $U_{limit} = 12m/s$.

7.5. Conclusion

The city-wide risk analysis showed that it is not necessary to simulate every potential inflow angle to get risk maps that contain an accurate representation of the inflow direction variability. Using 16 inflow angles yielded similar results as using 40 inflow angles. This would save significant computational time for CFD simulations. Therefore, other cities interested in generating their own risk maps can invest less computational resources. Additionally, it was shown that using an ensemble of relatively more inaccurate RANS simulations makes it feasible to generate city-wide risk maps. However, for a more detailed analysis in smaller problematic regions, an LES simulation can be made. The strength of this approach is that problematic regions are identified with RANS and then augmented with LES.

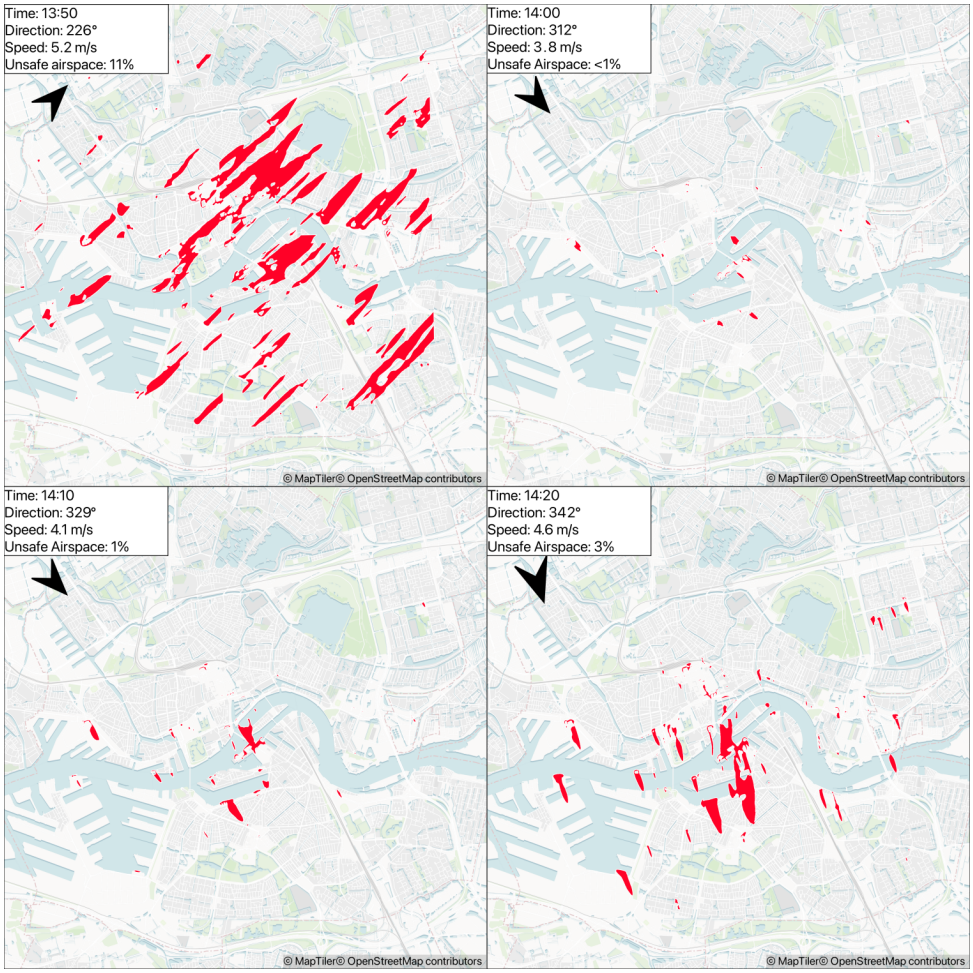

Figure 7.10: Unsafe airspace (red zones) for October 13, 2022, with speed safety threshold of $\alpha = 1$ and turbulence safety threshold of $\beta = 0.02$. The safe speed limit is set to $U_{limit} = 10$m/s at 60 metres above terrain. The speed shown on the images is the measured speed of the weather station at 10 metres above the ground.

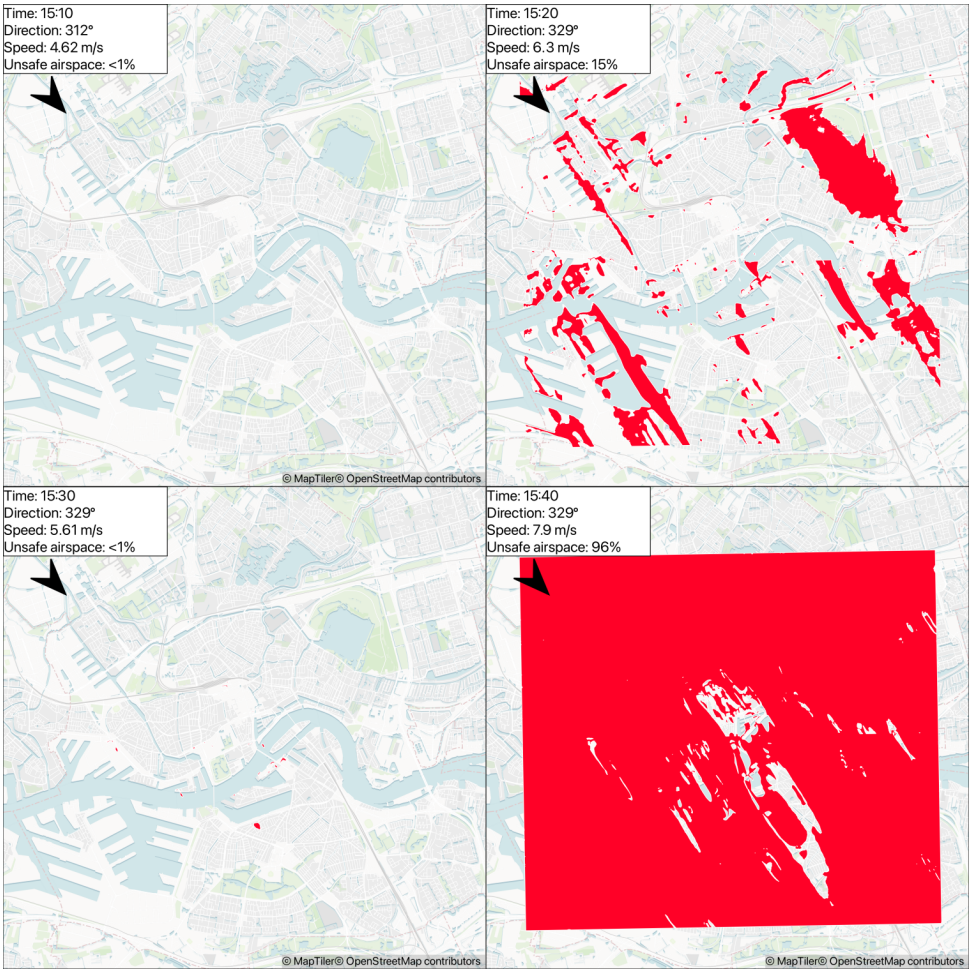

Figure 7.11: Unsafe airspace (red zones) for September 16, 2022 with speed safety threshold of $\alpha = 1$ and turbulence safety threshold of $\beta = 0.05$. The safe speed limit is set to $U_{limit} = 10$m/s at 60 metres above terrain. The speed shown on the images is the measured speed of the weather station at 10 metres above the ground.

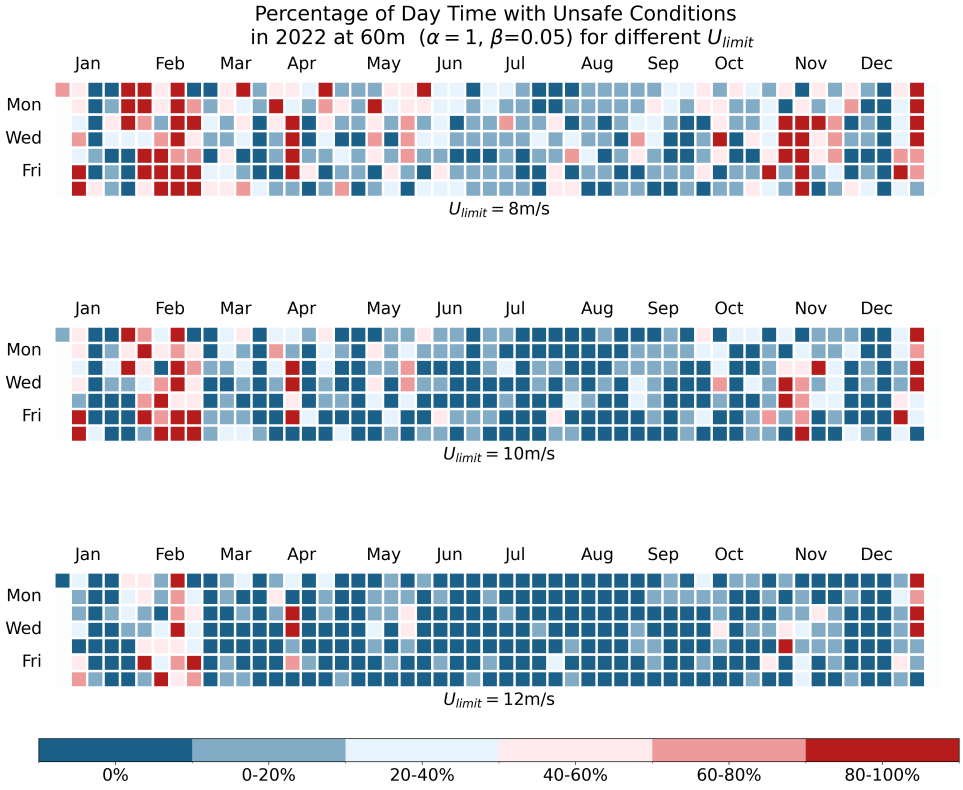

Figure 7.12: Seasonal patterns of unsafe airspace conditions at 60m altitude throughout 2022 in Rotterdam. Each calendar heatmap displays the percentage of daytime with unsafe conditions. An unsafe condition occurs when more than 10% of the airspace contains areas that exceed the speed ($\alpha = 1$) and turbulence ($\beta = 0.05$) safety thresholds for different drone speed limits (U_{limit}).

The city-wide analysis also illustrated that drones should at least withstand a medium amount of turbulence (safety threshold $\beta = 0.05$) in order to have a lower probability of encountering unsafe airspace at around 20m height with a speed limit of 10m/s. This for the more conservative condition, where it is checked if either speed **OR** turbulence thresholds are exceeded. Additionally, it is important to note that these checks were performed when the probability of exceeding one of the thresholds was equal to 1. In reality, the airspace regulators and drone manufacturers should decide the acceptable risk. For this reason, the simulation results and post-processing scripts are shared in the supplementary dataset.

It was also observed that if drones could withstand a turbulence safety threshold of $\beta = 0.05$, the limiting factor for operations in 2022 was the speed limit. Drones could have been operational about 90% during that year in Rotterdam up to 60 metres. Nevertheless, this does not account for potential downtime caused right before and after the airspace was unsafe. The downtime may be potentially reduced if there is accurate forecasting of wind conditions.

The short-term variable scenarios showed that the airspace can quickly change from almost completely safe to completely unsafe within 10 minutes. Moreover, it was seen that drones with a speed limit of 12 m/s and a medium turbulence threshold, still had about 11 days in February 2022 with significant downtime. This uncertainty is something that airspace operators will need to account for to reach the 90% operational time or increase the drone safety thresholds.

Note that for the flight operational feasibility analysis, the 10-minute window time steps were rebuilt from the 40 inflow angles because using only 16 inflow angles is less accurate when matching directions. Therefore, in future work, the Uncertainty Quantification framework can be extended to rebuild any inflow angles that were not via the polynomial chaos expansion. In this work, it was only used to select the relevant inflow angles.

Another limitation of this work, is the assumption of a neutral atmospheric boundary layer. The urban heat island effect in Rotterdam can create around a 2 $°C$ difference between air in the city and the inflow air temperature [67] in some places. It was seen in [29] that including this temperature differential leads to increased turbulence kinetic energy. Therefore, extending the flight operational feasibility analysis to consider temperature differentials should be furthered studied to capture additional restrictions on the yearly operational time. Moreover, extending the analysis to include more weather stations would help isolate the relevant important inflow and boundary conditions

Although this work mostly focuses on situations where airspace is deemed unsafe. Another aim of this work was to provide realistic wind fields to augment drone research. The wind will have an effect on path-planning and may cause delays even when the airspace is mostly safe. Studies like [68–70] could be improved by providing a more detailed wind field and potentially illustrate the robustness of their planning algorithms.

Finally, further research is needed to define allowable speed and turbulence limits. There will likely not be a single threshold but will depend on the aircraft

type, mission, and flight elevation. Drone manufacturers and urban airspace regulators should work together to be clearer about airspace rules for different flight phases and wind conditions.

References

[1] A. Morfin Veytia, A. Patil, I. Pađen, J. Hoekstra, C. García-Sánchez and J. Ellerbroek. *Investigating the Operational Feasibility for Drones Using Wind Simulations in Rotterdam*. Available at SSRN. 2025. DOI: 10.2139/ssrn.5366294. URL: https://ssrn.com/abstract=5366294.

[2] IPCC. *Climate Change 2023: Synthesis Report. Contribution of Working Groups I, II and III to the Sixth Assessment Report of the Intergovernmental Panel on Climate Change*. Geneva, Switzerland: IPCC, 2023, pp. 35–115. DOI: 10.59327/IPCC/AR6-9789291691647.

[3] P. Jaramillo, S. Kahn Ribeiro, P. Newman, S. Dhar, O. E. Diemuodeke, T. Kajino, D. S. Lee, S. B. Nugroho, X. Ou, A. Hammer Strømman and J. Whitehead. 'Transport'. In: *Climate Change 2022: Mitigation of Climate Change. Contribution of Working Group III to the Sixth Assessment Report of the Intergovernmental Panel on Climate Change*. Ed. by P. R. Shukla, J. Skea, R. Slade, A. Al Khourdajie, R. van Diemen, D. McCollum, M. Pathak, S. Some, P. Vyas, R. Fradera, M. Belkacemi, A. Hasija, G. Lisboa, S. Luz and J. Malley. Cambridge, UK and New York, NY, USA: Cambridge University Press, 2022. DOI: 10.1017/9781009157926.012.

[4] F. Yan, E. Winijkul, D. G. Streets, Z. Lu, T. C. Bond and Y. Zhang. 'Global emission projections for the transportation sector using dynamic technology modeling'. In: *Atmospheric Chemistry and Physics* 14.11 (2014), pp. 5709–5733. DOI: 10.5194/acp-14-5709-2014. URL: https://acp.copernicus.org/articles/14/5709/2014/.

[5] J. I. Levy, J. J. Buonocore and K. von Stackelberg. 'Evaluation of the public health impacts of traffic congestion: a health risk assessment'. In: *Environmental Health* 9 (Oct. 2010), p. 65. DOI: 10.1186/1476-069X-9-65. URL: https://doi.org/10.1186/1476-069X-9-65.

[6] R. Louf and M. Barthelemy. 'How congestion shapes cities: from mobility patterns to scaling'. In: *Scientific Reports* 4.1 (July 2014), p. 5561. ISSN: 2045-2322. DOI: 10.1038/srep05561. URL: https://doi.org/10.1038/srep05561.

[7] TomTom. *Annual TomTom Traffic Index Major Traffic Trends Shaping Cities Globally in 2023*. Tech. rep. TomTom, 2023. URL: https://a.storyblok.com/f/178460/x/863802b48e/major-traffic-trends-shaping-cities-globally-in-2023-eu.pdf.

[8] J. K. Stolaroff, C. Samaras, E. R. O'Neill, A. Lubers, A. S. Mitchell and D. Ceperley. 'Energy use and life cycle greenhouse gas emissions of drones for commercial package delivery'. en. In: *Nature Communications* 9.1 (2018), p. 409. DOI: 10.1038/s41467-017-02411-5.

[9] A. Vidović, I. Štimac, T. Mihetec and S. Patrlj. 'Application of Drones in Urban Areas'. In: *Transportation Research Procedia* 81 (2024). 13th International Conference on Air Transport – INAIR 2024, Challenging the Status Quo in Aviation, pp. 84–97. ISSN: 2352-1465. DOI: https://doi.org/10.1016/j.trpro.2024.11.010. URL: https://www.sciencedirect.com/science/article/pii/S2352146524002606.

[10] V. Garg, S. Niranjan, V. Prybutok, T. Pohlen and D. Gligor. 'Drones in last-mile delivery: A systematic review on Efficiency, Accessibility, and Sustainability'. In: *Transportation Research Part D: Transport and Environment* 123 (2023), p. 103831. ISSN: 1361-9209. DOI: https://doi.org/10.1016/j.trd.2023.103831. URL: https://www.sciencedirect.com/science/article/pii/S1361920923002286.

[11] N. B. Roberts, E. Ager, T. Leith, I. Lott, M. Mason-Maready, T. Nix, A. Gottula, N. Hunt and C. Brent. 'Current summary of the evidence in drone-based emergency medical services care'. In: *Resuscitation Plus* 13 (2023), p. 100347. ISSN: 2666-5204. DOI: https://doi.org/10.1016/j.resplu.2022.100347. URL: https://www.sciencedirect.com/science/article/pii/S2666520422001473.

[12] H. Gupta and O. P. Verma. 'Monitoring and surveillance of urban road traffic using low altitude drone images: a deep learning approach'. In: *Multimedia Tools and Applications* 81.14 (June 2022), pp. 19683–19703. ISSN: 1573-7721. DOI: 10.1007/s11042-021-11146-x. URL: https://doi.org/10.1007/s11042-021-11146-x.

[13] Single European Sky ATM Research 3 Joint Undertaking. *U-space : blueprint*. Publications Office, 2017. URL: https://data.europa.eu/doi/10.2829/335092.

[14] FAA. *Urban Air Mobility Concept of Operations*. Tech. rep. Version 2.0. Federal Aviation Administration, 2023. URL: https://www.faa.gov/sites/faa.gov/files/Urban%20Air%20Mobility%20%28UAM%29%20Concept%20of%20Operations%202.0_0.pdf.

[15] Port of Rotterdam Authority. *Drones in the port of Rotterdam*. Port of Rotterdam. 2025. URL: https://www.portofrotterdam.com/en/port-future/innovation/drones (visited on 08/05/2025).

[16] Single European Sky ATM Research 3 Joint Undertaking. *European drones outlook study: unlocking the value for Europe*. Publications Office, 2017. URL: https://data.europa.eu/doi/10.2829/085259.

[17] T. McCarthy, L. Pforte and R. Burke. 'Fundamental Elements of an Urban UTM'. In: *Aerospace* 7.7 (2020). ISSN: 2226-4310. DOI: 10.3390/aerospace7070085.

[18] H. A. Blom, C. Jiang, W. B. Grimme, M. Mitici and Y. S. Cheung. 'Third party risk modelling of Unmanned Aircraft System operations, with application to parcel delivery service'. In: *Reliability Engineering & System Safety* 214 (2021), p. 107788. ISSN: 0951-8320. DOI: https://doi.org/10.1016/j.ress.2021.107788. URL: https://www.sciencedirect.com/science/article/pii/S0951832021003124.

[19] C. A. Roseman and B. M. Argrow. 'Weather Hazard Risk Quantification for sUAS Safety Risk Management'. en. In: *Journal of Atmospheric and Oceanic Technology* (July 2020). Section: Journal of Atmospheric and Oceanic Technology. DOI: 10.1175/JTECH-D-20-0009.1. URL: https://journals.ametsoc.org/view/journals/atot/37/7/jtechD200009.xml (visited on 18/09/2024).

[20] M. Gao, C. H. Hugenholtz, T. A. Fox, M. Kucharczyk, T. E. Barchyn and P. R. Nesbit. 'Weather constraints on global drone flyability'. In: *Scientific Reports* 11.1 (June 2021), p. 12092. ISSN: 2045-2322. DOI: 10.1038/s41598-021-91325-w. URL: https://doi.org/10.1038/s41598-021-91325-w.

[21] A. Oakey and T. Cherrett. 'Quantifying Weather Tolerance Criteria for Delivery Drones - A UK Case Study'. In: *2023 International Conference on Unmanned Aircraft Systems (ICUAS)*. 2023, pp. 1005–1012. DOI: 10.1109/ICUAS57906.2023.10156144.

[22] T. Lundby, M. P. Christiansen and K. Jensen. 'Towards a Weather Analysis Software Framework to Improve UAS Operational Safety'. In: *2019 International Conference on Unmanned Aircraft Systems (ICUAS)*. 2019, pp. 1372–1380. DOI: 10.1109/ICUAS.2019.8798271.

[23] K. O. Ploetner, C. Al Haddad, C. Antoniou, F. Frank, M. Fu, S. Kabel, C. Llorca, R. Moeckel, A. T. Moreno, A. Pukhova, R. Rothfeld, M. Shamiyeh, A. Straubinger, H. Wagner and Q. Zhang. 'Long-term application potential of urban air mobility complementing public transport: an upper Bavaria example'. In: *CEAS Aeronautical Journal* 11.4 (Dec. 2020), pp. 991–1007. ISSN: 1869-5590. DOI: 10.1007/s13272-020-00468-5. URL: https://doi.org/10.1007/s13272-020-00468-5.

[24] M. Patterson, L. Kohlman and K. Antcliff. 'A Proposed Approach to Studying Urban Air Mobility Missions Including an Initial Exploration of Mission Requirements'. In: *AHS Annual Forum and Technology Display*. May 2018.

[25] D. S. Nithya, G. Quaranta, V. Muscarello and M. Liang. 'Review of Wind Flow Modelling in Urban Environments to Support the Development of Urban Air Mobility'. In: *Drones* 8.4 (2024). ISSN: 2504-446X. DOI: 10.3390/drones8040147. URL: https://www.mdpi.com/2504-446X/8/4/147.

[26] A. Mohamed, M. Marino, S. Watkins, J. Jaworski and A. Jones. 'Gusts Encountered by Flying Vehicles in Proximity to Buildings'. In: *Drones* 7.1 (2023). ISSN: 2504-446X. DOI: 10.3390/drones7010022. URL: https://www.mdpi.com/2504-446X/7/1/22.

[27] M. Gianfelice, H. Aboshosha and T. Ghazal. 'Real-time Wind Predictions for Safe Drone Flights in Toronto'. In: *Results in Engineering* 15 (2022), p. 100534. ISSN: 2590-1230. DOI: https://doi.org/10.1016/j.rineng.2022.100534. URL: https://www.sciencedirect.com/science/article/pii/S2590123022002043.

[28] S. Jiang, J. Wang, C. Li, J. Ou, P. Duan and L. Li. 'Identification of no-fly zones for delivery drone path planning in various urban wind environments'. In: *Physics of Fluids* 36.8 (Aug. 2024), p. 085166. ISSN: 1070-6631. DOI: 10.1063/5.0221281. eprint: https://pubs.aip.org/aip/pof/article-pdf/doi/10.1063/5.0221281/20121043/085166_1_5.0221281.pdf. URL: https://doi.org/10.1063/5.0221281.

[29] S. Giersch, O. El Guernaoui, S. Raasch, M. Sauer and M. Palomar. 'Atmospheric flow simulation strategies to assess turbulent wind conditions for safe drone operations in urban environments'. In: *Journal of Wind Engineering and Industrial Aerodynamics* 229 (2022), p. 105136. ISSN: 0167-6105. DOI: https://doi.org/10.1016/j.jweia.2022.105136. URL: https://www.sciencedirect.com/science/article/pii/S016761052200232X.

[30] M. Chrit and M. Majdi. 'Improving Wind Speed Forecasting for Urban Air Mobility Using Coupled Simulations'. en. In: *Advances in Meteorology* 2022.1 (2022), p. 2629432. ISSN: 1687-9317. DOI: 10.1155/2022/2629432. URL: https://onlinelibrary.wiley.com/doi/abs/10.1155/2022/2629432 (visited on 18/09/2024).

[31] D. Seon and S. Jeong. 'Terrain-Driven Wind Environment Generation for UAM'. In: *The Proceedings of the 2021 Asia-Pacific International Symposium on Aerospace Technology (APISAT 2021), Volume 2*. Ed. by S. Lee, C. Han, J.-Y. Choi, S. Kim and J. H. Kim. Singapore: Springer Nature Singapore, 2023, pp. 531–541. ISBN: 978-981-19-2635-8.

[32] S. B. Pope. *Turbulent Flows*. Cambridge University Press, 2000.

[33] M. Chrit. 'Reconstructing urban wind flows for urban air mobility using reduced-order data assimilation'. In: *Theoretical and Applied Mechanics Letters* 13.4 (2023), p. 100451. ISSN: 2095-0349. DOI: https://doi.org/10.1016/j.taml.2023.100451. URL: https://www.sciencedirect.com/science/article/pii/S2095034923000223.

[34] J. Sousa and C. Gorlé. 'Computational urban flow predictions with Bayesian inference: Validation with field data'. In: *Building and Environment* 154 (2019), pp. 13–22. ISSN: 0360-1323. DOI: https://doi.org/10.1016/j.buildenv.2019.02.028. URL: https://www.sciencedirect.com/science/article/pii/S0360132319301313.

[35] D. Xiu and G. E. Karniadakis. 'Modeling uncertainty in flow simulations via generalized polynomial chaos'. In: *Journal of Computational Physics* 187.1 (2003), pp. 137–167. ISSN: 0021-9991. DOI: https://doi.org/10.1016/S0021-9991(03)00092-5. URL: https://www.sciencedirect.com/science/article/pii/S0021999103000925.

[36] C. García-Sánchez, G. Van Tendeloo and C. Gorlé. 'Quantifying inflow uncertainties in RANS simulations of urban pollutant dispersion'. In: *Atmospheric Environment* 161 (2017), pp. 263–273. ISSN: 1352-2310. DOI: https://doi.org/10.1016/j.atmosenv.2017.04.019. URL: https://www.sciencedirect.com/science/article/pii/S1352231017302571.

[37] H. Bijl. *Uncertainty quantification in computational fluid dynamics*. Vol. 92. Lecture notes in computational science and engineering. 1 online resource (xi, 333 pages) : illustrations (some color). Cham: Springer, 2013. ISBN: 9783319008851. DOI: 10.1007/978-3-319-00885-1. URL: https://tudelft.on.worldcat.org/oclc/859778838.

[38] C. L. Archer and M. Z. Jacobson. 'Evaluation of global wind power'. In: *Journal of Geophysical Research: Atmospheres* 110.D12 (2005). DOI: https://doi.org/10.1029/2004JD005462.

[39] K. Schweiger, R. Schmitz and F. Knabe. 'Impact of Wind on eVTOL Operations and Implications for Vertiport Airside Traffic Flows: A Case Study of Hamburg and Munich'. In: *Drones* 7.7 (2023). ISSN: 2504-446X. DOI: 10.3390/drones7070464. URL: https://www.mdpi.com/2504-446X/7/7/464.

[40] DronePort Rotterdam. *DronePort Rotterdam prepares strategic projects and initiatives for an impactful 2025*. DronePort Rotterdam. 19th Nov. 2024. URL: https://www.droneportrotterdam.com/news/droneport-rotterdam-prepares-strategic-projects-and-initiatives-for-an-impactful-2025/ (visited on 08/05/2025).

[41] ATMOSYS. *Unique model of Antwerp offers superior insights in air quality, wind comfort and wind energy potential*. ATMOSYS - VITO's atmospheric modeling team. VITO, 2024. URL: https://atmosys.vito.be/en/unique-model-antwerp-offers-superior-insights-air-quality-wind-comfort-and-wind-energy-potential (visited on 10/06/2025).

[42] R. Peters, B. Dukai, S. Vitalis, J. van Liempt and J. Stoter. 'Automated 3D reconstruction of LoD2 and LoD1 models for all 10 million buildings of the Netherlands'. English. In: *Photogrammetric Engineering and Remote Sensing* 88.3 (2022), pp. 165–170. ISSN: 0099-1112. DOI: 10.14358/PERS.21-00032R2.

[43] F. Biljecki, H. Ledoux and J. Stoter. 'An improved LOD specification for 3D building models'. In: *Computers, Environment and Urban Systems* 59 (2016), pp. 25–37. ISSN: 0198-9715. DOI: https://doi.org/10.1016/j.compenvurbsys.2016.04.005. URL: https://www.sciencedirect.com/science/article/pii/S0198971516300436.

[44] Cadastre (LV-BGT). *Large-Scale Topography Basic Registry (OGC API)*. URL: https://api.pdok.nl/lv/bgt/ogc/v1/.

[45] AHN. *Home*. Landingspagina. Publisher: AHN. URL: https://www.ahn.nl/.

[46] I. Paden, C. Garcia-Sanchez and H. Ledoux. 'Towards Automatic Reconstruction of 3D City Models Tailored for Urban Flow Simulations'. In: *Frontiers in Built Environment* 8 (2022). ISSN: 2297-3362. DOI: 10.3389/fbuil.2022.899332.

[47] B. Blocken. ‘Computational Fluid Dynamics for urban physics: Importance, scales, possibilities, limitations and ten tips and tricks towards accurate and reliable simulations’. In: *Building and Environment*. Fifty Year Anniversary for Building and Environment 91 (2015), pp. 219–245. ISSN: 0360-1323. DOI: 10.1016/j.buildenv.2015.02.015.

[48] R. B. Stull. *An Introduction to Boundary Layer Meteorology*. Vol. 13. Atmospheric and Oceanographic Sciences Library. Springer Dordrecht, 1988, p. 670. ISBN: 978-90-277-2768-8. DOI: 10.1007/978-94-009-3027-8.

[49] B. E. Launder and D. Spalding. ‘The numerical computation of turbulent flows’. In: *Computer Methods in Applied Mechanics and Engineering* 3.2 (1974), pp. 269–289. ISSN: 0045-7825. DOI: https://doi.org/10.1016/0045-7825(74)90029-2.

[50] H. G. Weller, G. Tabor, H. Jasak and C. Fureby. ‘A tensorial approach to computational continuum mechanics using object-oriented techniques’. In: *Computer in Physics* 12.6 (Nov. 1998), pp. 620–631. ISSN: 0894-1866.

[51] T. O. Foundation. *OpenFOAM | Free CFD Software | The OpenFOAM Foundation*. en-GB. URL: https://openfoam.org/ (visited on 21/09/2023).

[52] S. Patankar. *Numerical Heat Transfer and Fluid Flow*. 1st edition. Boca Raton, Florida: CRC Press, 1980.

[53] H. Jasak. ‘Error Analysis and Estimation for the Finite Volume Method with Applications to Fluid Flows’. In: *PhD. Thesis, Imperial College, University of London* (1996).

[54] D. M. Hargreaves and N. G. Wright. ‘On the use of the k–epsilon model in commercial CFD software to model the neutral atmospheric boundary layer’. In: *Journal of Wind Engineering and Industrial Aerodynamics* 95.5 (2007), pp. 355–369. ISSN: 0167-6105. DOI: https://doi.org/10.1016/j.jweia.2006.08.002.

[55] J. Wieringa. ‘Updating the Davenport roughness classification’. In: *Journal of Wind Engineering and Industrial Aerodynamics* 41.1 (1992), pp. 357–368. ISSN: 0167-6105. DOI: https://doi.org/10.1016/0167-6105(92)90434-C.

[56] P. Luchini. ‘Universality of the Turbulent Velocity Profile’. In: *Phys. Rev. Lett.* 118 (22 June 2017), p. 224501. DOI: 10.1103/PhysRevLett.118.224501. URL: https://link.aps.org/doi/10.1103/PhysRevLett.118.224501.

[57] Royal Netherlands Meteorological Institute (KNMI). *Wind - wind speed, direction, standard deviation at a 10 minute interval*. Dataset. URL: https://dataplatform.knmi.nl/dataset/windgegevens-1-0 (visited on 12/05/2025).

[58] N. Wiener. ‘The Homogeneous Chaos’. In: *American Journal of Mathematics* 60.4 (1938), pp. 897–936. ISSN: 00029327, 10806377. URL: http://www.jstor.org/stable/2371268 (visited on 02/04/2025).

[59] B. M. Adams, W. J. Bohnhoff, K. R. Dalbey, M. S. Ebeida, J. P. Eddy, M. S. Eldred, R. W. Hooper, P. D. Hough, K. T. Hu, J. D. Jakeman, M. Khalil, K. A. Maupin, J. A. Monschke, E. E. Prudencio, E. M. Ridgway, P. Robbe, A. A. Rushdi, D. T. Seidl, J. A. Stephens, L. P. Swiler and J. G. Winokur. *Dakota 6.21.0 documentation*. Tech. rep. SAND2024-15492O. Albuquerque, NM: Sandia National Laboratories, Nov. 2024. URL: http://snl-dakota.github.io.

[60] DJI. *DJI FlyCart 30 Combo*. 2025. URL: https://www.dji.com/flycart-30 (visited on 07/05/2025).

[61] Matternet. *M2 Drone*. 2025. URL: https://www.matternet.com/our-system-aircraft (visited on 07/05/2025).

[62] Zipline. *Safety at Zipline*. 2025. URL: https://www.flyzipline.com/safety (visited on 07/05/2025).

[63] Wing. *Meet the drones taking delivery to new heights*. 2025. URL: https://wing.com/technology (visited on 07/05/2025).

[64] E. U. A. S. Agency. *Certified Category — Civil Drones*. 2025. URL: https://www.easa.europa.eu/en/domains/drones-air-mobility/operating-drone/certified-category-civil-drones (visited on 07/05/2025).

[65] A. Morfin Veytia, A. Patil, I. Pađen, J. Ellerbroek, C. Garcia Sanchez and J. Hoekstra. *Supporting data and code for: Investigating the Operational Feasibility for Drones Using Wind Simulations in Rotterdam*. 2025. DOI: 10.4121/908dd8a2-821e-485b-b659-21995f273e4e.

[66] A. Patil and C. Garcia-Sanchez. *riskMap - An OpenFOAM utility to compute directionally averaged risk metrics for RANS simulations*. Version 0.1.0. May 2024. DOI: 10.5281/zenodo.11207890. URL: https://github.com/AkshayPatil1994/riskMap.git.

[67] Atlas Natural Capital. *Climate control in cities*. Online resource. 2024. URL: https://www.atlasnatuurlijkkapitaal.nl/en/node/681 (visited on 15/05/2025).

[68] Ö. Gürel and S. Serdarasan. 'Drone-Assisted Last-Mile Delivery Under Windy Conditions: Zero Pollution Solutions'. In: *Smart Cities* 7.6 (2024), pp. 3437–3457. ISSN: 2624-6511. DOI: 10.3390/smartcities7060134. URL: https://www.mdpi.com/2624-6511/7/6/134.

[69] A. Thibbotuwawa, G. Bocewicz, G. Radzki, P. Nielsen and Z. Banaszak. 'UAV Mission Planning Resistant to Weather Uncertainty'. In: *Sensors* 20.2 (2020). ISSN: 1424-8220. DOI: 10.3390/s20020515. URL: https://www.mdpi.com/1424-8220/20/2/515.

[70] Y. Chan, K. K. Ng, C. Lee, L.-T. Hsu and K. Keung. 'Wind dynamic and energy-efficiency path planning for unmanned aerial vehicles in the lower-level airspace and urban air mobility context'. In: *Sustainable Energy Technologies and Assessments* 57 (2023), p. 103202. ISSN: 2213-1388. DOI: https://doi.org/10.1016/j.seta.2023.103202. URL: https://www.sciencedirect.com/science/article/pii/S2213138823001959.

8

Discussion and Recommendations

This thesis compared and evaluated different airspace designs and rules and presented a method to quantify the risk and operational time due to local wind conditions. Vienna and Rotterdam were used as the two main cities for evaluation. This chapter presents a discussion of the main findings of the thesis and provides recommendations for future work.

8.1. Overall discussion

The two main goals of this thesis were to **(1)** develop and compare different airspace designs and rules that improved conflict prevention, and **(2)** evaluate risk and operational feasibility due to local wind conditions. These airspace designs, rules, and wind conditions have a direct effect on the observed safety and efficiency in the airspace. For this thesis, there are two main views for safety. For goal **(1)**, safety was evaluated with observed conflicts and intrusions between interacting drones. While, for goal **(2)**, safety was defined by the ability of drones to withstand certain wind speeds and turbulence created by the wind interacting with the urban environment. The efficiency evaluation refers to how route duration or route distance changes with different airspace designs and rules (goal **(1)**). These research goals were presented in Ch. 1 and aimed to answer research question RQ1.

8.1.1. Constrained urban airspace design considerations

Ch. 2 outlined urban airspace design considerations to answer research question RQ2. In this chapter, different airspace structures were presented, but it was stated that the focus is in constrained airspace design. In urban environments where there are tall buildings or other infrastructure, the routes of drones may be limited to a constrained network. This means that it may not be feasible for small aircraft to fly above the highest building. Additionally, even if there aren't any physical constraints, airspace managers may limit aircraft to only pre-defined routes in an attempt to limit third-party risk, privacy or other reasons.

The main considerations used to achieve goal **(1)** were airspace designs and rules that make use of the limited vertical and horizontal space in the urban environment. This thesis did not study the interactions of drones with general aviation and/or civil aviation. Therefore, it is assumed that drones only operate in ZU airspace [1] which is typically defined away from airports and up to 500 feet above the ground level.

The interaction between wind and the urban environment creates complex situations where there are areas locally high average wind speed and/or turbulence. Therefore, for goal **(2)**, the thesis aimed to study the effects of this local wind. The focus was on evaluating risk areas and yearly operational time for drone flights, considering when the airspace is unsafe to fly in. Although not a focus, the thesis has shown wind speeds and turbulence are of an order of magnitude that will affect path planning and mission time and distance even when the airspace is considered safe to operate.

8.1.2. Thesis goal 1: Conflict prevention with airspace design and rules

This thesis goal was focused on analysing airspace designs and rules that benefited conflict prevention. In general, the goal of conflict prevention is to reduce the probability that aircraft interact in a manner that creates conflicts and leads to a loss of separation. Conflict prevention acts at a higher level than

conflict resolution and should organise traffic such that aircraft have enough space for conflict resolution if necessary. This can be achieved by effectively organising traffic along the vertical and horizontal airspace. Thesis goal **(1)** was achieved by answering research questions RQ3 and RQ4 and will be discussed in the following sections.

Vertical: airspace structure utilisation and aircraft allocation

Research question RQ3 analysed how airspace layering strategies and height allocation methods, focusing on vertical airspace, affect safety and efficiency across varying traffic demand levels in the airspace of Vienna. Vertical airspace is a limited resource in urban environments. Previous research has made estimates of air traffic densities orders of magnitude higher than what is currently flying today [2, 3]. At these high traffic densities, vertical airspace will be limited in order to reduce interactions with general and civil aviation. Therefore, this vertical space should be allocated and used effectively by drones and drone operators.

Ch. 3 focused on vertical utilisation of airspace and aircraft allocation in this space in a constrained environment (refer to Sec. 2.3). The first experiment of the chapter compared two different structures. These structures contained layers with different utilisations (cruise or turn layers). One had relatively more layers for cruising (similar to [4, 5]), while the other had relatively more layers for turning space. It was observed that at relatively low traffic demand levels, there are small differences in safety between the two structures. However, as density increased, cruising space became more important and the intrusions per flight were lower in the structure with more cruising layers.

One important aim of airspace design and rules is to reduce the probability that aircraft will interact. The goal is to act on the conflict prevention level rather than on the conflict resolution level. This was also an important part of studies in the Metropolis project [6]. The results of Ch. 3 result highlighted an apparent contradiction that is observable in the first experiment. The structure with more cruising space had more conflicts per flight than the structure with more turn space at high traffic demand levels. Conversely, the structure with more cruise space had fewer intrusions per flight at the same high traffic demand level. Although fewer conflicts are generally desirable, fewer conflicts does not always mean one structure is safer than another. This is because tactical conflict resolution is used as the method of communication between aircraft. That is to say, provided enough space to resolve conflicts, which the structure with more cruise layers provides, then it is possible to have a higher intrusion prevention rate to lower the overall intrusions.

The second experiment of the chapter compared four different strategies to allocate aircraft to a layered airspace structure across different traffic demand levels. One strategy gave aircraft more freedom by allowing them to fly as low as possible. The other three strategies pre-allocated aircraft to a specific height based on density, flight distance and random chance. In this experiment, it was observed that the strategy allowing for more freedom was slightly safer at lower

demand levels. However, as the demand level increased, the random or density allocation strategies tended to be safer because aircraft were more predictable and did not perform as many vertical manoeuvres. Therefore, it can be concluded that as traffic demand level increases, airspace rules should constrain aircraft manoeuvres so the movements of the aircraft are more predicable. A similar conclusion was reached in [7], where turning layers were completely removed. At low traffic demand levels, it makes sense to give aircraft more freedom to choose where they fly. Because there are fewer aircraft in the air, there is more space for aircraft to focus on reducing local density only when necessary. Finally, in terms of travel time, the strategy that allowed aircraft freedom to choose their travel height also travelled longer. However, this was a difference of about 2%. The low difference in travel time is because in both cases, aircraft take a similar horizontal route, and they typically do not slow down during vertical transitions.

Horizontal: decentralised dynamic capacity balancing

Urban air missions will need to be more ad-hoc if they are expected to replace a significant portion of current ground traffic. Recently, Amazon [8] was delivering via drone for orders needed within an hour of placing them. This uncertainty can make demand difficult to predict and plan for via centralised separation management. Additionally, aircraft operators may be interested in sharing only limited information about their mission.

For these reason, a decentralised dynamic capacity balancing method inspired by [9] was developed in Ch. 4. This method was developed to answer research questions RQ4, which asked how a decentralised dynamic capacity balancing method can reduce local density and complexity with real-time and historical flow data of urban air operations.

In this method, the goal of the central actor is to gather current flow information (conflicts, positions, and intrusions) and attempt to reduce local traffic density and complexity by dynamically altering the cost of flying through the airspace. Nevertheless, it is expected that the predictability of traffic demand will be limited but still not completely unpredictable. This is why the extended method in Ch. 5 incorporates historical data into the real-time decentralised dynamic capacity balancing method from Ch. 4. These two chapters aimed to tackle the problem of horizontal organisation of aircraft in the airspace.

The method developed in Ch. 4 compared different data sources to identify zones of high traffic density or complexity. Aircraft receive an updated cost of flying in the airspace and attempt to replan their routes with new paths that avoid these areas. It was observed that depending only on traffic density is not sufficient to increase safety in the airspace. It is more helpful to track complexity metrics that show where aircraft are converging. The results show that using current conflicts to identify high-complexity areas significantly improves safety with an additional 6% increase in distance travelled when comparing to a case where there is no replanning, except at low traffic demand levels. At low demand levels, there is not enough conflict information to be used effectively and isolate areas of high-complexity.

This result also highlights another view of the conflict contradiction mentioned in the previous section. The method in Ch. 4 depends on measuring conflicts in order to improve safety. Conflicts are needed in order to solve them and reduce the amount of intrusions. This highlights that conflicts are an important data source for conflict prevention. This is why at low traffic demand levels there is no safety improvement shown by the method. Fewer live conflicts are occurring, so it is more difficult to dynamically find the areas where aircraft are converging.

This conflict contradiction led to the work presented in Ch. 5. This aims to incorporate historical data into the decentralised dynamic capacity balancing method. It does this by pre-dividing the airspace into zones using historical data. Nevertheless, the method still uses current conflict information of those zones to alter the cost of the pre-defined zones. When compared to the original method developed in Ch. 4, it was observed that at low traffic densities, there were 30 percent fewer intrusions and about 10 % more distance travelled compared to a case where aircraft do not change their original route. However, as the density increases, using only real-time data (method in Ch. 5) is safer because the dynamic nature of identifying zones allows the method to be more effective at finding zones with high local complexity.

8.1.3. Thesis Goal 2: Local wind effects on urban air operations

The interaction of the wind flow with buildings, vegetation, water and other parts of cities can create complex flows for drones. Whereas traditional air traffic tends to operate high in the atmosphere where the air is more predictable, drones will operate inside the turbulent atmospheric boundary layer. This complex three-dimensional air flow will create areas with higher relative risk and limit the operational time for missions. Therefore, the wind flow will likely limit where and when drones can operate in a city. This is why research question RQ5 aimed to learn how local wind conditions affect the risk and operational feasibility of urban air operations.

Ch. 6 compared wind measurements to two Computational Fluid Dynamics (CFD) simulations in the centre of The Hague. It was shown that in some places, the CFD model has similar results to the measured wind data. However, other places had large discrepancies in speed and direction. This is due to several factors. One is that the computation geometry does not always represent the actual situation on the ground. For example, these simulations did not include the effects of vegetation and assumed a flat terrain. Additionally, the low level of detail in the building models will reduce the accuracy of the CFD results. Nevertheless, the measurements and simulations showed the complexity of urban air flows. In some areas both the measurements and the simulations showed air flow that was perpendicular to the direction of the streets and also situations where the air flow does not align with the global meteorological direction.

There is an important trade-off that is made when simulating the urban air flow. Typically, Reynolds Averaged Navier Stokes (RANS) simulations are performed because they have relatively lower computational cost. However, they typically only provide an average view of the turbulent field and velocity. This

is why sometimes Large Eddy Simulations (LES) are performed [10]. However, these have very high computational cost, so it is difficult to perform a city-wide analysis. Therefore, Ch. 7 used an ensemble of RANS simulations with different inflow conditions chosen with a polynomial chaos expansion to run city-wide simulations for Rotterdam.

Additionally, buildings, water bodies, vegetation, and the varying terrain were included in these simulations to capture the diversity of Rotterdam. Then, using the annual wind data measured from a weather station, it is possible to create a probabilistic risk map and perform a flight operational feasibility analysis. The risk is based on varying speed and turbulence safety thresholds that drones should withstand. These limits will likely vary depending on flight phase, mission type, and aircraft type. This is why the analysis is performed with varying limits. Additionally, the code and results were shared so that limits not shared in this work can also be analysed.

An interesting result was that it is possible to build a comprehensive city-wide risk map considering the yearly wind conditions, combining 16 simulation results. It yielded similar results as when using 40 simulations. Therefore, if another city wants to create their own city-wide risk maps, they can have a reduced number of CFD simulations. However, it is recommended that once the risk areas are identified, that a more accurate simulation is performed using by performing an LES with a smaller domain accompanied by an increased level of detail in the building models. This is important during take-off and landing, since the drones can be closer to buildings during that part of the flight.

The flight operational analysis recreated the wind conditions of 2022 every 10 minutes. Then the analysis consisted of identifying zones where a certain wind speed or turbulence threshold were exceeded. It showed that inside Rotterdam, drones needed to withstand a medium level of turbulence and a wind speed of 12 metres per second to be operational 90% of the time in 2022 up to 60 metres above the ground. This assumes that drone operators and airspace managers are able to accurately forecast when conditions will become unsafe. In reality, this will be difficult, and an operational time of 90% could be difficult to achieve.

8.2. Recommendations for future research

Based on the results of this thesis, two general paths of research are recommended. The first path recommends options to continue building upon the work presented. The second path recommends research that was out of scope for this thesis.

8.2.1. Further studies along line of work of thesis

Airspace layer functions and pre-allocation of cruise heights

Ch. 3 studied the trade-off of assigning layers different functions in limited vertical space. However, the work only considered the trade-off between cruising and turning layers. These separate layer functions were also considered in [4, 5] but provide a limited view on what a layer can provide. Other works in urban

airspace design proposed separate layers for de-confliciton [11]. It might also be necessary to reserve layers for emergency missions, such as police or medical missions. Other research has also observed that turn layers may not be necessary [12]. Therefore, it is recommended to continue studies that aim to make the most effective use of the limited vertical space by analysing other functions for a layered airspace or performing an optimisation analysis.

The research on pre-allocation of cruise heights in Ch. 3 can also be further extended. In this work, it was observed that at low demand levels, there is no significant safety difference between the density allocation versus the dynamic redistribution method. Therefore, it may be interesting to explore an adaptive structure. If there is very low density, then it is unnecessary to force drones to fly to the highest layer. Then, as the density increases, there will be a point when it becomes necessary to make aircraft more predictable. An adaptive structure that is based on the current density could provide a balance between safety and route duration and distance. However, this transition will be difficult for aircraft in the air at the time of the transition.

Decentralised Dynamic Capacity Balancing

Ch. 4 and Ch. 5 developed a method for decentralised dynamic capacity balancing, in which high-complexity zones are identified either with only real-time data or by also including historical data. In this work, the role of the central authority is only in gathering the data and then applying the additional cost of the airspace. The individual aircraft receive an updated cost in the airspace and attempt to plan around them. The Metropolis II [13] showed that a hybrid method that splits the responsibility for separation management and flight planning can provide increased safety over a fully centralised or decentralised system. For this reason, it is recommended to combine the proposed method for capacity balancing with a centralised flight planner. It might be possible to further reduce local traffic complexity and density with a cohesive combination.

Urban wind studies

Although the results of Ch. 6 and Ch. 7 showed that CFD simulations provide valuable insight into airspace risk and operational feasibility, it required a significant amount of computational resources that may be out of reach for some cities. Therefore, it is recommended that research continues on developing high quality reduced ordered models. It is possible to extend the uncertainty quantification analysis in Ch. 7 to build inflow cases that were not simulated. It is then important to check if a rebuilt inflow case matches a simulated result.

The RANS simulations performed in Chs. 6 and 7 are relatively less accurate than an LES. However, the RANS approach is significantly less computationally extensive. Therefore, it is recommended that in other cities, a RANS risk analysis is first performed to identify regions with high velocity and/or turbulent kinetic energy. Then, in these smaller regions that are of the scale of city-blocks, an LES can be performed to get a more accurate view of the regions.

This thesis specifically focused on the neutral atmospheric boundary layer of Rotterdam. The Urban Heat Island in Rotterdam can create a 2 $°C$ difference between the air inside and outside the city [14]. The buoyant effects have been shown to increase turbulence in urban environments, especially from ground level to around 500 metres (see Fig. 3 in [10]). This could increase the flight risk and decrease the yearly operational time for drone missions. Moreover, this thesis provided generic and parametrized wind and turbulence thresholds safety thresholds. It is recommended for drone operators to provide more information about their performance under turbulent conditions. Different aircraft types, mission types, and even routes will likely have an effect on the acceptable thresholds. Therefore, along with drone manufactures being more open about the drone limitations, government authorities should work to establish guidelines for setting these limitations.

The results in Ch. 7 focused mainly on risk and operational feasibility. Nevertheless, it is possible to use the resulting wind fields and include them in other areas of drone research. For example, studies like [15, 16] will benefit from more realistic wind fields to test their path planning algorithms. This is one reason for sharing the wind fields in the supplementary dataset of Ch. 7. These results could also be useful for airspace design in general and conflict resolution studies.

8.2.2. Other areas of study

This thesis provided guidelines and considerations for urban airspace design and rules of travel. However, it has limitations that were considered out of scope but may significantly affect constrained airspace design, rules, and risk. Some of these are listed below:

- **Mixed airspace design**: The urban airspace is not always fully open or constrained. Therefore, more focus should be on mixed airspace structures and rules such as in [13].
- **Take-off and landing**: Take-off and landing procedures were not seriously considered in this thesis. Strategies such as those considered in [17] should be integrated into airspace designs and rules.
- **Vertiport locations**: The locations of vertiports were randomly selected. In reality, the locations of vertiports can be more organised and could create converging and diverging traffic patterns.
- **Communication uncertainty**: This thesis assumed that there is perfect knowledge of state-information. However, drone locations may not always be communicated with certainty and without time delay. This will likely limit the allowable traffic densities.
- **Environmental emissions**: It is generally assumed that drones will have less greenhouse gas emissions than current ground traffic. However, this assumption should be furthered studied to ensure that it is the case.

- **Other environmental factors**: Other factors such as noise pollution and interactions with wild life may mean that drone traffic is significantly disruptive to the environment. This should be studied further and could limit the allowable traffic densities.
- **Interactions with civil/military aviation**: This thesis assumed that drones remain below a certain height and have limited interactions with civil and military aviation. This does not mean that there will not be any interactions, so this should be furthered studied.
- **Elevation standards**: It is assumed in this thesis that drones will always fly at similar altitudes above the ground. Elevation standards may be difficult to standardise and will require significant effort. The varying terrain of the urban environment will need to be incorporated into the urban airspace design and rules.
- **Wind forecasting**: The forecasting of accurate wind conditions will largely affect the available safe airspace and operational time for drone missions.

References

[1] C. Barrado, M. Boyero, L. Brucculeri, G. Ferrara, A. Hately, P. Hullah, D. Martin-Marrero, E. Pastor, A. P. Rushton and A. Volkert. 'U-Space Concept of Operations: A Key Enabler for Opening Airspace to Emerging Low-Altitude Operations'. In: *Aerospace* 7.3 (2020). ISSN: 2226-4310. DOI: 10.3390/aerospace7030024. URL: https://www.mdpi.com/2226-4310/7/3/24.

[2] Single European Sky ATM Research 3 Joint Undertaking. *European drones outlook study: unlocking the value for Europe*. Publications Office, 2017. URL: https://data.europa.eu/doi/10.2829/085259.

[3] M. Doole, J. Ellerbroek and J. Hoekstra. 'Estimation of traffic density from drone-based delivery in very low level urban airspace'. en. In: *Journal of Air Transport Management* 88 (2020), p. 101862. DOI: 10.1016/j.jairtraman.2020.101862.

[4] M. Doole, J. Ellerbroek, V. L. Knoop and J. Hoekstra. 'Constrained Urban Airspace Design for Large-Scale Drone-Based Delivery Traffic'. en. In: *Aerospace* 8.2 (2021). DOI: 10.3390/aerospace8020038.

[5] M. Ribeiro, J. Ellerbroek and J. Hoekstra. 'Velocity Obstacle Based Conflict Avoidance in Urban Environment with Variable Speed Limit'. In: *Aerospace* 8 (2021). DOI: 10.3390/aerospace8040093.

[6] E. Sunil, J. Hoekstra, J. Ellerbroek, F. Bussink, D. Nieuwenhuisen, A. Vidosavljevic and S. Kern. 'Metropolis: Relating Airspace Structure and Capacity for Extreme Traffic Densities'. en. In: *ATM seminar 2015, 11th USA/EUROPE Air Traffic Management R&D Seminar*. 2015.

[7] C. Badea, A. Morfin Veytia, J. Ellerbroek, J. Hoekstra, N. Patrinopoulou, I. Daramouskas, V. Lappas and V. Kostopoulos. 'Tactical conflict detection and resolution for a decentralised U-space traffic management system'. Unpublished. 2023.

[8] K. Roose. 'Are Amazon's Drones Finally Ready for Prime Time?' In: *The New York Times* (Dec. 2024). URL: https://www.nytimes.com/2024/12/20/technology/amazon-prime-air-drone-delivery.html (visited on 10/01/2025).

[9] K. Bilimoria and H. Lee. 'Analysis of Aircraft Clusters to Measure Sector-Independent Airspace Congestion'. In: *AIAA 5th ATIO and16th Lighter-Than-Air Sys Tech. and Balloon Systems Conferences*. Arlington, Virginia, 2005.

[10] S. Giersch, O. El Guernaoui, S. Raasch, M. Sauer and M. Palomar. 'Atmospheric flow simulation strategies to assess turbulent wind conditions for safe drone operations in urban environments'. In: *Journal of Wind Engineering and Industrial Aerodynamics* 229 (2022), p. 105136. ISSN: 0167-6105. DOI: https://doi.org/10.1016/j.jweia.2022.105136. URL: https://www.sciencedirect.com/science/article/pii/S016761052200232X.

[11] T. McCarthy, L. Pforte and R. Burke. 'Fundamental Elements of an Urban UTM'. In: *Aerospace* 7.7 (2020). ISSN: 2226-4310. DOI: 10.3390/aerospace7070085.

[12] C. A. Badea, A. Morfin Veytia, N. Patrinopoulou, I. Daramouskas, J. Ellerbroek, V. Lappas, V. Kostopoulos and J. Hoekstra. 'Unifying Tactical Conflict Prevention, Detection, and Resolution Methods in Non-Orthogonal Constrained Urban Airspace'. en. In: *Aerospace* 10.5 (2023), p. 423. DOI: 10.3390/aerospace10050423.

[13] A. Morfin Veytia, C. A. Badea, J. Ellerbroek, J. Hoekstra, N. Patrinopoulou, I. Daramouskas, V. Lappas, V. Kostopoulos, P. Menendez, P. Alonso, J. Rodrigo, V. Terrazas, D. Bereziat, A. Vidosavljevic and L. Sedov. 'Metropolis II: Benefits of Centralised Separation Management in High-Density Urban Airspace'. In: *12th SESAR Innovation Days*. 2022.

[14] Atlas Natural Capital. *Climate control in cities*. Online resource. 2024. URL: https://www.atlasnatuurlijkkapitaal.nl/en/node/681 (visited on 15/05/2025).

[15] Ö. Gürel and S. Serdarasan. 'Drone-Assisted Last-Mile Delivery Under Windy Conditions: Zero Pollution Solutions'. In: *Smart Cities* 7.6 (2024), pp. 3437–3457. ISSN: 2624-6511. DOI: 10.3390/smartcities7060134. URL: https://www.mdpi.com/2624-6511/7/6/134.

[16] Y. Chan, K. K. Ng, C. Lee, L.-T. Hsu and K. Keung. 'Wind dynamic and energy-efficiency path planning for unmanned aerial vehicles in the lower-level airspace and urban air mobility context'. In: *Sustainable Energy Technologies and Assessments* 57 (2023), p. 103202. ISSN: 2213-1388. DOI: https://doi.org/10.1016/j.seta.2023.103202. URL: https://www.sciencedirect.com/science/article/pii/S2213138823001959.

[17] Y. Zheng, D. Li, Z. Shen, C. Li and Z. Zhang. 'Optimized Airspace Structures and Sequencing Method for Urban Logistics Droneport'. In: *Aerospace* 12.3 (2025). ISSN: 2226-4310. DOI: 10.3390/aerospace12030257. URL: https://www.mdpi.com/2226-4310/12/3/257.

A

Appendix for Chapter 4

A.1. Hypothesis testing results

This appendix will illustrate the formal hypothesis testing results for the hypotheses presented in Section 4.3.1. The safety levels of the clustering strategies and baseline case will be compared based on the observed intrusions per flight with a Wilcoxon signed-rank test [1] . The intrusions per flight metric is chosen as the relevant metric because it represents aircraft converging at distances less than the safe separation distance.

The null hypothesis is that the differences between strategies is not statistically significant, therefore the null hypotheses will be rejected when $p_{value} < 0.01$

A.1.1. H1 hypothesis test

Hypothesis **H1** states that all three clustering strategies will be safer than the baseline case. The null hypothesis is that the baseline case is not statistically different from any of the three clustering strategies. The p_{value} comparing the baseline case to the three clustering strategies is seen in Table A.1. Each column represents how that particular strategy compares to the baseline. Hypothesis **H1** was partially accepted because the clustering strategies only have higher safety levels at the higher traffic demand levels.

A.1.2. H2 hypothesis test

Hypothesis **H2** states that two traffic complexity clustering strategies (conflict-based and intrusion-based) will have higher safety levels than the traffic density strategy (position-based). The null hypothesis is that the position-based strategy is not statistically different from the conflict-based and intrusion-based strategy. The p_{value} comparing the position-based case to the two traffic complexity clustering strategies is seen in Table A.2. Each column represents how that particular strategy

[1] Frank Wilcoxon, "Individual Comparisons by Ranking Methods," *Biometrics Bulletin* 1, no. 6 (1945): 80–83, https://doi.org/10.2307/3001968.

A

Table A.1: p_{values} comparing the baseline (no clustering) case to the three clustering strategies. Highlighted cells refer to the cases where the null hypothesis can be rejected.

	Clustering strategies compared to the baseline (no clustering) case		
Traffic demand level	**Conflict-based** p_{value}	**Intrusion-based** p_{value}	**Position-based** p_{value}
100	0.5	0.23	0.41
200	<0.01	0.89	0.72
300	<0.01	<0.01	<0.01
400	<0.01	<0.01	<0.01
500	<0.01	<0.01	<0.01

compares to the position-based strategy. Hypothesis **H2** was partially accepted because the conflict-based strategy has higher safety levels than the position-based, starting at 200 aircraft in the air.

Table A.2: p_{values} comparing the position-based strategy to the two traffic complexity strategies (conflict-based and intrusion-based). Highlighted cells refer to the cases where the null hypothesis can be rejected.

	Clustering strategies compared to the position-based case	
Traffic demand level	**Conflict-based** p_{value}	**Intrusion-based** p_{value}
100	0.65	0.01
200	<0.01	0.84
300	<0.01	0.06
400	<0.01	0.67
500	<0.01	<0.01

A.1.3. H3 hypothesis test

Hypothesis **H3** states that the intrusion-based strategy will have higher safety level than the conflict-based strategy. The null hypothesis is that the strategies are not statistically different from each other. The p_{value} comparing both complexity strategies is seen in Table A.3. Hypothesis **H3** was rejected because the conflict-based strategy had a higher level of safety at most traffic demand levels.

Table A.3: p_{values} comparing the conflict-based strategy and intrusion-based strategies. Highlighted cells refer to the cases where the null hypothesis can be rejected.

Traffic demand level	p_{value}
100	0.03
200	<0.01
300	<0.01
400	<0.01
500	<0.01

B

Appendices for Chapter 7

B.1. Scaling the inflow speeds

For the simulations, we selected an inflow speed of 10 m/s at the reference height of 10 metres. However, as it can be seen in Fig. 7.4a, there are countless different speeds measured in 2022. The inflow speed profile is set to follow the log-law (Eq. 7.5) and it is assumed that the raw simulation results can be scaled linearly for other inlet speeds. This is due to the asymptotic behaviour of the bulk Reynolds number ($Re_b = U_{\text{in}}H/\nu \gg 10^6$), where H is the representative height of the tallest building in the domain [1].

Below, we show an example of how the raw simulation results are scaled to other inflow conditions. Fig. B.1a shows the log-law model for an inflow speed (γ) of 10 m/s at 10 m height in red and the corresponding OpenFOAM results at the inlet for Region 1. The profile in blue is the log-law model for an inflow speed of 4 m/s at 10 m height. The blue dashed line represents the scaling of the raw OpenFOAM results to the inflow case of 4 m/s at 10 m.

The process to achieve this scaling is as shown in Eq. B.1.

$$U_\gamma = U_{sim}\phi(\gamma, x_3) \tag{B.1}$$

Here U_{sim} is the speed simulation results, which are shown in red dashed lines in Fig. B.1a. U_γ represents the scaled speed to another inflow speed (γ). For our example, γ is set to 4 m/s at 10 metres and the example shows this results in blue-dashed lines. $\phi(\gamma, x_3)$ is the scaling function that scales the simulated results to different inflow profiles.

This scaling function is derived by using the of the results of the log-law. In our example, we look at how the simulation results would be scaled at a height of 20 metres for an inflow profile with a speed of 4 m/s at 10 metres height. Therefore, the scaling function at 20 metres height is:

[1] Paolo Luchini, "Universality of the Turbulent Velocity Profile," *Physical Review Letters* 118, no. 22 (2017): 224501, https://doi.org/10.1103/PhysRevLett.118.224501.

$$\phi(4m/s, 20m) = \frac{U_{\gamma=4m/s}(20m)}{U_{\gamma=10m/s}(20m)} \tag{B.2}$$

B

$U_{\gamma=4m/s}(20m)$ is the speed derived from the log-law at 20 metres height, when the reference inflow speed at 10 metres is 4 m/s. Similarly, $U_{\gamma=10m/s}(20m)$ is the speed derived from the log-law at 20 metres height when the reference inflow speed at 10 metres is 10 m/s.

We solve for $U_{\gamma=10m/s}(20)$ from the log-law, and recall that the friction velocity u^* is derived by solving the log-law model for the given inflow speed and reference height. For the inflow speed of 10 m/s at 10 m, $u^* = 1.35$ m/s. The constants of the log law model are the von Kármán constant (κ =0.41) and the aerodynamic roughness (z_0 =0.5):

$$U_{\gamma=10m/s}(20m) = \frac{1.35m/s}{\kappa} \ln\left(\frac{20 + z_0}{z_0}\right) = 12.20m/s \tag{B.3}$$

Then, we solve for $U_{\gamma=4m/s}(20)$ which requires a new friction velocity calculation, $u^* = 0.54$ m/s:

$$U_{\gamma=4m/s}(20m) = \frac{0.54m/s}{\kappa} \ln\left(\frac{20 + z_0}{z_0}\right) = 4.88m/s \tag{B.4}$$

The scaling function for speed values at 20 metres height with inflow speed of 4 m/s at 10 m is:

$$\phi(4m/s, 20m) = \frac{4.88m/s}{12.20m/s} = 0.4 \tag{B.5}$$

Therefore, to get the scaled velocity field with profile of an inflow speed with 4 m/s at 10 metres height from the raw simulation results:

$$U_{\gamma=4m/s} = U_{sim}0.4 \tag{B.6}$$

Note that for this work, the reference height for all inflow conditions is 10 metres because that is the height of the weather station. This is the reason why the scaling function ends up being a ratio of the inflow speeds. In the example above, it was 4 m/s divided by 10 m/s which is 0.4. However, this processes also applies when the reference height is different from 10 m. In that case, the scaling function will not be a ratio of the reference inflow speeds.

Scaling the turbulent kinetic energy follows a similar process. The turbulent kinetic energy at the inflow is modelled as follows [2]:

$$k = \frac{u_*^2}{\sqrt{C_\mu}} \tag{B.7}$$

[2]Stephen B. Pope, *Turbulent Flows* (Cambridge: Cambridge University Press, 2000).

The friction velocity u^* varies per inflow speed and is calculated using the inflow speed at the reference height. C_μ is an empirical constant equal to 0.09. The process for scaling the turbulence is:

$$k_\gamma = k_{sim}\phi(\gamma, x_3)^2 \tag{B.8}$$

Therefore, to scale the raw results at 20 metres to the case with a reference inflow speed of 4m/s at 10m:

$$k_{\gamma=4m/s} = k_{sim}0.4^2 \tag{B.9}$$

B.2. Additional city-wide risk contours

This section shows additional unsafe airspace percentage contour plots. Fig. B.2 shows the contour plot that is similar to Fig. 7.9. Note that this figure shows the unsafe percentage built with 16 inflow angles. The airspace is unsafe when the probability condition (**AND** or **OR**) is greater than or equal to 1. Note that it is quite similar to the plot with 40 inflow angles.

It is also helpful to study the unsafe airspace would look with a lower probability condition. Fig. B.3 shows the contour plot with unsafe airspace only for the **OR** condition for the case when we accept either 0.9 (Fig. B.3a) or 0.8 (Fig. B.3b). Note how more of the airspace would be unsafe in this case. This is built with 40 inflow angles.

To generate the additional risk maps at different heights, please refer to the supplementary dataset.

B.3. Additional flight operational feasibility analysis results

This section will show some additional operational feasibility tables for 2023 and 2024. Figs. B.4a and B.4b show the probability distribution of the speed and the wind rose for 2023, respectively. Similarly, Figs. B.5a and B.5b show the probability distribution of the speed and the wind rose for 2024, respectively. The data for November 2024 and December 2024 was not available at the time of writing, so it is not included in the plots. Note that the mean speed value in 2023 and 2024 was 4.6 and 4.2 metres per second, compared to 4.1 metres per second in 2022.

Tables B.1 and B.2 shows the yearly operation for 2023 and 2024, respectively. Note that this calculation is less accurate than what was shown in Table 7.2 because the wind rose is different, so the relevant directions will vary slightly for 2023 and 2024. However, it is clear that the higher wind speed average of 2023 led to lower overall operational time percentage when compared to 2022. This is especially true at 60 metres, where the wind speed limitation is more important. The differences between 2024 and 202 are less pronounced but may vary once the complete year is available.

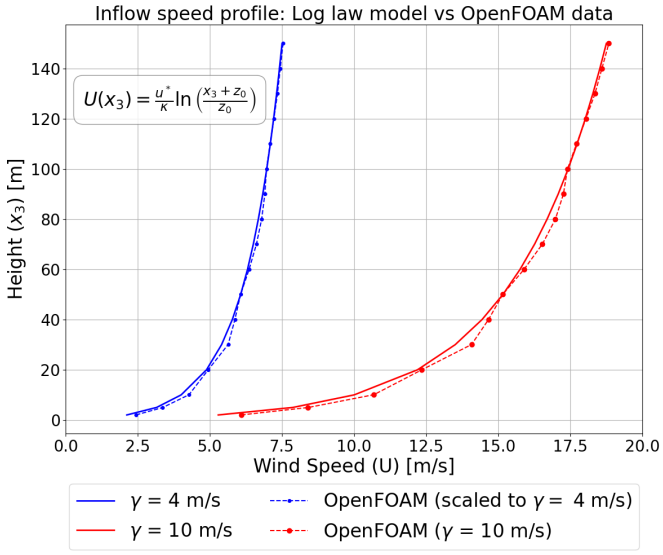

(a) This figure shows the log-law (Eq. 7.5) model at the inflow (red) and a raw result taken from the simulation at the inflow (red-dash) in Region 1. Additionally, it shows an example profile of scaling to a different inflow speed (blue).

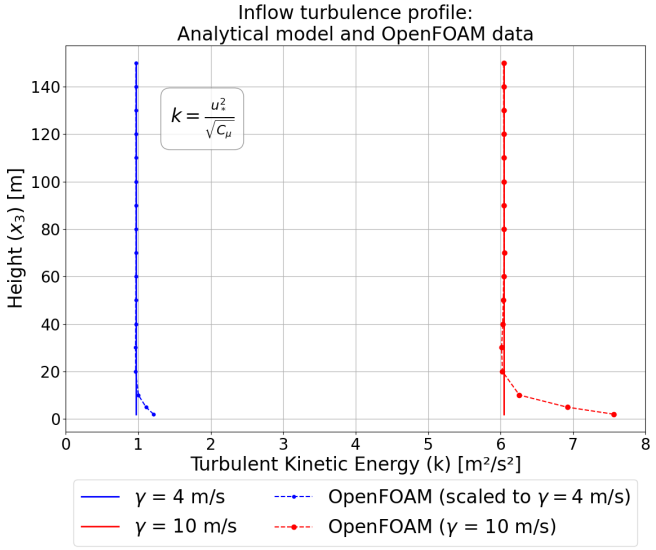

(b) This figure shows the k analytical model (Eq. B.7) model at the inflow (red) and a result taken from the simulation at the inflow (red-dash) in Region 1. Additionally, it shows an example profile of scaling to a different inflow speed (blue)

Figure B.1: Scaling example for the velocity magnitude and turbulent kinetic energy in Region 1.

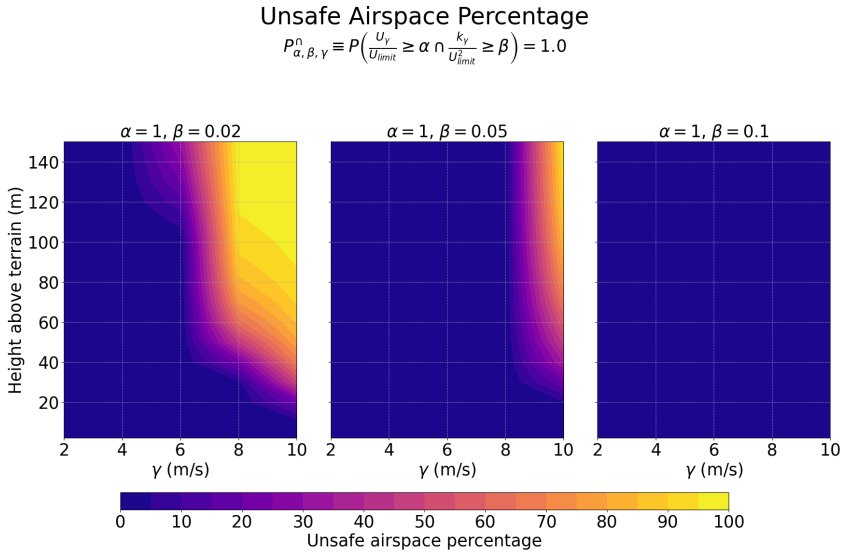

(a) Contour plot showing the **AND** condition for 16 inflow angles.

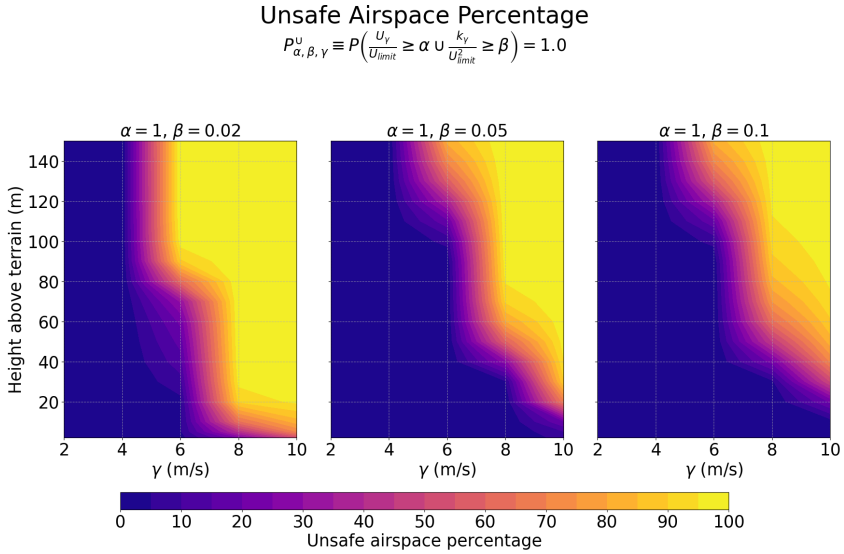

(b) Contour plot showing the **OR** condition for 16 inflow angles.

Figure B.2: Contour plot of unsafe airspace with 16 inflow angles for $U_{limit} = 10m/s$ and different inflow speeds, γ. The different plots correspond to certain speed, α, and turbulence, β safety thresholds. The plot shows the percent of unsafe airspace, considering areas where the velocity magnitude and turbulence thresholds are exceeded.

B

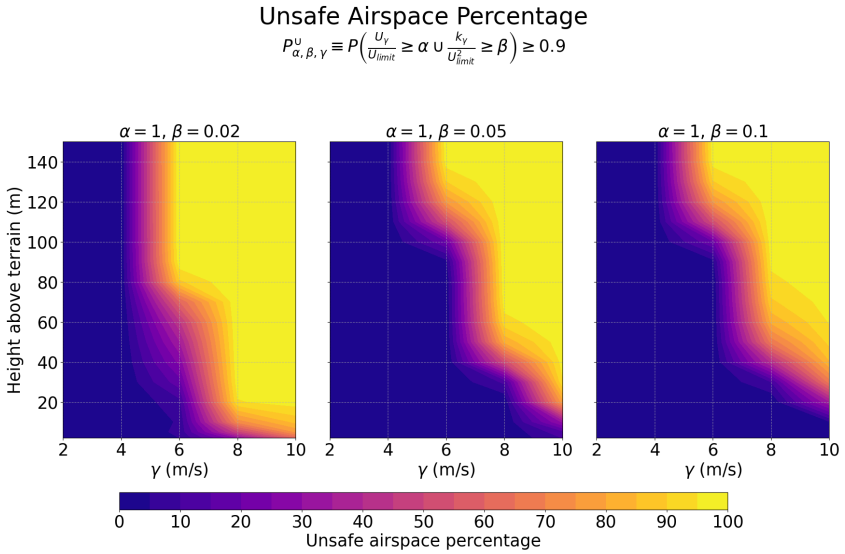

(a) Contour plot showing the **AND** condition for 40 inflow angles and probability condition less than 0.9.

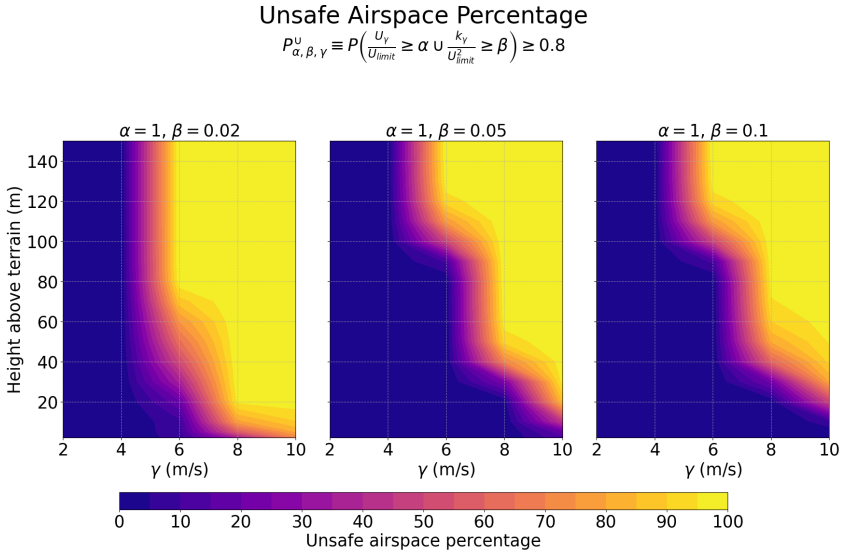

(b) Contour plot showing the **AND** condition for 40 inflow angles and probability condition less than 0.8.

Figure B.3: Contour plot of unsafe airspace with 16 inflow angles for $U_{limit} = 10m/s$ and different inflow speeds, γ. The different plots correspond to certain speed, α, and turbulence, β safety thresholds. The plot shows the percent of unsafe airspace, considering areas where the velocity magnitude and turbulence thresholds are exceeded.

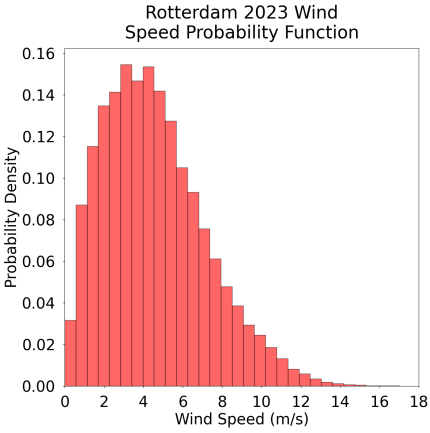

(a) Wind speed probability density function of Rotterdam.

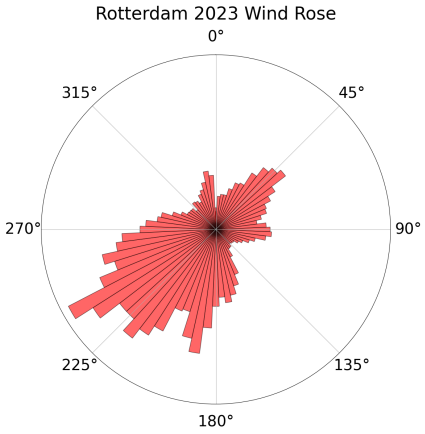

(b) Wind rose of Rotterdam.

Figure B.4: Measured speed probability density function and wind rose for a weather station located at the Rotterdam-The Hague Airport in 2023. Note that the wind rose refers to the direction from which the wind is coming; 0 degrees corresponds to North and 90 degrees to East.

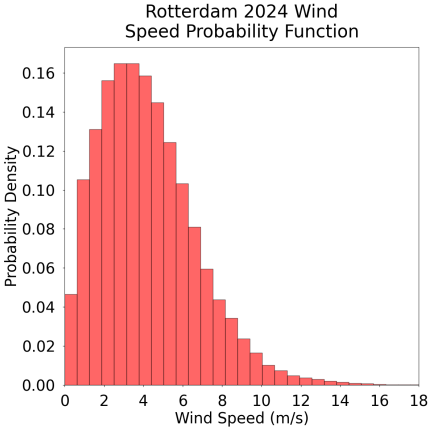

(a) Wind speed probability density function of Rotterdam.

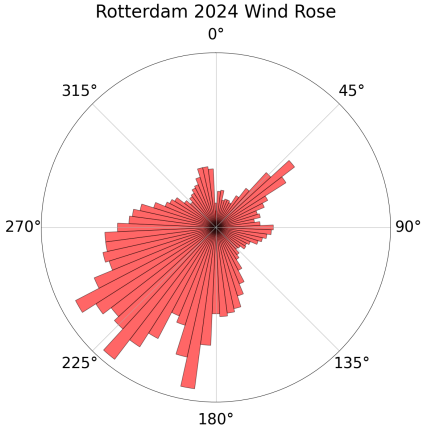

(b) Wind rose of Rotterdam.

Figure B.5: Measured speed probability density function and wind rose for a weather station located at the Rotterdam-The Hague Airport in 2024. Note that the wind rose refers to the direction from which the wind is coming; 0 degrees corresponds to North and 90 degrees to East. **Note that the data does not yet contain information about November and December of 2024.**

B

Table B.1: This table shows the amount of time as a percentage of 2023 that the airspace is operational for drones with different turbulence safety thresholds (β), and safe speed limits (U_{limit}) (The speed safety threshold is set to $\alpha = 1$ for all cases).

Yearly operational time as percentage of 2023 in Rotterdam						
	Height = 20 m			**Height = 60 m**		
U_{limit}	$\beta = 0.02$	$\beta = 0.05$	$\beta = 0.1$	$\beta = 0.02$	$\beta = 0.05$	$\beta = 0.1$
8 m/s	50%	75%	76%	48%	62%	62%
10 m/s	66%	87%	88%	63%	76%	76%
12 m/s	77%	94%	95%	75%	86%	86%

Table B.2: This table shows the amount of time as a percentage of January 2024 to October 2024, that the airspace is operational for drones with different turbulence safety thresholds (β), and safe speed limits (U_{limit}) (The speed safety threshold is set to $\alpha = 1$ for all cases).

Yearly operational time as percentage of 2024 in Rotterdam						
	Height = 20 m			**Height = 60 m**		
U_{limit}	$\beta = 0.02$	$\beta = 0.05$	$\beta = 0.1$	$\beta = 0.02$	$\beta = 0.05$	$\beta = 0.1$
8 m/s	56%	81%	82%	54%	68%	68%
10 m/s	72%	92%	92%	69%	82%	82%
12 m/s	83%	97%	97%	81%	91%	91%

Acknowledgements

Somehow, the acknowledgments are the last bit for me to write. It has been some weeks since the last version of the thesis was approved. Nevertheless, I could not seem to get started on this part. There was always something else to do. I had designed the cover, gotten my ISBN, electronic link. Just have been avoiding coming here. Even minutes ago, I was trying to find something else to do.

Was I ignoring them? yes, but why. Maybe I did not want the PhD to end? No that is probably not it. Perhaps I just don't know how to sum up these four years (heh, more like 5). I do know that I felt a sense of unease. I no longer have to follow a structure. There are no nice plots to describe, no need for a literature review. But there are conclusions to draw, that is something I can do.

I would first like to thank my supervisors. Your expert knowledge, input, and advice was invaluable in helping me compose this dissertation. I also appreciate the freedom you gave in pursuing my academic curiosities. Aside from the work, I enjoyed chatting about the smart home and swimming in North Sea.

My PhD colleagues were very important to me during these years and I am glad that I can call you friends. I think we can agree that we were quite lucky with the group we got. Even though I met most of you at the start of COVID, we managed to stay connected and work together. The time spent at dinners, conferences, Pizza-bakkers, and weddings was always fun. Additionally, I am very grateful that you indulged me with countless Catan nights.

Apart from my supervisors and PhD colleagues, I want to thank the people that I met as part of the broader TU Delft community. This includes professors, students, and staff. Additionally, I want to thank the people at the 3D geoinformation group, in another life, I would like to have been a PhD there.

It is true that I also have a life outside the University. These times helped me create some temporary distance from the thesis. Therefore, I want to thank all the friends I met in The Hague and Delft. As you know, I try not to venture further.

I also want to thank the people that I met before I began this PhD adventure. This includes my friends and family from Mexico, Miami, Bratislava, Switzerland, and Forlì (yes these are cities and countries in one list, but this is how they live in my head). Although, we do not see each other often, I am always ready to visit and hoping for your visits.

As I alluded to in my last proposition, scheduled dog walks are helpful for productivity. So I thank Coco for forcing me to leave my desk. Finally, without Barbora preventing my inevitable spirals when simulations inevitably failed, I would not have completed this thesis. You truly are amazing and your faith is - and continues to be - essential to my life.

Curriculum Vitæ

Andres Morfin Veytia

21-10-1991 Born in Guadalajara, Mexico.

Education

2010–2014 Bachelor of Science in Civil Engineering
Major in International Studies
Minor in Mathematics
University of Miami

2017–2019 Double Master of Science in Aerospace Engineering and Mechanical Engineering
Università di Bologna & Kungliga Tekniska högskolan
Thesis: Interscale transport of Reynolds stresses in wall-bounded flows

2020–2025 PhD. Aerospace Engineering
Technische Universiteit Delft
Thesis: Constrained Urban Airspace Design: Exploring future rules, strategies, and risk
Promotor: Dr. ir. J. Ellerbroek
Promotor: Prof. dr. ir. J.M. Hoekstra

Experience

2014–2017 Structural Engineer at UNITED Engineering, Inc.
Miami, Florida, United States

2020 Aeroelasticity Intern at NASA Langley Research Center
Hampton, Virginia, United States

Awards

2022 1st Place in EUROCONTROL's Innovation Masterclass Competition

2024 Best Paper Award in the UAS/UAM/Space track at ICRAT 2024

List of Publications

13. C. Badea, A. Morfin Veytia, M. Ribeiro, M. Doole, J. Ellerbroek and J. Hoekstra. 'Limitations of Conflict Prevention and Resolution in Constrained Very Low-Level Urban Airspace'. In: *11th SESAR Innovation Days*. 2021

12. N. Patrinopoulou, I. Daramouskas, V. Lappas, V. Kostopoulos, A. Morfin Veytia, C. A. Badea, J. Ellerbroek, J. Hoekstra, V. de Vries, J. van Ham, E. Sunil, P. M. Ponte Alonso, J. Pedrero Gonzalez, D. Bereziat, A. Vidosavljevic and L. Sedov. 'Metropolis II: Investigating the Future Shape of Air Traffic Control in Highly Dense Urban Airspace'. In: *2022 30th Mediterranean Conference on Control and Automation (MED)*. 2022. DOI: 10.1109/MED54222.2022.9837201

11. C. A. Badea, J. Groot, A. Morfin Veytia, M. Ribeiro, J. Ellerbroek and J. Hoekstra. 'Lateral and Vertical Air Traffic Control Under Uncertainty Using Reinforcement Learning'. In: *12th SESAR Innovation Days*. 2022

10. A. Morfin Veytia, C. A. Badea, J. Ellerbroek, J. Hoekstra, N. Patrinopoulou, I. Daramouskas, V. Lappas, V. Kostopoulos, P. Menendez, P. Alonso, J. Rodrigo, V. Terrazas, D. Bereziat, A. Vidosavljevic and L. Sedov. 'Metropolis II: Benefits of Centralised Separation Management in High-Density Urban Airspace'. In: *12th SESAR Innovation Days*. 2022

9. M. Giliam, J. Ellerbroek, C. A. Badea, A. Morfin Veytia and J. Hoekstra. 'A Tactical Conflict Resolution Method for UAVs in Geovectored Airspace'. In: *12th SESAR Innovation Days*. 2022

8. C. A. Badea, A. Morfin Veytia, N. Patrinopoulou, I. Daramouskas, J. Ellerbroek, V. Lappas, V. Kostopoulos and J. Hoekstra. 'Unifying Tactical Conflict Prevention, Detection, and Resolution Methods in Non-Orthogonal Constrained Urban Airspace'. en. In: *Aerospace* 10.5 (2023), p. 423. DOI: 10.3390/aerospace10050423

7. N. Patrinopoulou, I. Daramouskas, C. A. Badea, A. M. Veytia, V. Lappas, J. Ellerbroek, J. Hoekstra and V. Kostopoulos. 'Dynamic Capacity Management for Air Traffic Operations in High Density Constrained Urban Airspace'. In: *Drones* 7.6 (2023). DOI: 10.3390/drones7060395

6. A. Morfin Veytia, C. A. Badea, N. Patrinopoulou, I. Daramouskas, J. Ellerbroek, V. Lappas, V. Kostopoulos and J. Hoekstra. 'U-Space Utilisation of Airspace under Various Layer Function Assignments and Allocations'. In: *Drones* 7.7 (2023). ISSN: 2504-446X. DOI: 10.3390/drones7070444. URL: https://www.mdpi.com/2504-446X/7/7/444

5. C. Badea, A. Morfin Veytia, J. Ellerbroek and J. Hoekstra. 'Urban Wind Measurement and Modelling for U-space Operations'. English. In: *Proceedings International Conference on Research in Air Transportation*. Ed. by E. Neiderman, M. Bourgois, D. Lovell and H. Fricke. International Conference on Research in Air Transportation, ICRAT 2024 ; Conference date: 01-07-2024 Through 04-07-2024. 2024

4. A. Morfin Veytia, J. Ellerbroek and J. Hoekstra. ‘Decentralised Traffic Management for Constrained Urban Airspace: Dynamically Generating and Acting Upon Aggregate Flow Data’. In: *Journal of Open Aviation Science* 2.1 (2024). DOI: 10.59490/joas.2024.7716. URL: https://journals.open.tudelft.nl/joas/article/view/7716

3. A. Veytia, J. Ellerbroek and J. Hoekstra. ‘Dynamic capacity balancing in urban airspace: comparing historical and real-time aggregate flow data’. In: *14th SESAR Innovation Days*. 2024

2. C. A. Badea, A. Morfin Veytia, A. Vidosavljević, J. Ellerbroek and J. Hoekstra. ‘Very-low-level U-space Conflict Detection and Resolution: Focused Developments, Analysis, and Future Prospects’. In: *Journal of Open Aviation Science* 3.1 (May 2025). DOI: 10.59490/joas.2025.7921. URL: https://journals.open.tudelft.nl/joas/article/view/7921

1. A. Morfin Veytia, A. Patil, I. Pađen, J. Hoekstra, C. García-Sánchez and J. Ellerbroek. *Investigating the Operational Feasibility for Drones Using Wind Simulations in Rotterdam*. Available at SSRN. 2025. DOI: 10.2139/ssrn.5366294. URL: https://ssrn.com/abstract=5366294

Propositions

accompanying the dissertation

Constrained Urban Airspace Design

Exploring future rules, strategies, and risk.

by

Andres MORFIN VEYTIA

1. Air traffic designs should prioritise flexibility at low densities and predictability at high densities (this thesis).
2. Successful airspace designs transform air conflicts from safety hazards to useful information (this thesis).
3. Depending only on real-time data for local capacity management is possible when traffic density is high enough to generate meaningful data (this thesis).
4. Accurate forecasting of rapid changes in local wind conditions in cities is necessary for future high-density urban air operations (this thesis).
5. The term ”unmanned” is both inaccurate and objectionable.
6. Achieving successful open science is significantly more difficult and significantly more valuable.
7. Scientists developing novel methods to solve problems should compare them against solutions that (1) do nothing and (2) act randomly.
8. It is more urgent to reduce our energy consumption than to improve our energy efficiency.
9. Variations of the OR6A2 gene improve empathy in Mexicans living abroad.[1]
10. Scheduled dog walks help productivity for completing a doctoral’s student dissertation.

These propositions are regarded as opposable and defendable, and have been approved as such by the promotors Dr. ir. J. Ellerbroek and Prof. dr. ir. J.M. Hoekstra.

[1] The OR6A2 gene is the likely cause of a soapy taste in coriander